HZDR-031

Wissenschaftlich-Technische Berichte
HZDR-031 2013 · ISSN 2191-8708

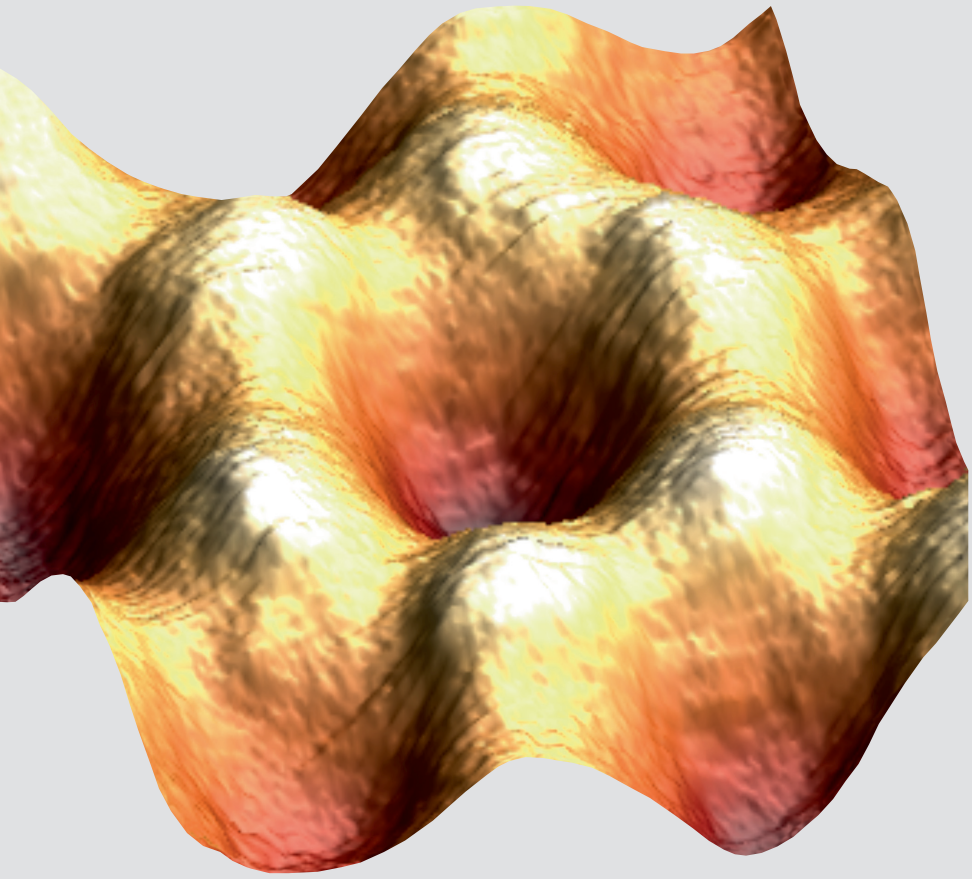

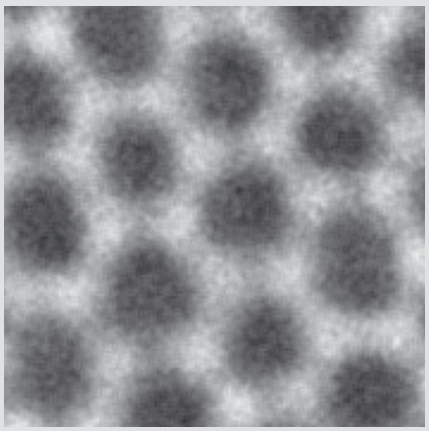

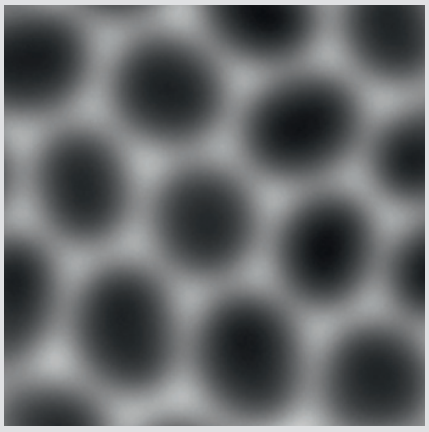

ANNUAL REPORT 2012

INSTITUTE OF ION BEAM PHYSICS AND MATERIALS RESEARCH

HZDR

HELMHOLTZ ZENTRUM DRESDEN ROSSENDORF

Wissenschaftlich-Technische Berichte
HZDR–031

Annual Report 2012

Institute of Ion Beam Physics and Materials Research

Editors

A. L. Cordeiro, J. Fassbender,
V. Heera, M. Helm

HZDR

HELMHOLTZ
ZENTRUM DRESDEN
ROSSENDORF

Cover Picture

Atomic force microscope image (100 x 100 nm^2) showing a hole structure in a Ge surface induced by irradiation with 5 keV Ga^+ ions. These self-organized nanostructures are formed in a hexagonally ordered pattern with a characteristic length of 48 nm during ion irradiation. The upper right image shows a 200 x 200 nm^2 scanning electron microscope image of the pattern. Using a continuum equation for pattern formation by ion irradiation the hexagonal ordering as well as details of the structures can be reproduced (lower right image).

For further information see:
M. Fritzsche et al., Appl. Phys. Lett. **100**, 223108 (2012),
reprinted at pp. 34 - 37 of this Annual Report.

Print edition: ISSN 2191-8708
Electronic edition: ISSN 2191-8716

Qucosa: http://fzd.qucosa.de/startseite/
Published by Helmholtz-Zentrum Dresden-Rossendorf e.V.

This report is also available at http://www.hzdr.de/FWI

Helmholtz-Zentrum Dresden-Rossendorf e.V.
Institute of Ion Beam Physics and Materials Research
P.O. Box 51 01 19
01314 Dresden
Germany

Directors	Prof. Dr. M. Helm	Prof. Dr. J. Fassbender
Phone	+ 49 (351) 260 2260	+ 49 (351) 260 3096
Fax	+ 49 (351) 260 3285	+ 49 (351) 260 3285
Email	m.helm@hzdr.de	j.fassbender@hzdr.de

http://www.hzdr.de/FWI

Preface by the directors

In 2012 the HZDR, and in consequence also the Institute of Ion Beam Physics and Materials Research (IIM) including its Ion Beam Center (IBC), has undergone a scientific evaluation. The evaluation committee composed of the Scientific Advisory Board and numerous external experts in our field of research concluded that “the overall quality of the scientific work is excellent”, that “there are an impressive number of young scientists working enthusiastically on a variety of high-level projects” and that “the choice of these projects represents a clear underlying strategy and vision”. We feel honored and are proud that the external view on our scientific achievements is that extraordinary. In view of this outstanding result we would like to express our gratitude to all our staff members for their commitment and efforts!

In the past year, we continued our integration into the Helmholtz Association of German Research Centers (HGF) with our Institute mostly active in the research area “Matter”, but also involved in a number of activities in the research area “Energy”. In this respect, many consultations were held with the Helmholtz centers contributing to common research areas to precisely define the role we will play in the newly established HGF program “**From Matter to Materials and Life**” (see schematic below). Our IBC has been recognized as a large-scale user facility for ion beam analysis and modification of materials, i.e., specializing on materials science. In particular, the IBC plays a prominent role in the recently approved Helmholtz Energy Materials Characterization Platform (HEMCP), which mainly concentrates on the development of dedicated analytical tools for the characterization of materials required for future energy technologies. The successes achieved by the IBC allows us to invest 7200 k€ to further improve and strengthen the ion beam capabilities at the Institute. In addition to this infrastructure-related grant, we were also successful in our funding application for the establishment of the International Helmholtz Research School for Nanoelectronic Networks (IHRS NANONET), aiming at promoting the next generation of leading scientists in the field of nanoelectronics. The IHRS NANONET is coordinated by our Institute and offers a well-structured PhD program to outstanding students of all nationalities with emphasis on interdisciplinary research and comprehensive training in technical and professional skills.

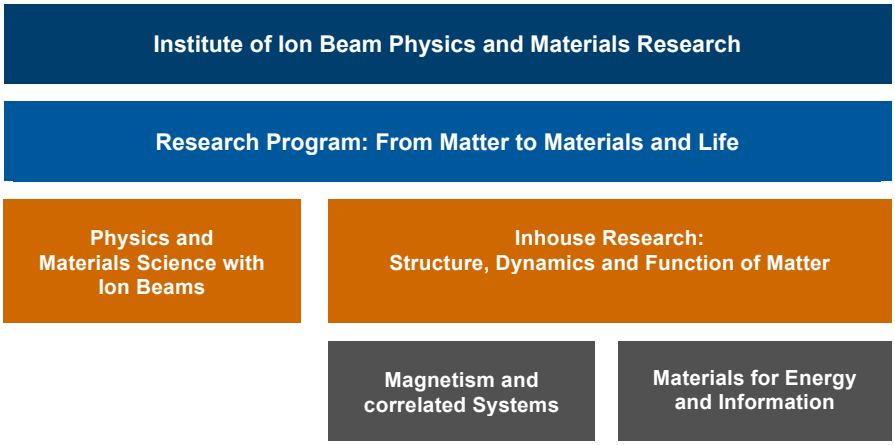

We owe the success of our Institute to our excellent researchers. Prof. Dr. Sibylle Gemming, head of the division “Scaling Phenomena”, received a Helmholtz-funded full professor position at TU Chemnitz, allowing us to strengthen the ties between TU Chemnitz and the HZDR. The research of Prof. Gemming focuses on the multiscale modeling of materials with special emphasis on the atomistic structure, physical properties and function relationships. In addition, several of our scientists received

awards in 2012. Most prominently Dr. Shengqiang Zhou, head of the Helmholtz Young Investigators Group “Functional Materials”, received the IBMM Young Scientist Award 2012 at the 18th International Conference on Ion Beam Modification of Materials. This award is attributed to outstanding young scientists. Within the HZDR, Dr. Stephan Winnerl received the HZDR Research Award 2012 for his outstanding contributions to terahertz science, and Dr. Stefan Facsko was appointed “HZDR Research Fellow”, allowing him to leave administrative burdens behind and concentrate on science for the next five years. In 2012 three of our longstanding scientists, Dr. Arndt Mücklich (responsible for transmisson electron microscopy), Dr. Reinhard Kögler (expert in defect engineering with ion beams), and Dr. Helfried Reuther (responsible for Mössbauer spectroscopy and Auger electron spectroscopy) have left the Institute for early retirement. We wish them all the best for their next period of life.

Together with colleagues from the IFW Dresden we organized the 17th International Conference on Superlattices, Nanostructures, and Nanodevices (ICSNN 2012). For one week in July, 250 semiconductor scientists were gathering in the Congress Center Dresden. Also in 2012 the TU Dresden was awarded the status of excellence by the Federal Ministry of Education and Research. In this framework, the cluster of excellence “Center for Advancing Electronics Dresden (cfAED), with significant participation of scientists from our institute, was granted. Both achievements will clearly strengthen our visibility in the field semiconductor nanoelectronics.

With respect to publications, 2012 was a very successful year. This Annual Report provides 16 selected publications out of 152 articles in refereed journal and book chapters in the field of semiconductor physics, magnetism and materials science using ion beams. In addition, our scientists delivered 49 invited talks at international conferences.

Finally we would like to cordially thank all partners, friends, and organizations who supported our progress in 2012. Special thanks are due to the Executive Board of the Helmholtz-Zentrum Dresden-Rossendorf, the Minister of Science and Arts of the Free State of Saxony, and the Minister of Education and Research of the Federal Government of Germany. Numerous partners from universities, industry and research institutes all around the world contributed essentially, and play a crucial role for the further development of the institute. Last but not least, the directors would like to thank again all IIM staff for their efforts and excellent contributions in 2012.

Prof. Manfred Helm

Prof. Jürgen Fassbender

Contents

Selected Publications

Statistics

Selected Publications

Photo: HZDR / J. Jeibmann

Copyright remarks

The following journal articles are reprinted with kind permission from:

Jacob, R.; Winnerl, S.; Fehrenbacher, M.; Bhattacharyya, J.; Schneider, H.; Wenzel, M. T.; von Ribbeck, H.-G.; Eng, L. M.; Atkinson, P.; Schmidt, O. G.; Helm, M.
Intersublevel spectroscopy on single InAs-quantum dots by terahertz near-field microscopy
Nano Letters, Vol. **12**, Issue 8, pp. 4336-4340

DOI: 10.1021/nl302078w

El-Said, A. S.; Wilhelm, R. A.; Heller, R.; Facsko, S.; Lemell, C.; Wachter, G.; Burgdörfer, J.; Ritter, R.; Aumayr, F.
Phase diagram for nanostructuring CaF_2 surfaces by slow highly charged ions
Physical Review Letters, Vol. **109**, Issue 11, Art.-No. 117602

DOI: 10.1103/PhysRevLett.109.117602

Krause, M.; Mücklich, A.; Oates, T. W. H.; Zschornak, M.; Wintz, S.; Endrino, J. L.; Baehtz, C.; Shalimov, A.; Gemming, S.; Abrasonis, G.
Tilting of carbon encapsulated metallic nanocolumns in carbon-nickel nanocomposite films by ion beam assisted deposition
Applied Physical Letters, Vol. **101**, Issue 5, Art.-No. 053112

DOI: 10.1063/1.4739417

Heera, V.; Fiedler, J.; Voelskow, M.; Mücklich, A.; Skrotzki, R.; Herrmannsdörfer, T.; Skorupa, W.
Superconductor-insulator transition controlled by annealing in Ga implanted Si
Applied Physical Letters, Vol. **100**, Issue 26, Art.-No. 262602

DOI: 10.1063/1.4732081

Liedke, M. O.; Körner, M.; Lenz, K.; Grossmann, F.; Facsko, S.; Fassbender, J.
Magnetic anisotropy engineering: Single-crystalline Fe films on ion eroded ripple surfaces
Applied Physical Letters, Vol. **100**, Issue 24, Art.-No. 242405

DOI: 10.1063/1.4729151

Fritzsche, M.; Mücklich, A.; Facsko, S.
Nanohole pattern formation on germanium induced by focused ion beam and broad beam Ga^+ irradiation
Applied Physical Letters, Vol. **100**, Issue 22, Art.-No. 223108

DOI: 10.1063/1.4721662

Bhattacharyya, J.; Zybell, S.; Winnerl, S.; Helm, M.; Hopkinson, M.; Wilson, L. R.; Schneider, H.
In-plane interdot carrier transfer in InAs/GaAs quantum dots
Applied Physical Letters, Vol. **100**, Issue 15, Art.-No. 152101

DOI: 10.1063/1.3701578

Wagner, M.; Teich, M.; Helm, M.; Stehr, D.
Temperature dependence of the intraexcitonic AC Stark effect in semiconductor quantum wells
Applied Physical Letters, Vol. **100**, Issue 5 Art.-No. 051109

DOI: 10.1063/1.3681399

Bürger, D.; Zhou, S.; Höwler, M.; Ou, X.; Kovacs, G.; Reuther, H.; Mücklich, A.; Skorupa, W.; Helm, M.; Schmidt, H.
Hysteretic anomalous Hall effect in a ferromagnetic, Mn-rich Ge:Mn nanonet
Applied Physical Letters, Vol. **100**, Issue 1, Art.-No. 012406

DOI: 10.1063/1.3674981

The following abstracts of journal articles are reprinted with kind permission from:

Wintz, S.; Strache, T.; Körner, M.; Bunce, C.; Banholzer, A.; Mönch, I.; Mattheis, R.; Raabe, J.; Quitmann, C.; McCord, J.; Erbe, A.; Lenz, K.; Fassbender, J.
Control of vortex pair states by post-deposition interlayer exchange coupling modification
Physical Review B, Vol. **85**, Issue 13, Art.-No. 134417

DOI: 10.1103/PhysRevB.85.134417

Prucnal, S.; Zhou, S.; Ou, X.; Reuther, H.; Liedke, M. O.; Mücklich, A.; Helm, M.; Zuk, J.; Turek, M.; Pyszniak, K.; Skorupa, W.
InP nanocrystals on silicon for optoelectronic applications
Nanotechnology, Vol. **23**, Issue 48, Art.-No. 485204

DOI: 10.1088/0957-4484/23/48/485204

Philipp, P.; Bischoff, L.; Schmidt, B.
Taming of Ga droplets on DLC layers – Size tuning and local arrangement with nanometer accuracy
Nanotechnology, Vol. **23**, Issue 47, Art.-No. 4753044

DOI: 10.1088/0957-4484/23/47/475304

Böttger, R.; Bischoff, L.; Facsko, S.; Schmidt, B.
Quantitative analysis of the order of Bi ion induced dot patterns on Ge
EPL, Vol. **98**, Issue 1, Art.-No. 16009

DOI: 10.1209/0295-5075/98/16009

Abrasonis, G.; Wintz, S.; Liedke, M. O.; Aksoy Akgul, F.; Krause, M.; Kuepper, K.; Banerjee, D.; Liu, Z.; Gemming, S.
Environment controlled dewetting of Rh−Pd bilayers: A route for core−shell nanostructure synthesis
Journal of Physical Chemistry C, Vol. **116**, Issue 27, 14401-14407.

DOI: 10.1021/jp302908x

Winnerl, S.; Hubrich, R.; Mittendorff, M.; Schneider, H.; Helm, M.
Universal phase relation between longitudinal and transverse fields observed in focused terahertz beams
New Journal of Physics, Vol. **14**, Art.-No.103049.

DOI: 10.1088/1367-2630/14/10/103049

Heintze, C.; Hernández-Mayoral, M.; Ulbricht, A.; Bergner, F.; Shariq, A.; Weissgärber, T. Frielinghaus, H.
Nanoscale characterization of ODS Fe-9%Cr model alloys compacted by spark plasma sintering
Journal of Nuclear Materials, Vol. **428**, Issue 1-3, 139-146.

DOI: 10.1016/j.jnucmat.2011.08.053

NANO LETTERS
Letter
pubs.acs.org/NanoLett

Intersublevel Spectroscopy on Single InAs-Quantum Dots by Terahertz Near-Field Microscopy

Rainer Jacob,[†] Stephan Winnerl,*[,†] Markus Fehrenbacher,[†] Jayeeta Bhattacharyya,[†] Harald Schneider,[†] Marc Tobias Wenzel,[‡] Hans-Georg von Ribbeck,[‡] Lukas M. Eng,[‡] Paola Atkinson,[§] Oliver G. Schmidt,[§] and Manfred Helm[†,‡]

[†]Institute of Ion Beam Physics and Materials Research, Helmholtz-Zentrum Dresden-Rossendorf, P.O. Box 51 01 19, 01314 Dresden, Germany

[‡]Institut für Angewandte Photophysik, Technische Universität Dresden, 01062, Dresden, Germany

[§]Institute for Integrative Nanosciences, IFW Dresden, Helmholtzstrasse 20, 01069 Dresden, Germany

ABSTRACT: Using scattering-type near-field infrared microscopy in combination with a free-electron laser, intersublevel transitions in buried single InAs quantum dots are investigated. The experiments are performed at room temperature on doped self-assembled quantum dots capped with a 70 nm GaAs layer. Clear near-field contrast of single dots is observed when the photon energy of the incident beam matches intersublevel transition energies, namely the p-d and s-d transition of conduction band electrons confined in the dots. The observed room-temperature line width of 5−8 meV of these resonances in the mid-infrared range is significantly below the inhomogeneously broadened spectral lines of quantum dot ensembles. The experiment highlights the strength of near-field microspectroscopy by demonstrating signals from bound-to-bound transitions of single electrons in a probe volume of the order of $(100\ \mathrm{nm})^3$.

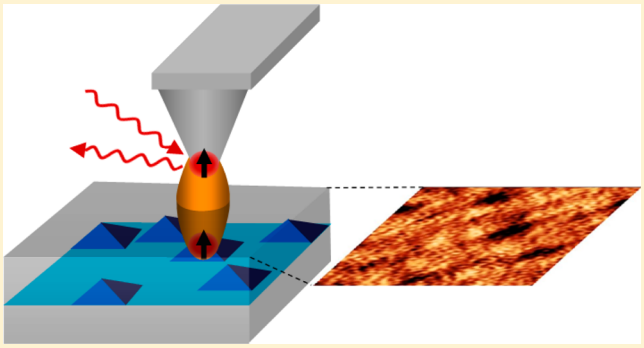

KEYWORDS: *Spectroscopy on single quantum dots, self-assembled quantum dots, near-field microscopy, intersublevel transitions*

Quantum dots have attracted remarkable interest for the last years. Because of the three-dimensional confinement, they exhibit atom-like electronic states rather than energy bands which are typical for bulk semiconductors or semiconductor quantum wells. Optical transitions between discrete levels of carriers confined in the valence band and the conduction band (interband transitions) are relevant for application purposes in quantum dot lasers,[1] for research on spin dynamics[2] as well as for quantum information processing in solid-state systems.[3] While many studies can be performed on ensembles of self-assembled quantum dots grown by the Stranski-Krastanov growth mode, for example, InAs dots on GaAs,[4] an increasing number of studies is focusing these days on single quantum dots. Optical spectroscopy on single quantum dots has been achieved, for example, by microphotoluminescence[5,6] measurements, and coherent spectroscopy[7] employing aperture-based near-field microscopes. Furthermore, scattering-type near-field microscopy has been employed to study interband transitions in Ge[8] and InAs[9] quantum dots. Apart from interband transitions of confined charge carriers, also the intersublevel transitions of electrons and holes within the conduction or valence band are of interest both from basic science and application-oriented viewpoints. For example, polaronic coupling can be studied in doped self-assembled quantum dots.[10] Intersublevel transitions are also the basis for quantum dot infrared photodetectors that operate in the mid-infrared.[11,12] However, while single-dot spectroscopy is well established for interband transitions, only few studies on intersublevel single dot spectroscopy have been reported so far. Houel et al.[13] have excited intersublevel transitions in buried InAs quantum dots and measured the surface deformation caused by the local heating with an atomic-force microscope (AFM). Signatures of local heating from single dots were identified, however, the main part of the measured signal stemmed from groups of quantum dots, which could not be resolved individually. The signals obtained for photon energies around 120 meV were attributed to the s-d intersublevel transition. With the same technique, Sauvage et al.[14] investigated the s-p intersublevel transition (∼50 meV) of InGaAs quantum dots embedded in a thin GaAs membrane in order to minimize phononic absorption in the GaAs matrix.

In this work, we present near-field terahertz microscopy measurements on buried single InAs quantum dots in resonance with electron intersublevel transitions. We used a

Received: June 1, 2012
Revised: July 5, 2012
Published: July 9, 2012

dx.doi.org/10.1021/nl302078w | *Nano Lett.* 2012, 12, 4336−4340

scattering-type near-field infrared microscope (s-SNOM) in combination with a free-electron laser (FEL) to map optical transitions between bound electron states. By scanning the wavelength and recording the near-field amplitude above and beside an InAs quantum dot, we were able to determine the transition energies as well as the homogeneous broadening of the transition at room temperature. In our experiment, the spatial resolution is significantly higher as compared to the distance between quantum dots, hence the recorded signals can be clearly attributed to individual single quantum dots.

The self-assembled quantum dots were grown in the Stranski-Krastanov growth mode on GaAs by molecular beam epitaxy at a substrate temperature of 515 °C. The growth rate was 0.007 ML/s. The conduction band electrons (approximately two electrons per dot) are provided by Si δ-doping 2 nm below the dot layer. The quantum dots were capped by a 70 nm thick undoped GaAs layer followed by δ-doping of nominally 1×10^{15} cm^{-2} at the surface in order to avoid surface depletion of the quantum dots. To suppress indium segregation, the GaAs overgrowth was started at a substrate temperature of 470 °C, which subsequently was ramped up to 570 °C. The dot density was of the order of 1×10^{9} cm^{-2}, which is 40 times less than used by Houel et al.[13]

The quantum dot ensemble was first characterized by photoluminescence (PL) spectroscopy. In Figure 1, a PL spectrum obtained at 15 K (excitation energy 2.33 eV, excitation power 40 mW, spot size ~100 μm) is shown. The three distinct peaks are attributed to emission from the electronic ground state (s-level) and the first two excited electron states (p- and d-level), respectively. The PL emission lines with a separation of around 55 and 120 meV for the s-p and s-d transitions, respectively, show typical behavior for this type of self-organized quantum dots. Measurements at room temperature revealed a full width at half-maximum (fwhm) of the PL lines of 30 meV and a significant red shift (not shown). However, the line separation remained unchanged, which is in agreement with previous reports.[15] Hence, the line separation at 15 K is a good measure for estimating the intersublevel separation in the conduction band also at room temperature. To this end it is crucial to take into account the interband−transition selection rules as indicated in Figure 1(a). In particular, since electrons from the electronic p-level recombine to the first excited hole state while electrons from the s and d-level recombine to the hole ground state, the energy difference between the hole ground state and the first excited state has to be considered. Furthermore different exciton binding energies may play a role. The electron confinement energy is roughly 70% of the combined confinement energy of electrons and holes observed in the PL emission.[16,17] Following this argument we expect the electronic intersublevel transitions of our quantum dots at energies of approximately 56 meV × 0.7 = 39 meV, 110 meV − 39 meV = 71 meV, and 110 meV for the s-p, p-d, and s-d transition, respectively.

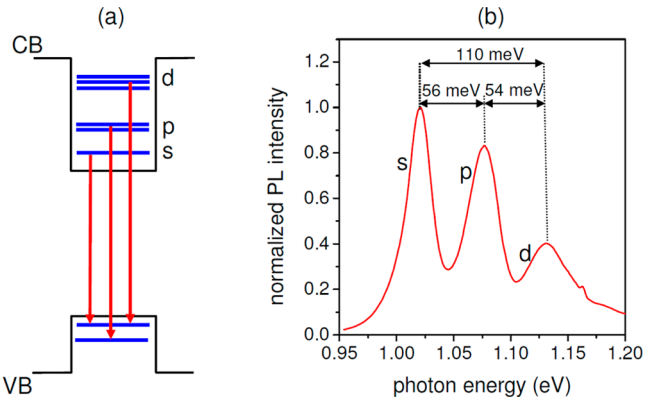

Figure 1. Simplified scheme of confined states in the conduction band (CB) and valence band (VB) (a). The conduction band states classified as s-p-d levels exhibit a 1-2-3 fold near-degeneracy, respectively. The transitions observed by photoluminescence spectroscopy are indicated as red arrows. Photoluminescence spectrum obtained at a sample temperature of 15 K (b).

For near-field nanospectroscopy of the buried quantum dots, the s-SNOM technique as illustrated in Figure 2a is applied. The tip of an AFM cantilever is illuminated and the backscattered radiation is detected.[18−20] The polaritonic polarization excited in the tip interacts with an image-charge dipole in the sample.[21] This principle allows us to probe the local dielectric properties of the sample with a spatial resolution that is determined by the tip diameter and the tip−sample distance only, and therefore is wavelength-independent. Separation of the near-field signal from the far-field background is achieved by harmonic demodulation of the measured signal.[21] To this end, lock-in detection at harmonics of the cantilever oscillation frequency is applied. Our setup consists of a home-built AFM which employs the widely tunable FEL (photon energy 5−300 meV, relative spectral width 0.5−2%) at the Helmholtz−Zentrum Dresden−Rossendorf as a radiation source.[22,23] Commercially available platinum−iridium-coated cantilevers with nominal resonance frequency of 170 kHz and radius below 50 nm are used. The sample topography was recorded in true noncontact AFM mode simultaneously with the s-SNOM signals, mercury−cadmium−telluride (MCT) detectors were employed for the s-SNOM measurements.

A topography image of our buried quantum dot sample is shown in Figure 2b. Signatures of several overgrown quantum dots appear as structures of 2 nm height and lateral dimensions of 100 nm × 300 nm. We note that this does not resemble the shape of the quantum dots, rather the flattened, enlarged, and elongated along the [$\bar{1}$10] direction shape is a typical result of the overgrowth process.[24] From the growth conditions and the PL spectra we conclude that the buried dots are lens shaped with typical base dimensions of ~25 nm and a height of 3−4 nm.[15,17] At an excitation energy of 85 meV, the individual quantum dots clearly appear as well-separated dark areas in the s-SNOM image. At slightly larger energies (91 meV), three dots marked with circles are still barely visible, while the other dots, which are clearly visible in the upper part of Figure 2c, disappear. This energy dependence rules out that the observed s-SNOM contrast is a topography artifact. Furthermore it is an indication that the intersublevel separation, which differs slightly from dot to dot, is responsible for the contrast. To corroborate this further, the photon energy was scanned over a range of 20 meV while monitoring the single quantum dot behavior. In Figure 3, the normalized near-field contrast defined as $C = (S_{dot} - S_{no\_dot})/S_{no\_dot}$ is plotted as a function of the excitation energy. Here S_{dot} is the near-field signal recorded over the buried quantum dot, while S_{no_dot} denotes the reference signal recorded far away from a buried quantum dot. In both cases, the near-field signal is demodulated at the second harmonic of the cantilever oscillation. The measured data can be fitted with a Lorentzian function centered at 84 ± 1 meV with a full width at half-maximum (fwhm) of 8 ± 2 meV.

dx.doi.org/10.1021/nl302078w | Nano Lett. 2012, 12, 4336−4340

Nano Letters Letter

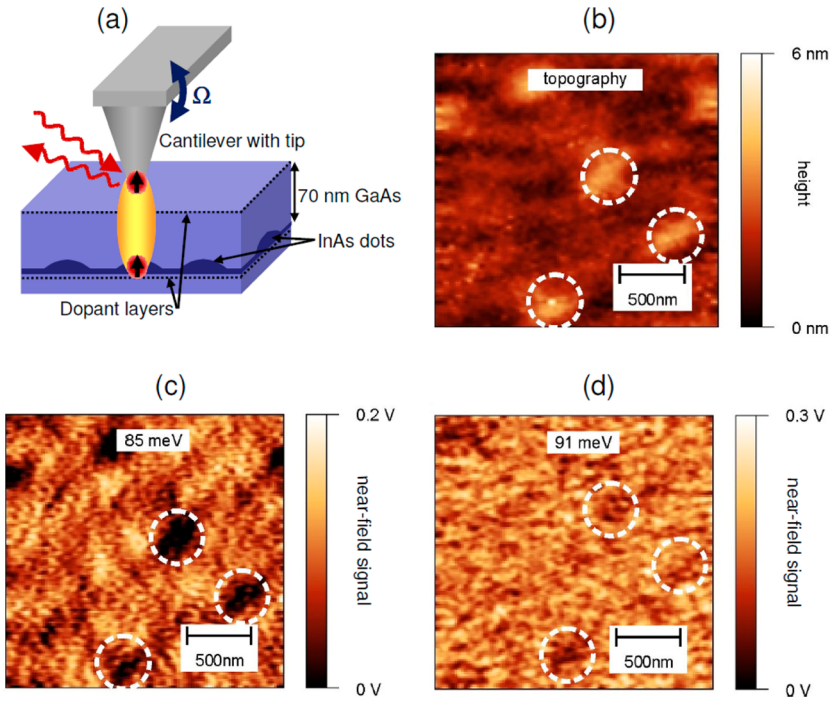

Figure 2. Principle of s-SNOM on buried InAs quantum dots (a) The arrows on the tip and the quantum dot indicate the interacting polarization dipoles. Topography as recorded by AFM (b), and s-SNOM images (second harmonic) of the same location recorded at two different photon energies (c,d). The dotted circles mark the positions of three dots that are clearly visible as surface mounds in the topography scan (b) and in the near-field signal using 85 meV excitation (c), but only weakly visible in using 91 meV excitation.

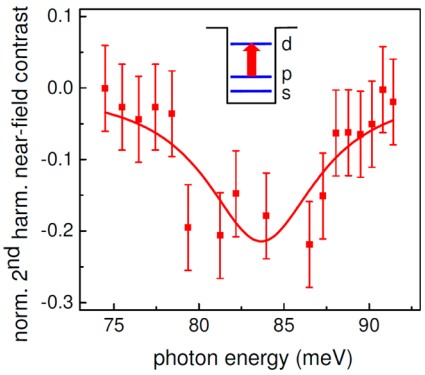

Figure 3. Near-field contrast of a single quantum dot excited at energies around the p-d intersublevel transition. The dots represent measured data and the solid line is a Lorentzian fit to the data with a fwhm of 8 ± 2 meV.

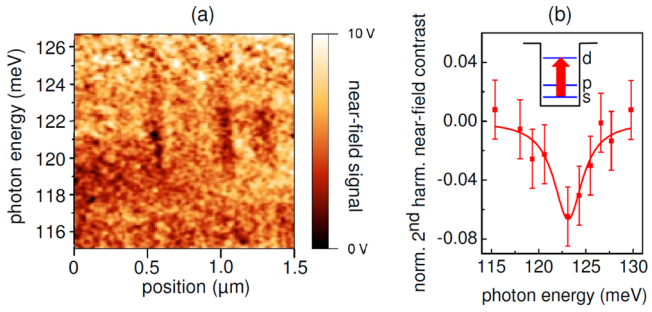

Figure 4. Line scans at different photon energies showing three quantum dots excited around the s-d intersublevel transition (a). Near-field contrast of a single quantum dot excited at energies around the s-d intersublevel transition (b). The dots represent measured data and the solid line is a Lorentzian fit to the data.

Theoretically maximum s-SNOM signals are expected at energies, where the real part of the dielectric function reaches a minimum, that is, at slightly higher energies as compared to the peak position of an absorption line. Hence the observed resonance in the s-SNOM signal can be consistently attributed to the p-d intersublevel transition. Any other contrast mechanism arising, for instance, from strain effects or a local change in the dielectric constant caused by the different phononic properties of InAs dots and the GaAs matrix, can be ruled out since the reported near-field contrast is resonant within a narrow energy band only. We note that the p-d intersublevel transition is enabled in the doped dots by the finite population in the p-level at room temperature.

Next we discuss s-SNOM signals for the excitation at energies around the s-d intersublevel transition. Line scans were performed in one lateral dimension only while the photon energy was changed slightly for subsequent scans. The results of these measurements are shown in Figure 4a. Three quantum dots become clearly visible when the sample is excited at around 122 meV. Again the lateral position of the s-SNOM signals is consistent with the topography signal observed by AFM (not shown). The normalized contrast of a single dot is displayed in Figure 4b. Here the fit reveals a position of 123 ± 1 meV and a fwhm of 5 ± 2 meV. Again the peak position is blue shifted with respect to the s-d level separation obtained by the PL measurement. We attribute the significantly smaller normalized contrast as compared to the p-d transition to the smaller oscillator strength of the transition. For atomic levels as well as for a harmonic Fock model the s-d transition is parity forbidden. In more realistic eight band **k·p** models[25] and calculations based on density functional theory,[26] however, this transition has a nonvanishing oscillator strength. Correspond-

dx.doi.org/10.1021/nl302078w | Nano Lett. 2012, 12, 4336–4340

ingly s-d transitions have frequently been observed at energies around 120 meV in self-organized InAs quantum dots.[13]

We did not observe near-field contrast in the energy range 35−55 meV, where the s-p intersublevel transition is expected. We suggest that the absorption due to the GaAs reststrahlen region (absorption coefficient >100 cm^{-1} between 31 and 39 meV[27]) prevented the observation of s-SNOM contrast caused by the dots. The absorption not only reduces the transmission through the capping layer, more importantly it results in local heating of the crystal lattice. The heating in turn reduces the electronic absorption in the quantum dots, since it results in a distribution where the s- and p-level could be almost equally populated.

The linewidths of single-dot transitions observed in our s-SNOM experiments of ∼5 and ∼8 meV for s-d and the p-d transitions, respectively, are significantly below the inhomogeneously broadened line width (∼30 meV) observed in the PL measurements. Several processes contribute to this homogeneous line width. At room temperature, the most important process is scattering by longitudinal optical phonons. We expect the induced broadening to be comparable or somewhat less than for interband transitions, where homogeneous broadening of about 10 meV is observed,[28] which is consistent with our present observation. Further broadening may be expected to arise from anisotropy splitting of the excited states, which could be different for p and d-levels. Additionally the quantum confined Stark effect induced by fluctuating charges surrounding the quantum dots, for example, at the δ-doped layers, may contribute to the line broadening. However, from theoretical studies this effect is expected to contribute less than 1 meV to the line broadening.[29] A comparison of our s-SNOM results with the results of the local absorption spectroscopy by Houel et al.[13] and Sauvage et al.[14] further corroborates this interpretation: by local absorption spectroscopy homogeneous linewidths of 2.5 and 10 meV were observed for the s-p and the s-d intersublevel transitions, respectively.

At low temperatures, the carrier lifetime resulting from polaronic coupling depends strongly on the electron energy.[10,30] Dephasing times for the s-p transition (∼53 meV) of almost 100 ps have been observed at low temperatures for ensembles of InAs quantum dots.[31] This corresponds to a homogeneous line width of 15 μeV, which increases to 150 μeV as the temperature is raised from 10 to 120 K. We expect that extending our s-SNOM study to low temperatures will be of great interest as it will allow us to study the homogeneous line width on a single dot level and therefore provide new insights into the microscopic processes. We point out that these processes correspond to quite a different and basically unexplored regime as compared to the study of single undoped quantum dots in micro-PL experiments. Because of doping, both the carrier−carrier scattering as well as the polaronic interaction of electrons and phonons differ significantly from the excitonic behavior observed in PL experiments on undoped quantum dots.

The spatial resolution in our experiment measures ∼100 nm, corresponding to a subwavelength resolution of $\sim\lambda/150$. For objects at the surface, the spatial resolution of s-SNOM is basically determined by the tip diameter.[21] It has been shown that objects can also be resolved if they are buried under capping layers of a thickness comparable to the tip diameter.[19,22,32] In this case, the contrast is reduced and the spatial resolution blurred. Quantitatively the resolution in a certain depth can be approximated by the resolution at the surface plus the thickness of the capping layer (50 nm + 70 nm in our case).[32] It has been pointed out previously that s-SNOM is extremely sensitive in the infrared and terahertz spectral range.[33] In a study on semiconductor nanodevices, it has been shown that the Drude absorption stemming from a few hundred electrons in the volume probed by s-SNOM provides the near-field contrast.[33] Our experiment involving bound-to-bound transitions of quantum-confined electrons demonstrates directly the intriguing opportunity to visualize one or two electrons in a probe volume of the order of $(100\ nm)^3$.

While our results clearly point to electronic intersublevel transitions being responsible for the s-SNOM contrast observed at resonant energies, we do not provide a quantitative theoretical description. To this end, modeling of the local polarizability of the tip and the sample is required. For the sample a realistic description of the complex dielectric function in the infrared is needed locally, which is beyond the scope of the present study. For a sample, which is large compared to the tip diameter and the tip−sample distance, the dipole model predicts increased near-field amplitudes, when the real part of the dielectric constant becomes negative.[21] Hence, one could expect increased s-SNOM amplitudes for excitation energies slightly above the central energy of a pronounced absorption line. In our experiment, however, we observe a decrease of the s-SNOM signal from the dots, when they are excited around the electronic resonances. We attribute this to a particle size effect. For InGaAs nanoparticles on GaN it has been found that InGaAs particles of 100−200 nm diameter yield increased s-SNOM signals as expected from the dielectric constant. On the other hand, imaging particles of 10−20 nm diameter, which is smaller than the tip diameter, results in an inverted contrast, that is, in this case the s-SNOM amplitude from the nanoparticle is smaller as compared to the signal from the surrounding GaN.[34] Similar contrast reversal has been observed for gold and polystyrene nanoparticles on Si.[35] Furthermore this behavior has been found for vibrational absorption in Si_3N_4 nanoislands and explained by a model that takes into account the changes in the dielectric constant on a nanometer scale.[36] The striking contrast reversal can be understood in the following way: for particles smaller than the tip diameter, the dipole coupling between the tip and particle becomes very small. On the other hand, the particle effectively reduces the coupling between the tip and the surrounding substrate, resulting in a reduced signal when the tip is above the particle.[35] Since our quantum dots are smaller than both the tip diameter and the tip-dot separation, a contrast reversal due to the nanosize effect can be expected, which is accord with our experimental findings.

In conclusion, we have shown that s-SNOM is capable to clearly resolve signals from single overgrown semiconductor quantum dots. The near-field contrast corresponds to electronic intersublevel transitions. The homogeneous line width of 5−8 meV, which is well below the inhomogeneously broadened width for transitions of an ensemble, reflects the rapid dephasing at room temperature as well as the anisotropy splitting of the excited states. Extending these studies toward lower temperatures opens up fascinating new possibilities to investigate the dephasing mechanisms on a single-dot level for doped quantum dots.

AUTHOR INFORMATION

Corresponding Author

*E-mail: s.winnerl@hzdr.de.

Nano Letters Letter

Notes

The authors declare no competing financial interest.

■ ACKNOWLEDGMENTS

We gratefully acknowledge the funding by the German Science Foundation DFG (projects HE 3352/4-1 and EN 434/22-1) and by the German Ministry of Education and Research (BMBF; Grant 05K10BRA and 05K10ODB). Furthermore, we thank the whole ELBE team for their dedicated support. We are especially indebted to A. Rastelli for discussions concerning the sample design.

■ REFERENCES

(1) Arakawa, Y.; Sakaki, H. *Appl. Phys. Lett.* **1982**, *40*, 939.
(2) Paillard, X.; Marie, X.; Renucci, P.; Amand, T.; Jbeli, A.; Gérard, J. M. *Phys. Rev. Lett.* **2001**, *86*, 1634.
(3) Imamoglu, A.; Awschalom, D. D.; Burkard, G.; Di Vincenzo, D. P.; Loss, D.; Sherwin, M.; Small, A. *Phys. Rev. Lett.* **1999**, *83*, 4204.
(4) Grundmann, M.; Stier, O.; Bimberg, D. *Phys. Rev. B* **1995**, *52*, 11969.
(5) Hess, H. F.; Betzig, E.; Harris, T. D.; Pfeiffer, L. N.; West, K. W. *Science* **1994**, *264*, 5166.
(6) Shields, A. J. *Nat. Photonics* **2007**, *1*, 215.
(7) Guest, J. R.; Stievater, T. H.; Chen, G.; Tabak, E. A.; Orr, B. G.; Steel, D. G.; Gammon, D.; Katzer, D. S. *Science* **2001**, *293*, 2224.
(8) Ogawa, Y.; Minami, F.; Abate, Y.; Leone, S. R. *Appl. Phys. Lett.* **2010**, *96*, 063107.
(9) Skacel, M.; Francardi, M.; Gerardino, A.; Alloing, B.; Li, L. H.; Fiore, A. *J. Phys. Conf. Ser.* **2010**, *245*, 012040.
(10) Zibik, E. A.; Grange, T.; Carpenter, B. A.; Porter, N. E.; Ferreira, R.; Bastard, G.; Stehr, D.; Winnerl, S.; Helm, M.; Liu, H. Y.; Skolnick, M. S.; Wilson, L. R. *Nat. Mater.* **2009**, *8*, 803.
(11) Pan, D.; Towe, E.; Kennerly, S. *Appl. Phys. Lett.* **1998**, *73*, 1937.
(12) Maimon, S.; Finkman, E.; Bahir, G.; Schacham, S. E.; Garcia, J. M.; Petroff, P. M. *Appl. Phys. Lett.* **1998**, *73*, 2003.
(13) Houel, J.; Sauvage, S.; Boucaud, P.; Dazzi, A.; Prazeres, R.; Glotin, F.; Ortéga, J. M.; Miard, A.; Lemaître, A. *Phys. Rev. Lett.* **2007**, *99*, 217404−217404.
(14) Sauvage, S.; Driss, A.; Réveret, F.; Boucaud, P.; Dazzi, A.; Prazeres, R.; Glotin, F.; Orétga, J.-M.; Miard, A.; Halioua, Y.; Raineri, F.; Sagnes, I.; Lemaître, A. *Phys. Rev. B* **2011**, *83*, 035302.
(15) Joyce, P. B.; Krzyzewski, T. J.; Bell, G. R.; Malik, T. S. J. S.; Childs, D.; Murray, R. *Phys. Rev. B* **2000**, *62*, 10891.
(16) Aslan, B.; Song, C. Y.; Liu, H. C. *Appl. Phys. Lett.* **2008**, *92*, 253118.
(17) Williamson, A. J.; Wang, L. W.; Zunger, A. *Phys. Rev. B* **2000**, *62*, 12963.
(18) Knoll, B.; Keilmann, F. *Nature* **1999**, *399*, 134.
(19) Samson, J. S.; Wollny, G.; Bründermann, E.; Berger, A.; Hecker, A.; Schwaab, G.; Wiek, A. D.; Havenith, M. *Phys. Chem. Chem. Phys.* **2006**, *8*, 753.
(20) Kehr, S. C.; Cebula, M.; Mieth, O.; Härting, T.; Seidel, J.; Grafsrtöm, S.; Eng, L. M.; Winnerl, S.; Stehr, D.; Helm, M. *Phys. Rev. Lett.* **2008**, *100*, 256403.
(21) Knoll, B.; Keilmann, F. *Opt. Commun.* **2000**, *182*, 321.
(22) Jacob, R.; Winnerl, S.; Schneider, H.; Helm, M.; Wenzel, M. T.; von Ribbeck, H.-G.; Eng, L. M.; Kehr, S. C. *Opt. Express* **2010**, *18*, 26206.
(23) Kehr, S. C.; Liu, Y. M.; Martin, L. W.; Yu, P.; Gajek, M.; Yang, S.-Y.; Yang, C. -H.; Wenzel, M. T.; Jacob, R.; von Ribbeck, H.-G.; Helm, M.; Zhang, X.; Eng, L. M.; Ramesh, R. *Nat. Comm.* **2011**, *2*, 249.
(24) Joyce, P. B.; Krzyzewski, T. J.; Steans, P. H.; Bell, G. R.; Neave, J. H.; Jones, T. S. *Surf. Sci.* **2001**, *492*, 345.
(25) Boucaud, P.; Sauvage, S. *C. R. Physique* **2003**, *4*, 1133.
(26) Leburton, J.-P.; Fonseca, L. R. C.; Shumway, J; Ceperly, D.; Martin, R. M. *Jpn. J. Appl. Phys.* **1999**, *38*, 357.
(27) Blakemore, J. S. *J. Appl. Phys.* **1982**, *53*, R123.
(28) Matsuda, K.; Ikeda, K.; Saiki, T.; Tsuchiya, H; Saito, H.; Nishi, K. *Phys. Rev. B* **2001**, *63*, 121304(R).
(29) Abbarchi, M.; Troiani, F.; Mastrandrea, C.; Goldoni, G.; Kuroda, T.; Mano, T.; Sakoda, K.; Koguchi, N.; Sanguinetti, S.; Vinattieri, A.; Gurioli, M. *Appl. Phys. Lett.* **2008**, *93*, 162101.
(30) Zibik, E. A.; Wilson, L. R.; Green, R. P.; Bastard, G.; Ferreira, R.; Phillips, P. J.; Carder, D. A.; Wells, J.-P. R.; Cockburn, J. W.; Skolnick, M. S.; Steer, M. J.; Hopkinson, M. *Phys. Rev. B* **2004**, *70*, 161305(R).
(31) Zibik, E. A.; Grange, T.; Carpenter, B. A.; Ferreira, R.; Bastard, G.; Vinh, N. Q.; Phillips, P. J.; Steer, M. J.; Hopkinson, M.; Cockburn, J. W.; Skolnick, M. S.; Wilson, L. R. *Phys. Rev. B* **2008**, *77*, 041307(R).
(32) Krutokhvostov, R.; Govyadinov, A. A.; Stiegler, J. M.; Huth, F.; Chuvilin, A.; Carney, P. S.; Hillenbrand, R. *Opt. Express* **2012**, *20*, 593.
(33) Huber, A. J.; Keilmann, K.; Wittborn, J.; Aizpura, J.; Hillenbrand, R. *Nano Lett.* **2008**, *8*, 3766.
(34) Kim, Z. H.; Ahn, S.-H.; Liu, B.; Leone, S. R. *Nano Lett.* **2007**, *7*, 2258.
(35) Cvitkovic, A; Ocelic, N.; Hillenbrand, R. *Nano Lett.* **2007**, *7*, 3177.
(36) Stiegler, J. M.; Abate, Y.; Cvitkovic, A.; Romanyuk, Y. E.; Huber, A. J.; Leone, S. R.; Hillenbrand, R. *ASC Nano* **2011**, *5*, 6494.

PRL 109, 117602 (2012) PHYSICAL REVIEW LETTERS week ending 14 SEPTEMBER 2012

Phase Diagram for Nanostructuring CaF_2 Surfaces by Slow Highly Charged Ions

A. S. El-Said*
Institute of Ion Beam Physics and Materials Research, Helmholtz-Zentrum Dresden-Rossendorf, 01328 Dresden, Germany, EU; Physics Department, Faculty of Science, Mansoura University, 35516 Mansoura, Egypt

R. A. Wilhelm, R. Heller, and S. Facsko†
Institute of Ion Beam Physics and Materials Research, Helmholtz-Zentrum Dresden-Rossendorf, 01328 Dresden, Germany, EU

C. Lemell, G. Wachter, and J. Burgdörfer
Institute for Theoretical Physics, Vienna University of Technology, Wiedner Hauptstr. 8-10, A-1040 Vienna, Austria, EU

R. Ritter and F. Aumayr‡
Institute of Applied Physics, TU Wien-Vienna University of Technology, 1040 Vienna, Austria, EU
(Received 24 February 2012; published 14 September 2012)

The impact of individual slow highly charged ions (HCI) on alkaline earth halide and alkali halide surfaces creates nano-scale surface modifications. For different materials and impact energies a wide variety of topographic alterations have been observed, ranging from regularly shaped pits to nano-hillocks. We present experimental evidence for the creation of thermodynamically stable defect agglomerations initially hidden after irradiation but becoming visible as pits upon subsequent etching. A well defined threshold separating regions with and without etch-pit formation is found as a function of potential and kinetic energies of the projectile. Combining this novel type of surface defects with the previously identified hillock formation, a phase diagram for HCI induced surface restructuring emerges. The simulation of the energy deposition by the HCI in the crystal provides insight into the early stages of the dynamics of the surface modification and its dependence on the kinetic and potential energies.

DOI: 10.1103/PhysRevLett.109.117602 PACS numbers: 79.20.Rf, 34.35.+a, 61.80.Jh

Studies of the interactions of slow ($v < v_{\mathrm{Bohr}}$), highly charged ions (HCIs) with solid surfaces were originally aimed at gaining an understanding of the dynamical processes governing neutralization, relaxation, and eventual dissipation of the very high potential energy density ($\sim$ keV/Å^3) within a few femtoseconds ([1] and references therein). This potential energy carried into the collision is given by the sum of binding energies of all missing electrons. More recently, the focus has shifted to material-science driven applications, specifically to the development of novel techniques for material modification [2–5] and improved surface analysis [6,7]. Various types of surface nanostructures such as nanosized hillocks, pits or craters have so far been observed after the impact of individual HCI on different materials [8–11]. Their topography, appearance, and long-time stability seem to depend sensitively on the material properties as well as on the potential energy (charge state) and kinetic energy of the incident ion (for a recent review see Ref. [12]).

Surprisingly, even for very similar prototypical wide-band-gap insulators, ionic crystals of alkali halides and alkaline earth halides, vastly different and seemingly contradictory results have been found. Irradiation of KBr single crystals by individual highly charged Xe ions leads to the formation of pits of one atomic layer depth [11] while irradiation of CaF_2 single crystals produces nanometer high hillocks protruding from the surface [8]. In both cases the surface nanostructures were shown to be the result of individual ion impacts; i.e., every structure is caused by the impact of a single ion and a threshold value for the potential energy of the projectile has to be surpassed before the nanostructure can be observed. However, while for KBr this threshold potential energy for pit formation strongly decreases with increasing kinetic energy of the HCI [11], for hillock formation in CaF_2 only a slight yet noticeable increase with increasing kinetic energy is observed [8].

In this Letter we present experimental evidence which supplies the missing pieces to this puzzle and allows us to construct a phase diagram as a function of kinetic and potential energies for the formation of different nanosized defect structures in CaF_2. In addition, simulation of the early stages of dissipation of the energy deposited by the HCIs reveals characteristic differences in the relaxation dynamics as a function of potential and kinetic energies which can be considered to be the precursors of the eventual formation of different stable surface structures. The key is the search for previously unobserved "hidden" surface structures after irradiation by ions with potential energies below the threshold for nano-hillock formation. By etching the samples we discover a second threshold at lower potential energy above which CaF_2 undergoes a nanoscale structural transformation even though it is not evident as a topographic change. It becomes, however,

visible in the form of triangular pits after chemical etching. This threshold depends on both the potential and the kinetic energies of the HCIs closely resembling the threshold behavior found for pit formation on KBr. Accompanying molecular dynamics simulations suggest this second threshold to be associated with lattice defect aggregation in CaF_2 following electronic excitations caused by the HCI-surface interaction.

Thin platelets of CaF_2 were prepared by cleaving a high purity single-crystal block grown from melt in an inert atmosphere along the (111) plane. This cleavage is known to produce atomically flat fluorine-terminated surfaces which are ideal for observing surface topographic changes down to the nanometer scale [13]. $^{129}Xe^{q+}$ ions were extracted from the electron beam ion trap at the Two-Source-Facility of the Helmholtz-Zentrum Dresden-Rossendorf using an electrostatic potential of 4.5 kV. By using a two stage deceleration system and adjusting the potential difference between source and target from 4.5 kV down to 0.18 kV, highly charged Xe^{q+} projectiles over a wide range of charge states ($10 \leq q \leq 33$, corresponding to potential energies of 0.8 keV $\leq E_{pot} \leq$ 21.2 keV) and kinetic impact energies (6 keV $\leq E_{kin} \leq$ 150 keV) could be produced. The applied ion fluences were chosen between 0.5 and 5×10^8 ions/cm^2, small enough to avoid overlapping of impact sites and high enough to obtain reasonable statistics. The time averaged current density varied between $\sim 10^4$ and $\sim 3 \times 10^5$ ions/s/cm^2 as derived from the ion count rate and a circular beam spot with a diameter of 6 mm. The surfaces of the irradiated samples were investigated using atomic force microscopy (AFM) (Veeco Multimode). The AFM was operated in contact mode with a constant loading force of less than 5 nN using nonconductive Si_3N_4 sensors (Veeco Instruments) with cantilevers of force constants ~ 0.1 Nm. The image processing was performed using the WSXM software [14]. Ion-irradiated CaF_2 samples were chemically etched using a HNO_3 solution (10% vol.) at room temperature without agitation [13]. Each platelet was immersed once in the etchant, subsequently in deionized water, and was finally dried in a stream of dry nitrogen. It should be emphasized that we use much shorter etching times t_e than applied in standard etching techniques. For the latter, typically $t_e \gtrsim 1$ minute yields etch pits even starting from randomly occurring atomic-scale dislocations and much of the sensitivity to hidden defect aggregates would be lost. Due to the dramatically enhanced etching speed in regions with a high defect density caused by the HCIs (~ 20 nm/s compared to a regular lateral etching speed of less than 3 nm/s [13]), $t_e =$ 10 s turned out to be the optimum etching time combining good visibility of etch pits in AFM while selecting only defect clusters created by HCI impact. The presented structures with dimensions in the range of a few 100 nm in lateral and vertical direction are by far larger than the topographic resolution of the ambient AFM in contact mode.

The observation of a pattern of well-defined irradiated and masked areas (Fig. 1) for 150 keV Xe^{33+} ion impact on

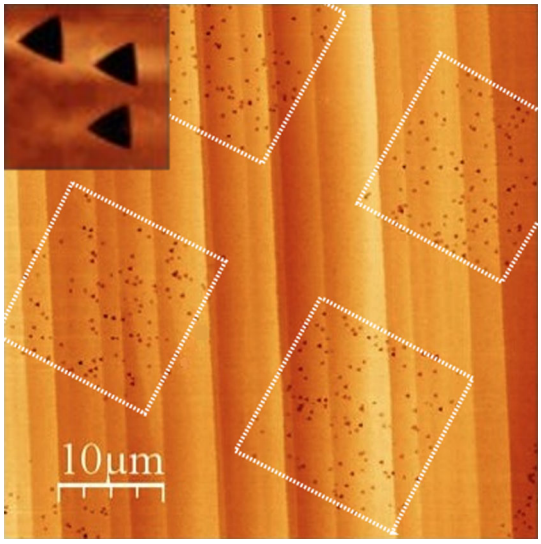

FIG. 1 (color online). AFM topographic image (50×50 μm^2) of a CaF_2 surface showing etch pits after exposure to 150 keV Xe^{33+} ions. The sample was irradiated through a mask (indicated by dotted lines) and subsequently chemically etched using HNO_3. The inset in the upper left corner shows a magnification of the etch pits (1.5×1.5 μm^2).

CaF_2 (111) is direct evidence of HCI induced surface defects which can be clearly distinguished from randomly occurring dislocations and surface damage. In irradiated areas, etch pits of regularly structured 3-faced symmetric triangular depressions appear which are similar to those observed after irradiation and etching of BaF_2 [15]. This particular geometrical shape originates from the (111) crystal lattice orientation of the CaF_2 sample [13]. The number of pits is in good agreement with the applied ion fluence; i.e., each etch pit is created by a single ion impact. We suppose the pits are localized at the sites where HCI impact created hillocks were situated prior to etching. The charge state ($q = 33$) of the incident ion corresponds to a potential energy well above the threshold for nanohillock formation.

Lowering the charge state to values below the potential energy threshold for hillock formation ($q_{th} \approx 28$ for Xe; $E_{pot} = 12$ keV) reveals the appearance of similar pits in the absence of preceding hillocks (Fig. 2). At the same kinetic energy of $E_{kin} = 40$ keV for "low" charge states ($q \lesssim 18$) no damage of the etched surface is visible, whereas at a higher charge state ($q = 25$, $E_{pot} = 8.1$ keV) etch pits appear.

In order to investigate the influence of both potential and kinetic energies on etch pit formation, we performed systematic irradiations with $^{129}Xe^{q+}$ projectiles of different charge states ($q = 10$ to 33) and with varying kinetic energy on CaF_2. The resulting thermodynamically stable damage structures and modifications can be summarized by a "phase diagram" with potential and kinetic energies as state variables (Fig. 3). Three different phases pertaining to surface

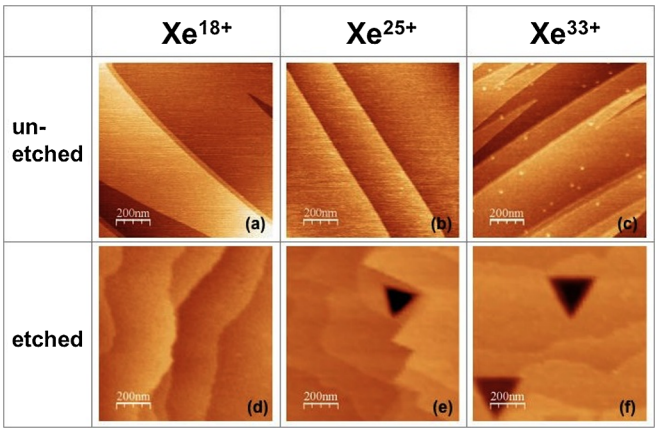

FIG. 2 (color online). Topographic contact-mode AFM images of CaF_2 (111) samples irradiated by 40 keV Xe ions in different charge states (columns): (a), (d) Xe^{18+}, (b), (e) Xe^{25+}, and (c), (f) Xe^{33+}. In each frame an area of 1 μm × 1 μm is displayed. Upper row: resulting images without etching (a), (b), (c). Lower row: images after etching by HNO_3 (d), (e), (f). Ion fluences were 2×10^8 ions/cm^2 for (e), (f) and 1–2 × 10^9 ions/cm^2 for (a), (b), (c), (d).

restructuring can be distinguished: the stability region *A* without detectable surface modification after HCI impact [Figs. 2(a) and 2(d)], region *B* in which defect clusters become visible as regularly shaped pits only upon etching [Figs. 2(b) and 2(e)], and the nanohillock region *C* [Figs. 2(c) and 2(f)] in which hillocks resulting from nanomelting can be observed after irradiation. The nanomelting arises from the transfer of high local energy density during HCI impact and is followed by a rapid quenching resulting in the formation of a hillock-like structure (nanohillock) [8]. Pits appear in phase *C* only after etching presumably at the

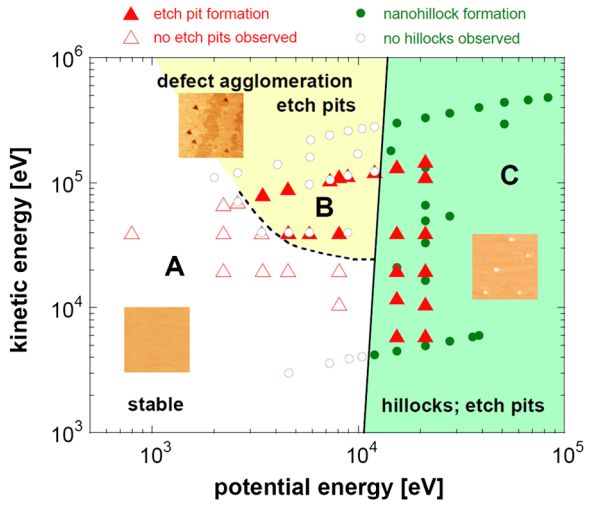

FIG. 3 (color online). Hillock and etch pit formation on CaF_2 (111) induced by irradiation with highly charged Xe ions. Full (open) green circles show pairs of potential and kinetic energies where hillocks are produced (absent) after irradiation, full (open) red triangles indicate pairs where pits are present (missing) after etching the irradiated samples.

positions of the hillocks which could not be found on the etched surface.

While the threshold for hillock formation strongly depends on potential energy but only weakly on kinetic energy [8,12] implying an almost vertical boundary of region *C* in Fig. 3, the border separating the stability region *A* and the defect agglomeration region *B* (etch pits) is strongly dependent on both kinetic and potential energies. Ions with lower kinetic energy require more potential energy to create etchable damage than faster ones. Such synergistic effects of kinetic and potential energies have previously been observed for pit formation in KBr [11], however, with the difference that no chemical etching was a prerequisite for the pits to be observed. This may be related to the much higher defect mobility in KBr than in CaF_2 leading to a more efficient transport of defects to the surface immediately followed by material desorption.

These experimental findings suggest a scenario for nanostructure formation on alkaline earth halides and alkali halides involving initial heating of electrons by multiple electron transfer and Auger relaxation, hot electron transport and dissipation with accompanying lattice heating by electron-optical phonon coupling, and finally atomic motion in the heated crystal which results in dislocations, defects, and structural weakening of the cooled lattice. The early stages of defect formation can be simulated within a three-step model exploiting disparate time scales of the underlying processes: the initial electronic energy deposition of the HCIs occurring on the (sub) femtosecond time scale can be described by the classical-over-barrier model [16], the hot electron transport and lattice heating occurring on a sub-picosecond time scale by classical electron-transport simulations [17], and finally the atomic motion by a molecular-dynamics (MD) simulation which we follow for up to 15 ps [18]. It should be noted that accurate potential surfaces for ionic crystals, in particular, in the presence of excitations and charge transfer entering the MD simulation, are not available. Following the system on longer time scales and reaching the regime of formation of thermodynamically stable phases is, thus, not possible. Our simulation results can therefore provide only qualitative, yet important, insights into the early stages of defect formation and aggregation. The following qualitative trends can be readily extracted. For HCIs in "low" charge states (Fig. 4, left) only a few (i.e., low density) individual defects (point defects, single vacancies) are created at or below the surface, where we take the distance individual fluorine atoms travel during ~15 ps as measure for the eventual defect formation probability. These defects either remain below the surface, easily anneal or are too small to be detected by means of AFM. Since the etchability of CaF_2 is strongly coupled to the creation of large defect aggregates [19] rather than to point defects, no pits are observed after etching. Our MD simulations do not yield any significant number of lattice displacements for low q (well below ~1%).

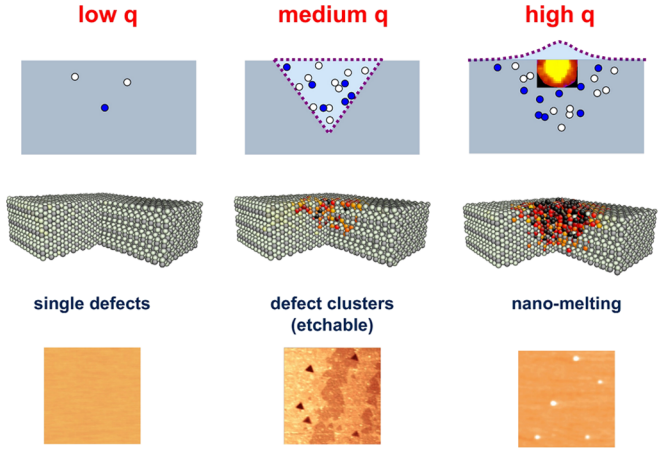

FIG. 4 (color online). Scenario for surface modification as a function of charge q or, equivalently, potential energy of the HCIs. Upper row: the charge state controls the created surface modification from nonetchable single defects (low q) to defect aggregates (medium q) and to locally molten zones (high q), schematically. Lower row: AFM images. Center row: typical results of molecular dynamics simulations showing that the initial electronic excitation of the surface and energy transfer to the lattice leads to a considerable number of displacements (center column) even before melting of the surface sets in (right column); center figures created using AtomEye [28].

For larger q and, correspondingly, larger potential energy, the sputtering yield [20] as well as the density of defects (excitons, color centers, Ca enriched regions due to F_2 formation) strongly increase. The latter is now large enough to lead to defect clusters and aggregates (Fig. 4, center column). Depending on their mobility, defects may diffuse to the surface, leading to defect-mediated desorption [21] and thus form (monoatomic) pits as observed in the case of the alkali halide KBr [11]. The defect-mediated desorption mechanism is less probable in CaF_2 since color center recombination below the surface is much more likely [22] due to the small energy gain of color center pair formation as well as the formation of more complex (and therefore immobile) defect agglomerates [23,24]. The material in the vicinity of the impact region is not ablated but structurally weakened and forms the nucleus of an etchable defect subsequently removed by a suitable etchant [15]. The synergistic effect induced by the accompanying kinetic energy originates from kinetically induced defects created in the collision cascade which enhance the trapping of the color centers created by potential energy [25] and therefore increases defect agglomeration. Consequently, the borderline between the regions A (stable) and B (etchable surface defects) has a negative slope in the phase diagram (Fig. 3). While our MD simulation cannot directly account for the defect cluster formation (due to the lack of realistic binary potentials for color centers and charge-exchanged constituents), it shows in the regime of phase B atomic displacements of the order of a few percent of the impact region, the overwhelming majority of which are fluorine atoms (Fig. 4, center). This is believed to be a necessary precursor for defect aggregation.

At still higher potential energies (Fig. 4, right column), heating of the lattice atoms by primary and secondary electrons from the deexcitation of the HCIs surpasses the melting threshold of the solid [8,18]. Heat and pressure deforms the surface and after rapid quenching a hillock remains at the surface. With increasing kinetic energy, the region where the potential energy of the HCIs is deposited, extends slightly deeper into the target [8]. Therefore, the kinetic energy dependence of the borderline between the region of nanohillock formation (region C) and defect clustering without protrusion (region B) is only weak with a slightly positive slope. The overall surface damage (lattice distortion, defect aggregations) extends well beyond the molten core. While the latter determines the diameter of the hillock, the former determines the size of the nucleus of the etch pit. Within the MD simulations a much larger number of displacements ($\sim 25\%$) is observed in region C, a significant fraction of which are calcium atoms.

Even though the present scenario is demonstrated specifically for CaF_2, we surmise that it should hold for other halide crystals as well. While borderlines between different regions A, B, and C will, of course, depend on the specific target material, we expect the phase diagram (Fig. 3) to remain qualitatively valid. For BaF_2 (111) and KBr (001), for example, we have previously observed the A and B phases [15,26]. The phase diagram predicts that by further increasing the potential energy of the HCIs we should be able to reach region C, i.e., hillock formation (or melting) in line with first indications for hillock formation on BaF_2 [27].

In summary, we have established a phase diagram for stable nanoscale surface modification of alkaline earth halides and alkali halides by highly charged ion impact with its potential and kinetic energies as control parameters. In addition to the region of predominantly potential energy driven melting and hillock formation, a second region was identified in which a sufficient number of defects agglomerate such that chemical etchants are able to remove material leaving triangular shaped pits on the surface. The etchability of the defect cluster not only depends on the potential energy of the HCIs but also strongly on the kinetic energy of the projectile. This scenario seems to be generally applicable to other alkaline earth and alkali halide surfaces as well.

A. S. E. thanks the Alexander von Humboldt Foundation for financial support. The Deutsche Forschungsgemeinschaft (DFG) is gratefully acknowledged for financial support under Project No. HE 6174/1-1. R. R. is a recipient of a DOC-fellowship of the Austrian Academy of Sciences. Support from the Austrian Science Foundation FWF under Project No. SFB-041 ViCoM and the International Max Planck Research School of Advanced Photon Science APS (G. W.) is acknowledged.

*a.s.el-said@hzdr.de
†s.facsko@hzdr.de
‡aumayr@iap.tuwien.ac.at

[1] A. Arnau, F. Aumayr, P. M. Echenique, M. Grether, W. Heiland, J. Limburg, R. Morgenstern, P. Roncin, S. Schippers, R. Schuch, N. Stolterfoht, P. Varga, T. J. M. Zouros, and H. P. Winter, Surf. Sci. Rep. **27**, 113 (1997).
[2] A. V. Hamza, M. W. Newman, P. A. Thielen, H. W. H. Lee, T. Schenkel, J. W. McDonald, and D. H. Schneider, Appl. Phys. Lett. **79**, 2973 (2001).
[3] M. Tona, H. Watanabe, S. Takahashi, N. Nakamura, N. Yoshiyasu, M. Sakurai, T. Terui, S. Mashiko, C. Yamada, and S. Ohtani, Nucl. Instrum. Methods Phys. Res., Sect. B **256**, 543 (2007).
[4] J. M. Pomeroy, H. Grube, A. C. Perrella, and J. Gillaspy, Appl. Phys. Lett. **91**, 073506 (2007).
[5] R. E. Lake, J. M. Pomeroy, H. Grube, and C. E. Sosolik, Phys. Rev. Lett. **107**, 063202 (2011).
[6] A. V. Hamza, T. Schenkel, A. V. Barnes, and D. H. Schneider, J. Vac. Sci. Technol. A **17**, 303 (1999).
[7] M. Tona, S. Takahashi, K. Nagata, N. Yoshiyasu, C. Yamada, N. Nakamura, S. Ohtani, and M. Sakurai, Appl. Phys. Lett. **87**, 224102 (2005).
[8] A. S. El-Said, R. Heller, W. Meissl, R. Ritter, S. Facsko, C. Lemell, B. Solleder, I. C. Gebeshuber, G. Betz, M. Toulemonde, W. Möller, J. Burgdörfer, and F. Aumayr, Phys. Rev. Lett. **100**, 237601 (2008).
[9] M. Tona, H. Watanabe, S. Takahashi, N. Nakamura, N. Yoshiyasu, M. Sakurai, T. Terui, S. Mashiko, C. Yamada, and S. Ohtani, Surf. Sci. **601**, 723 (2007).
[10] M. Tona, Y. Fujita, C. Yamada, and S. Ohtani, Phys. Rev. B **77**, 155427 (2008).
[11] R. Heller, S. Facsko, R. A. Wilhelm, and W. Möller, Phys. Rev. Lett. **101**, 096102 (2008).
[12] F. Aumayr, S. Facsko, A. S. El-Said, C. Trautmann, and M. Schleberger, J. Phys. Condens. Matter **23**, 393001 (2011).
[13] C. Motzer and M. Reichling, J. Appl. Phys. **105**, 064309 (2009).
[14] I. Horcas, R. Fernandez, J. M. Gomez-Rodriguez, J. Colchero, J. Gomez-Herrero, and A. M. Baro, Rev. Sci. Instrum. **78**, 013705 (2007).
[15] A. S. El-Said, R. Heller, F. Aumayr, and S. Facsko, Phys. Rev. B **82**, 033403 (2010).
[16] J. Burgdörfer, P. Lerner, and F. W. Meyer, Phys. Rev. A **44**, 5674 (1991).
[17] B. Solleder, C. Lemell, K. Tökesi, N. Hatcher, and J. Burgdörfer, Phys. Rev. B **76**, 075115 (2007).
[18] G. Wachter, Diplom thesis, TU Wien-Vienna University of Technology, 2009 (unpublished), http://www.ub.tuwien.ac.at/dipl/2009/AC07452619.pdf.
[19] C. Trautmann, K. Schwartz, and O. Geiss, J. Appl. Phys. **83**, 3560 (1998).
[20] F. Aumayr and H. P. Winter, Phil. Trans. R. Soc. A **362**, 77 (2004).
[21] G. Hayderer, M. Schmid, P. Varga, H. Winter, F. Aumayr, L. Wirtz, C. Lemell, J. Burgdörfer, L. Hagg, and C. O. Reinhold, Phys. Rev. Lett. **83**, 3948 (1999).
[22] R. T. Williams, Radiat. Eff. Defects Solids **109**, 175 (1989).
[23] S. Rix, U. Natura, M. Letz, C. Felser, and L. Parthier, Proc. SPIE Int. Soc. Opt. Eng. **7504**, 75040J (2009).
[24] S. Rix, Ph.D. thesis, Johannes Gutenberg-University Mainz, 2011 (unpublished).
[25] G. Hayderer, S. Cernusca, M. Schmid, P. Varga, H. P. Winter, F. Aumayr, D. Niemann, V. Hoffmann, N. Stolterfoht, C. Lemell, L. Wirtz, and J. Burgdörfer, Phys. Rev. Lett. **86**, 3530 (2001).
[26] S. Facsko, R. Heller, A. S. El-Said, W. Meissl, and F. Aumayr, J. Phys. Condens. Matter **21**, 224012 (2009).
[27] A. S. El-Said, R. Heller, and S. Facsko, Nucl. Instrum. Methods Phys. Res., Sect. B **269**, 901 (2011).
[28] J. Li, Model. Simulat. Mater. Sci. Eng. **11**, 173 (2003).

APPLIED PHYSICS LETTERS **101**, 053112 (2012)

Tilting of carbon encapsulated metallic nanocolumns in carbon-nickel nanocomposite films by ion beam assisted deposition

Matthias Krause,[1,2,a)] Arndt Mücklich,[1] Thomas W. H. Oates,[3] Matthias Zschornak,[1] Sebastian Wintz,[1] Jose Luis Endrino,[4] Carsten Baehtz,[1,5] Artem Shalimov,[1,5] Sibylle Gemming,[1] and Gintautas Abrasonis[1]

[1]*Helmholtz-Zentrum Dresden-Rossendorf, PF-510119, 01314 Dresden, Germany*
[2]*Technische Universität Dresden, D-01062 Dresden, Germany*
[3]*Leibniz-Institut für Analytische Wissenschaft, ISAS e.V., Albert-Einstein-Str. 9, 12489 Berlin, Germany*
[4]*Surfaces and Coatings Department, Instituto de Ciencia de Materiales de Madrid, c/Sor Juana Ines de la Cruz 3, Cantoblanco, 28049 Madrid, Spain*
[5]*Rossendorf Beamline, European Synchrotron Radiation Facility, F-38043 Grenoble, France*

(Received 25 May 2012; accepted 12 July 2012; published online 31 July 2012)

The influence of assisting low-energy (~50-100 eV) ion irradiation effects on the morphology of C:Ni (~15 at. %) nanocomposite films during ion beam assisted deposition (IBAD) is investigated. It is shown that IBAD promotes the columnar growth of carbon encapsulated metallic nanoparticles. The momentum transfer from assisting ions results in tilting of the columns in relation to the growing film surface. Complex secondary structures are obtained, in which a significant part of the columns grows under local epitaxy via the junction of sequentially deposited thin film fractions. The influence of such anisotropic film morphology on the optical properties is highlighted. © *2012 American Institute of Physics*. [http://dx.doi.org/10.1063/1.4739417]

Nanocomposites (NCs) are heterogeneous materials, wherein the lateral extension of at least one component is smaller than ~100 nm.[1] Interface, size and shape effects synergistically influence their properties on the macro-scale. For NC films, this leads to new properties and new functionalities which cannot be predicted from those of the constituting phases alone.[1] Therefore, the control over the NC film microstructure and morphology is of utmost importance.

Thin film growth includes many interacting kinetic processes (surface and bulk diffusion, repeated nucleation (RN), shadowing, surface reaction, etc.) which are influenced by external parameters such as temperature or growth rate.[2,3] Ion irradiation during growth is widely employed to influence the thin film microstructure.[4,5] On one hand, ions provide an amount of energy per incorporated material atom of the order of ~1-100 eV per atom.[6] This energy is much larger than that provided by any other process such as solidification, recrystallization, interface energy minimization, thermal activation, phase transformation, etc. which is around or below ~1 eV/atom.[6] This property of ion irradiation has been broadly explored to influence thin film characteristics by densification, interface mixing, enhanced phase separation, and/or enhancement of ad-atom mobility.[2] On the other hand, directionality due to momentum transfer is another specific property of ion beams. It allows a high level of biaxial crystallographic texturing on polycrystalline or even amorphous substrates as has been demonstrated for metallic or ceramic thin films.[7–10]

In contrast to single phase thin films, the microstructure of nanocomposites is not only determined by the interplay of nucleation, surface and bulk diffusion processes but also by phase segregation.[11–13] Recent studies have shown that under oblique incidence, ionized physical vapour deposition (iPVD) can simultaneously induce self-organization of the separating phases into multilayers with well defined periodicity and tilting of this layered phase structure in relation to the growing film surface.[14,15] However, the ion effect is entangled in the structure formation in a complex manner as the energetic species are also film forming species themselves. A systematic study of the effects of the assisting ion irradiation acting as a pure energy and momentum transfer agent on the phase morphology of NCs is lacking.

In this letter, we report another type of the ion energy and directionality effect which occurs during the growth of nanocomposite C:Ni films. We demonstrate that ion enhanced surface mobility due to energy transfer reduces RN of metal rich nanoparticles (NPs) thus enhancing the columnar growth. Moreover, the momentum transfer induces a surface atomic drift which results in tilting of metal rich nanocolumns in relation to the advancing film surface. The tilting effect does not depend on the metal phase (nickel carbide or fcc nickel). The possibility of sculpting by changing the ion beam direction with respect to the film surface is demonstrated and the influence of such anisotropic structures on the optical properties is highlighted. The technique holds great potential for large-area fabrication of metamaterials.

The C:Ni (~15 at. %) NC films were grown by IBAD. A 6 in. graphite target covered by a 1.5 mm wide Ni stripe was sputtered at an off normal angle of ~22° by an Ar^+ beam of 1 keV ion energy and 40 mA beam current produced with a 3 cm Kaufmann type ion source (IonTech, Inc.). The sputtered atoms were deposited on a 2×2 cm^2 Si (100) or SiO_2 (~0.5 μm)/Si substrate positioned on a heatable sample holder (for more details see Refs. 16 and 17). The growing film was irradiated at an oblique incidence of ~58° relative to the surface normal by an assisting Ar^+ ion beam (energy 50-100 eV, total beam current of 9 mA) produced by a 4 cm 3-grid Kaufmann type ion source ISQ40K-F (Ion-Tech GmbH, Germany). The focusing grid optics results in an irradiated area with a lateral dimension of ~20 mm. The

[a)]Electronic mail: matthias.krause@hzdr.de. Tel.: +49-351-260-3578.

estimated Ar^+ ion to atom ratio is ~50. The base pressure in the deposition chamber was $(1.3 \pm 0.3) \times 10^{-5}$ Pa. The substrate temperatures were ~60 °C, ~300 °C and 500 °C, and the deposition time was 1 h if not differently specified. The film composition and areal density were determined by Rutherford back scattering (RBS). The phase structure was analyzed by x-ray diffraction (XRD) measured using a D-5000 (Bruker-AXS) diffractometer with Cu K_α (1.5406 Å) radiation in a θ-2θ configuration. The film microstructure was analysed by cross-sectional transmission electron microscopy (XTEM, microscope Titan 80-300 (FEI)). Two different cross sections were prepared for each sample: one was oriented perpendicular to the plane of ion incidence, the other one parallel to it, thus including the ion direction. The film morphology was determined by grazing incidence small angle x-ray scattering (GISAXS). Two-dimensional (2D) GISAXS measurements were recorded by a 2D position sensitive detector (Pilatus 100 k from Dectris, Ltd.) at the Rossendorf Beamline ROBL BM 20, ESRF, Grenoble, France. The x-ray beam with a wavelength of 0.689 Å at the incidence angle of $\alpha_i = 0.125°$ (larger than the critical angle of total external reflection) was used. The optical response of a number of characteristic samples was measured using visible and mid-infrared (MIR) ellipsometry. Measurements were taken at orthogonal planes of incidence, either perpendicular or parallel to the direction of ion irradiation. Variable-angle of incidence (55°, 65° and 75° from the normal) MIR measurements were performed using a custom-built Fourier-transform infrared (FTIR) spectroscopic ellipsometer, in the spectral range from 1500 to 7000 cm^{-1}.

The C:Ni NC thin films contain 83 ± 2 at. % C, 15 ± 1 at. % Ni, 2 ± 1 at. % Ar independently on the ion energy and the growth temperature. Traces (~0.15 at. %) of a heavy element with a mass close to that of W are found in all the samples, most probably originating from the tungsten filaments of the ion sources. The thickness and the areal density of the films grown without ion assistance at 60 °C and 300 °C are 61 nm (Fig. 1(a)) and 6.4×10^{17} cm^{-2} and 6.0×10^{17} cm^{-2}, respectively. With ion irradiation, the thickness and the areal densities of the C:Ni films grown at 60 °C are (48 ± 3) nm and $(5.7 \pm 0.6) \times 10^{17}$ cm^{-2}, independently on the specific ion energy. The lack of preferential material loss effects hints towards ion induced/enhanced desorption instead of sputtering. The combined effect of thickness (−20%) and areal density (−12%) reduction at constant atomic composition can be attributed to ion induced densification. The C:Ni IBAD films deposited at 50 V ion energy at 300 °C and 500 °C have a thickness of 52 nm and 55 nm as well as areal densities of 3.9×10^{17} cm^{-2} and 4.3×10^{17} cm^{-2}. This indicates a higher loss rate and a less dense film structure than for deposition at 60 °C.

Without ion assistance, the microstructure of C:Ni NC thin films grown at ~60 °C consists of homogenously distributed spherical Ni_3C particles in an amorphous carbon matrix (Fig. 1(a)). This is similar to the observations in the literature[13,16,18] and is consistent with a RN dominated growth regime.[2,16] IBAD promotes the columnar growth (Fig. 1(b)). The TEM cross section parallel to the ion plane of incidence reveals that columns are formed throughout the entire thin film. These are not oriented perpendicular to the film surface

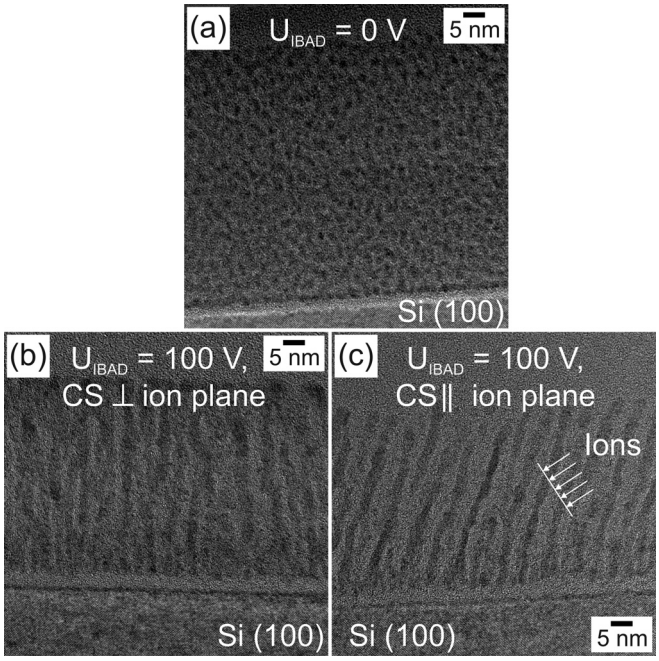

FIG. 1. XTEM images of C:Ni NC thin films deposited at ~60 °C without (a) and with (b) and (c) an assisting Ar^+ beam of 100 eV ion energy. Panel (b) (panel (c)) shows the film cross section oriented perpendicular (parallel) to the plane of ion incidence.

but tilted (Fig. 1(c)). The nanocolumn diameter of (1.8 ± 0.2) nm is the same as that of the particles in C:Ni NCs grown without ion irradiation. The tilt angle of the nanocolumns at a constant deposition temperature of 60 °C is $(13 \pm 5)°$ for ion energies of 50−100 eV. The nanocolumns grown at ~100 eV ion energy exhibit the largest aspect ratio and the highest degree of parallel orientation of all tilted nanocolumns prepared in the parameter field of this study. The spherical-columnar transition can be attributed to the enhanced surface mobility due to the energy transfer from the assisting ion beam equivalent to the temperature increase.[2,16,19] The observed tilt hints towards an ion-induced atomic drift along the growing film surface.

At constant ion energy of 50 eV, the increase of the deposition temperature from 60 °C via 300 °C to 500 °C has significant effects on the film morphology (Figs. 2(a)–2(c)): (i) the diameter of the nanocolumns increases with temperature from 1.8 nm via 3.8 nm to 17 nm, (ii) the inter-particle distance increases from ~4 nm at 60 °C, via ~7 nm at 300 °C to ~25 nm at 500 °C; and (iii) the tilt angle relative to the surface normal of the film increases concomitantly with the growth temperature from 16° via 25° to 38°. These changes are highlighted by fast Fourier transforms (FFTs) of the corresponding TEM images which show two asymmetric intensity lobes due to column tilting (see insets of Figs. 2(a)–2(c)). The decreasing reciprocal lattice vector represents the increase in the inter-particle distance.

All C:Ni NC films deposited at 60 °C are x-ray amorphous. According to the HTEM analysis, they consist mainly of amorphous and to a minor extend of crystalline Ni_3C nano-particles and -columns embedded in amorphous carbon. In the series deposited at the ion energy of 50 V, the C:Ni NC film grown at 300 °C shows the XRD pattern of

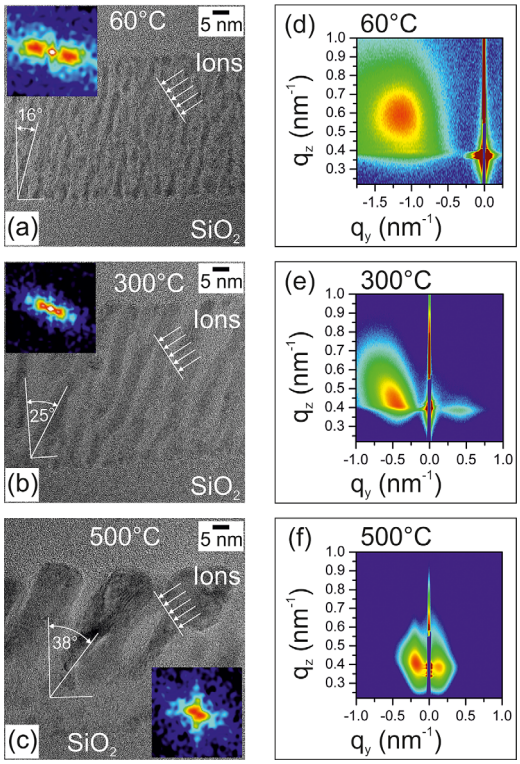

FIG. 2. Film morphology measured by XTEM ((a)-(c)) and GISAXS ((d)-(f)) of C:Ni films grown with an assisting Ar^+ beam of 50 eV ion energy at ~60 °C (a) and (d), at 300 °C (b) and (e), and at 500 °C (c) and (f). The insets in ((a)-(c)) show the FT's of the XTEM images. A logarithmic colour scale was used in ((d)-(f)).

Ni_3C, while the diffraction pattern of fcc-Ni is found for the film grown at 500 °C. Neither the x-ray diffraction patterns nor the HTEM images show any ion induced texture. Note the nickel surface enrichment and the partial graphitic ordering parallel to the nickel nanocolumns at 500 °C (Fig. 2(c)). This effect is attributed to the phenomenon of metal induced crystallization of carbon which is caused by activated bulk diffusion at this high temperature.[13,20] The partial graphitisation might account for the less dense film structure indicated by the ratio of thickness and the areal density discussed earlier.

2D GISAXS images represent essentially the Fourier transformation (FT) of the density contrast autocorrelation function. Taking into account that the incidence and scattering angles are small, the horizontal and vertical components of the scattering vector $\mathbf{q}(q_y,q_z)$ are expressed as

$$\mathbf{q} = \frac{2\pi}{\lambda}[\sin 2\theta_{sc}\cos\alpha_{sc}, \sin\alpha_i + \sin\alpha_{sc}]. \quad (1)$$

α_i is the x-ray angle of incidence, α_{sc} and θ_{sc} are out-of-plane and in-plane scattering angles, respectively (for more details, see Ref. 14). The 2D GISAXS images from a macroscopic sample region (~mm^2) closely resemble the upper part of the FFT patterns of the local area probed by TEM (Figs. 2(d) and 2(e)), confirming that the observed asymmetries are a global property of the material. Within the incidence plane, the scattering lobe at $q_y < 0$ corresponds to columns tilted in the opposite real space direction, i.e. $y > 0$.[21] For the given IBAD conditions, GISAXS patterns allowed us to determine the column tilting direction, which is *towards* the incoming ions. Similar GISAXS patterns have been reported for tilted TiO_2 columns grown by glancing angle deposition (GLAD).[21]

In analogy to the sculpted films produced by GLAD,[22] more complex nanostructures have been produced. As an example, a sequential deposition was carried out at 300 °C with the Ar^+ energy of 50 eV. The sample was rotated by 180° after the first half. The resulting structure is characterized by an almost complete match of Ni_3C nanocolumns and carbon rich regions at the junction between both parts of the NC thin film (Fig. 3). It resembles a timber frame structure on a nanometre scale. The nanocolumns keep their tilt angle with an accuracy of ±1°. Despite the fact that the vacuum chamber was vented to rotate the sample around its normal in between the sequential depositions, about 30% of the tilted nanocolumns grow under local atomic epitaxy across the junction. This is illustrated in detail for the (113) crystal planes of one Ni_3C column (Fig. 3(b)). Another epitaxial nanocolumn junction is shown at the very right edge of the same figure.

In order to discuss the growth mechanisms which are responsible for the observed microstructure, it has to be distinguished between the effect of the energy transfer that is responsible for the enhanced columnar growth at

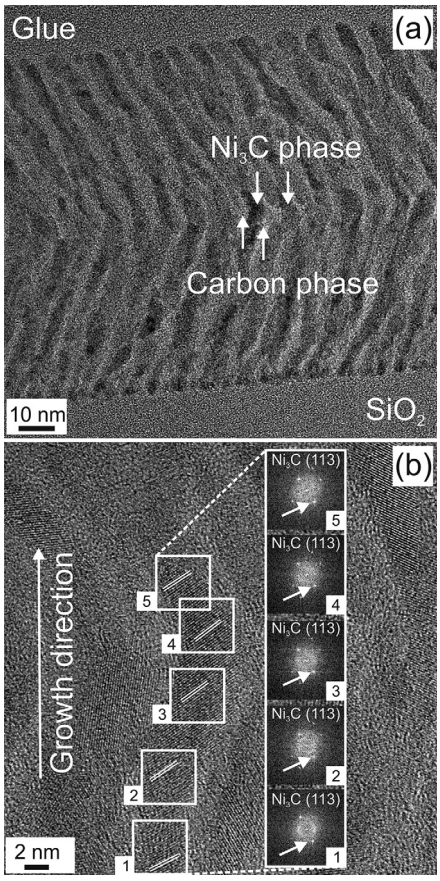

FIG. 3. XTEM analysis of a C:Ni NC timber frame. The sample was rotated by ~180° around its surface normal after the first half of the deposition, giving a total deposition time of 2 h. (a) Overview XTEM image (185 k magnification). The arrows indicate exemplarily the areas of the Ni_3C and the a-C phase. (b) HTEM image (620 k magnification) highlighting the local epitaxial growth of Ni_3C (113) crystal planes across the junction of sequentially deposited film fractions. The insets show the FFTs of the corresponding white squared areas.

temperatures, where bulk diffusion is negligible, i.e., $\leq$300 °C, and that of the momentum transfer that results in nanocolumn tilting at all deposition temperatures. The growth of the NC films is essentially a phase separation assisted by thin film growth processes, such as deposition, nucleation, surface and bulk diffusion, epitaxy, etc.[2,11,23] The observed NP coarsening with the growth temperature is consistent with temperature enhanced diffusion.[23,24] Higher diffusivity allows longer average diffusion paths before the atoms are covered by depositing species.[23]

RN is due to the formation of a covering layer, blocking further growth. This can be due to segregation of one of the components, changes in composition or phase during growth, chemical reaction etc. A high RN rate results in the spherical or elongated spherical NP shape in C:Ni NC grown without ion irradiation at temperatures $\leq$300 °C.[16] In general, the following surface diffusion processes are of high relevance for controlling the morphology of metal-rich (metal or metal-carbide) NPs: (i) matrix atom diffusion on the metal-rich NPs, (ii) metal diffusion on the carbon matrix, and (iii) metal and matrix atoms approaching and crossing the NP/carbon interface. A recent study on the substrate influence on the Ni nanocolumn morphology in C:Ni films has shown that the process (i) is not the limiting factor.[25] A comparison of morphologies of carbon based nanocomposites grown at similar conditions but employing different metals (V, Co, Cu) shows that all the metals exhibit spherical NPs (RN regime) at RT, copper showing the largest diameter.[17] The diameter of Cu at RT is similar to that of Co at a significantly higher temperature of ~300 °C.[17] At this temperature, however, the columnar growth takes place for both Cu and Co. In the former case, NPs are spherical while in the latter NPs are columnar, indicating different growth regimes at similar metal diffusivities. This implies that the process (ii) as well is not the driving one for RN. This discussion strongly suggests the crossing of the Me/C interface as the limiting factor. This is not surprising as carbon adatoms can start to form strong covalent bonds with the adjacent C matrix atoms upon approaching the phase boundaries. This significantly increases the activation energy to jump across the boundary. The growth of the carbon phase from the boundaries inwards over the metal-rich NPs takes place. As a result, curved graphenic sheets encapsulating metal-rich NPs are observed.[26] Such overgrowth provokes RN of metal-rich NPs. On the other hand, ion irradiation can easily break the covalent C-C bonds thus facilitating the NP/C interface crossing probability and enhancing the columnar growth even at low temperatures. Such a scenario is consistent with the observations of the current study (see Fig. 1).

The phenomenological tangent rule relating the column tilting angle to the deposition angle due to shadowing for GLAD (Ref. 22) is not relevant for the current process. This is due to the fact that the no tilting is observed without ion irradiation as the film forming species arrive almost perpendicularly to the surface. Therefore, the effect is related to the assisting ion irradiation. Also note, that the tilting direction is opposite to that reported for self-organized multilayers grown with iPVD conditions.[14] For iPVD, the sub-plantation of energetic depositing film forming species play a key role resulting in the self-organized phase layering and tilting of this layered structure.[15] In the present case, the low energy of Ar ions (~50 eV) implies even lower energy of Ni and C recoils. Therefore, the recoil sub-plantation effects can be neglected and the ion effects can be confined to the growing surface with high level of confidence. We propose the following mechanism. Incident ions generate atomic recoils with favored motion along the initial ion direction.[27] For the oblique incidence conditions, as in this work, there is a component of this motion along the surface. This results in a ballistic drift of carbon and Ni ad-atoms. Let us consider the surface of a metal-rich NP. Such a drift results in a flux of C ad-atoms with an effective flux component along the ion beam direction towards the NP edge. An accumulation of carbon on the ion beam averted side of the NP occurs. Similar arguments are valid for Ni ad-atoms arriving from the carbon matrix from the other side of the metal-rich NP, resulting in metal accumulation on the opposite side of the NP. This results in an asymmetric NP growth, which leads to a tilt towards the ion beam. The number of drifting atoms is proportional to the NP area, i.e., $\sim r^2$, where r is the NP diameter. The part of the NP circumference where the flux of ad-atoms arrives is $\sim r$. The drift flux arriving at the Me/C interface is proportional to the ratio of drifting atoms per unit of the circumference and thus is proportional to $\sim r$. Therefore, the drift effects are expected to be more pronounced for larger NPs. This is consistent with the observed temperature dependence of this study (Fig. 2).

The results of the ellipsometry measurements of two samples deposited at 300 °C, with and without IBAD, are shown in Fig. 4. The ellipsometric parameter tan Ψ displayed in this work is defined as the real part of the ratio of the

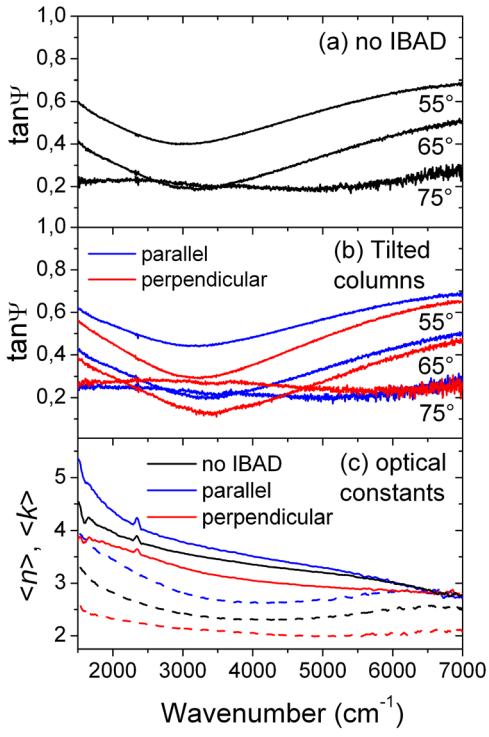

FIG. 4. Variable angle FTIR spectroscopic ellipsometry of two selected C:Ni films grown at 300 °C: (a) grown without assisting ions, (b) grown using assisting Ar^+ ions of 50 eV, for two orthogonal measurement planes, and (c) the effective pseudo-refractive indices ($\langle n \rangle$ solid lines, $\langle k \rangle$ dashed lines) extracted from the applied model.

complex p- and s-polarized reflection coefficients.[28] The sample without IBAD showed no dependence on the measurement plane of incidence. In contrast, the tanΨ values for the IBAD sample in the MIR differed greatly depending on whether the measurement plane was parallel or perpendicular to the ion incidence direction. This indicates anisotropy in the in-plane optical properties. By modelling the data using a three-layer slab model (substrate, film, ambient), we extracted the optical properties of the film. Since the dimensions of the metal-rich structures are much smaller than the light wavelength in the MIR (ca. 10 μm), we assume that the optical properties are homogenous and assign an effective complex refractive index, $n + ik$. By fixing the film thickness to that measured by XTEM, the ellipsometric data may be inverted to provide an unique effective refractive index. Although we have assumed an isotropic optical tensor, the IBAD film should in fact be modelled with an anisotropic tensor and fit to generalized (i.e., cross-polarization sensitive) ellipsometric data. Thus, the refractive indices shown are termed pseudo-indices (denoted $\langle n \rangle$ and $\langle k \rangle$), as is commonly done in ellipsometric analysis.[29] The pseudo-refractive indices show that the film without IBAD has an optical density approximately midway between the two unequal orthogonal curves for the IBAD film (Fig. 4(c), from the 55° data). An optically denser material is observed in the measurement plane parallel to the ion incidence.

In summary, we have demonstrated that assisting low energy ion irradiation has a dramatic effect on the phase morphology of C:Ni films. On the one side, the energy transfer from the Ar^+ ions promotes the columnar growth of carbon encapsulated Ni_3C NPs. On the other side, the momentum transfer induces the tilting of the metal-rich (Ni_3C and Ni) nanocolumns. The sculpting possibility using this approach has been demonstrated. The influence of the morphological anisotropy on the optical response has been shown. In contrast to GLAD, which is based on shadowing effects of the low energy atom beam on the free standing structures,[22] the formation of the tilted nanostructures here is due to ion guided surface phase separation. The energetic ion irradiation is a compulsory component. Moreover, the sculpted metallic structures are automatically encapsulated in the protecting carbon matrix. In addition, the ion irradiation results in the formation of dense structures. As the underlying driving force is based on physical effects, we believe that the effects observed in this study will also operate for other nanocomposite systems. Encapsulation and densification means that an appropriate choice of the matrix material is expected to have a protective effect against the environmental degradation of the functional metallic nanostructures. We predict that the use of plasmonic materials such as gold and silver, instead of nickel, would significantly enhance the anisotropy, particularly in the visible and near-IR spectral range. Additionally, the use of a transparent dielectric embedding medium, such as SiO_2 should open the way to the large-area bottom-up production of tailored metamaterials with hyperbolic dispersion[30] and chirality.[31]

This work was funded by the EU, "European regional development fund," Project ECEMP-D1 (13857/2379), "Nanoskalige Funktionsschichten auf Kohlenstoffbasis." We thank the ESRF, Grenoble, France, for providing synchrotron radiation facilities. T.O. acknowledges funding by the European Community's 7th Framework Programme under grant agreement no. 228637 NIM NIL (www.nimnil.org). Technical assistence of R. Heller, A. Kolitsch, J. Wagner, A. Kunz, M. Missbach, A. Scholz (all HZDR), and B. Dastmalchi (Kepler University, Linz, Austria) is acknowledged.

[1]P. M. Ajayan, L. S. Schadler, and P. V. Braun, *Nanocomposite Science and Technology* (Wiley-VCH, Weinheim, 2003).
[2]I. Petrov, P. B. Barna, L. Hultman, and J. E. Greene, J. Vac. Sci. Technol. A **21**, S117 (2003).
[3]Z. Y. Zhang and M. G. Lagally, Science **276**, 377 (1997).
[4]F. A. Smidt, Int. Mater. Rev. **35**, 61 (1990).
[5]J. M. E. Harper, J. J. Cuomo, R. J. Gambino, and H. R. Kaufman, Nucl. Instrum. Methods Phys. Res. B **7–8**, 886 (1985).
[6]J. M. E. Harper and K. P. Rodbell, J. Vac. Sci. Technol. B **15**, 763 (1997).
[7]L. S. Yu, J. M. E. Harper, J. J. Cuomo, and D. A. Smith, Appl. Phys. Lett. **47**, 932 (1985).
[8]C. P. Wang, K. B. Do, M. R. Beasley, T. H. Geballe, and R. H. Hammond, Appl. Phys. Lett. **71**, 2955 (1997).
[9]J. Xiong, V. Matias, H. Wang, J. Y. Zhai, B. Maiorov, D. Trugman, B. W. Tao, Y. R. Li, and Q. X. Jia, J. Appl. Phys. **108**, 083903 (2010).
[10]J. M. E. Harper, Mater. Res. Soc. Symp. Proc. **1150**, 3 (2009).
[11]M. Atzmon, D. A. Kessler, and D. J. Srolovitz, J. Appl. Phys. **72**, 442 (1992).
[12]N. Yasui, R. Horie, Y. Ohashi, K. Tanji, and T. Den, Adv. Mater. **19**, 2797 (2007).
[13]G. Abrasonis, G. J. Kovacs, L. Ryves, M. Krause, A. Mucklich, F. Munnik, T. W. H. Oates, M. M. M. Bilek, and W. Moller, J. Appl. Phys. **105**, 083518 (2009).
[14]G. Abrasonis, T. W. H. Oates, G. J. Kovacs, J. Grenzer, P. O. A. Persson, K. H. H. Heinig, A. Martinavicius, N. Jeutter, C. Baehtz, M. Tucker, M. M. M. Bilek, and W. Muller, J. Appl. Phys. **108**, 043503 (2010).
[15]G. Abrasonis, G. J. Kovacs, M. D. Tucker, R. Heller, M. Krause, M. C. Guenette, F. Munnik, J. Lehmann, A. Tadich, B. C. C. Cowie, L. Thomsen, M. M. M. Bilek, and W. Moller, Appl. Phys. Lett. **97**, 163108 (2010).
[16]G. Abrasonis, M. Krause, A. Mucklich, K. Sedlackova, G. Radnozi, U. Kreissig, A. Kolitsch, and W. Moller, Carbon **45**, 2995 (2007).
[17]M. Berndt, M. Krause, G. Abrasonis, A. Mucklich, F. Munnik, A. Kolitsch, and W. Moller, Plasma Process. Polym. **6**, S902 (2009).
[18]K. Sedlackova, P. Lobotka, I. Vavra, and G. Radnoczi, Carbon **43**, 2192 (2005).
[19]A. Anders, Thin Solid Films **518**, 4087 (2010).
[20]M. Berndt, G. Abrasonis, G. J. Kovacs, M. Krause, F. Munnik, R. Heller, A. Kolitsch, and W. Moller, J. Appl. Phys. **109**, 063503 (2011).
[21]L. Gonzalez-Garcia, A. Barranco, A. M. Paez, A. R. Gonzalez-Elipe, M. C. Garcia-Gutierrez, J. J. Hernandez, D. R. Rueda, T. A. Ezquerra, and D. Babonneau, Chemphyschem **11**, 2205 (2010).
[22]M. M. Hawkeye and M. J. Brett, J. Vac. Sci. Technol. A **25**, 1317 (2007).
[23]K. Fukutani, K. Tanji, T. Saito, and T. Den, J. Appl. Phys. **98**, 033507 (2005).
[24]K. Fukutani, K. Tanji, T. Motoi, and T. Den, Adv. Mater. **16**, 1456 (2004).
[25]G. Abrasonis, G. J. Kovacs, A. Mucklich, S. Q. Zhou, D. Babonneau, A. Martinavicius, M. Berndt, F. Munnik, M. Vinnichenko, K. H. Heinig, J. Grenzer, A. Kolitsch, H. Schmidt, and W. Moller, J. Phys. Chem. C **113**, 8645 (2009).
[26]S. Q. Zhou, M. Berndt, D. Burger, V. Heera, K. Potzger, G. Abrasonis, G. Radnoczi, G. J. Kovacs, A. Kolitsch, M. Helm, J. Fassbender, W. Moller, and H. Schmidt, Acta Mater. **57**, 4758 (2009).
[27]G. Carter and V. Vishnyakov, Phys. Rev. B **54**, 17647 (1996).
[28]T. W. H. Oates, H. Wormeester, and H. Arwin, Prog. Surf. Sci. **86**, 328 (2011).
[29]T. W. H. Oates, M. Ranjan, S. Facsko, and H. Arwin, Opt. Express **19**, 2014 (2011).
[30]J. Yao, Z. Liu, Y. Liu, Y. Wang, C. Sun, G. Bartal, A. M. Stacy, and X. Zhang, Science **321**, 930 (2008).
[31]J. K. Gansel, M. Thiel, M. S. Rill, M. Decker, K. Bade, V. Saile, G. von Freymann, S. Linden, and M. Wegener, Science **325**, 1513 (2009).

APPLIED PHYSICS LETTERS **100**, 262602 (2012)

Superconductor-insulator transition controlled by annealing in Ga implanted Si

V. Heera,[1,a)] J. Fiedler,[1,2] M. Voelskow,[1] A. Mücklich,[1] R. Skrotzki,[3,4] T. Herrmannsdörfer,[3] and W. Skorupa[1]

[1]*Institute of Ion Beam Physics and Materials Research, Helmholtz-Zentrum Dresden-Rossendorf (HZDR), P.O. Box 51 01 19, D-01314 Dresden, Germany*

[2]*Experimental Physics, Institute of Physics, Ilmenau University of Technology, Weimarer Str. 32, 98693 Ilmenau, Germany*

[3]*Dresden High Magnetic Field Laboratory (HLD), Helmholtz-Zentrum Dresden-Rossendorf (HZDR), P.O. Box 51 01 19, D-01314 Dresden, Germany*

[4]*Department of Chemistry and Food Chemistry, TU Dresden, D-01062 Dresden, Germany*

(Received 17 April 2012; accepted 14 June 2012; published online 27 June 2012)

Heavily Ga implanted Si nanolayers covered with a thin SiO_2 layer exhibit a superconductor-insulator transition in dependence on annealing conditions. The transition characteristics resemble those of ultrathin quench-condensed metal films although the implanted layer differs clearly in composition, width, and nanostructure. This implies a general physical mechanism for the superconductor-insulator transition in thin, disordered layers which is supposed to be a quantum phase transition between dual states—the superconducting and the superinsulating one. There is a resistance criterion for the phase transition closely associated with a critical hole concentration. [http://dx.doi.org/10.1063/1.4732081]

Recently, it has been shown that Ga rich Si nanolayers with robust superconducting properties can be fabricated on Si chips below a SiO_2 capping layer by ion implantation and rapid thermal annealing (RTA).[1,2] These nanolayers have a width of about 10 nm and critical parameters (temperature $T_C \sim$ 6-7 K, magnetic field $B_C \sim 9$ T, current density $j_C \sim 1$ kA/cm^2) that are competitive with those of Nb or Al films commonly used in superconducting quantum interference devices.[3] Previous investigations[2] revealed that the nanolayer consists of amorphous precipitates containing Ga, Si, and O which are embedded in a nanocrystalline Si matrix.

It is known that the electrical transport in thin and, in particular, disordered or granular films substantially deviates from that of homogeneous bulk materials because of dimensional and blocking effects (e.g., classical and quantum percolation, Coulomb blockade). Metal-insulator and even superconductor-(super)insulator transitions controlled by structure (film thickness, grain size), composition, or magnetic field were observed in films of quench-condensed metals,[4–9] metal-insulator mixtures,[10–12] and high temperature superconductors.[13,14] In addition, the critical parameters of superconductivity in these films can exceed those of homogeneous bulk materials.[10,13] Therefore, such layers are interesting for both fundamental and applied research.

The superconductor-superinsulator transition is supposed to be a continuous quantum phase transition[15,16] between electron and vortex pairing occurring in disordered, two-dimensional Fermi systems. The insulating quantum state is superinsulating in the sense that the resistance grows with decreasing temperature in a double-exponential manner and becomes practically infinite immediately below the transition temperature.[17] Some experimental results and theoretical models indicate that there is a universal critical resistance close to the pair quantum value $R_Q = h/(4e^2) = 6.45$ kΩ separating the superconducting from the superinsulating state.[12,14,16] However, this universality hypothesis is still under discussion and critical resistances between 6 and 25 kΩ have been reported.[18–20] It is an open question whether the Ga rich nanolayers at the Si/SiO_2 interface exhibit a similar superconductor-insulator transition controlled by a critical resistance.

In recent studies, it was demonstrated that the formation and transport properties of the Ga rich nanolayer on Si depend sensitively on the annealing conditions.[1,2] For a 60 s annealing, a narrow temperature window between 600 °C and 700 °C was found to produce nanolayers with superconducting properties. At temperatures of 800 °C and above, Ga outdiffusion prevents the nanolayer synthesis. Ga accumulation at the SiO_2/Si interface is a necessary but not sufficient condition for superconductivity as demonstrated in Refs. 1 and 2. Already after annealing at 500 °C, the Ga concentration at the interface is comparable to those observed in the superconducting layers but no superconducting state was observed.

Because the annealing temperature commonly effects crystal growth, impurity diffusion, and chemical reactions in an exponential manner (Arrhenius-type law), the variation of annealing time is better suited to study the gradual evolution of the Ga rich layers. Therefore, we conducted a systematic study on the annealing time dependence of the electrical transport in heavily Ga implanted Si. As in the previous studies,[1,2] we used Czochralski-grown, n-tpye Si wafers with (100) orientation and resistivity of about 1 kΩcm which was covered with 30 nm SiO_2 by sputtering. A heavily p-type doped, amorphous layer of about 90 nm width was fabricated by 80 keV, 4×10^{16} cm^{-2} Ga^+ ion implantation at room temperature. The as-implanted Ga profile has a full width at half maximum of about 40 nm and a Ga peak concentration of 11

a)Electronic mail: heera@hzdr.de.

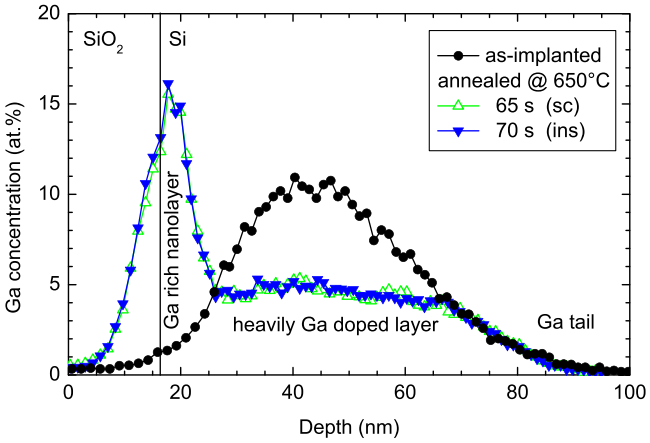

FIG. 1. Ga depth distribution calculated from the results of RBS measurements for selected samples. There are no differences between the Ga profiles of the superconducting (sc) and the insulating (ins) sample. The notion for different depth regions used in the text is indicated.

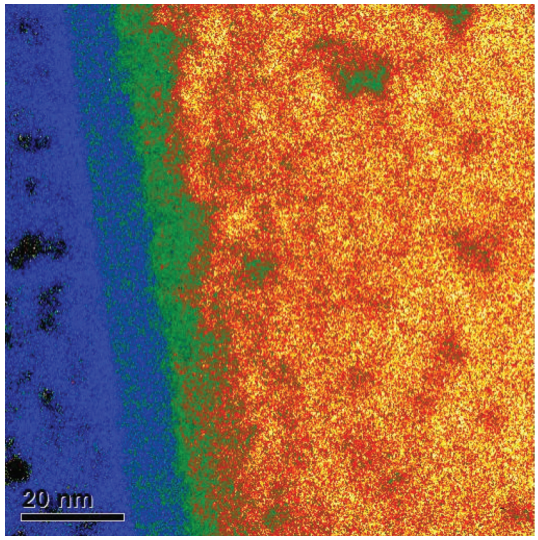

FIG. 2. Pseudocolor image of the silicon distribution in the cross section of the sample annealed at 600 °C for 60 s obtained from EFTEM. Ga accumulation and oxygen intermixing close to the interface lead to local Si depletion. The silicon concentration decreases from orange to blue. The multilayer structure is clearly mapped: glue, SiO_2 layer, Ga rich nanolayer, and heavily doped Si with few impurity rich precipitates (from left to right).

at. % 30 nm beneath the SiO_2/Si interface as measured by Rutherford backscattering spectrometry (RBS) (Fig. 1). Sample pieces of 1 cm^2 were subjected to RTA at temperatures of 600 °C, 650 °C, and 700 °C under flowing Ar atmosphere. The annealing time was varied from 1 s to 90 s. This processing leads to Ga redistribution and the formation of a Ga rich nanolayer at the SiO_2/Si interface (Fig. 1). Already after RTA at lowest temperature and duration, the nanolayer has formed and does not change substantially with increasing thermal load. Its typical width and peak concentration are 10 nm and 16 at. %, respectively. Underneath this Ga rich nanolayer, a heavily Ga doped, about 40 nm deep Si zone with an almost plateau-like Ga concentration of about 5 at. % is observed. Energy filtered transmission electron microscopy (EFTEM) in the range of the Si $L_{2,3}$ absorption edge (99 eV) confirms strong Si depletion as consequence of Ga accumulation and oxygen intermixing close to the interface. As an example, a pseudocolor image of the silicon distribution in the cross section of a sample annealed at 600 °C for 60 s is shown in Fig. 2. Due to sputtering during the high fluence Ga implantation, the SiO_2 layer is thinned from 30 nm to about 15 nm.

The temperature dependence of the electrical transport in the Ga implanted Si samples was investigated by resistance and Hall effect measurements in van der Pauw geometry.[21] Some sheet resistance curves of samples annealed at 650 °C and different annealing times are shown in Fig. 3 as function of temperature. For interpreting these results, one has to consider the multilayer structure of the samples: n-type substrate, p-type Ga tail region, heavily Ga doped plateau region, and Ga rich nanolayer (Fig. 1). The high temperature behaviour is influenced by leakage currents through the weakly n-doped Si substrate. However, in the temperature range below 20 K, the current path is constricted to the Ga containing layers because the substrate electrons are frozen out. The low temperature part ($T < 10$ K) of the curves shown in Fig. 3 clearly illustrates the drastic effect of the annealing conditions on the electrical transport properties. Whereas annealing times below 70 s result in layers with a superconducting state, longer annealing leads to layers with insulating properties. There is a general trend in the evolution of the normal-state sheet resistance. The sheet resistance and its negative temperature gradient increase with increasing annealing time. Additionally, the width of the superconducting transition and the residual resistance increase whereas the critical temperature decreases with annealing time. Quite similar observations were made for the resistance evolution of ultrathin quench-condensed Ga films with increasing thickness (1.2–1.5 nm).[4] In our case, this trend is partially broken in the critical time window (60 s-70 s) for the superconductor-insulator transition. It can be assumed that in the critical range already little differences in the as-implanted state of the sample and/or the annealing cycle cause pronounced changes of the transport behaviour.

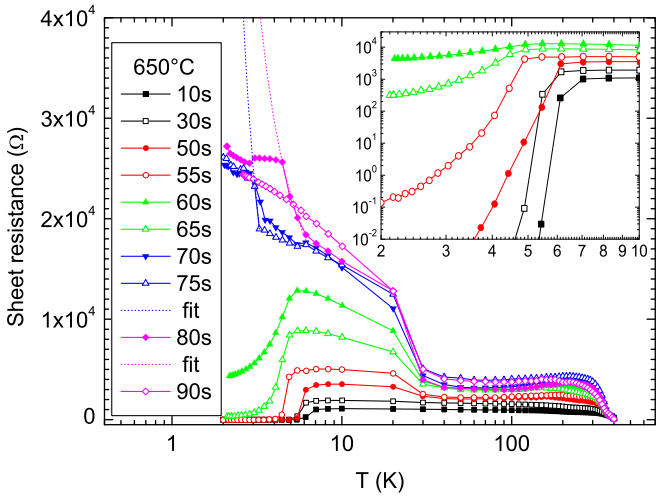

FIG. 3. Sheet resistance $R_\square$ as function of temperature for samples annealed at 650 °C at various annealing times. The inset shows the transition to the superconducting state in more detail. Zero residual resistance is observed for normal state resistances below 6 kΩ. The dashed lines are Arrhenius fits $R = R_0 \exp(T_0/T)$ with $R_0 = 865$ Ω, 6944 Ω and $T_0 = 10.1$ K, 5.8 K for the samples annealed at 75 s and 80 s, respectively.

Interestingly, in insulating samples with annealing times below 90 s, a steep increase of the resistance is observed in the same temperature region as for the superconducting transition. This finding and even details in the temperature-resistance curve such as a weak minimum appearing at 5.5 K are in accordance to the results of Jaeger *et al.*[4] However, they found that the resistance in the insulating state continuously grows over orders of magnitude with decreasing temperature whereas we observe a finite jump of about 7 kΩ. This behaviour may be explained by the multilayer structure of our samples. In addition to the Ga-rich nanolayer at the interface, a parallel normal-state conduction channel is present in the heavily Ga doped layer underneath as proven in previous experiments where the nanolayer was etched away.[1,2] Therefore, the sheet resistance leaps to and, then, follows the resistance of this layer when the Ga-rich nanolayer becomes insulating below the critical temperature. The resistance curve can be fitted in the transition region by an Arrhenius law, indicating that the nanolayer is indeed insulating.[20] The dashed lines shown in Fig. 3 are fits according to $R = R_0 \exp(T_0/T)$ with $R_0 = 865$ Ω, 6944 Ω and $T_0 = 10.1$ K, 5.8 K for the samples annealed at 75 s and 80 s, respectively. The extrapolated part of the curves demonstrates approximately the temperature dependence of the sheet resistance without the shunting layer beneath. In analogy to the resistance drop in the superconducting case, one can speculate that the resistance leap is caused by the transition into the superinsulating state.

It should be noted that in both states, the superconducting and the insulating one, the global Ga depth distribution as determined by RBS measurements (see Fig. 1) is the same. Even by XTEM analysis, distinct structural or compositional changes could not be detected. However, subtle modifications of grain size, distribution, or composition are difficult to resolve by this analysis. In this context, one should remember that in quench-condensed metal films a thickness variation in the range of 0.1 nm is sufficient for the phase transition.[4] In Al granular materials, the metal-insulator transition occurs when the thickness of the insulating coating (Ge or Al_2O_3) increases by less than 0.5 nm.[22] However, if the sheet resistance is the key parameter for the phase transition, not the kind of structural changes but only their impact on the global resistance is of importance.

In order to address the question whether a resistance criterion holds for the superconductor-insulator transition in the Ga rich nanolayers, the sheet resistances at 10 K as function of the annealing time obtained for three annealing temperatures are compiled in Fig. 4. In fact, there is a resistance gap (11.5 kΩ–15.2 kΩ) separating the superconducting samples from the insulating ones which is in good agreement with the results of Jaeger *et al.*,[4] although our Ga rich nanolayers are rather different in structure and composition. Parshin *et al.*[23] found that the critical thickness of quench-deposited Ga films substantially changes when using different substrates, but the critical temperature scales with the sheet resistance. These results corroborate the idea of a resistance criterion for the superconductor-insulator transition. For an appropriate characterization of a quantum-phase transition, the critical resistance at zero temperature extrapolated from finite-temperature results or extracted from scaling laws

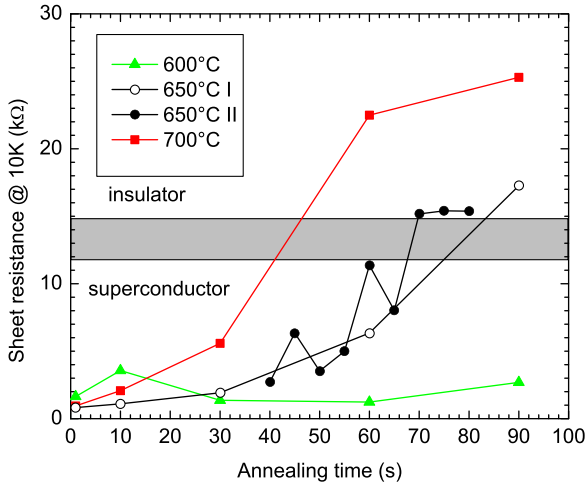

FIG. 4. The sheet resistance $R_\square$ measured at 10 K as function of annealing time for different annealing temperatures. The resistance gap between superconducting and insulating samples is indicated. There are two independent experimental series (I & II) for annealing at 650 °C. The lines are only to guide the eye.

should be considered.[15,16] Jaeger *et al.*[4] defined the critical value as the upper limit of the normal-state resistance at which the samples pass into the superconducting state with zero residual resistance and have found it in the vicinity of the pair quantum resistance, i.e., 6.45 kΩ. Our data point to a value less than 6 kΩ (see inset of Fig. 3).

One problem that makes the data analysis difficult is the presence of the parallel conduction channel in the heavily Ga doped layer beneath the Ga rich nanolayer which reduces the total sheet resistance. Unfortunately, it is impossible to determine the depth profile of resistivity and carriers generated by Ga acceptors in Si or present in the Ga rich nanolayer from the Hall effect measurements. Instead, only the total sheet resistance and the sheet carrier concentration $p_\square = 1/(eR_{H\square})$ can be calculated where $R_{H\square}$ and e are the sheet Hall coefficient and the elementary charge, respectively. The Hall coefficient was determined from field-dependent measurements of the Hall resistance. All low temperature, Hall measurements resulted in a positive Hall coefficient indicating that the hole conduction dominates. The superconducting samples are metallic in the normal state in the sense that their carrier concentration is independent of temperature. Thus, the temperature dependence of the resistance is determined by grain boundary barriers leading to a thermally activated mobility.[24] The mobilities at 10 K are in the range of 0.1 to 5 cm^2/Vs, decreasing with increasing hole concentration.

The results of the Hall effect and sheet resistance measurements can be used to set up a tentative phase diagram shown in Fig. 5 for data measured at 10 K. In addition to the resistance gap between the superconducting and insulating state, there is a critical value for the sheet hole concentration. In the vicinity of the phase transition, the data of the 650 °C series can be fitted by the power law $p_\square \sim R_\square^{-1.6}$. Exponents derived from the model of progressive Coulomb blockade in granular structures (−0.5) or scaling rules of the transport in 3d percolating systems (∼−0.15) are quite different.[10] No power law does exist in 2d percolating systems because the Hall coefficient does not diverge at the percolation threshold.

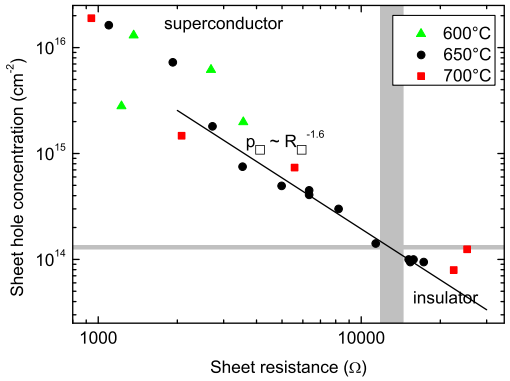

FIG. 5. Tentative sheet hole concentration $p_\square$ – sheet resistance $R_\square$ (@10 K) phase diagram of the superconductor-insulator transition. The separation of the phase regions is indicated (grey bars). In the vicinity of the transition point, the data of the 650 °C annealing follow a power law (solid line).

Hence, our system cannot be attributed to one of these model systems.

The intersection of the power law curve with the critical sheet hole concentration $p_c = 1.3 \times 10^{14}\,cm^{-2}$ is at $R_C = 12.9$ kΩ. However, these values change with temperature. Taking the data very close to the critical temperatures (6 K), the same exponent was found in the power law within our measurement accuracy but p_C and R_C changes to $1.1 \times 10^{14}\,cm^{-2}$ and 15.7 kΩ, respectively. The fact that the resistance separatrix between the superconducting and the insulating state is a function of temperature was also reported by Baturina *et al.*[20] for the phase transition in TiN. They concluded that this phase transition cannot be described by a single-parameter scaling with the universal resistance at the transition. On the other hand, our critical resistance near the transition temperature is very close to the universal resistance $R^* = (8/\pi)\ R_Q = 16.4$ kΩ calculated by Fisher.[18] In order to decide, whether the phase transition observed in Ga implanted Si follows strict scaling rules further experiments on current and field dependence are necessary.[9,15,16]

In conclusion, we have demonstrated that heavily Ga implanted Si with a thin SiO_2 cover layer undergoes a superconductor-insulator transition in dependence on annealing conditions. Since the global Ga depth distribution remains unchanged the transition must be associated with fine changes of the layer nanostructure, leading to higher hole concentration and lower sheet resistance. Surprisingly, the phase transition is very similar to those observed in ultrathin quench-condensed metal films although our layer stack differs strongly in composition, width, and nanostructure. One can speculate that the steep step observed in the resistance-versus-temperature curves of some insulating samples indicates the onset of superinsulation—a quantum phase dual to superconductivity—partly masked by a parallel conduction channel in our samples. Obviously, there is a resistance criterion for the phase transition closely associated with a critical sheet hole concentration. Evaluating the resistance-hole concentration phase diagram in the vicinity of the critical temperature, we obtain a critical resistance of about 16 kΩ whereas the criterion of vanishing residual resistance provides an upper limit of 6 kΩ. It is not yet clear which critical quantity is the primary one and whether the phase transition follows a universal scaling law.

The financial support by Deutsche Forschungsgemeinschaft under Contract No. HE 2604/7 is gratefully acknowledged. The authors thank M. Helm, J. Wosnitza, and G. Gobsch for stimulating discussions.

[1]R. Skrotzki, J. Fiedler, T. Herrmannsdörfer, V. Heera, M. Voelskow, A. Mücklich, B. Schmidt, W. Skorupa, G. Gobsch, M. Helm, and J. Wosnitza Appl. Phys. Lett. **97**, 192505 (2010).
[2]J. Fiedler, V. Heera, R. Skrotzki, T. Herrmannsdörfer, M. Voelskow, A. Mücklich, S. Oswald, B. Schmidt, W. Skorupa, G. Gobsch, J. Wosnitza, and M. Helm, Phys. Rev. B **83**, 214504 (2011).
[3]*The SQUID Handbook, Vol. I, Fundamentals and Technology of SQUIDs and SQUID Systems*, edited by J. Clarke and A. I. Braginski (WILEY-VCH, Weinheim, 2004).
[4]H. M. Jaeger, D. B. Haviland, A. M. Goldman, and B. G. Orr, Phys. Rev. B **34**, 4920 (1986).
[5]D. B. Haviland, Y. Liu, and A. M. Goldman, Phys. Rev. Lett. **62**, 2180 (1989).
[6]A. Frydman, O. Naaman, and R. C. Dynes, Phys. Rev. B **66**, 052509 (2002).
[7]K. A. Parendo, K. H. Sarwa B. Tan, and A. M. Goldman, Phys. Rev. B **76**, 100508(R) (2007).
[8]A. M. Goldman, Low Temp. Phys. **36**, 884 (2010).
[9]Y.-H. Lin and A. M. Goldman, Phys. Rev. Lett. **106**, 127003 (2011).
[10]G. Deutscher, *Superconductivity—Conventional and Unconventional Superconductors*, Nanostructured Superconductors Vol. 1, edited by K. H. Bennemann and J. B. Ketterson (Sringer, Berlin, 2008), p. 259.
[11]L. Nagarajan, R. A. De Souza, D. Samuelis, I. Vavlov, A. Börger, J. Janek, K.-D. Becker, P. C. Schmidt, and M. Martin, Nature Mater. **7**, 391 (2008).
[12]M. A. Steiner, N. P. Breznay, and A. Kapitulnik, Phys. Rev. B **77**, 212501 (2008).
[13]C. B. Eom, M. K. Lee, J. H. Choi, L. J. Belenky, X. Song, L. D. Cooley, M. T. Naus, S. Patnaik, J. Jiang, M. Rikel, A. Polyanskii, A. Gurevich, X. Y. Cai, S. D. Bu, S. E. Babcock, E. E. Hellstrom, D. C. Larbalestier, N. Rogado, K. A. Regan, M. A. Hayward, T. He, J. S. Slusky, K. Inumaru, M. K. Haas, and R. J. Cava, Nature (London) **411**, 558 (2001).
[14]A. T. Bollinger, G. Dubuis, J. Yoon, D. Pavuna, J. Misevich, and I. Bozovic, Nature (London) **472**, 458 (2011).
[15]S. L. Sondhi, S. M. Girvin, J. P. Carini, and D. Shahar, Rev. Mod. Phys. **69**, 315 (1997).
[16]V. F. Gantmakher and V. T. Dolgopolov, Phys. Usp. **53**, 1 (2010).
[17]V. M. Vinokur, T. I. Baturina, M. V. Fistul, A. Yu. Mironov, M. R. Baklanov, and Ch. Strunk, Nature (London) **452**, 613 (2008).
[18]M. P. A. Fisher, G. Grinstein, and S. M. Girvin, Phys. Rev. Lett. **64**, 587 (1990).
[19]N. Markovic, C. Christiansen, A. M. Mack, W. H. Huber, and A. M. Goldmann, Phys. Rev. B **60**, 4320 (1999).
[20]T. I. Baturina, A. Yu. Mironov, V. M. Vinokur, M. R. Baklanov, and C. Strunk, Phys. Rev. Lett. **99**, 257003 (2007).
[21]P. Blood and J. W. Orton, *The Electrical Characterization of Semiconductors: Majority Carriers and Electron States* (Academic, London, 1992).
[22]Y. Shapira and G. Deutscher, Thin Solid Films **87**, 29 (1982).
[23]I. A. Parshin, I. L. Landau, and L. Rinderer, Phys. Rev. B **54**, 1308 (1996).
[24]J. W. Orton and M. J. Powell, Rep. Prog. Phys. **43**, 81 (1980).

APPLIED PHYSICS LETTERS **100**, 242405 (2012)

Magnetic anisotropy engineering: Single-crystalline Fe films on ion eroded ripple surfaces

M. O. Liedke, M. Körner, K. Lenz,[a] F. Grossmann, S. Facsko, and J. Fassbender
Institute of Ion Beam Physics and Materials Research, Helmholtz-Zentrum Dresden-Rossendorf e.V., P.O. Box 510119, 01314 Dresden, Germany

(Received 7 December 2011; accepted 29 May 2012; published online 12 June 2012)

We present a method to preselect the direction of an induced in-plane uniaxial magnetic anisotropy (UMA) in thin single-crystalline Fe films on MgO(001). Ion beam irradiation is used to modulate the MgO(001) surface with periodic ripples on the nanoscale. The ripple direction determines the orientation of the UMA, whereas the intrinsic cubic anisotropy of the Fe film is not affected. Thus, it is possible to superimpose an in-plane UMA with a precision of a few degrees—a level of control not reported so far that can be relevant for example in spintronics. © *2012 American Institute of Physics*. [http://dx.doi.org/10.1063/1.4729151]

The magnetic patterning of samples on the nanoscale is crucial for spintronic designs. Commonly, electron beam lithography is used to obtain the required nanometer precision. However, this technique is slow and therefore limited to small sample areas not suitable for high throughput production. Hence, fast large-area structuring processes are highly demanded.

In contrast to cleaning and smoothing single crystal substrates, broad beam ion sputtering can also be employed to form nanoscale periodic ripple patterns over large areas.[1,2] They are of quasi-sinusoidal shape with several nanometers height compared to stepped/vicinal surfaces with monoatomic steps and preferential orientation. The ripple formation by ion beam irradiation can be described by the linear instability theory by Bradley and Harper[3] further extended by others.[4–6] Ripple patterns formed by ion irradiation have been found on various materials, like metals,[7–10] semiconductors,[11,12] and oxides.[13–15] The ripple wavelength is set by the ion beam energy, where ≈10 nm seems to be a lower limit.

It is well known that a periodic roughness in ferromagnetic films generates dipolar stray fields, which in turn give rise to an uniaxial magnetic anisotropy (UMA).[16,17] Thus, ferromagnetic (FM) rippled films gained attraction in recent years[18–21] and inspired usage in magnetic sensors.[22,23] It was shown that the ripple pattern wavelength controls the strength of the UMA,[24] or creates an additional orange peel (Néel) coupling in interlayer exchange coupled films.[25] Recently, Landeros and Mills calculated the spinwave response in such periodically perturbed films.[17]

To prepare thin rippled, ferromagnetic films one has two options: (i) The post-growth ion sculpturing of a FM film grown on a planar substrate.[8–10,20,26] This just modulates the surface of the FM film only. However, this method suffers from the fact that it is almost impossible to create *homogeneously thin* films of a few nanometers thickness, since due to the sputter removal the starting thickness must be much larger. Therefore we dedicate our efforts to (ii) the bottom-up approach, i.e., where the thin film is grown onto previously patterned ripple substrates.[21,24,25,27] These films exhibit the ripple morphology on the substrate–FM interface *as well as* on the top.

To investigate the influence of periodically modulated Fe films, MgO(001) substrates were used due to their good epitaxial relation to Fe.[28] The rippled MgO(001) surface was created by Ar^+ ion beam irradiation from conventional planar MgO(001), using an Ar^+ primary energy of $E = 0.6$ keV, a fluence of 5×10^{17} ions·cm^{-2}, an incident angle of 50°, and a substrate temperature of $T = 0$ °C. The ion gun was a Kaufman type source with a single graphite extraction grid with 5 cm diameter. Further details of the underlying general erosion process are described elsewhere.[3,29] By choosing the sputter direction (azimuth), the ripple crest direction ϕ_{ripple} can be set to any arbitrary angle with respect to the MgO⟨100⟩ directions. A series of samples with varying ϕ_{ripple} as well as planar reference samples were prepared. The morphology and ripple-wavelength prior to the film deposition was evaluated using atomic force microscopy (AFM). Figures 1(a) and 1(b) show AFM images for ripple directions of $\phi_{\text{ripple}} = 0°$ and 52°, respectively. The periodical surface modulation with an average amplitude of ≈ 1 nm and a wavelength of ≈18 nm (see inset linescan in Fig. 1) is clearly visible. Subsequently the samples were sonicated in isopropanol, transferred to a molecular beam epitaxy system, and annealed at 200 °C for 10 min. The 10 nm thick Fe film followed by a 3 nm thick Cr protective layer were deposited at room temperature by molecular beam evaporation under normal incidence. The deposition rate was ≈0.2 Å/s. The pressure during evaporation was below 1×10^{-9} mbar.

The Fe films were investigated by means of low energy electron diffraction (LEED) yielding always a cubic structure proving the epitaxial single-crystalline growth [inset Fig. 2(b)]. Due to the lattice mismatch, the Fe lattice is rotated by 45° with respect to the MgO lattice, i.e., the well known relation Fe⟨110⟩||MgO⟨100⟩,[28] and therefore the ripple direction in the Fe coordinate system is $\phi^{\text{Fe}}_{\text{ripple}} := \phi_{\text{ripple}} - 45°$ as depicted in Fig. 1(c). High-resolution cross-sectional transmission electron microscopy (TEM) was used to examine the Fe films and its interfaces as shown in Fig. 2. The rippled MgO surface still exhibits its *single-crystalline* structure. No amorphization at the MgO–Fe interface is found as the lattice planes continue through the Fe film as

[a]Author to whom correspondence should be addressed. Electronic mail: k.lenz@hzdr.de.

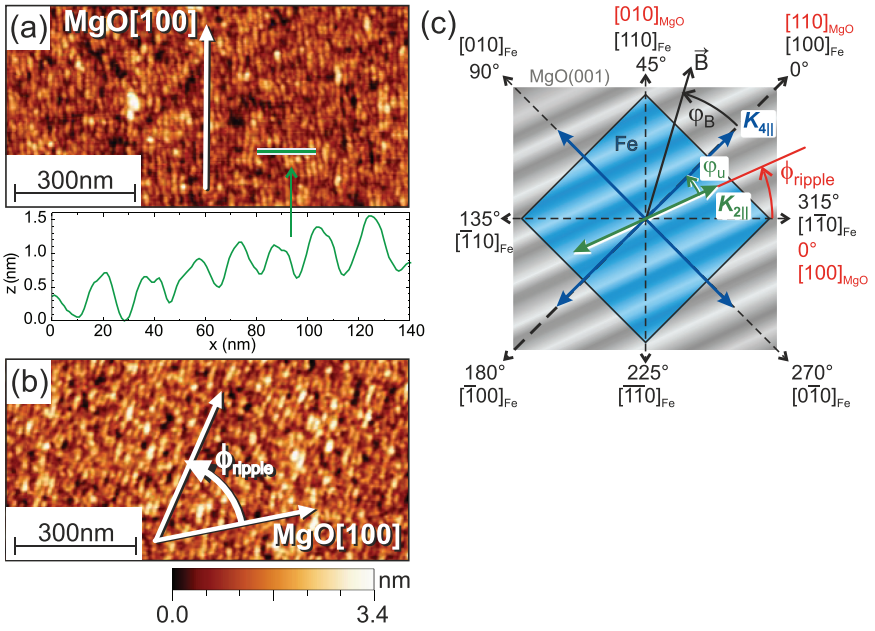

FIG. 1. AFM images and linescan of rippled MgO(001) with (a) $\phi_{\text{ripple}} = 0°$ and (b) $\phi_{\text{ripple}} = 52°$. (c) Sketch of the anisotropy axes and lattice directions.

depicted exemplarily by the yellow guide lines in Fig. 2(c). Hence, the Fe/Cr layers on top grow clearly epitaxially and pseudomorphically, taking over the lattice and surface corrugation given by the MgO substrate. The Fe/Cr surface shows the same ripples the MgO substrate induces [white lines in Fig. 2(a)]. A further proof against amorphization is the fact that a polycrystalline film (as a result on an amorphous substrate) would not show the fourfold cubic in-plane anisotropy as shown later.

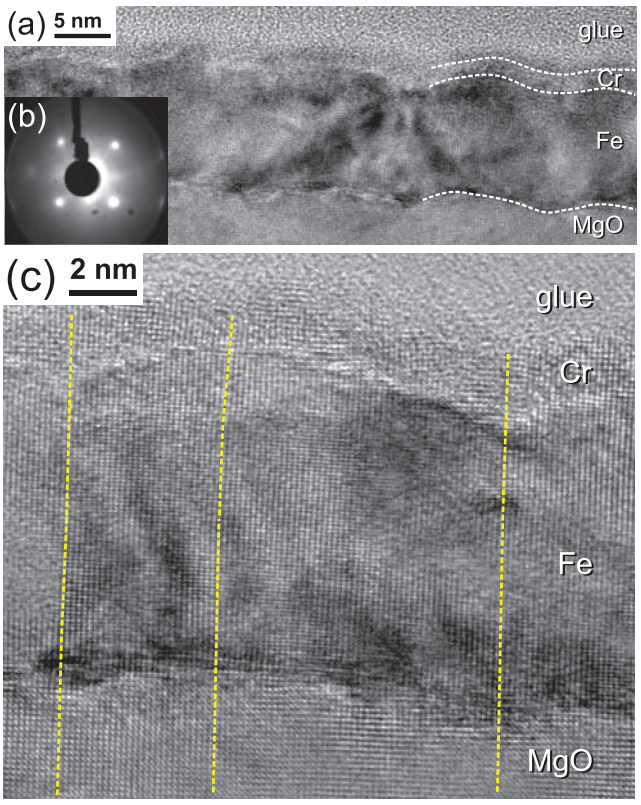

FIG. 2. (a) TEM cross-section of a rippled Cr/Fe/MgO sample. Dashed lines are eye-guides for the interfaces. (b) LEED image (136 eV). (c) Magnified HR-TEM image with dashed yellow lines depicting the continuous lattice planes.

The magnetic properties were determined by magneto-optical Kerr effect (MOKE) magnetometry and vector network analyzer ferromagnetic resonance (VNA-FMR).

In Fig. 3, three magnetization reversal (MR) curves are presented for in-plane field angles of $\varphi_B = -45°$, $-25°$, and $5°$. The ripple crest orientation for this sample was $\phi^{\text{Fe}}_{\text{ripple}} = -15°$. The MR curves exhibit certain irreversible jumps of the magnetization, i.e., single, double, or triple magnetization switching processes. This is a sign for UMA superimposed on the cubic magnetic anisotropy, but also for the nucleation and fast propagation of 180° or 90° domain walls. It should be noted that, although the switching fields were mostly below 10 mT, the saturation fields were typically close to 80 mT. The arrows in Fig. 3 denote the orientation of the magnetic domains in this system during reversal. First, at a field angle of $\varphi_B = -45°$ [Fig. 3(a)] the magnetization reverses by a one-jump process that corresponds to a rapid propagation of 180° domain walls. Second, the two-jump process found at $\varphi_B = 5°$ [Fig. 3(c)] indicates nucleation and propagation of 90° domain walls for both jumps,[30] whereas the three-jump process at $\varphi_B = -25°$ [Fig. 3(b)] represents a sequence of 90°, 180°, and again 90° domain wall displacements (based on Kerr microscopy investigations, not shown). Zhan *et al.*[31] have reported and unambiguously described the three-jump process MR curves in Fe/MgO(001) systems, where the strength and orientation of the UMA were *altered* either by ion sputtering or by oblique-incidence MBE growth. However, in contrast to our investigations any direct proof of precise orientation *control* of the in-plane UMA was not given.

The FMR was carried out in field-sweep mode, i.e., sweeping the external magnetic field with the microwave frequency fixed to $f = 15$ GHz. The samples were mounted on a coplanar waveguide. The FMR spectra taken at different in-plane field angles φ_B were evaluated by using a complex Lorentzian fit function. From the resulting angle-dependent resonance field data $B_{\text{res}}(\varphi_B)$, the magnetic anisotropy parameters were determined from a fit with the resonance equation as described, e.g., in Ref. 32. The contributions to the free energy density are

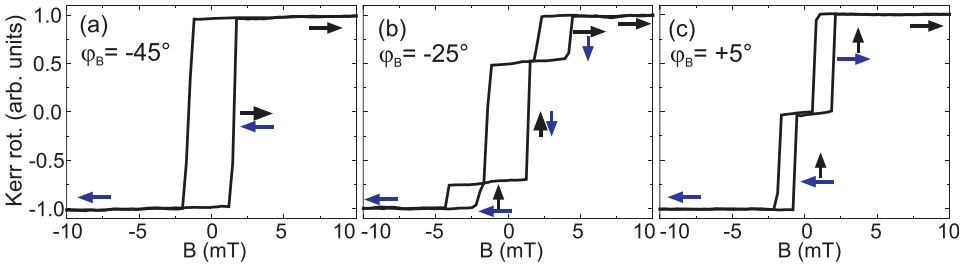

FIG. 3. Magnetization reversal curves of 10 nm Fe/MgO with $\phi^{\mathrm{Fe}}_{\mathrm{ripple}} = -15°$ for 3 different in-plane field angles φ_B. Arrows denote the orientation of domains.

$$F = -MB[\sin\theta\sin\theta_B\cos(\varphi-\varphi_B)+\cos\theta\cos\theta_B] - \left(\frac{1}{2}\mu_0 M^2 - K_{2\perp}\right)\sin^2\theta - K_{2\parallel}\sin^2\theta\cos^2(\varphi-\varphi_B) - \frac{1}{8}K_{4\parallel}(3+\cos 4\varphi)\sin^4\theta, \quad (1)$$

where θ (θ_B) and φ (φ_B) are the out-of-plane and in-plane angles of the magnetization M (external field B), respectively. $K_{4\parallel}$ is the cubic anisotropy and $K_{2\perp}$ ($K_{2\parallel}$) the uniaxial out-of-plane (in-plane) anisotropy. The uniaxial anisotropy direction with respect to the cubic direction is denoted by φ_u. The in-plane angles φ, φ_B, φ_u are counted from the Fe[100] direction, as depicted in Fig. 1(c).

Figure 4(a) shows the angle-dependent FMR data for an Fe film with a ripple orientation of $\phi^{\mathrm{Fe}}_{\mathrm{ripple}} = -45°$, i.e., with the ripple crests along MgO[100] ∥ Fe[1$\bar{1}$0]. The red curve is a fit according to the resonance equation providing the anisotropy fields and directions. The angular dependence of the resonance field is mainly characterized by a strong cubic anisotropy field of $\frac{2K_{4\parallel}}{M} = 63.2$ mT superimposed by a small in-plane UMA field of $\frac{2K_{2\parallel}}{M} = 4.28$ mT. This can be seen directly by the difference in the resonance field maxima marked with the green dotted lines. The uniaxial easy axis is rotated by $\varphi_u = -45°$ with respect to the cubic one, i.e., pointing along Fe[1$\bar{1}$0]. Hence, the UMA axis is parallel to the ripple crests, which were previously set by the ion erosion process of the substrate. Thus, the in-plane UMA is induced by ≈1 nm high ripples, which generate dipolar stray fields at the Fe/MgO and Fe/Cr interfaces.[17] In contrast, the cubic anisotropy direction and magnitude is an intrinsic feature of the Fe lattice.[33] The effective magnetization $\mu_0 M_{\mathrm{eff}} = \mu_0 M - \frac{2K_{2\perp}}{M} = 2.05$ T is close to the Fe bulk value.

To further confirm these findings, other ripple directions were prepared and investigated. Figure 4(b) shows the corresponding result for $\phi^{\mathrm{Fe}}_{\mathrm{ripple}} = 7°$. Now the ripple crests lie close to the cubic easy axis direction and in turn the UMA axis is rotated only by $\varphi_u = 10°$. The cubic anisotropy field and effective magnetization are similar to the previous sample. The UMA field is slightly smaller, i.e., $\frac{2K_{2\parallel}}{M} = 2.78$ mT.

The results for all investigated ripple directions are listed in Table I. One can see that the values for $\mu_0 M_{\mathrm{eff}}$ and $\frac{2K_{4\parallel}}{M}$ are similar for all samples, except the planar reference sample. This means that the ripple direction does not influence the intrinsic Fe anisotropy. In comparison to the planar 10 nm thick reference sample, the cubic anisotropy is twice as large. However, only 12% larger than the Fe bulk value. For the cubic anisotropy strain plays an important role.[33] X-ray diffraction studies (not shown) prove that the planar Fe reference sample is definitely subject to strain and much rougher compared to the ripple templates, whereas the Fe films on ripples are in the nearly fully relaxed state. This strain explains the lower cubic anisotropy and effective magnetization of the planar sample.

The values for the in-plane UMA field $\frac{2K_{2\parallel}}{M}$ vary only slightly between 2.8 and 6.4 mT. This could be due to small differences in the ripple height and elongation of the ripples. These values also match estimations derived from the spin-wave spectra calculations using the theory of Landeros and Mills.[17] Apart from that, the key of our work, i.e., the match of the UMA direction with the preset ripple direction is perfectly confirmed. The small mismatch (less than 10%) found between $\phi^{\mathrm{Fe}}_{\mathrm{ripple}}$ and φ_u stems from the uncertainty of $\phi^{\mathrm{Fe}}_{\mathrm{ripple}}$. The ripple directions were determined from AFM measurements with the substrate edges as reference. A slight misalignment or even edge-miscut would be an explanation.

In conclusion, we have shown that the direction of an induced in-plane UMA can be precisely preset by the sputter direction of the substrates. Fe films on these rippled MgO templates grow in single-crystalline fashion. The UMA is

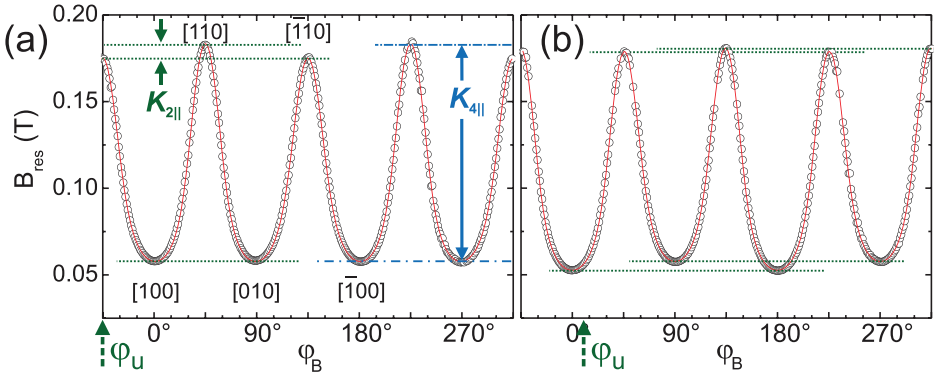

FIG. 4. In-plane angle-dependent FMR of 10 nm Fe on MgO ripples ($\lambda = 18$ nm) with (a) $\phi^{\mathrm{Fe}}_{\mathrm{ripple}} = -45°$ and (b) $\phi^{\mathrm{Fe}}_{\mathrm{ripple}} = 7°$. The UMA direction φ_u is marked with dashed arrows. The red curve is a fit with the resonance equation. Dashed and dotted lines are guides to the eye.

TABLE I. Anisotropy and ripple parameters.

ϕ_{ripple} (deg)	$\phi_{\text{ripple}}^{\text{Fe}}$ (deg)	φ_{u} (deg)	$\frac{2K_{2\parallel}}{M}$ (mT)	$\frac{2K_{4\parallel}}{M}$ (mT)	$\mu_0 M_{\text{eff}}$ (mT)
Bulk	…	…	…	55	2144
Planar	…	0	0	33.2	1900
0	−45	−45	4.28	63.2	2052
23	−22	−20	3.30	59.4	2037
30	−15	−16	3.16	59.8	2050
44	−1	3	3.54	52.0	2011
52	7	10	2.78	64.8	2071
78	33	30	6.38	63.0	2035

superimposed with the intrinsic cubic anisotropy of the Fe film. This opens possibilities to select and pin the easy magnetization axis in a certain direction in spintronic devices, like multi-axial magnetic sensors for application. If the UMA will be further increased by optimized ripple structures, a 6-fold but non-symmetric easy axis system could be created.

We thank A. Mücklich, T. Strache, A. Shalimov, and M. Ranjan for their help. We thank P. Landeros for fruitful discussions and calculations. This work has been supported by the Deutsche Forschungsgemeinschaft (Grant No. FA 314/6-1). In memoriam, D. L. Mills.

[1]M. Navez, C. Sella, and D. Chaperot, C. R. Hebd. Acad. Sci. **254**, 240 (1962), Available at http://gallica.bnf.fr/ark:/12148/bpt6k3206x/f248.
[2]W. L. Chan and E. Chason, J. Appl. Phys. **101**, 121301 (2007).
[3]R. M. Bradley and J. M. E. Harper, J. Vac. Sci. Technol. A **6**, 2390 (1988).
[4]M. A. Makeev, R. Cuerno, and A. L. Barabasi, Nucl. Instrum. Methods B **197**, 185 (2002).
[5]J. Munoz-Garcia, M. Castro, and R. Cuerno, Phys. Rev. Lett. **96**, 086101 (2006).
[6]S. A. Norris, M. P. Brenner, and M. J. Aziz, J. Phys.: Condens. Matter **21**, 224017 (2009).
[7]S. Rusponi, G. Costantini, F. Buatier de Mongeot, C. Boragno, and U. Valbusa, Appl. Phys. Lett. **75**, 3318 (1999).
[8]F. Bisio, R. Moroni, F. B. de Mongeot, M. Canepa, and L. Mattera, Appl. Phys. Lett. **89**, 052507 (2006).
[9]K. Zhang, F. Rotter, M. Uhrmacher, C. Ronning, J. Krauser, and H. Hofsäss, New J. Phys. **9**, 29 (2007).
[10]R. Moroni, D. Sekiba, F. Buatier de Mongeot, G. Gonella, C. Boragno, L. Mattera, and U. Valbusa, Phys. Rev. Lett. **91**, 167207 (2003).
[11]J. Erlebacher, M. J. Aziz, E. Chason, M. B. Sinclair, and J. A. Floro, Phys. Rev. Lett. **82**, 2330 (1999).
[12]T. K. Chini, D. P. Datta, and S. R. Bhattacharyya, J. Phys.: Condens. Matter **21**, 224004 (2009).
[13]S. Camelio, D. Babonneau, D. Lantiat, L. Simonot, and F. Pailloux, Phys. Rev. B **80**, 155434 (2009).
[14]H. Zhou, Y. Wang, L. Zhou, R. L. Headrick, A. S. Özcan, Y. Wang, G. Özaydin, K. F. Ludwig, and D. P. Siddons, Phys. Rev. B **75**, 155416 (2007).
[15]T. Luttrell and M. Batzill, Phys. Rev. B **82**, 035408 (2010).
[16]R. Arias and D. L. Mills, Phys. Rev. B **59**, 11871 (1999).
[17]P. Landeros and D. L. Mills, Phys. Rev. B **85**, 054424 (2012).
[18]F. Bisio, R. Moroni, F. Buatier de Mongeot, M. Canepa, and L. Mattera, Phys. Rev. Lett. **96**, 057204 (2006).
[19]J. Briones, F. Montaigne, D. Lacour, G. Lengaigne, S. Girod, and M. Hehn, Appl. Phys. Express **3**, 073002 (2010).
[20]F. Büttner, K. Zhang, S. Seyffarth, T. Liese, H.-U. Krebs, C. A. F. Vaz, and H. Hofsäss, Phys. Rev. B **84**, 064427 (2011).
[21]K. V. Sarathlal, D. Kumar, and A. Gupta, Appl. Phys. Lett. **98**, 123111 (2011).
[22]M. J. Carey, J. R. Childress, E. E. Fullerton, and S. Maat, U.S. patent no. 7,360,300 (22 April 2008).
[23]M. J. Carey, J. R. Childress, and S. Maat, U.S. patent no. 7,529,066 (05 May 2009).
[24]J. Fassbender, T. Strache, M. O. Liedke, D. Markó, S. Wintz, K. Lenz, A. Keller, S. Facsko, I. Mönch, and J. McCord, New J. Phys. **11**, 125002 (2009).
[25]M. Körner, K. Lenz, M. O. Liedke, T. Strache, A. Mücklich, A. Keller, S. Facsko, and J. Fassbender, Phys. Rev. B **80**, 214401 (2009).
[26]K. Zhang, M. Uhrmacher, H. Hofsäss, and J. Krauser, J. Appl. Phys. **103**, 083507 (2008).
[27]M. O. Liedke, B. Liedke, A. Keller, B. Hillebrands, A. Mücklich, S. Facsko, and J. Fassbender, Phys. Rev. B **75**, 220407(R) (2007).
[28]H. Fuke, A. Sawabe, and T. Mizoguchi, Jpn. J. Appl. Phys. **32**, L1137 (1993).
[29]A. Keller, S. Roßbach, S. Facsko, and W. Möller, Nanotechnology **19**, 135303 (2008).
[30]R. P. Cowburn, S. J. Gray, and J. A. C. Bland, Phys. Rev. Lett. **79**, 4018 (1997).
[31]Q. F. Zhan, S. Vandezande, K. Temst, and C. Van Haesendonck, Phys. Rev. B **80**, 094416 (2009).
[32]K. Zakeri, I. Barsukov, N. K. Utochkina, F. M. Römer, J. Lindner, R. Meckenstock, U. von Hörsten, H. Wende, W. Keune, M. Farle, S. S. Kalarickal, K. Lenz, and Z. Frait, Phys. Rev. B **76**, 214421 (2007).
[33]Y. V. Goryunov, N. N. Garif'anov, G. G. Khaliullin, I. A. Garifullin, L. R. Tagirov, F. Schreiber, T. Mühge, and H. Zabel, Phys. Rev. B **52**, 13450 (1995).

APPLIED PHYSICS LETTERS **100**, 223108 (2012)

Nanohole pattern formation on germanium induced by focused ion beam and broad beam Ga^+ irradiation

Monika Fritzsche, Arndt Muecklich, and Stefan Facsko[a)]
Institute of Ion Beam Physics and Materials Research, Helmholtz-Zentrum Dresden-Rossendorf, P.O. Box 510119, 01314 Dresden, Germany

(Received 21 March 2012; accepted 9 May 2012; published online 30 May 2012)

Hexagonally ordered nanohole patterns were produced on Ge(100) surfaces by focused Ga^+ ion beam and broad Ga^+ ion beam irradiations with 5 keV energy under normal incidence. Identical patterns were obtained by irradiations with a scanning focused ion beam under different irradiation conditions and with a broad Ga^+ beam without scanning and five orders of magnitude smaller ion flux. Thus, we could demonstrate that nanohole pattern formation is independent of ion flux over several orders of magnitude and scanning of a focused ion beam under appropriate conditions is identical to broad ion beam irradiation. © *2012 American Institute of Physics*. [http://dx.doi.org/10.1063/1.4721662]

The morphology of surfaces and interfaces strongly influences optical, electrical, and magnetic properties of thin films. Furthermore, nanopatterned surfaces are interesting templates for functional metallic films[1,2] as well as for bioactive surfaces.[3] Low energy ion beam irradiations can change the surface morphology drastically either by smoothing or by roughening mechanisms. Under special conditions, the interplay of these mechanisms leads to self-organized periodic patterns.[4] For oblique ion incidence, ripple patterns with periodicity in the nanometer range have been obtained on metals, semiconductors, and insulators.[5] For normal ion incidence, hexagonal dot patterns on compound materials[6] or on surfaces with intentional or unintentional co-deposition of metal atoms were found.[7,8] Beside these well known ripple and dot patterns, a third kind of highly ordered self-organized nanostructures were observed using 5 keV Ga^+ focused ion beam (FIB) irradiation of Ge at normal incidence, namely periodic nanohole patterns.[9]

FIBs are commonly used for direct patterning of surfaces.[10] However, due to the linear writing only small areas can be patterned in acceptable times. On the other hand, self-organized patterns appear also when surfaces are irradiated with a defocused FIB.[11–13] In this case, the ion irradiation differs in many aspects from the usually used noble gas broad beam (BB) irradiations. First, the Ga^+ ion beam already implants Ga into the surface, thus a two component system is present at the surface after the steady-state condition is reached at fluences of a few 10^{16} ions/cm^2. Second, the ion beam focus is smaller than 1 μm and can be even focussed down to a few tenths of nanometers. In order to pattern a larger area, the ion beam is scanned over the surface mimicking a larger homogeneously irradiated area. Until now there is no consensus whether a scanning focused ion beam is identical to a broad ion beam for self-organized pattern formation.[14] And finally, the local flux in the ion beam can be orders of magnitude higher than in a broad beam. If thermal diffusion is effective, a strong flux dependence is expected.[4] However, in many systems ion induced smoothing mechanisms have been found exhibiting no flux dependence.[15] In this letter, we present a comparison of hole pattern formation on Ge surfaces induced by FIB and by BB irradiations. Thus, we address the question if FIB produced self-organized patterns are similar to the well known noble gas broad ion beam induced patterns.

Figure 1 shows a comparison of the irradiation schemes. The square indicates the sample, whereas the large circle represents the size of the broad beam with a radius r_{BB}. Due to the large size of the broad beam which is approximately 5 mm no scanning is necessary. In contrast, the focused ion beam is scanned over the surface. The small filled blue circles are indicating the points where the FIB stands for a certain time, called dwell time. These points have a certain distance in x and y direction, the step size Δx and Δy. The radius of the FIB, indicated by the small circles with a radius r_{FIB}, is in the range of 150 nm and much larger than the step size of only 5 nm. Hence, a large overlap is used and guided pattern formation is not expected. The beam is scanned over the surface in a meander like way, indicated by the red lines with arrows. The scanning of the FIB over the whole area is repeated for a given number of loops with a velocity called beam speed. Taking into account the scanning of the FIB two fluxes can be defined. The first is a local flux in the beam given by the beam current and the second one, the total areal flux, is the mean ion flux in the scanning area. For a FIB, the local flux is much higher than the total areal flux. In case of a broad beam, both fluxes are equal due to a standing beam.

For studying the nanohole pattern dynamics on Ge surfaces a 5 keV Ga^+ FIB was used. All FIB patterns were created using a Zeiss NVision 40 CrossBeam® combined with a Raith Elphy Plus. In all cases, epiready Ge (100) substrates were irradiated at room temperature (RT) and an angle of 0° with respect to the surface normal. In Fig. 2, scanning electron microscopy (SEM) images of hexagonally ordered nanohole patterns are shown which were created using an ion fluence of 2.5×10^{18} ions/cm^2. A reference pattern, shown in Fig. 2(c), was created using a 150 pA current (corresponding to a local flux of 1.3×10^{18} ions/(cm^{2}s)), a dwell time of 0.667 μs, a step size of 5 nm in both directions, 1000 loops, and a beam speed of 7.5 mm/s. All these values are summarized in Table I. A closer look at the pattern

[a)]Author to whom correspondence should be addressed. Electronic mail: s.facsko@hzdr.de.

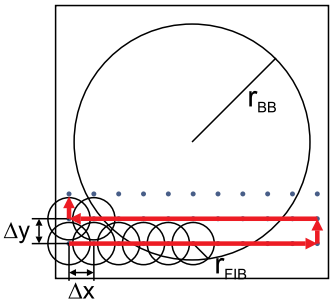

FIG. 1. Scheme of broad beam and FIB irradiation (not to scale).

reveals a periodicity of the nanoholes of 48 nm. Each hole is surrounded by 6 small elevations which appear as white points at the edges of a honeycomb like structure. The connections of these elevations separate the holes from each other. The hole domains exhibit a short range hexagonal order with an extension of approximately 500 nm. However, the domains are oriented arbitrary with no correlation to the crystal structure of the Ge (100) surface. Between the domains point defects are found, which are higher than the surrounding pattern.

In order to investigate the influence of beam scanning and local flux on the pattern formation, beam current, dwell time, and number of loops were changed. The different dwell times and loops are shown in Table I. Bold values indicate changed parameters using different currents. The 150 pA current is used as a reference to compare the pattern of different currents. So it can either be placed in the upper or in the lower row of Fig. 2. After changing the current to 80 pA and 700 pA, the dwell time was increased and decreased, respectively, in order to get the same fluence per loop. The patterns created after a total fluence of 2.5×10^{18} ions/cm^2 are shown in Figs. 2(a) and 2(b), respectively. Apparently, the same pattern appears. There is no difference in periodicity although the dwell time changed from 1.25 μs (80 pA) to 0.206 μs (700 pA). Due to the changed dwell time also the scan speed changed from 4.0 mm/s (80 pA) to 29.2 mm/s (700 pA). After changing the dwell time, the number of loops was changed keeping the dwell time constant. In all cases, the total fluence (not to be confused with the fluence per loop) was kept constant at 2.5×10^{18} ions/cm^2. Although the

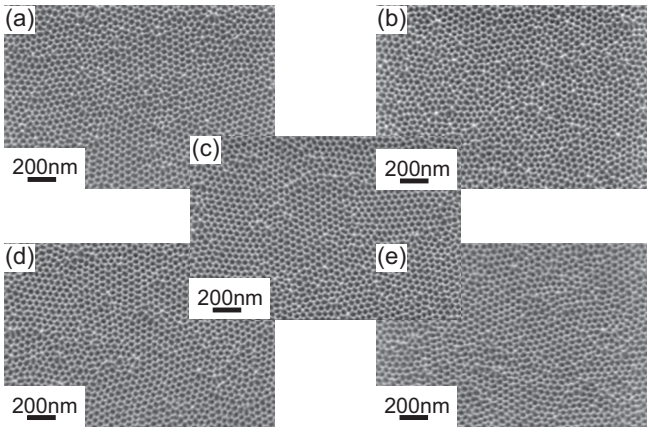

FIG. 2. Flux dependence and scanning dependence of FIB produced nanoholes on Ge (100) at RT using the parameters given in Table I.

number of loops was changed from 214 (700 pA) to 1875 (80 pA) again the same nanohole pattern with the same periodicity is obtained (Figs. 2(d) and 2(e), respectively). We can thus conclude that ion flux, dwell time, number of loops, and scan speed have no influence on the pattern formation.

To analyse the effect of scanning of the FIB, a comparison of a pattern created by FIB and another pattern created with the same parameters but using a broad Ga^+ beam was performed. The broad beam experiment was done using a Danfysik 1050 low energy broad beam implanter. To reduce the influence of surrounding material, the Ge sample was mounted on a holder which was fully covered by Ge. In case of the broad beam, a fluence of 3.0×10^{18} ions/cm^2 was used which is comparable to the fluence used for FIB (Fig. 2). This pattern (Fig. 3) was created using an energy of 5 keV and Ga^+ ions at normal incidence and RT. A comparison of the local flux which was 4.3×10^{13} ions/(cm^{2}s) using broad beam irradiation and 1.3×10^{18} ions/(cm^{2}s) for FIB irradiation illustrates immediately that the flux was five orders of magnitude lower for broad beam irradiation. A comparison of both SEM images (Figs. 2(c) and 3) shows very similar nanohole pattern. Again a honeycomb like structure with hexagonally ordered holes is appearing. Also, the periodicities are equal within the measuring accuracy and have the same value like before in FIB produced pattern (48 nm). We can thus conclude that scanning does not affect the pattern formation. In order to compare patterns by FIB and broad beam in more detail, cross-sectional transmission electron microscopy (TEM) analysis was performed. These patterns were created using a 5 keV Ga^+ beam at normal incidence and a fluence of 2.0×10^{17} ions/cm^2. SEM and corresponding TEM images of FIB produced pattern are shown in Figs. 4(a) and 4(c), respectively, whereas the pattern produced by broad beam irradiations are shown in Figs. 4(b) and 4(d). A comparison of the two SEM images (Figs. 4(a) and 4(b)) shows again nanohole patterns which cannot be distinguished neither in periodicity nor in ordering. A comparison of Figs. 4(a) and 4(b) with Figs. 2(c) and 3, respectively, shows that the ordering is increasing with increasing fluence for FIB produced patterns as well as for broad beam produced patterns. In the TEM images of these two samples, the dark areas in the lower part of the images are the single crystalline Ge substrate. The brighter areas on top of the dark areas are amorphous layers which were confirmed by high resolution TEM of these areas (not shown). The depth of the nanoholes is approximately 7 nm, whereas the amorphous layer has a thickness of 12 nm. This is valid both for the FIB and for the broad beam produced patterns (Figs. 4(c) and 4(d), respectively). As expected, Ga is enriched in the amorphous layer as measured by energy-dispersive x-ray spectroscopy (EDX) (not shown here). No difference in the height of the structures or in the thickness of the amorphous layer is found for patterns irradiated using FIB or broad beam.

Pattern formation induced by ion irradiation is commonly described by continuum equations.[4,16] They are generic partial differential equations derived from Sigmund's sputter theory or, more general, from averaged "crater functions" resulting from molecular dynamics simulations.[17] Originally, the hole pattern observed during irradiation of Ge surfaces with Ga^+ FIB has been modelled by the damped

TABLE I. Parameters of the FIB produced nanoholes shown in Fig. 2.

Current pA	Dwell time μs	Loops	Beam speed mm/s	Step size nm	Total areal flux ions/cm^{2}s	Total fluence ions/cm^2	Fig.
80	**1.250**	1000	4.0	5	3.0×10^{14}	2.5×10^{18}	2(a)
700	**0.206**	1000	29.2	6	2.7×10^{15}	2.5×10^{18}	2(b)
150	**0.667**	**1000**	7.5	5	5.7×10^{14}	2.5×10^{18}	2(c)
80	0.667	**1875**	7.5	5	3.0×10^{14}	2.5×10^{18}	2(d)
700	0.667	**214**	7.5	5	2.7×10^{15}	2.5×10^{18}	2(e)

Kuramoto-Sivashinsky (dKS) equation[18] with good qualitative agreement.[9] However, it is now commonly accepted that the damping term proportional to the height in the dKS equation has no physical grounds.[19] In addition, under normal incidence an additional smoothing mechanism caused by the ion induced drift of surface atoms is expected to dominate over roughening.[16,20] However, Bradley and Shipman (BS) proposed recently that if more than one species is present at the surface preferential sputtering and ion induced atomic drift can lead to an additional instability.[21,22] Thus, we assume that in the case of hole patterns on Ge, which are evolving during irradiation with Ga^+ ions under normal incidence, this instability is the dominant mechanism for pattern formation. We therefore modeled the pattern formation by their proposed coupled equations in which the surface topography is coupled to a surface layer of altered composition.[22] In compound materials, preferential sputtering leads to a changed composition at the surface. However, it also applies for concurrent deposition of impurities.[23] In our case, one species is the substrate material Ge and the other one is Ga which is continuously implanted into the surface by the Ga^+ ion beam. After a fluence of 2.0×10^{17} ions/cm^2, we determined with Auger electron spectroscopy a Ga atomic surface concentration of 18% in fair agreement with Tridyn[24] simulations of 20%. Figures 5(a) and 5(b) show snapshots of a simulation of the BS equations at integration times t of 250 and 1000, respectively. Immediately, the better ordering in case of higher time, i.e., fluence, is visible. Thus, the simulation confirms the observation of quality improvement seen by a comparison of Figures 4(a) and 4(b) with Figures 2(c) and 3, respectively. Figs. 4(a) and 2 are FIB produced patterns using the same parameters except the number of loops and therefore the fluence. The fluence was 2.0×10^{17} ions/cm^2 (Fig. 4(a)) and 2.5×10^{18} ions/cm^2 (Fig. 2(c)). The obtained pattern is the same but the ordering is much higher in case of the higher fluence. In Figure 4(a), only small hexagonally ordered domains (e.g., upper right of the picture) are present whereas the typical domain size in Figure 2(c) is 500 nm. The same effect is visible for the broad beam produced patterns (Figs. 4(b) and 3). This means that the domain size and therefore the ordering is increasing with increasing fluence.

To make the similarity between simulation and experiment as well as the similarity between FIB and BB produced pattern more visible some details of the pattern are shown in Figure 6. Fig. 6(a) is a zoom in the simulation, whereas Fig. 6(b) shows a SEM image of a FIB produced pattern with a picture width of 200 nm. In Fig. 6(c), an atomic force microscopy (AFM) image of a pattern produced using broad beam irradiation is shown. The AFM image corresponds to the SEM image shown in Fig. 4(b) and has a picture width of 100 nm and a height scale of 10.6 nm. In all cases, each hole is surrounded by six small elevations which appear as brighter areas in the simulation and the SEM image and are even more visible in the AFM image. The similarity between FIB and broad beam irradiation is also valid for higher energies. We used a 30 keV broad Ga^+ beam at RT, normal incidence and a fluence of 1.0×10^{18} ions/cm^2 and obtained a sponge like structure (not shown) which is also observed using FIB.[14]

In conclusion, normal incidence irradiation of Ge (100) surfaces with 5 keV Ga^+ ions produces self-organized nanohole patterns. The pattern formation has been discussed and modelled on the base of the recently proposed Bradley-Shipman model reaching a qualitative agreement with the experimentally observed patterns and the increasing ordering with fluence. However, predictive parameter choice is not possible at this stage. The comparison of nanohole patterns

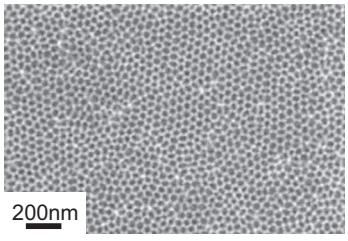

FIG. 3. Nanohole pattern produced using broad beam Ga^+ irradiation of Ge (100) at normal incidence, RT, 5 keV, and a fluence of 3.0×10^{18} ions/cm^2.

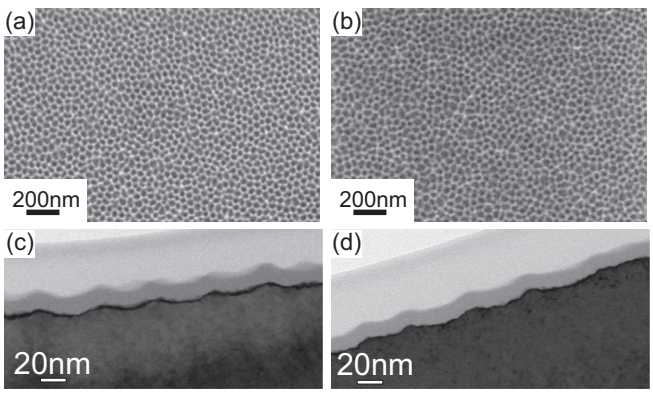

FIG. 4. SEM ((a) and (b)) and cross-sectional TEM images ((c) and (d)) of patterns created using a 5 keV Ga^+ beam at normal incidence, RT and a fluence of 2.0×10^{17} ions/cm^2, (a) and (c) FIB irradiation, (b) and (d) broad beam irradiation.

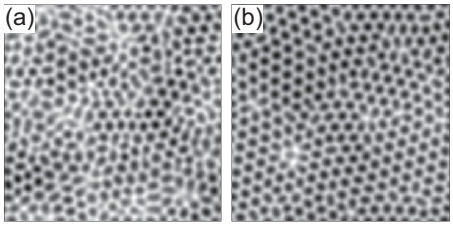

FIG. 5. Snapshot of a simulation of the BS equations at (a) $t = 250$; (b) $t = 1000$ using the following parameters: normal incidence of ions, $\lambda = -1$, $a = 0.25$, $b = 0.37$, $c = 1$, $\nu = 1$, $\eta = 0$, mesh size 200×200 points, spatial step size $\Delta x,y = 1$, time steps $\Delta t = 0.01$, and a starting surface with white noise. For the simulations we used the coupled equations (Eqs. (40) and (41)) and denomination of parameters according to Ref. 22.

on Ge produced by irradiation with a FIB and a broad beam of 5 keV Ga^+ clearly demonstrates that the mechanisms responsible for the self-organized pattern formation are the same, irrespectively of the characteristics of the ion beam. The regular hole pattern observed after the irradiation at different parameters of the FIB scanning and with a broad Ga^+ ion beam without scanning demonstrates conclusively that ion flux, scan speed, dwell time, and number of loops have no influence on the pattern formation. Thus, using a FIB with appropriate scanning with a large overlap of the beams during scanning mimics perfectly a broad beam.

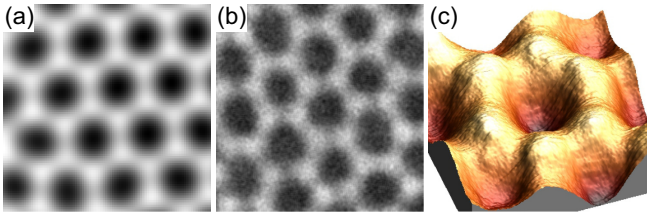

FIG. 6. (a) Zoom in simulation, (b) SEM image of a FIB produced pattern with a picture width of 200 nm, and (c) AFM image of a broad beam produced pattern with a picture width of 100 nm and a height of 10.6 nm.

We would like to acknowledge I. Winkler for technical support and DFG (FOR 845) for financial support.

[1]T. W. H. Oates, A. Keller, S. Facsko, and A. Muecklich, Plasmonics **2**, 47 (2007).
[2]J. Fassbender, T. Strache, M. O. Liedke, D. Marko, S. Wintz, K. Lenz, A. Keller, S. Facsko, I. Moench, and J. McCord, New J. Phys. **11**, 125002 (2009).
[3]M. S. Lord, M. Foss, and F. Besenbacher, Nanotoday **5**, 66 (2010).
[4]R. M. Bradley and J. M. E. Harper, J. Vac. Sci. Technol. A **6**, 2390 (1988).
[5]W. L. Chan and E. Chason, J. Appl. Phys. **101**, 121301 (2007).
[6]S. Facsko, T. Dekorsy, C. Koerdt, C. Trappe, H. Kurz, A. Vogt, and H. L. Hartnagel, Science **285**, 1551 (1999).
[7]B. Ziberi, F. Frost, M. Tartz, H. Neumann, and B. Rauschenbach, Appl. Phys. Lett. **92**, 063102 (2008).
[8]J. Zhou, S. Facsko, M. Lu, and W. Moeller, J. Appl. Phys. **109**, 104315 (2011).
[9]Q. M. Wei, X. L. Zhou, B. Joshi, Y. B. Chen, K. D. Li, Q. H. Wei, K. Sun, and L. M. Wang, Adv. Mat. **21**, 2865 (2009).
[10]A. Lugstein, B. Basnar, J. Smoliner, and E. Bertagnolli, Appl. Phys. A **76**, 545 (2003).
[11]S. Habenicht, K. P. Lieb, J. Koch, and A. D. Wieck, Phys. Rev. B **65**, 115327 (2002).
[12]S. Ichim and M. J. Aziz, J. Vac. Sci. Technol. B **23**, 1068 (2005).
[13]P. F. A. Alkemade, Phys. Rev. Lett. **96**, 107602 (2006).
[14]A. Cuenat and M. J. Aziz, Mater. Res. Soc. Symp. Proc. **707**, 113 (2002).
[15]C. C. Umbach, R. L. Headrick, and K. C. Chang, Phys. Rev. Lett. **87**, 246104 (2001).
[16]B. Davidovitch, M. J. Aziz, and M. P. Brenner, Phys. Rev. B **76**, 205420 (2007).
[17]S. A. Norris, M. P. Brenner, and M. J. Aziz, J. Phys. C **21**, 224017 (2009).
[18]S. Facsko, T. Bobek, A. Stahl, H. Kurz, and T. Dekorsy, Phys. Rev. B **69**, 153412 (2004).
[19]R. M. Bradley, Phys. Rev. B **83**, 075404 (2011).
[20]G. Carter and V. Vishnyakov, Phys. Rev. B **54**, 17647 (1996).
[21]R. M. Bradley and P. D. Shipman, Phys. Rev. Lett. **105**, 145501 (2010).
[22]P. D. Shipman and R. M. Bradley, Phys. Rev. B **84**, 085420 (2011).
[23]R. M. Bradley, Phys. Rev. B **83**, 195410 (2011).
[24]W. Moeller, W. Eckstein, and J. P. Biersack, Comput. Phys. Commun. **51**, 355 (1988).

APPLIED PHYSICS LETTERS **100**, 152101 (2012)

In-plane interdot carrier transfer in InAs/GaAs quantum dots

J. Bhattacharyya,[1,a)] S. Zybell,[1] S. Winnerl,[1] M. Helm,[1] M. Hopkinson,[2] L. R. Wilson,[3] and H. Schneider[1]
[1]*Institute of Ion Beam Physics and Materials Research, Helmholtz-Zentrum Dresden-Rossendorf, D-01314 Dresden, Germany*
[2]*EPSRC National Centre for III-V Technology, University of Sheffield, S1 3JD United Kingdom*
[3]*Department of Physics and Astronomy, University of Sheffield, Sheffield S3 7RH, United Kingdom*

(Received 27 January 2012; accepted 22 March 2012; published online 9 April 2012)

Using time resolved photoluminescence (PL) quenching measurements, we investigated inplane carrier transfer in InAs/GaAs self-assembled quantum dots (QDs). THz pulses from a free-electron laser tuned to the intersublevel transition energy were used to excite carriers to higher levels causing quenching in the PL. These carriers could either fall back to the lower energy states and recombine or get transferred to adjacent QDs. The relaxation of the carriers was directly reflected in the recovery of the PL signal. Comparing measurements from two samples, we found that the redistribution of carriers into the neighbouring QDs is the dominant mechanism of carrier relaxation. The data were fitted using a rate equation model to estimate the PL recovery time which we attribute to the interdot carrier transfer time. © *2012 American Institute of Physics*. [http://dx.doi.org/10.1063/1.3701578]

In a semiconductor quantum dot (QD), three-dimensional confinement of the electrons and holes results in discrete electronic states resembling a quasi atom-like system. Despite the narrow emission lines from individual dots, the optical emission spectrum from an ensemble of self-assembled QDs is inhomogeneously broadened, arising from the distribution of size and composition of the QDs. Due to the involvement of a large number of dots with different energy levels, the carrier dynamics of such an ensemble is strongly affected by contributions from interdot diffusion and trapped-carriers. Time resolved photoluminescence (PL) experiments[1–5] have been used to investigate the interband carrier relaxation mechanisms in QDs. THz spectroscopy[6] and THz modulated PL measurements[7–9] probe the intraband transitions in QD ensembles. However, most of the THz modulated experiments were performed in a time integrated mode and the carrier relaxation mechanisms for intraband transitions were not investigated. The carrier dynamics in QDs depend on the density, size, and composition of the dots. Though the properties of QDs grown under different conditions are diverse making a quantitative comparison of sample properties difficult, a qualitative understanding and identification of the processes are still useful. In general, carriers in higher energy levels in QDs can either relax directly to lower states or diffuse into adjacent dots. These relaxation paths can be tuned by post-growth annealing.[10] Time-resolved spectroscopy on samples with different intersublevel relaxation times gives insight into intraband carrier dynamics in these dots.

In this letter, we report on time resolved PL measurements on InAs QDs where carriers are excited quasi-resonantly by a near infrared (NIR) picosecond laser and redistributed by time-delayed THz pulses. When excited non-resonantly in the barrier, as was done in most of the previous measurements, all the QDs were equally populated and contributed to the PL. This made it difficult to distinguish different transition in different dots. We therefore excite below the barrier energy so that electron-hole pairs are generated only in selective QDs. Using a second THz pulse from a free electron laser (FEL), we induce quenching of the PL by re-exciting carriers to higher levels within the QDs. The analysis of the PL recovery allows us to investigate the underlying carrier relaxation mechanisms and their time constants.

The InAs QD samples were grown on a (100) GaAs substrate using molecular beam epitaxy, in the Stranski-Krastranow growth mode. The samples consisted of 80 layers of QDs separated by 50 nm wide GaAs barriers to ensure that there is no electrical or optical coupling between adjacent layers. The QD samples were annealed at different temperatures resulting in blue shifted PL and red shifted intersublevel transition (ISLT) energies.[11] Due to the phonon bottleneck, samples with different ISLT energies had intersublevel (ISL) relaxation times varying from a few picoseconds to nanoseconds.[10] The QD density was estimated to be about $4 \times 10^{10}\text{cm}^{-2}$ with an average base diameter of 20 nm and height of about 5 nm, before capping. The QDs were n-doped by a Si-layer grown ~2 nm below the QD layers, providing an average doping of one electron per dot. The PL excitation was performed using a tunable mode-locked Ti:sapphire laser, emitting ~4 ps long NIR pulses. The laser was tuned to energies below the wetting layer ground state energy for quasi-resonant excitation of the QDs. Typical PL spectra from the sample S850, for excitation energies close to resonance, are shown in Figure 1(a). Two phonon-mediated[12,13] ground state (s-state, as marked in Figure 1(b)) transitions of two subsets of QDs are observed at $\Delta E = 27$ meV and 36 meV, corresponding to InGaAs and GaAs LO phonons, respectively. ΔE is the difference of the excitation energy and the measured PL energy. However, at these excitation energies the PL emission is very weak. With increasing NIR photon energy (about 1.387 eV and higher), a

a)Electronic address: j.bhattacharyya@hzdr.de.

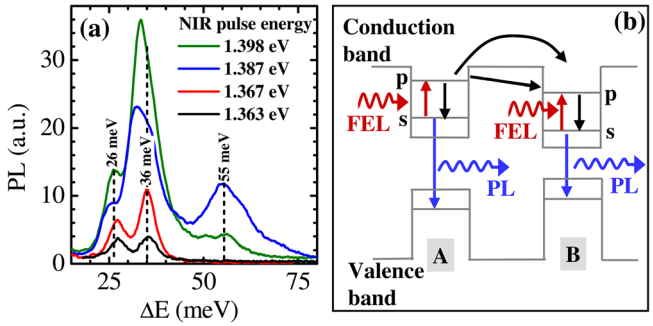

FIG. 1. (a) Typical PL spectra of S850 for quasi-resonant excitation where the horizontal axis gives the difference of the excitation energy and the measured PL energy. The black, red, green, and blue lines correspond to 1.363 eV, 1.367 eV, 1.387 eV, and 1.398 eV excitation energies, respectively. (b) The QD band diagram showing the FEL (THz) excitation in red, the PL recombination in blue and the relaxation paths in black arrows. As shown, the QD "A" loses carriers while QD "B" gains carries due to carrier redistribution after THz excitation. The NIR excitation is not shown.

second peak appears around 55 meV. This peak corresponds to emission from s-states of another subset of QDs, whose p-states are coupled to the incident photons via the 36 meV LO phonon. Due to the broad linewidth, some smaller QDs too have their ground state emission around the 36 meV. Thus for higher excitation energies, the peak around 36 meV consists of recombination from both p-like and s-like states. However, the s-state recombination is dominant, as will be clarified later. The peak farthest from the NIR excitation energy is the lower energy peak of the PL which is purely s-like.

In order to manipulate the carrier distribution, the QD ensemble was excited by strong THz pulses from the FEL at Helmholtz-Zentrum Dresden Rossendorf. The FEL was synchronized to the Ti:sapphire laser and its wavelength was tuned to the electron ISLT energy in the conduction band, as obtained from THz absorption measurements.[10] The details of the setup are discussed elsewhere.[14] Time and wavelength resolved PL was detected by a Hamamatsu streak camera coupled to a spectrometer. The time resolution of the measurements was ∼15 ps. The sample was cooled in a He cryostat to 8 K.

Figures 2(a) and 2(b) show typical streak camera images of the PL emission from the QD ensemble without and with THz pulse, respectively. The vertical axes give the emission energies and the horizontal axes represent time. Plots along the horizontal blue and red lines give the PL transients shown in Figures 2(c) and 2(d). The measurements were performed on two QD samples annealed at different temperatures and having parameters as listed in Table I. For quasi-resonant excitation of samples S850 and S900, the NIR photon energies were 1.397 eV and 1.442 eV, respectively. The plots in Figure 2 show PL from sample S900 excited about 40 meV above resonance but still below the wetting layer ground state energy. The bright spot around 100 ps (at 1.43 eV) is the scattered NIR excitation. Before the incidence of the THz pulse the PL intensity showed an initial rise and then decayed due to loss of carriers by radiative recombination [blue arrows in Figure 1(b)]. The THz pulse was made incident on the sample about 150 ps after the NIR pulse resulting in excitation of carriers to the higher levels in the

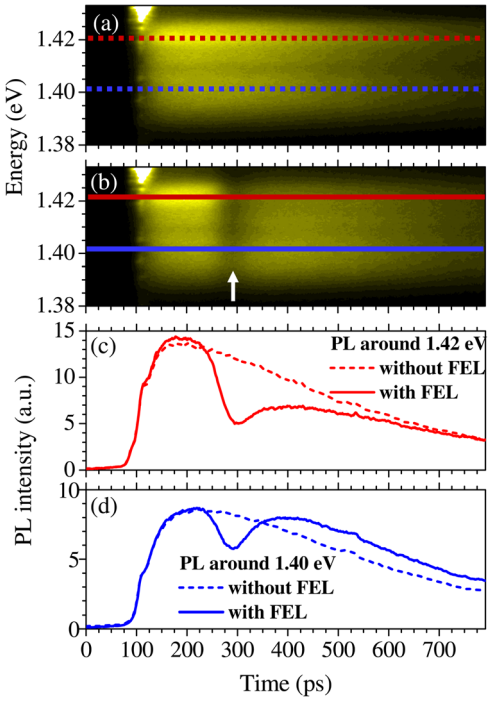

FIG. 2. Streak camera image of the PL transient at 8 K from the QD sample S900 for quasi-resonant excitation by the Ti:sapphire laser (a) without FEL pulse and (b) with FEL pulse (quenching by the FEL pulse is indicated by the arrow) of fluence 1 $\mu J/cm^2$. PL transient integrated over few meV around (c) 1.42 eV (red lines) and (d) 1.40 eV (blue lines) showing the quenching of the PL. The reference transients are shown by dashed lines.

QDs [red arrows in Figure 1(b)]. This caused decrease in the PL intensities appearing as dips in the PL transients in Figures 2(c) and 2(d). As reference plots, we measured the PL transient with the THz pulse temporally shifted away from the measured time window to nullify any lattice heating effect which would influence the PL dynamics. The observation of quenching in both PL peaks, for FEL photon energy resonant to the s-p electron transition, indicates that the high energy peak is dominantly s-like. The quenching is attributed to the THz excitation primarily of the electrons since the THz energy is non-resonant to the hole ISLT energies. The quenched and the reference plots show that eventually the PL signal recovers due to carriers relaxing back into the s-state [black arrows in Figure 1(b)] and recombining. However, this behaviour depends strongly on the PL energy. From comparison of Figures 2(c) and 2(d), we observe that the recovery of the quenched PL for the lower energy peak is much more pronounced. For the higher energy peak, the signal recovers but does not overshoot the reference value. This behavior is observed in both samples studied. The apparent loss of carriers for the higher energy peak and a gain in the lower energy end indicate a thermalization of carriers to

TABLE I. Sample details at 10 K (Ref. 10).

Sample #	Annealing temperature (°C)	PL peak at 8K (this work) (eV)	ISLT energy (meV)	ISL relaxation time (ps)	τ_{rec} at 8 K (this work) (ps)
S850	850	1.340	20	60	55
S900	900	1.396	15	1500	80

lower energy dots induced by the THz pulse. For quasi-resonant excitation, the PL is emitted primarily due to the excitation and recombination of excitons within the same QD. Thus the carriers cannot thermalize into QDs with lower energies. The THz excitation transfers the carriers to higher levels from which they can get redistributed into lower energy dots via the wetting layer or by tunneling. Such interdot carrier transfer in these samples has been reported earlier[9] leading to trapped-carrier luminescence. For comparison, in quantum well (QW) samples[15] where PL is emitted from only one energy level, the amount of recovery balances the number of quenched carriers for the given transition.

For a quantitative understanding we fitted our data with a multi-level rate equation model, which has been used for PL quenching in QWs.[15] Here we will discuss some of the basic features and modifications of the model. The PL intensity was proportional to the occupation number of the radiative state. The PL transient without the THz pulse was fitted with exponential curves having rise and decay time constants of about 30 ps and 400 ps, respectively. The measurement resolution was taken into account by convolving the fitting function by a Gaussian with a FWHM of 12 ps. At the time of incidence of the THz pulse, a fraction of the carriers "q" was excited to the higher energy states. The parameter "q" is therefore directly related to the PL dip depth at the quench. The recovery of the PL resulted from relaxation of the carriers from the excited state with a time constant τ_{rec}. For the QW sample in Ref. 15, the PL rise and recovery times were found to be practically identical. However, this does not hold for QD ensembles as the mechanism of relaxation of the carriers is different. For QWs, the intersubband relaxation is very fast (few ps) and the recovery time depends on the non-radiative relaxation of carriers by phonon scattering from high momentum states to the Γ-point. The PL rise time, too, involves the same non-radiative relaxation channel. However for QDs, the presence of spatially separated dots offers two recombination channels, (i) the carriers relax to the ground state of the same dot and recombine, and (ii) the carriers get redistributed into the neighbouring dots and then recombine, as shown in Figure 1(b). A fit of the data using just one relaxation channel, where the quenched carriers fall back into the same dots and no interdot transfer is allowed, is shown by the dashed lines in Figure 3. The fits are unable to account for the energy dependent recovery of the PL. The model was therefore modified and an additional recovery path, with the same time constant τ_{rec}, accounting for the interdot transfer was included. The interdot transfer flux defined by n_{QD} takes a negative (positive) value for loss (gain) of carriers and gives good fit to the experimental data as shown in Figure 3.

Measurements were performed on samples S900 and S850 for THz photon energies of 15 meV and 20 meV, respectively. Variation of q as a function of the THz fluence (defined by intensity per pulse) plotted in Figure 4(a) shows a saturation behaviour. This is explained by the complete depletion of the QD ground states. We attribute the stronger quenching in S900, compared to S850, to the fact that due to much broader ISL absorption feature in S900,[10] the THz pulse hits the ISLT resonance better. The higher value of q also tallies with the longer ISL relaxation time of S900. The amount of quenching of the two states for each sample is quite similar. However, the plots of n_{QD} in Figure 4(b) show a contrasting nature for the two transitions in both the samples. The low energy peak has a considerable gain of carriers shown by the high positive value while the high-energy peak exhibits mostly negative values for n_{QD}. The higher carrier transfer for S900 compared to S850 is due to the more pronounced quenching and weaker confinement of the levels in S900. The fitted value of τ_{rec} was typically 55 ps for S850 and 80 ps for S900. Even though the ISL relaxation times of S900 and S850 (1.5 ns and 60 ps, respectively) (Ref. 10) were orders of magnitude different, the τ_{rec} had quite similar values. The ISL relaxation times listed here were obtained from ISL absorption of the doped electrons. For PL measurements, due to the presence of extra electrons and holes (in addition to the doped electrons) excited by the NIR pulses, the relaxation times become faster via electron-hole scattering.[16] This, however, cannot account for differences in the recovery of the PL signal for different emission energies, indicating the strong influence of interdot carrier transfer. The carriers can either tunnel into adjacent dots or get transferred over the barrier with an effective time constant which can be associated with the τ_{rec} defined in the fitting model. Such re-excitation can be induced by multiphoton (THz) absorption. This is supported by the fast saturation of the q

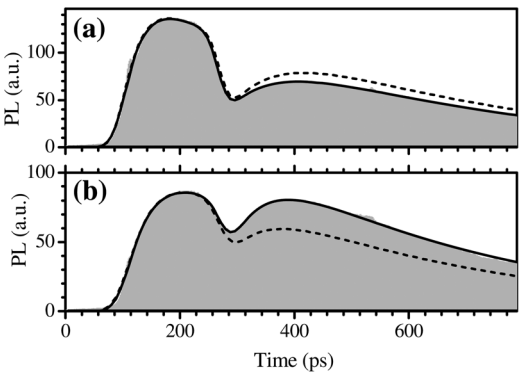

FIG. 3. Plot of the measured time resolved PL emission (gray filled region) from QD sample S900 at the (a) high and (b) low energy PL peaks for quasi resonant Ti:sapphire excitation. Quenching of the PL by the FEL pulse occur around 300 ps. The transients are fitted using rate equation model with (solid line) and without (dashed line) interdot carrier transfer channels.

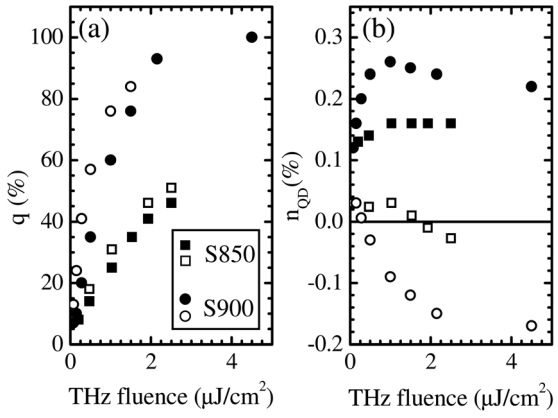

FIG. 4. The amount of (a) PL dip depth q and (b) interdot carrier transfer n_{QD} as obtained from the rate equation model fit. The circles and the squares represent samples S900 and S850, respectively. The open (solid) symbols correspond to the higher (lower) energy PL peak.

with THz fluence. In this whole argument, the contribution from the holes is ignored because the THz energy is non-resonant to the hole transitions. Also the hole relaxation is much faster (few ps), because of the valence band mixing, which cannot account for the observed recovery time.

In conclusion, we have performed time resolved PL spectroscopy of QD ensembles which were re-excited by a time delayed THz pulse. This THz pulse resulted in a transient quenching of the PL, which allowed us to investigate the carrier relaxation and to determine directly the intraband carrier dynamics in the QDs. Simultaneous measurements of PL transients at two different emission bands indicate an FEL-induced transfer of PL intensity between these two bands after recovery from the quenching. In addition, we found that the PL recovery time is much faster than the electron inter-sublevel relaxation time as obtained from pump probe measurements.[10] Both the spectral PL redistribution and the reduction in PL recovery time are attributed to inter-dot carrier transfer. Though a precise identification of the transfer mechanism is beyond the scope of this work, we have shown that even for low QD densities ($4 \times 10^{10}\text{cm}^{-2}$ in our case) the interdot carrier transfer influences intraband carrier dynamics in self assembled QDs.

We thank P. Michel, W. Seidel, and the FELBE Team for their dedicated support.

[1]B. Ohnesorge, M. Albrecht, J. Oshinowo, A. Forchel, and Y. Arakawa, Phys. Rev. B **54**, 11532 (1996).
[2]M. Paillard, X. Marie, E. Vanelle, T. Amand, V. K. Kalevich, A. R. Kovsh, A. E. Zhukov, and V. M. Ustinov, Appl. Phys. Lett. **76**, 76 (2000).
[3]S. Sanguinetti, M. Padovani, M. Gurioli, E. Grilli, M. Guzzi, A. Vinattieri, M. Colocci, P. Frigeri, and S. Franchi, Appl. Phys. Lett. **77**, 1307 (2000)
[4]L. Kong, Z. C. Feng, Z. Wu, and W. Lu, J. Appl. Phys. **106**, 013512 (2009).
[5]A. Chernikov, S. Horst, S. W. Koch, S. Chatterjee, W. W. Rühle, J. Sweet, B. Richards, J. Hendrickson, G. Khitrova, H. M. Gibbs, D. Litvinov, D. Gerthsen, and M. Wegener, Solid State Commun. **149**, 1485 (2009).
[6]S. Menzel, E. A. Zibik, P. Aivaliotis, J. W. Cockburn, and L. R. Wilson, Phys. Rev. B **77**, 153302 (2008).
[7]B. N. Murdin, A. R. Hollingworth, J. A. Barker, D. G. Clarke, P. C. Findlay, C. R. Pidgeon, J.-P. R. Wells, I. V. Bradley, S. Malik, and R. Murray, Phys. Rev. B **62**, R7755 (2000).
[8]R. A. Child, R. J. Nicholas, N. J. Mason, P. A. Shields, J.-P. R. Wells, I. V. Bradley, J. Phillips, and B. N. Murdin, Phys. Rev. B **68**, 165307 (2003).
[9]J. Bhattacharyya, M. Wagner, M. Helm, M. Hopkinson, L. R. Wilson, and H. Schneider, Appl. Phys. Lett. **97**, 031101 (2010).
[10]E. A. Zibik, T. Grange, B. A. Carpenter, N. E. Porter, R. Ferreira, G. Bastard, D. Stehr, S. Winnerl, M. Helm, H. Y. Liu, M. S. Skolnick, and L. R. Wilson, Nature Mater. **8**, 803 (2009).
[11]E. A. Zibik, W. H. Ng, L. R. Wilson, M. S. Skolnick, J. W. Cockburn, M. Gutierrez, M. J. Steer, and M. Hopkinson, Appl. Phys. Lett. **90**, 163107 (2007).
[12]F. Adler, M. Geiger, A. Bauknecht, D. Haase, P. Ernst, A. Dörnen, F. Scholz, and H. Schweizer, J. Appl. Phys. **83**, 1631 (1998).
[13]A. V. Baranov, V. Davydov, H. W. Ren, S. Sugou, and Y. Masumoto, J. Lumin. **87–89**, 503 (2000).
[14]J. Bhattacharyya, M. Wagner, S. Zybell, S. Winnerl, D. Stehr, M. Helm, and H. Schneider, Rev. Sci. Instrum. **82**, 103107 (2011).
[15]S. Zybell, H. Schneider, S. Winnerl, M. Wagner, K. Köhler, and M. Helm, Appl. Phys. Lett. **99**, 041103 (2011).
[16]E. Harbord, P. Spencer, E. Clarke, and R. Murray, Phys. Rev. B **80**, 195312 (2009).

APPLIED PHYSICS LETTERS **100**, 051109 (2012)

Temperature dependence of the intraexcitonic AC Stark effect in semiconductor quantum wells

M. Wagner,[a] M. Teich, M. Helm, and D. Stehr
Institute of Ion Beam Physics and Materials Research, Helmholtz-Zentrum Dresden-Rossendorf, P.O. Box 510119, 01314 Dresden, Germany

(Received 6 December 2011; accepted 13 January 2012; published online 2 February 2012)

We have investigated the temperature-dependent, intraexcitonic AC Stark effect that manifests itself in a line splitting of the heavy-hole 1s exciton transition in a GaAs/AlGaAs multi quantum well when the 1s-2p intraexciton transition is driven by intense THz light. The observed wavelength-dependent splitting at Helium temperature can still be distinguished at elevated temperatures up to 200 K. Although the thermal energy exceeds the exciton binding energy by a factor of 1.7, thermal exciton ionization influences the coherent nonlinear effect only indirectly via thermal line broadening. With a threefold transmission change on ultrafast timescales in a region accessible to Peltier-cooling the scheme could be promising for optical modulators. © *2012 American Institute of Physics*. [doi:10.1063/1.3681399]

Exciting a semiconductor material at its bandgap can create bound electron hole pairs known as excitons. With its oppositly charged constituents these quasiparticles perfectly behave as a hydrogen atom. However, its Rydberg energy is scaled down by 3 orders of magnitude resulting in a few meV binding energy. This energy range is accessible by the meanwhile well established techniques of terahertz (THz) spectroscopy by which it is now possible to investigate atomic physics in solid state semiconductor structures, giving insight in exciton formation and intraexcitonic transitions. For instance, several studies in the linear optical regime have addressed the dynamics of exciton formation[1–3] or proved optical gain for intraexcitonic transitions.[4] It is especially of interest how these artifical atoms behave in intense electromagnetic fields where strong nonlinear optical effects are expected.[5] THz fields of the order of 10 kV/cm and above are easily reached by free-electron lasers or recently also by table-top THz time domain systems.[6,7] In the perturbative regime where the polarization can still be expanded in a power series of the electric field, near-infrared THz sideband generation[8,9] was reported. Increasing the field strength results in a non-negligible population of the excited state that is coupled to the THz radiation. In this non-perturbative regime, combined light-matter states or dressed states occur and manifest themselves in Rabi oscillations in the time domain[10] and as AC Stark splitting[11,12] in the frequency-domain. Going beyond that regime strong field effects are predicted such as high-harmonic generation[13] or exciton field ionization that is known from strong dc electric fields.[14]

Recently we have discussed the AC Stark or Autler-Townes effect in GaAs/AlGaAs multiple quantum wells.[15] The effect revealed itself in the near-infrared (NIR) transmission spectrum as a distinct pump wavelength dependent line splitting of the heavy-hole hh(1s) exciton when the intraexcitonic 1s-2p transition is driven. Here, we extend the former low-temperature (10 K) study to higher lattice temperatures up to room-temperature using the same sample as investigated before.

The Dresden free-electron laser FELBE serves as high-power THz source to drive the intraexcitonic transition. Its beam is focused on the sample at normal-incidence via a parabolic off-axis mirror with 5 cm focal length as depicted in Fig. 1(a). Note that for this focal length at a photon energy of 2.5 THz a typical spot diameter is 400 μm, resulting in field strengths of up to 150 kV/cm for pulses of the order of 10 ps. A hole drilled in the mirror along the optical axis allows the NIR probe beam to pass for collinear propagation of pump and probe beam through the sample. The 78 MHz NIR light pulses originate from a 110 nm broadband Ti:Sapphire laser

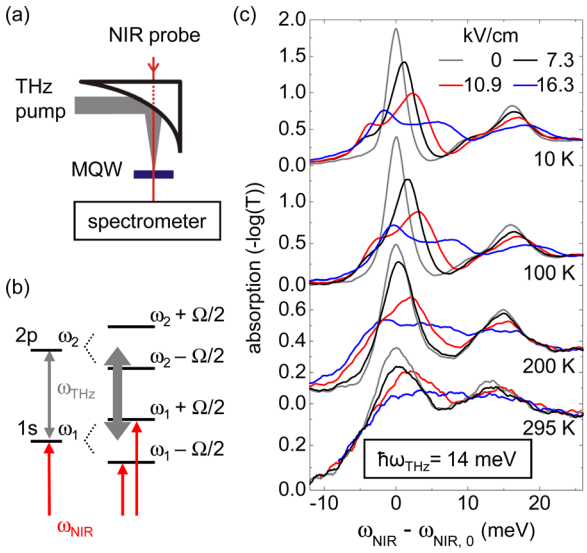

FIG. 1. (Color online) (a) Setup for measuring the NIR transmission of the multi-quantum well (MQW) sample under THz illumination. (b) Schematic splitting by the Rabi frequency Ω of the heavy-hole 1s and 2p states when resonantly coupled by intense THz light. (c) NIR absorption for different lattice temperatures at a THz photon energy of 14 meV (above the 1s-2p resonance). Absorption traces are plotted for different THz peak field strengths as indicated and are referenced to the temperature-dependent hh(1s) position $\omega_{NIR,0}$.

[a]Electronic mail: mwagner@physics.ucsd.edu.

(femtolasers: Femtosource Scientific sPro). In order to monitor only the THz induced spectral changes its repetition rate is reduced by an acousto optical pulse picker to the free-electron laser's 13 MHz. Both lasers are synchronized with a timing jitter of 1-2 ps. The sample is mounted in a liquid He flow cryostat. Z-cut Quartz windows transmit the THz and NIR beam while a grating spectrometer with a CCD camera detects the NIR transmission of the sample.

The sample is made of 60 alternating layers of 8.2 nm thin GaAs wells in between 19.6 nm thick $Al_{0.34}Ga_{0.66}As$ barriers. The GaAs substrate has been removed by wet etching after the sample was glued on NIR transparent ZnTe substrate. Employing NIR pump and broadband THz probe time-domain spectroscopy the intraexciton 1s-2p transition has been found to lie at 9 meV with a linewidth of 3 meV.

In Ref. 15 we have reported a distinct line splitting of the hh(1s) absorption peak given by the Rabi energy $\hbar\Omega$ when driving the system resonantly on the intraexciton 1s-2p transition, as schematically shown in Fig. 1(b). Illumination below and above resonance results in high- and low-energy Rabi sidebands, respectively. Note that the 2p state also splits but cannot be probed by interband NIR excitation due to selection rules. In Fig. 1(c) the 10 K absorption for a THz photon energy of 14 meV (above resonance) is plotted for different THz peak field strengths. Note that the traces are horizontally normalized to the hh(1s) peak position, i.e., without THz illumination (gray line) the hh(1s) absorption peak is found at 0 meV while the lh(1s) peak lies at 16 meV with the hh(2s) shoulder in between. With increasing THz field strength distinct spectral changes occur. At the lowest field strength of 7.3 kV/cm the Rabi sideband lies below the hh(1s) absorption line at −5 meV. A line broadening probably due to exciton field ionization[14] is already present and increases with field strength. For fields above approximately 16 kV/cm an asymmetry reversal is seen where the less pronounced Rabi sideband has been shifted over to the high-energy side. This behavior has been observed in our previous study; however, the field strengths applied here are higher due to a smaller THz focus. The asymmetry reversal might be attributed to a dynamical shift of the 1s-2p resonance with increasing field strength, since a symmetric splitting around the undriven hh(1s) position in two peaks of equal height is observed for 13 kV/cm (not shown) indicating that the intraexcitonic resonance has moved from the zero-field value of 9 meV to 14 meV at 13 kV/cm. However, an additional renormalization of the involved energy states is probably superimposed because the line shape becomes highly asymmetric as illustrated for 16.3 kV/cm peak field strength. The different peak fields have been chosen to demonstrate the temperature-dependent changes for the low-field regime where the Rabi sideband is on the low-energy side as expected from a simple two-level model, as well as for the high-field regime with the unexpected peak energetically above the undriven hh(1s) position.

At a lattice temperature of 100 K the absorption strongly resembles the low temperature case though the linewidth has increased slightly due to thermal broadening.[16] At an even higher temperature of 200 K the undriven absorption line has considerably broadened and decreased in height. However, the THz field dependent characteristics are still distinguishable, i.e., absorption at 10.9 kV/cm differs strongly from the one at 16.3 kV/cm. Compared to the 10 K absorption only the overall linewidths have increased. Finally, at room temperature the line broadening masks any Rabi sidebands. But still a strong field dependence is visible with a THz induced transmission increase at the hh(1s) exciton position.

So far the system has been driven above resonance. In Fig. 2(a) the near-resonant case with a THz photon energy of 10.5 meV is plotted for different temperatures. At 100 K and moderate THz peak field strength of 7 kV/cm we find a nearly symmetric splitting in contrast to the aforementioned pumping above resonance at this power. Increasing the field to 12.8 kV/cm the Rabi sideband is shifted in between the hh and lh peaks. At 200 K Rabi sidebands are still weakly observable but have vanished at room temperature.

Pumping with 6.1 meV THz photon energy, i.e., below resonance, in Fig. 2(b) results in a small Rabi sideband 6 meV above the hh(1s) exciton for 6.1 kV/cm. For 16.4 kV/cm the sideband has already merged with the lh state. Since the sideband is only weakly pronounced here it is not distinguishable any more at higher temperatures. However, for comparable field strengths of 6-7 kV/cm we find from Figs. 1(c) and 2 that the AC Stark effect is still observable at elevated lattice temperatures of 200 K with spectral features being distinctly different for varying THz photon energies. At room temperature only a THz induced decrease of the hh(1s) absorption occurs that is unspecific of the pump frequency. At 200 K the thermal energy of 17 meV well exceeds the exciton binding energy. There is only few literature related to the intraexciton 1s-2p transition at elevated temperatures or strong THz fields. Already for a lower temperature of 80 K, Kaindl *et al.*[3] have reported thermal exciton ionization in linear THz absorption measurements to occur on a time scale of a few picoseconds after optical excitation. The resulting ionized excitons and unbound electron-hole pairs lead to vanishing internal intraexcitonic transitions for these time delays. In intense THz fields Steiner *et al.*[13] have calculated decreasing Rabi sidebands in the THz response with a decreasing fraction of 1s excitons coexisting with a fixed correlated electron-hole plasma. However, in our measurement the nonlinear response does not appear to suffer

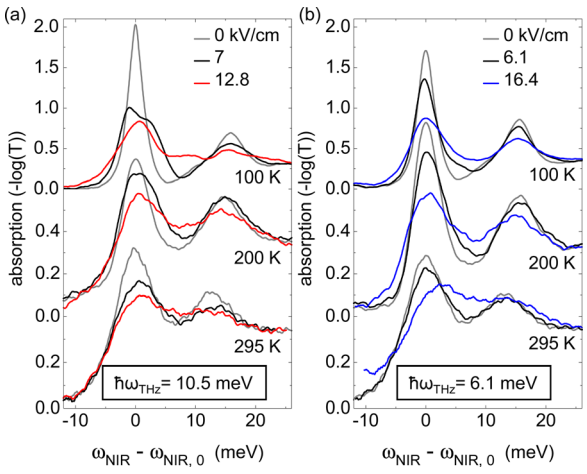

FIG. 2. (Color online) Lattice temperature-dependent NIR absorption traces for a THz photon energy of (a) 10.5 meV (near resonance) and (b) 6.1 meV (below resonance). Besides the undriven reference (gray line) two different THz peak field strengths are given as indicated in the legend.

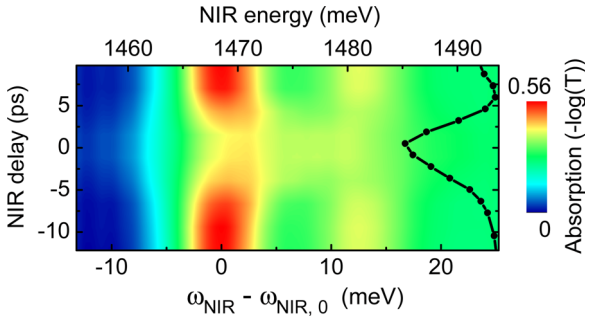

FIG. 3. (Color online) Absorption for different time delays between THz pump and NIR probe pulse at room temperature for an excitation near resonance (10.5 meV) at 14 kV/cm THz peak field strength. The vertical THz pulse profile on the right hand side is obtained from a NIR-THz cross-correlation measurement.

from thermal exciton ionization accompanied by a decaying 1s exciton population. Thermal broadening determines the linewidth of the observed Rabi sidebands but does not suppress them, since we probe a coherent effect insensitive to changes in the exciton population that occur after the probe pulse has passed.

Pumping above resonance (Fig. 1(c)) a transmission increase by a factor of 3 is found at 200 K at the hh(1s) spectral position and a 30% transmission change right below. This temperature is well in the range of Peltier cooling elements and demonstrates a possible concept for an optical modulator. At room temperature transmission increases by 60% for THz illumination at the hh(1s) exciton. These changes occur only in the presence of the driving THz pulse, as demonstrated in Fig. 3 for the near-resonant case at room temperature. Here, the synchronized NIR probe pulse is temporally shifted by time steps of 2.7 ps with respect to the THz pump pulse to obtain delay-dependent transmission spectra. These are compared to the THz pulse profile on the right hand side which is taken from the cross-correlation signal between NIR and THz pulse. It was detected in a 300 μm thin GaP crystal using intensity-based electro-optic sampling with a single Si photodiode.[17] The THz pulse length is consistent with the Fourier limit obtained from the spectrum. The adiabatic absorption change with constant signal height before and after the pulse on picosecond time scales also implies that excitons ionized by the strong THz field recover instantaneously when the THz pulse has vanished.

In conclusion, large changes in the NIR absorption of GaAs/AlGaAs quantum wells have been observed up to room temperature when the intraexcitonic 1s-2p transition is pumped. With strongest effects occurring when the system is driven above resonance, the distinct wavelength-dependent characteristics of the AC Stark effect can be distinguished up to 200 K. Demonstrated picosecond response times, thermal robustness of the excitonic system, a threefold transmission change at 200 K and a simple all-normal incidence geometry could be relevant for optical modulators. We emphasize that nonlinear optics of intraexcitonic transitions is still an active on-going field of research where other effects known from atomic physics such as high-harmonic generation have been predicted in the quasi-atomic excitonic system as well[13] but which are not yet proven experimentally.

The authors acknowledge A. M. Andrews and G. Strasser for sample growth and S. Schartner for processing the sample (all TU Vienna). We thank P. Michel, W. Seidel, and the FELBE Team for their dedicated support.

[1]R. Huber, R. A. Kaindl, B. A. Schmid, and D. S. Chemla, Phys. Rev. B **72**, 161314(R) (2005).
[2]I. Galbraith, R. Chari, S. Pellegrini, P. J. Phillips, C. J. Dent, A. F. G. van der Meer, D. G. Clarke, A. K. Kar, G. S. Buller, C. R. Pidgeon, B. N. Murdin, J. Allam, and G. Strasser, Phys. Rev. B **71**, 073302 (2005).
[3]R. A. Kaindl, D. Haegele, M. A. Carnahan, and D. S. Chemla, Phys. Rev. B **79**, 045320 (2009).
[4]R. Huber, B. A. Schmid, Y. R. Shen, D. S. Chemla, and R. A. Kaindl, Phys. Rev. Lett. **96**, 017402 (2006).
[5]K. Johnsen and A.-P. Jauho, Phys. Rev. Lett. **83**, 1207 (1999).
[6]A. Sell, A. Leitenstorfer, and R. Huber, Opt. Lett. **33**, 2767 (2008).
[7]Z. Chen, X. Zhou, C. A. Werley, and K. A. Nelson, Appl. Phys. Lett. **99**, 071102 (2011).
[8]J. Kono, M. Y. Su, T. Inoshita, T. Noda, M. S. Sherwin, S. J. Allen, and H. Sakaki, Phys. Rev. Lett. **79**, 1758 (1997).
[9]M. Wagner, H. Schneider, S. Winnerl, M. Helm, T. Roch, A. M. Andrews, S. Schartner, and G. Strasser, Appl. Phys. Lett. **94**, 241105 (2009).
[10]S. Leinss, T. Kampfrath, K. v. Volkmann, M. Wolf, J. T. Steiner, M. Kira, S. W. Koch, A. Leitenstorfer, and R. Huber, Phys. Rev. Lett. **101**, 246401 (2008).
[11]S. G. Carter, V. Birkedal, C. S. Wang, L. A. Coldren, A. V. Maslov, D. S. Citrin, and M. S. Sherwin, Science **310**, 651 (2005).
[12]A. D. Jameson, J. L. Tomaino, Y.-S. Lee, J. P. Prineas, J. T. Steiner, M. Kira, and S. W. Koch, Appl. Phys. Lett. **95**, 201107 (2009).
[13]J. T. Steiner, M. Kira, and S. W. Koch, Phys. Rev. B **77**, 165308 (2008).
[14]D. A. B. Miller, D. S. Chemla, T. C. Damen, A. C. Gossard, W. Wiegmann, T. H. Wood, and C. A. Burrus, Phys. Rev. B **32**, 1043 (1985).
[15]M. Wagner, H. Schneider, D. Stehr, S. Winnerl, A. M. Andrews, S. Schartner, G. Strasser, and M. Helm, Phys. Rev. Lett. **105**, 167401 (2010).
[16]D. Gammon, S. Rudin, T. L. Reinecke, D. S. Katzer, and C. S. Kyono, Phys. Rev. B **51**, 16785 (1995).
[17]G. M. H. Knippels, X. Yan, A. M. MacLeod, W. A. Gillespie, M. Yasumoto, D. Oepts, and A. F. G. van der Meer, Phys. Rev. Lett. **83**, 1578 (1999).

APPLIED PHYSICS LETTERS **100**, 012406 (2012)

Hysteretic anomalous Hall effect in a ferromagnetic, Mn-rich Ge:Mn nanonet

Danilo Bürger,[a] Shengqiang Zhou, Marcel Höwler, Xin Ou, György J. Kovacs, Helfried Reuther, Arndt Mücklich, Wolfgang Skorupa, Manfred Helm, and Heidemarie Schmidt

Institute of Ion Beam Physics and Materials Research, Helmholtz-Zentrum Dresden-Rossendorf, P.O. Box 510119, 01314 Dresden, Germany

(Received 25 August 2011; accepted 10 December 2011; published online 6 January 2012)

Ferromagnetic Ge:Mn has been fabricated by Mn implantation in intrinsic Ge wafers and by pulsed laser annealing with a pulse duration of 300 ns. Due to a segregation instability during laser annealing, Mn segregates at the liquid-solid interface and an approximately 40 nm thick Ge:Mn surface layer is strongly enriched with Mn. Plan-view images reveal a percolating Mn-rich nanonet. Hysteretic anomalous Hall effect has been observed up to 30 K, but it vanishes after etching away the 40 nm thick Mn-rich Ge:Mn surface layer. The nanonet seems to support the correlation between magnetization and hysteretic Hall resistance. Intrinsic scattering in the threads or vertices of this nanonet may lead to the observed anomalous Hall effect. © *2012 American Institute of Physics*. [doi:10.1063/1.3674981]

The fabrication of ferromagnetic semiconductors is one requisite step to realize semiconductor spintronic devices. Besides ferromagnetic GaAs:Mn, also Ge:Mn is a very interesting material for spintronics.[1–8] Electronic spin diffusion lengths larger than 100 μm have been demonstrated in Ge nanowires at 4.2 K.[9] Also electrical spin injection and transport have been demonstrated in weakly n-doped Ge up to 225 K.[10] In a previous work, we fabricated ferromagnetic Ge:Mn by Mn ion implantation and pulsed laser annealing (PLA) as a highly nonequilibrium method.[11] So far, PLA was applied to III-V semiconductors[6,7] and Ge:Mn.[8] Hysteretic Hall resistance has been observed in Ge:Mn at low temperatures.[11] Similarly to low temperature molecular beam epitaxy (LT-MBE),[1,3] the formation of Mn-rich ferromagnetic precipitates inside Ge:Mn has been observed. Especially, after PLA, the Mn segregation may lead to the formation of a Mn-rich surface layer.[11] In this work, we find that under specific PLA conditions and Mn implantation parameters, the Mn segregation at the liquid-solid interface leads to the formation of a percolating, Mn-rich, Ge:Mn nanonet in the 5–40 nm depth range. We applied chemical and physical etching to confirm the contribution of the nanonet to the observed correlated magnetization and hysteretic anomalous Hall effect.

Mn has been implanted in highly resistive (nearly intrinsic) n-type (001)-Ge wafers with liquid nitrogen cooling with a maximum implantation depth of 180 nm. PLA was performed by a scanning laser with 10 kHz repetition frequency, 40 μm × 2 mm large laser stripes and 75% modal overlap between adjacent laser stripes. The outcome of this is a lateral annealing periodicity of around 10 μm. Further details about the sample fabrication can be found in Ref. 11. Fig. 1 presents the Auger spectra that show the depth dependent Mn concentration from the surface into the sample (from left to right) for two different electron beam diameters, namely 1 μm and 15 μm. The relative error for the depth information amounts to ca. 30%. After PLA, the strong segregation of Mn within an only few nm thick surface layer of the Ge:Mn film is clearly visible. A second maximum in the depth dependent Mn concentration is visible at a depth of 60 nm for an AES spot diameter of 1 μm. That is a clear indication for a lateral variation of the depth distribution of Mn caused by the variation of the laser energy density. The inset of Fig. 1 presents the temperature dependent remanence of this sample after PLA measured by SQUID. The remanence strongly drops up to 30 K. Between 40 K and 120 K, the remanence is very sensitive

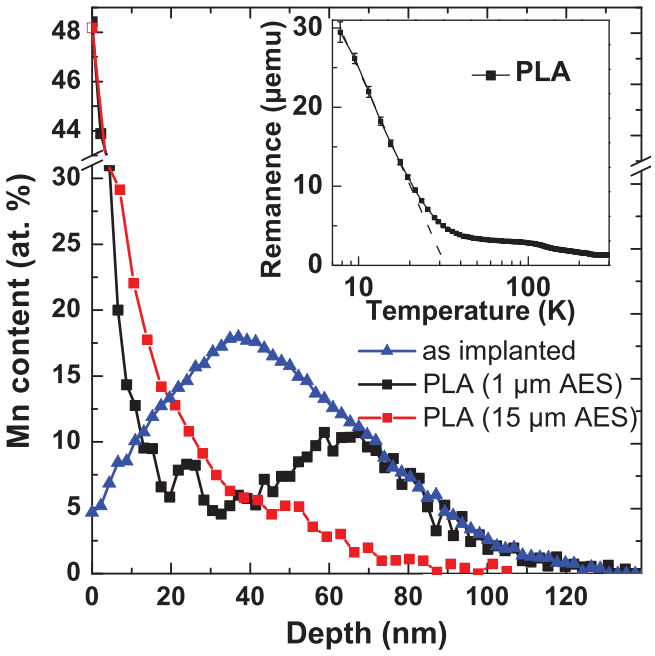

FIG. 1. (Color online) Auger electron spectroscopy measurements performed on the as-implanted Ge:Mn and the PLA Ge:Mn. The measurements with a 15 μm broad electron beam (15 μm AES) show a clear segregation of Mn towards the surface. Locally (1 μm AES) there exists also a slightly different Mn-distribution after PLA due to the lateral annealing periodicity of 10 μm. The inset shows the temperature dependent magnetic remanence of the Ge:Mn film after PLA from temperature dependent SQUID measurements.

[a]Electronic mail: d.buerger@hzdr.de.

towards small residual fields in the SQUID. Therefore, the measurement presented in the inset of Fig. 1 was performed after a complete warm up and cool down process of the SQUID system to prevent trapped magnetic flux in the SQUID coils. Small residual positive (negative) fields (5 Oe) lead to a larger (smaller) remanence. Above 120 K, the remanence measured by SQUID at small positive/negative fields is similar and vanishes at 220 K. Long time annealing (35 min) at 180 °C under Ar atmosphere increases the Curie temperature from 220 K to 250 K.[12] The temperature dependence of the remanence does not change if a 10 nm thick surface layer is etched away. Zero-field-cooled/field-cooled and M-T measurements after 10 nm etching show a similar behavior as already presented in Ref. 11. Therefore, we first recommend magnetotransport measurements to bring out the influence of specific PLA conditions on the properties of ferromagnetic Ge:Mn.

The AES data well agree with the results from transmission electron microscopy (TEM) measurements that are discussed in the following. TEM measurements were performed with a 300 kV Cs-corrected FEI Titan TEM device. Fig. 2 shows the plan-view (etched and non-etched) and the cross-section (XTEM) morphology of the annealed Ge:Mn film in detail. The film is covered by a thin polycrystalline Ge:Mn layer with a thickness of around 4 nm below the carbon glue (Fig. 2(a)). Fig. 2(b) shows the XTEM on a larger scale. Due to the amorphization during preparation of the XTEM sample, the polycrystalline character of this layer is only visible in the plan-view as shown in Fig. 2(c). A typical diffraction pattern of the plan-view TEM image is shown in Fig. 2(d). The diffraction rings can be assigned to Ge_2Mn_5 phases embedded in the top of the film, i.e., the approx. 4 nm thick top layer. The presence of other known Ge:Mn phases is very unlikely. Below this approx. 4 nm thick top layer, an approx. 35 nm thick layer consisting of a single-crystalline Ge:Mn matrix and Mn-rich tadpole-shaped precipitates[13] is visible (Figs. 2(a) and 2(b)). The nearly regular distribution of the tadpole-shaped precipitates (Fig. 2(b)) can be interpreted as a cut through a regularly formed nanonet. This becomes visible in the high angle annular dark field (HAADF) plan-view image[14] after etching the top 10 nm thick surface layer away (Figs. 2(e) and 2(f)). The nanonet is not visible in the non-etched plan-view sample because most probably a dephasing of the electron wave in the 4 nm thick polycrystalline top layer masks the structure of the underlying nanonet. For quantitative understanding of the TEM contrast appropriate TEM image simulation is necessary. In the single crystalline Ge:Mn surrounded by the nanonet in a depth of around 10 nm, the Mn concentration lies below the energy dispersive X-ray spectroscopy (EDX) detection limit of 10%. The amorphous nanonet contains more than 50 at. % Mn. This was determined by EDX measurements in XTEM. Moreover, EDX measurements were also performed in plan-view geometry. The results show that Mn is only detected at the analysing point 2 (Fig. 2(e)). The formation of similar structures has been experimentally observed and theoretically described by Narayan[15] for pulsed laser annealed silicon after ion implantation.

To clarify the contribution of the 4 nm thick Ge_2Mn_5 top layer and of the nanonet in a depth from 5 to 40 nm to the transport properties, it is necessary to remove them in two steps. Chemical etching as reported in Ref. 16 preferentially removes the 4 nm thick Ge_2Mn_5 layer and the Mn-rich nanonet and leaves the single crystalline Ge:Mn matrix behind.[12] We also used physical ion beam etching to homogeneously etch away the top 10 nm and 40 nm layers in two steps. The etching was done with 300 eV Ar^+ ions under an angle of 3° to the surface using the ion beam tool IonSys500 from Roth & Rau. The determined etching rate with an applied ion current of 34 $\frac{\mu A}{cm^2}$ was 2 nm/min. Smooth Ge:Mn surface etching was achieved by rotating the sample 10 times per minute during etching. After etching away 40 nm, nearly the entire nanonet was removed.[12]

The magnetotransport measurements were performed with a 9 T Hall measurement system from Lakeshore in van

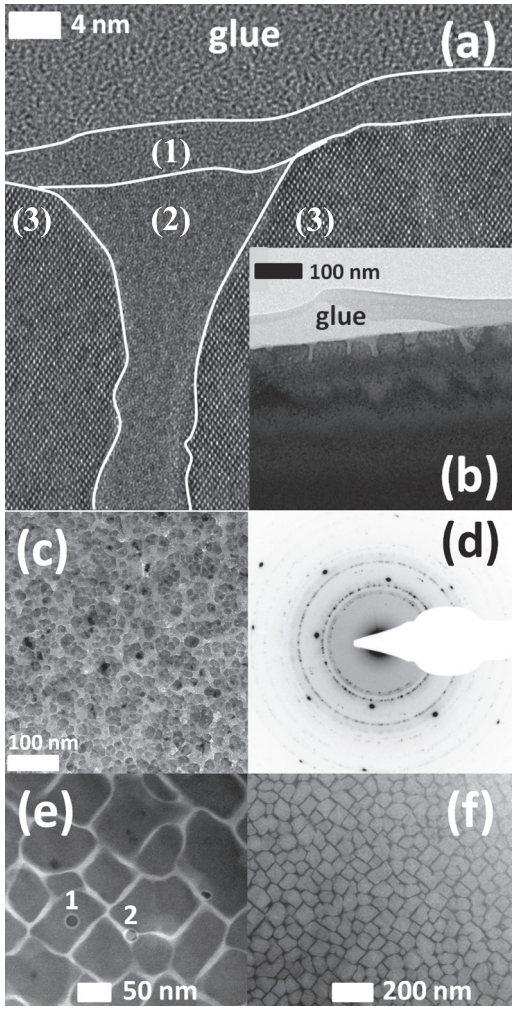

FIG. 2. TEM images of Mn implanted Ge annealed with PLA. (a) In the high resolution XTEM image, an approx. 4 nm thick polycrystalline layer is visible on top of the Ge:Mn film (1). The tadpole-shaped precipitate (2) is embedded in the crystalline Ge:Mn matrix (3). The white lines are guides to the eye. (b) An overview over nearly regularly distributed tadpole-shaped precipitates. (c) A plan-view image shows Mn-rich phases on top of the Ge:Mn film before etching. (d) The rings of the diffraction pattern from (c) can be assigned to nearly randomly oriented Ge_2Mn_5. (e) The HAADF plan-view image after etching reveals the Mn-rich amorphous Ge:Mn nanonet. EDX analysis on crystalline Ge:Mn (point 1) shows no detectable Mn, whereas EDX on the nanonet (point 2) reveals more than 50% Mn. (f) The conventional TEM image of the percolated Mn-rich nanonet reveals vertices with three and four threads.

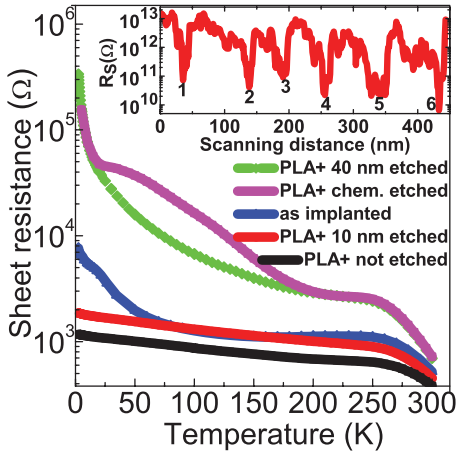

FIG. 3. (Color online) Sheet resistance of the as implanted, pulsed laser annealed Ge:Mn and after etching away a 10 nm and a 40 nm thick surface layer. After etching away 40 nm, there is an overall increase in the sheet resistance similar to the chemically etched Ge:Mn. This indicates that the polycrystalline Mn-rich top layer and the underlying nanonet are mainly responsible for the electrical properties in PLA Ge:Mn. The inset shows the SSRM data probed on a 450 nm long section line in the center of the 10 nm etched sample.

der Pauw geometry after implantation and annealing, and after etching. After annealing, the sheet resistance is smallest in the entire temperature range compared to the as-implanted and etched Ge:Mn sample (Fig. 3). After etching away the top 10 nm, the sheet resistance increases by a factor of 1.5 at 5 K. Further etching down to a depth of 40 nm and also chemical etching increases the sheet resistance by nearly two orders of magnitude at 5 K. These results indicate that the polycrystalline Mn-rich 4 nm thick top layer and the Mn-rich amorphous nanonet are highly conducting. An insulating behavior down towards low temperatures can only be observed without the percolating nanonet. Between 20 K and 200 K, the chemically etched sample shows an even higher sheet resistance. The difference possibly originates from the 4 nm thick amorphous layer on top of the physically etched film. Independent from TEM measurements, the successful removal of the nanonet has been confirmed by SQUID magnetization measurements. The saturation magnetic moment decreases by approx. 5% after 10 nm etching, by 70% after 40 nm etching and by 90% after chemical etching. Above 270 K, the drop of the sheet resistance for all samples can be fitted with a thermal activation energy close to 0.4 eV most probably due to the intrinsic conduction of Ge. A direct evidence for the percolating nature of the higher conductivity of the nanonet compared to the substrate has been observed by room temperature scanning spreading resistance microscopy (SSRM) measurements on a 10 nm etched sample. During SSRM, the current locally flows between the SSRM measurement position in the center of the quadratic sample (area 25 mm^2) and the sputtered gold contact at one edge of the sample.[17] The inset of Fig. 3 shows a 450 nm long linescan with a spatial resolution of around 4 nm. Six sharp drops of the spreading resistance R_S by two orders of magnitude have been found. This result can be expected from the TEM plan-view measurements and directly confirms the percolating nature of the highly conductive nanonet.

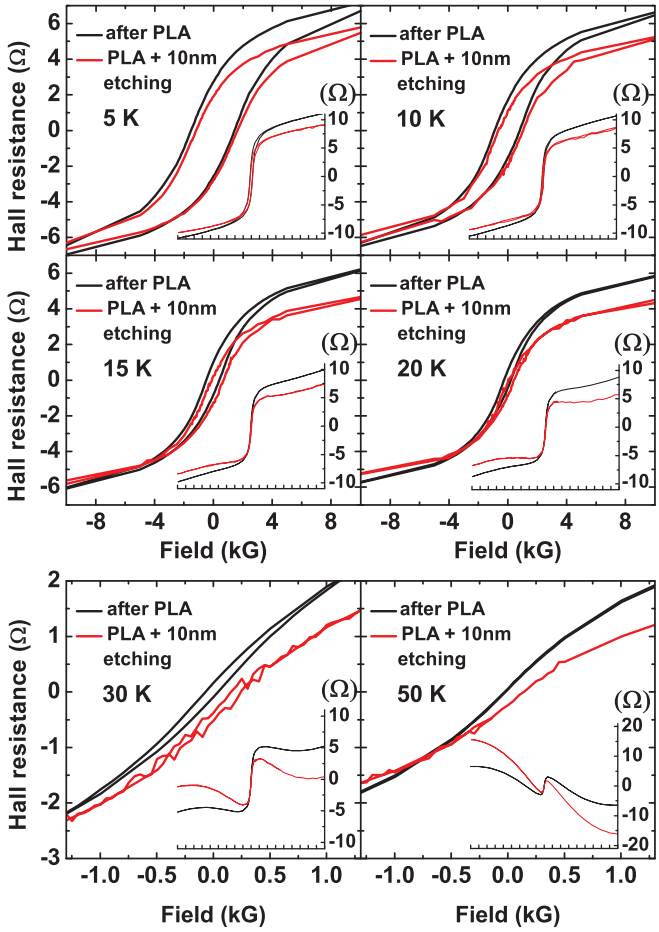

FIG. 4. (Color online) Hall resistance of Mn implanted Ge after PLA and after etching away 10 nm. The insets show an overview of the Hall resistance (in units of Ω) for both samples from −9 T to 9 T. A clear hysteresis at 30 K is visible for the non-etched sample, whereas 10 nm etching leads to a vanishing hysteresis at 30 K. At higher temperatures, the n-type substrate seems to influence the Hall resistance. The results indicate that the nanonet is responsible for the hysteretic anomalous Hall effect.

As it can be seen in Fig. 4, a clear hysteresis up to 30 K is visible in the Hall resistance for samples after PLA and after etching away 10 nm. This temperature correlates with the temperature above which the magnetic remanence of the nanonet has strongly decreased (shown in the inset of Fig. 1). The insets show the Hall resistance from −9 T up to +9 T. Due to the n-Ge substrate and/or the conductive nanonet, the Hall resistance of the 10 nm etched sample slightly changes at low temperatures which becomes more visible at 30 K and 50 K. Up to 30 K, a negative magnetoresistance is observed in the weak field region.[12] The magnetoresistance becomes positive when the hysteresis in the Hall resistance clearly vanishes. The Hall resistance measured on the sample after 40 nm etching reveals no hysteresis. The observed n-type conductivity reflects the influence of the n-doped substrate.[12,18] The n-type sheet carrier concentration of the PLA sample after etching 40 nm and of the virgin n-Ge substrate are similar and increase from around $10^{10}\,cm^{-2}$ to $10^{12}\,cm^{-2}$ between 5 K and 300 K, respectively. Layers deeper than 40 nm do not seem to contain a significant amount of electrically active Mn acceptors. Otherwise, p-type sheet carrier concentrations above $10^{15}\,cm^{-2}$ should be measured. Therefore, the hysteretic Hall resistance has its origin in the top Ge:Mn layer which consists of the

nanonet embedded in the single crystalline Ge. Guided by these findings, it can be assumed that the highly conductive nanonet strongly influences the transport properties. There exist two possible explanations for the observed hysteretic Hall resistance depending on the spin diffusion length. First, the free charge carriers in Ge:Mn are spin-polarized in the threads of the nanonet. In that case, only a relatively small spin diffusion length would be necessary. Second, the free charge carriers are subjected to preferential spin scattering in the vertices of the nanonet. In this case, the spin diffusion length has to be at least on the scale of the distance between two neighbouring vertices.

To summarize our observations, the structure and magnetotransport properties of Mn-implanted and pulsed laser annealed Ge:Mn have been investigated after different etching steps. During the PLA process, an embedded amorphous nanonet can be formed. After etching away the top 10 nm and the Mn-rich nanonet, the three main layers can be characterized as follows: A top layer including polycrystalline Ge_2Mn_5, a second, approx. 35 nm thick layer consisting of a Mn-rich nanonet embedded in crystalline Ge:Mn, and below that single crystalline Ge:Mn with a low Mn concentration. Intense research in the field of a controllable decomposition of Ge:Mn into Mn-rich areas with a large Curie temperature and the coupling to hysteretic anomalous Hall effects are of high interest.[19] Here, we present a new class of synthesized Ge:Mn that shows hysteretic magnetotransport and correlated magnetization. In the future, the formation of laterally grown Mn-rich nanonets may be optimized with respect to the Mn concentration and distribution and also by the pulsed laser annealing or postannealing conditions, in order to recrystallize the amorphous net and to increase the temperature up to which correlated magnetization and hysteretic anomalous Hall effects may be observed. By combining Mn-rich nanocolumnar growth from LT-MBE and lateral Mn-rich nanonet growth from pulsed laser annealing, three dimensional Mn-rich nanonetworks may be formed in Ge:Mn for spintronics applications.

The authors (D.B., G.J.K., and H.S) acknowledge financial funding from the Bundesministerium für Bildung und Forschung (FKZ13N10144). S.Z. thanks the funding from the Helmholtz-Gemeinschaft Deutscher Forschungszentren (HGF-VH-NG-713). We also thank Peter Oesterlin for pulsed laser annealing.

[1]M. Jamet, A. Barski, T. Devillers, V. Poydenot, R. Dujardin, P. Bayle-Guillemaud, J. Rothman, E. Bellet-amalric, A. Marty, J. Cibert *et al.* Nature Mater. **5**, 653 (2006).
[2]Y. D. Park, A. T. Hanbicki, S. C. Erwin, C. S. Hellberg, J. M. Sullivan, J. E. Mattson, T. F. Ambrose, A. Wilson, G. Spanos, and B. T. Jonker, Science **295**, 651 (2002).
[3]D. Bougeard, S. Ahlers, A. Trampert, N. Sircar, and G. Abstreiter, Phys. Rev. Lett. **97**, 237202 (2006).
[4]L. Ottaviano, A. Continenza, G. Profeta, G. Impellizzeri, A. Irrera, R. Gunnella, and O. Kazakova, Phys. Rev. B **83**, 134426 (2011).
[5]Y.-F. Qin, S.-S. Yan, S.-Q. Xiao, Q. Li, Z.-K. Dai, T.-T. Shen, S.-S. Kang, Y.-Y. Dai, G.-L. Liu, Y.-X. Chen, and L.-M. Mei, J. Appl. Phys. **109**, 083906 (2011).
[6]M. A. Scarpulla, B. L. Cardozo, R. Farshchi, W. M. H. Oo, M. D. McCluskey, K. M. Yu, and O. D. Dubon, Phys. Rev. Lett. **95**, 207204 (2005).
[7]M. A. Scarpulla, O. D. Dubon, K. M. Yu, O. Monteiro, M. R. Pillai, M. J. Aziz, and M. C. Ridgway, Appl. Phys. Lett. **82**, 1251 (2003).
[8]M. C. Dolph, T. Kim, W. Yin, D. Recht, W. Fan, J. Yu, M. J. Aziz, J. Lu, and S. A. Wolf, J. Appl. Phys. **109**, 093917 (2011).
[9]E.-S. Liu, J. Nah, K. M. Varahramyan, and E. Tutuc, Nano Lett. **10**, 3297 (2010).
[10]Y. Zhou, W. Han, L.-T. Chang, F. Xiu, M. Wang, M. Oehme, I. A. Fischer, J. Schulze, R. K. Kawakami, and K. L. Wang, Phys. Rev. B **84**, 125323 (2011).
[11]S. Zhou, D. Bürger, A. Mücklich, C. Baumgart, W. Skorupa, C. Timm, P. Oesterlin, M. Helm, and H. Schmidt, Phys. Rev. B **81**, 165204 (2010).
[12]See supplementary material at http://dx.doi.org/10.1063/1.3674981 for (1) further TEM measurements, (2) further magnetotransport results, and (3) further SQUID-magnetization measurements.
[13]Y. Wang, F. Xiu, J. Zou, K. L. Wang, and A. P. Jacob, Appl. Phys. Lett. **96**, 051905 (2010).
[14]Normally, the intensity of the HAADF image can be used for mapping elements. Heavy elements, e.g., Ge in comparison to Mn, scatter electrons to higher angles. Therefore, the HAADF image becomes bright at positions which contain more heavy elements. In our case, this explanation cannot be applied because the morphology also plays an important role and Mn-rich regions are amorphous in our samples. Therefore, the brightness of the HAADF image is no indication for Mn-rich or Mn-poor regions.
[15]J. Narayan, J. Appl. Phys. **52**, 1289 (1981).
[16]P. Gambardella, L. Claude, S. Rusponi, K. J. Franke, H. Brune, J. Raabe, F. Nolting, P. Bencok, A. T. Hanbicki, B. T. Jonker, C. Grazioli, M. Veronese, and C. Carbone, Phys. Rev. B **75**, 125211 (2007).
[17]X. Ou, P. D. Kanungo, R. Kögler, P. Werner, U. Gösele, W. Skorupa, and X. Wang, Nano Lett. **10**, 171 (2010).
[18]N. Sircar, S. Ahlers, C. Majer, G. Abstreiter, and D. Bougeard, Phys. Rev. B **83**, 125306 (2011).
[19]I.-S. Yu, M. Jamet, T. Devillers, A. Barski, P. Bayle-Guillemaud, C. Beigné, J. Rothman, V. Baltz, and J. Cibert, Phys. Rev. B **82**, 035308 (2010).

PHYSICAL REVIEW B **85**, 134417 (2012)

Control of vortex pair states by post-deposition interlayer exchange coupling modification

Sebastian Wintz,[1,*] Thomas Strache,[1,†] Michael Körner,[1] Christopher Bunce,[1,‡] Anja Banholzer,[1] Ingolf Mönch,[2] Roland Mattheis,[3] Jörg Raabe,[4] Christoph Quitmann,[4] Jeffrey McCord,[1,§] Artur Erbe,[1] Kilian Lenz,[1] and Jürgen Fassbender[1]

[1]*Helmholtz-Zentrum Dresden-Rossendorf, 01328 Dresden, Germany*

[2]*Institute for Integrative Nanosciences, IFW Dresden, 01069 Dresden, Germany*

[3]*Institut für Photonische Technologien, 07702 Jena, Germany*

[4]*Swiss Light Source, Paul Scherrer Institut, 5232 Villigen, Switzerland*

(Received 27 January 2012; revised manuscript received 22 March 2012; published 9 April 2012)

We report on both the global and micromagnetic properties of interlayer exchange coupled spin systems. Irradiation with Ne ions is employed to achieve a phase transition from antiferromagnetic to ferromagnetic coupling. For extended trilayer films a full quantitative analysis of the bilinear and biquadratic coupling constants is performed. With increasing ion fluence we observe a steady increase of the bilinear coupling constant at an almost negligible decrease in saturation magnetization. The mixing of atoms at the layer interfaces is identified as the origin for this. The effects of ion modification on the magnetic microstructure are studied for the model system of layered vortex pairs. X-ray microscopy is used to directly image the individual magnetization circulations in trilayer disks. The circulation configuration is found to be determined by the film coupling for both coupling orientations with a homogenous coupling angle throughout the structure. For the vortex cores, however, micromagnetic simulations indicate that due to the significant local demagnetization fields, parallel states are always energetically preferred. Nevertheless antiparallel configurations are metastable, having their signature in reduced core diameters. Our study provides new results on spin structures in interlayer exchange coupled trilayers and it demonstrates a promising way to control the local interlayer coupling post-deposition.

DOI: 10.1103/PhysRevB.85.134417 PACS number(s): 75.70.Kw, 81.40.Rs, 75.75.−c, 68.37.Yz

IOP Publishing Nanotechnology
Nanotechnology **23** (2012) 485204 (8pp) doi:10.1088/0957-4484/23/48/485204

InP nanocrystals on silicon for optoelectronic applications

Slawomir Prucnal[1,2], Shengqiang Zhou[1], Xin Ou[1], Helfried Reuther[1], Maciej Oskar Liedke[1,3], Arndt Mücklich[1], Manfred Helm[1], Jerzy Zuk[2], Marcin Turek[2], Krzysztof Pyszniak[2] and Wolfgang Skorupa[1]

[1] Institute of Ion Beam Physics and Materials Research, Helmholtz-Zentrum Dresden-Rossendorf, PO Box 510119, D-01314 Dresden, Germany
[2] Maria Curie-Sklodowska University, Pl. M. Curie-Sklodowskiej 1, 20-035 Lublin, Poland

E-mail: s.prucnal@hzdr.de

Received 5 July 2012, in final form 8 October 2012
Published 9 November 2012
Online at stacks.iop.org/Nano/23/485204

Abstract
One of the solutions enabling performance progress, which can overcome the downsizing limit in silicon technology, is the integration of different functional optoelectronic devices within a single chip. Silicon with its indirect band gap has poor optical properties, which is its main drawback. Therefore, a different material has to be used for the on-chip optical interconnections, e.g. a direct band gap III–V compound semiconductor material. In the paper we present the synthesis of single crystalline InP nanodots (NDs) on silicon using combined ion implantation and millisecond flash lamp annealing techniques. The optical and microstructural investigations reveal the growth of high-quality (100)-oriented InP nanocrystals. The current–voltage measurements confirm the formation of an n–p heterojunction between the InP NDs and silicon. The main advantage of our method is its integration with large-scale silicon technology, which allows applying it for Si-based optoelectronic devices.

(Some figures may appear in colour only in the online journal)

IOP PUBLISHING NANOTECHNOLOGY
Nanotechnology **23** (2012) 475304 (7pp) doi:10.1088/0957-4484/23/47/475304

Taming of Ga droplets on DLC layers—size tuning and local arrangement with nanometer accuracy

Peter Philipp, Lothar Bischoff and Bernd Schmidt

Institute of Ion Beam Physics and Materials Research, Helmholtz-Zentrum Dresden-Rossendorf, Germany

E-mail: p.philipp@hzdr.de

Received 6 July 2012, in final form 24 September 2012
Published 1 November 2012
Online at stacks.iop.org/Nano/23/475304

Abstract
A new method for the fabrication of spherical gallium nanoparticles (Ga-NPs) on diamond-like carbon (DLC) layers with high precision in their desired diameter and positioning is presented. The basic principle is the pre-patterning of a DLC film by focused Ga^+ ion beam irradiation and subsequent annealing. During thermal treatment the evolution of single Ga-NPs with spherical shape on irradiated areas is driven by phase separation and surface segregation of Ga from the supersaturated DLC layer. The shape and size of the implanted areas as well as the ion fluence serve as a Ga reservoir for the nanoparticle (NP) evolution which is strongly correlated with the NP diameter. For the formation of segregation seeds to avoid random segregation of the NPs small spots are additionally implanted with Ga within the irradiated areas. The NP evolution is then assessed with respect to the seed position and the material for the Ga-NP growth is gathered from the surrounding reservoir. Using this technique Ga-NPs were fabricated with a diameter ranging from 40 nm up to several hundred nm. Prospective applications, i.e. in the field of plasmonics, arise from the arrangement in chains as well as in periodical two-dimensional arrays with defined NP size and interparticle distance.

(Some figures may appear in colour only in the online journal)

A Letters Journal Exploring the Frontiers of Physics

April 2012

EPL, **98** (2012) 16009
doi: 10.1209/0295-5075/98/16009

www.epljournal.org

Quantitative analysis of the order of Bi ion induced dot patterns on Ge

R. Böttger[(a)], L. Bischoff, S. Facsko and B. Schmidt

Institute of Ion Beam Physics and Materials Research, Helmholtz-Zentrum Dresden-Rossendorf - POB 51 01 19, D-01328 Dresden, Germany, EU

received 14 December 2011; accepted in final form 9 March 2012
published online 11 April 2012

PACS 62.23.Eg – Nanodots
PACS 07.05.Pj – Image processing
PACS 05.65.+b – Self-organized systems

Abstract – We demonstrate that the temperature-dependent focused ion beam irradiation of (100) Ge surfaces with 20 keV Bi^+ ions leads to variably ordered hexagonal dot patterns. We show that the average information gain about the spatial order can be significantly increased by image preprocessing transforming the power spectral density into the pair correlation function. Order parameters are derived from the pair correlation function for the comparison of highly ordered patterns.

THE JOURNAL OF PHYSICAL CHEMISTRY C
Article
pubs.acs.org/JPCC

Environment Controlled Dewetting of Rh−Pd Bilayers: A Route for Core−Shell Nanostructure Synthesis

Gintautas Abrasonis,*[,†] Sebastian Wintz,[†] Maciej O. Liedke,[†] Funda Aksoy Akgul,[‡,§] Matthias Krause,[∥] Karsten Kuepper,[⊥] Dipanjan Banerjee,[#,▽] Zhi Liu,[‡] and Sibylle Gemming[†]

[†]Institute of Ion Beam Physics and Materials Research, Helmholtz-Zentrum Dresden-Rossendorf, P.O. Box 51 01 19, 01314 Dresden, Germany

[‡]Advanced Light Source, Lawrence Berkeley National Laboratory, Berkeley, California 94720, United States

[§]Physics Department, Nigde University, 51240 Nigde, Turkey

[∥]Institut für Festkörperphysik, Technische Universität Dresden, 01062 Dresden, Germany

[⊥]Institute of Solid State Physics, University of Ulm, Albert-Einstein-Allee 11, 89069 Ulm, Germany

[#]Institute of Resource Ecology, Helmholtz-Zentrum Dresden-Rossendorf, 01314 Dresden, Germany

[▽]The Rossendorf Beamline (ROBL), European Synchrotron Radiation Facility (ESRF), BP 220, 38043 Grenoble, France

Supporting Information

ABSTRACT: Chemical environment plays a significant role on the size, shape, or surface composition of nanostructures. Here, the chemical environment effects are studied in the context of core−shell nanoparticle synthesis. The environment driven dynamics and kinetics of Rh/Pd bilayers is investigated by in situ ambient pressure X-ray photoelectron spectroscopy. Thin Rh (∼1.5 nm)/Pd (∼ 1.5 nm) bilayers were grown on thermally oxidized Si substrates. The films were heated in CO or NO environments or heated in vacuum with a subsequent NO/CO cycling. This study demonstrates that not the initial stacking sequence but the chemical environment plays a crucial role in controlling the surface composition. Heating in CO results in a surface enrichment of Pd at ∼200 °C and is followed by film dewetting at ∼300 °C. Heating in NO results in progressive oxidation of Rh starting at ∼150 °C, which stabilizes the film continuity up to >∼375 °C. The film rupture correlates with the thermal destabilization of the surface oxide. Heating in vacuum results in a significant increase in surface Pd concentration, and the following NO/CO cycling induces periodic surface composition changes. The quasi-equilibrium states are ∼50% and ∼20% of Rh/(Rh + Pd) for NO and CO environments, respectively. Possible surface composition change and dewetting mechanisms are discussed on the basis of the interplay of thermodynamic (surface/oxide energy and surface wetting) and kinetic (surface oxidation and thermally induced and chemically enhanced diffusion) factors. The results open alternative ways to synthesize supported (core−shell) nanostructures with controlled morphology and surface composition.

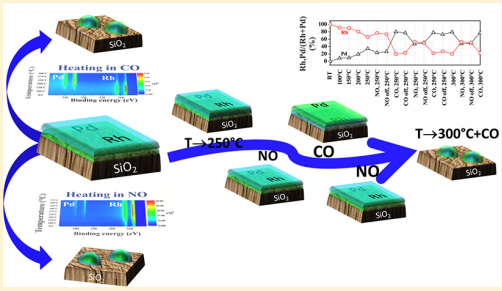

New Journal of Physics
The open-access journal for physics

Universal phase relation between longitudinal and transverse fields observed in focused terahertz beams

S Winnerl[1,3], R Hubrich[1], M Mittendorff[1,2], H Schneider[1] and M Helm[1,2]

[1] Helmholtz-Zentrum Dresden-Rossendorf, PO Box 510119, 01314 Dresden, Germany
[2] Technische Universität Dresden, 01062 Dresden, Germany
E-mail: s.winnerl@hzdr.de

New Journal of Physics **14** (2012) 103049 (12pp)
Received 6 September 2012
Published 30 October 2012
Online at http://www.njp.org/
doi:10.1088/1367-2630/14/10/103049

Abstract. We directly observe longitudinal electromagnetic fields in focused freely propagating terahertz (THz) beams of radial and linear polarization. Employing electro-optic detection, which is phase sensitive, allows one to selectively detect longitudinal and transverse field components. A phase shift of $\pi/2$ between the transverse and longitudinal field components is revealed. This phase shift is of universal nature, as it does not depend on the mode, frequency and focusing conditions. We show that the universal phase relation is a direct consequence of the divergence-free nature of electromagnetic waves in vacuum. In the experiments, we observe the phase shift of $\pi/2$ for all frequency components of single-cycle THz radiation pulses of both radial and linear polarization. Additionally, we show that the longitudinal field of a radially polarized THz beam has a smaller spot size as compared with the transverse field of a linearly polarized beam that is focused under the same conditions. For field-sensitive measurements this property can be exploited even for moderate focusing conditions. Furthermore, the phase-sensitive detection of longitudinal electromagnetic fields opens up new possibilities to study their interaction with electronic excitations in semiconductor nanostructures.

[3] Author to whom any correspondence should be addressed.

Journal of Nuclear Materials 428 (2012) 139–146

Contents lists available at SciVerse ScienceDirect

Journal of Nuclear Materials

journal homepage: www.elsevier.com/locate/jnucmat

Nanoscale characterization of ODS Fe–9%Cr model alloys compacted by spark plasma sintering

C. Heintze [a,*], M. Hernández-Mayoral [b], A. Ulbricht [a], F. Bergner [a], A. Shariq [c], T. Weissgärber [d], H. Frielinghaus [e]

[a] Helmholtz-Zentrum Dresden-Rossendorf, Germany
[b] CIEMAT, Madrid, Spain
[c] Fraunhofer-Center for Nanoelectronic Technologies, Dresden, Germany
[d] Fraunhofer-Institut IFAM, Dresden, Germany
[e] Jülich Centre for Neutron Science, Forschungszentrum Jülich, Garching, Germany

ARTICLE INFO

Article history:
Available online 21 September 2011

ABSTRACT

Ferritic/martensitic high-chromium steels are leading candidates for fission and fusion reactor components. Oxide dispersion strengthening is an effective way to improve properties related to thermal and irradiation-induced creep and to extend their elevated temperature applications. An extensive experimental study focusing on the microstructural characterization of oxide-dispersion strengthened Fe–9wt%Cr model alloys is reported. Several material variants were produced by means of high-energy milling of elemental powders of Fe, Cr and commercial yttria powders. Consolidation was based on spark plasma sintering. Special emphasis is placed on the characterization of the nano-particles using transmission electron microscopy, small-angle neutron scattering and atom probe tomography. The microstructure of the investigated alloys and the role of the process parameters are discussed. Implications for the reliability of the applied characterization techniques are also highlighted.

Statistics

Image: AIFilm

Publications and patents

Books and chapters

1. Altstadt, E.
Lower head failure
In: Sehgal, B.R. (Ed.); Nuclear Safety in Light Water Reactors: Severe Accident Phenomenology, Amsterdam: Academic Press Elsevier, 2012, 145-155

2. Butterling, M.; Bergner, F.; Heintze, C.; Anwand, W.; Ulbricht, A.
Application of positron annihilation spectroscopy to irradiated Fe-Cr alloys
In: Ganguly, B.N.; Brauer, G. (Eds.); Near Surface Depth Profiling by Mono-Energetic Positrons, Switzerland: Trans Tech Publisher, 2012, 165-179

3. Čížek, J.; Prochazka, I.; Kuriplach, J.; Anwand, W.; Brauer, G.; Cowan, T. E.; Grambole, D.; Schmidt, H.; Skorupa, W.
Characterization of H-plasma treated ZnO crystals by positron annihilation and atomic force microscopy
In: Ganguly, B.N.; Brauer, G. (Eds.); Near Surface Depth Profiling by Mono-Energetic Positrons, Switzerland: Trans Tech Publisher, 2012, 113-125

4. Čížek, M. Vlček; Lukáč, F.; Melikhova, O.; Procházka, I.; Anwand, W.; Butterling, M.; Wagner, A.; Brauer, G.
Low background digital coincidence spectrometer – A tool for investigation of positron annihilation in flight
In: Ganguly, B.N.; Brauer, G. (Eds.); Near Surface Depth Profiling by Mono-Energetic Positrons, Switzerland: Trans Tech Publisher, 2012, 53-73

5. Čížek, M. Vlček; Lukáč, F.; Vlach, M.; Prochazka, I.; Brauer, G.; Anwand, W.; Muecklich, A.; Wagner, S.; Uchida, H.; Pundt, A.
Structural studies of nanocrystalline thin Pd films electrochemically doped with hydrogen
In: Ganguly, B.N.; Brauer, G. (Eds.); Near Surface Depth Profiling by Mono-Energetic Positrons, Switzerland: Trans Tech Publisher, 2012, 137-147

6. Drachenko, O.; Helm, M.
Cyclotron resonance spectroscopy
In: Patane A., Balkan, N. (Eds.); Semiconductor Research, Berlin-Heidelberg: Springer-Verlag, 2012, 283-307

7. Foerst, M.; Hoffmann, M.; Dienst, A.; Kaiser, S.; Rini, M.; Tobey, R. I.; Gensch, M.; Manzoni, C.; Cavalleri, A.
THz control in correlated electron solids: sources and applications
In: Peiponen, K.-E.; Zeitler, A.; Kuwata-Gonokami, M. (Eds): Terahertz Spectroscopy and Imaging, Springer Series in Optical Sciences Vol. 171, Berlin Heidelberg: Springer-Verlag, 2012

8. Kögler, R.; Anwand, W.; Richter, A.; Butterling, M.; Mücklich, A.; Ou, X.; Reuther, H.; Chen, C.-L.; Wagner, A.
Investigation of dual-beam-implanted oxide-dispersed-strengthened FeCrAl alloy by positron annihilation spectroscopy
In: Ganguly, B.N.; Brauer, G. (Eds.); Near Surface Depth Profiling by Mono-Energetic Positrons, Switzerland: Trans Tech Publisher, 2012, 149-163

9. Potzger, K.; Liedke, M.
Application of positron beams to the investigation of memristive materials and diluted magnetic semiconductors
In: Ganguly, B.N.; Brauer, G. (Eds.); Near Surface Depth Profiling by Mono-Energetic Positrons, Switzerland: Trans Tech Publisher, 2012, 235-251

Publications in journals

1. Abd El-Rahman, A.; Raaif, M.; Mohamed, S.; Kolitsch, A.
Mechanical and ellipsometry measurements of thin TiN layer prepared by PIII
Materials Chemistry and Physics **132**, 91 (2012)

2. Abrasonis, G.; Morawetz, K.
Instability types at ion-assisted alloy deposition: from two-dimensional to three-dimensional nanopattern growth
Physical Review B **86**, 085452 (2012)

3. Abrasonis, G.; Wintz, S.; Liedke, M. O.; Aksoy Akgul, F.; Krause, M.; Kuepper, K.; Banerjee, D.; Liu, Z.; Gemming, S.
Environment controlled dewetting of Rh−Pd bilayers: A route for core−shell nanostructure synthesis
Journal of Physical Chemistry C **116**, 14401 (2012)

4. Adelmann, C.; Conard, T.; Franquet, A.; Brijs, B.; Munnik, F.; Burgess, S.; Witters, T.; Meersschaut, J.; Kittl, J. A.; Vandervorst, W.
Compositional depth profiling of TaCN thin films
Journal of Vacuum Science & Technology A **30**, 041510 (2012)

5. Audronis, M.; Abrasonis, G.; Munnik, F.; Heller, R.; Chapon, P.; Bellido-Gonzalez, V.
Diffusive racetrack oxidation in a Ti sputter target by reactive high power impulse magnetron sputtering
Journal of Physics D: Applied Physics **45**, 1 (2012)

6. Bali, R.; Marchetto, H.; Barcza, A.; Blamire, M. G.; Dhesi, S. S.
Direct imaging of spin relaxation in stepped α-Fe_2O_3/$Ni_{81}Fe_{19}$ bilayers using X-ray photo emission electron microscopy
Applied Physics Letters **101**, 052403 (2012)

7. Barlak, M.; Piekoszewski, J.; Werner, Z.; Sartowska, B.; Waliś, L.; Starosta, W.; Kierzek, J.; Kowalska, E.; Wilhelm, R. A.; Pochrybniak, C.; Woźnica, M.
High-temperature oxidation resistance in yttrium implanted stainless steel
Nukleonika **57**, 473 (2012)

8. Baudisch, M.; Wagner, M.; Schneider, H.; Stehr, D.; Helm, M.; Atkinson, P.; Huo, Y.; Schmidt, O. G.; Andrews, A. M.; Strasser, G.
Fano effect due to ponderomotive coupling in intersubband response of semiconductor quantum wells
Physical Review B **86**, 075305 (2012)

9. Beyer, R.; von Borany, J.
Determination of size and density of embedded Ge nanocrystals in SiO_2 by scanning force microscopy using a tomographic approach
Surface and Interface Analysis **44**, 1018 (2012)

10. Bhattacharyya, J.; Zybell, S.; Winnerl, S.; Helm, M.; Hopkinson, M.; Wilson, L. R.; Schneider, H.
In-plane interdot carrier transfer in InAs/GaAs quantum dots
Applied Physics Letters **100**, 152101 (2012)

11. Bischoff, L.; Heinig, K.-H.; Schmidt, B.; Facsko, S.; Pilz, W.
Self-organization of Ge nanopattern under erosion with heavy Bi monomer and cluster ions
Nuclear Instruments and Methods in Physics Research B **272**, 198 (2012)

12. Boppel, S.; Lisauskas, A.; Mundt, M.; Seliuta, D.; Minkevičius, L.; Kašalynas, I.; Valušis, G.; Krozer, V.; Mittendorff, M.; Winnerl, S.; Roskos, Hartmut, G.
CMOS integrated antenna-coupled field-effect-transistors for the detection of radiation from 0.2 to 4.3 THz
IEEE Transactions on Microwave Theory and Techniques **60**, 3834 (2012)

13. Böttger, R.; Bischoff, L.; Facsko, S.; Schmidt, B.
Quantitative analysis of the order of Bi ion induced dot patterns on Ge
EPL - Europhysics Letters **98**, 16009 (2012)

14. Böttger, R.; Bischoff, L.; Heinig, K.-H.; Pilz, W.; Schmidt, B.
From sponge to dot arrays on (100) Ge by increasing the energy of ion impacts
Journal of Vacuum Science & Technology B **30**, 06FF12 (2012)

15. Bottomleya, D.; Stuckert, J.; Hofmann, P.; Tocheny, L.; Hugon, M.; Journeau, C.; Clément, B.; Weber, S.; Guentay, S.; Hozer, Z.; Herranz, L.; Schumm, A.; Oriolo, F.; Altstadt, E.; Krause, M.; Fischer, M.; Khabensky, V. B.; Bechta, S. V.; Veshchunov, M. S.; Palagin, A. V.; Kiselev, A. E.; Nalivaev, V. I.; Goryachev, A. V.; Zhdanov, V.; Baklanov, V.
Severe accident research in the core degradation area: An example of effective international cooperation between the European Union (EU) and the Commonwealth of Independent States (CIS) by the International Science and Technology Center
Nuclear Engineering and Design **252**, 226 (2012)

16. Brandt, R.; Tibus, S.; Springer, F.; Fassbender, J.; Rohrmann, H.; Albrecht, M.; Schmidt, H.
Influence of intergranular exchange coupling on the magnetization dynamics of CoCrPt:SiO_2 granular media
Journal of Applied Physics **112**, 033918 (2012)

17. Briechle, B. M.; Kim, Y.; Ehrenreich, P.; Erbe, A.; Sysoiev, D.; Huhn, T.; Groth, U.; Scheer, E.
Current-voltage characteristics of single-molecule diarylethene junctions measured with adjustable gold electrodes in solution
Beilstein Journal of Nanotechnology **3**, 798 (2012)

18. Brombacher, C.; Schubert, C.; Daniel, M.; Liebig, A.; Beddies, G.; Schumann, T.; Skorupa, W.; Donges, J.; Häberlein, S.; Albrecht, M.
Chemical ordering of FePt films using millisecond flash-lamp annealing
Journal of Applied Physics **111**, 023902 (2012)

19. Bürger, D.; Seeger, M.; Zhou, S.; Skorupa, W.; Schmidt, H.
Transition metal diffusion in diluted magnetic Si and GaAs prepared by pulsed laser processing
Journal of Applied Physics **111**, 054914 (2012)

20. Bürger, D.; Zhou, S.; Höwler, M.; Ou, X.; Kovacs, G.; Reuther, H.; Mücklich, A.; Skorupa, W.; Helm, M.; Schmidt, H.
Hysteretic anomalous Hall effect in a ferromagnetic, Mn-rich Ge:Mn nanonet
Applied Physics Letters **100**, 012406 (2012)

21. Chen, C.-L.; Richter, A.; Kögler, R.; Wu, L.-T.
Dual-beam irradiation of friction stir spot welding of nanostructured ferritic oxide dispersion strengthened alloy
Journal of Alloys and Compounds **536S**, S194 (2012)

22. Cheng, F.; Ding, B.; Pan, F.; Yao, S.; Potzger, K.; Zhou, S.
Investigation on the structural and magnetic properties of Co^+ implanted rutile TiO_2
Nuclear Instruments and Methods in Physics Research B **286**, 180 (2012)

23. Dai, X. M.; Xu, S. J.; Gu, Q. L.; Ling, C. C.; Brauer, G.; Anwand, W.; Skorupa, W.
Emission bands of nitrogen-implantation induced luminescent centers in ZnO crystals: Experiment and theory
Journal of Applied Physics **112**, 046102 (2012)

24. de Boor, J.; Kim, D. S.; Ao, X.; Becker, M.; Hinsche, N. F.; Mertig, I.; Zahn, P.; Schmidt, V.
Thermoelectric properties of porous silicon
Applied Physics A **107**, 789 (2012)

25. Dekov, V. M.; Kamenov, G. D.; Abrasheva, M. D.; Capaccioni, B.; Munnik, F.
Mineralogical and geochemical investigation of seafloor massive sulfides from Panarea Platform (Aeolian Arc, Tyrrhenian Sea)
Chemical Geology **335**, 136 (2012)

26. Delga, A.; Carras, M.; Trinité, V.; Guériaux, V.; Doyennette, L.; Nedelcu, A.; Schneider, H.; Berger, V.
Master equation approach of classical noise in intersubband detectors
Physical Review B **85**, 245414 (2012)

27. Ding, B.; Cheng, F.; Pan, F.; Fa, T.; Yao, S.; Potzger, K.; Zhou, S.
The correlation between structure and magnetism of Ni-implanted TiO_2 annealed at

different temperatures
Journal of Magnetism and Magnetic Materials **324**, 33 (2012)

28. Donchev, A.; Schütze, M.; Kolitsch, A.; Yankov, R.
Enhancing the high temperature capability of Ti-alloys
Steel Research International **83**, 938 (2012)

29. Donchev, A.; Schütze, M.; Kolitsch, A.; Yankov, R.
Optimization of the fluorine effect for improving the oxidation resistance of TiAl alloys
Materials Science Forum **706-709**, 1061 (2012)

30. El-Said, A. S.
Nanostructures created in SiO_2 surface: A comparison between the impingement by slow highly charged ions and by swift heavy ions
Nuclear Instruments and Methods in Physics Research B **282**, 63 (2012)

31. El-Said, A. S.; Wilhelm, R. A.; Heller, R.; Facsko, S.; Lemell, C.; Wachter, G.; Burgdörfer, J.; Ritter, R.; Aumayr, F.
Phase diagram for nanostructuring CaF_2 surfaces by slow highly charged ions
Physical Review Letters **109**, 117602 (2012)

32. Endrino, J. L.; Anders, A.; Andersson, J.; Horwat, D.; Vinnichenko, M.
Plasma and ion-beam assisted materials processing introduction
Journal of Materials Research **27**, 741 (2012)

33. Fassbender, J.
The chemical way to ion irradiation
Nature Nanotechnology **7**, 554 (2012)

34. Fechner, M.; Zahn, P.; Ostanin, S.; Bibes, M.; Mertig, I.
Switching magnetization by 180° with an electric field
Physical Review Letters **107**, 197206-1 (2012)

35. Feige, J.; Wallner, A.; Winkler, Stephan R.; Merchel, S.; Fifield, L. Keith; Korschinek, G.; Breitschwerdt, D.
The search for supernova-produced radionuclides in terrestrial deep-sea archives
Publications of the Astronomical Society of Australia (PASA) **29**, 109 (2012)

36. Fiedler, J.; Heera, V.; Skrotzki, R.; Herrmannsdörfer, T.; Voelskow, M.; Mücklich, A.; Facsko, S.; Reuther, H.; Perego, M.; Heinig, K.-H.; Schmidt, B.; Skorupa, W.; Gobsch, G.; Helm, M.
Superconducting Ga-overdoped Ge layers capped with SiO_2 – structural and transport investigations
Physical Review B **85**, 134530 (2012)

37. Fitting, H.-J.; Fitting-Kourkoutis, L.; Schmidt, B.; Liedke, B.; Ivanova, E. V.; Zamoryanskaya, M. V.; Pustovarov, V. A.; Zatsepin, A. F.
Electron microscopic imaging of an ion beam mixed SiO_2/Si interface correlated with photo- and cathodoluminescence
Physica Status Solidi (A) **209,** 1101 (2012)

38. Fritzsche, M.; Mücklich, A.; Facsko, S.
Nanohole pattern formation on germanium induced by focused ion beam and broad beam Ga^+ irradiation
Applied Physics Letters **100**, 223108 (2012)

39. Gago, R.; Redondo-Cubero, A.; Vinnichenko, M.; Lehmann, J.; Munnik, F.; Palomares, F. J.
Spectroscopic evidence of NO_x formation and band-gap narrowing in N-doped TiO_2 films grown by pulsed magnetron sputtering
Materials Chemistry and Physics **136**, 729 (2012)

40. Gonzalez-Arrabal, R.; Munnik, F.; González, M.; Romero, P.; Heller, R.; Leardini, F.; Perlado, J. M.
Ion beam analysis of as-received, H-implanted and post implanted annealed fusion steels
Nuclear Instruments and Methods in Physics Research B **270**, 27 (2012)

41. Gordillo, N.; González-Arrabal, R.; Rivera, A.; Munnik, F.; Agulló-López, F.
Stopping power dependence of nitrogen sputtering yields in copper nitride films under

swift-ion irradiation: exciton model approach
Nuclear Instruments and Methods in Physics Research B **289**, 74 (2012)

42. Gradhand, M.; Fedorov, D. V.; Pientka, F.; Zahn, P.; Mertig, I.; Györfy, B. L.
First-principles calculations of the Berry curvature of Bloch states for charge and spin transport of electrons
Journal of Physics: Condensed Matter **24**, 213202 (2012)

43. Gradhand, M.; Fedorov, D. V.; Zahn, P.; Mertig, I.; Otani, Y.; Niimi, Y.; Vila, L.; Fert, A.
Perfect alloys for spin Hall current induced magnetization switching
SPIN **2**, 1250010 (2012)

44. Grebing, J.; Fassbender, J.; Erbe, A.
Time efficient fabrication of ultra large scale nano dot arrays using electron beam lithography
Microelectronic Engineering **97**, 55 (2012)

45. Hämäläinen, J.; Holopainen, J.; Munnik, F.; Hatanpää, T.; Heikkilä, M.; Ritala, M.; Leskelä, M.
Lithium phosphate thin films grown by atomic layer deposition
Journal of the Electrochemical Society **159**, A259 (2012)

46. Hämäläinen, J.; Holopainen, J.; Munnik, F.; Heikkilä, M.; Ritala, M.; Leskelä, M.
Atomic layer deposition of aluminum and titanium phosphates
Journal of Physical Chemistry C **116**, 5920 (2012)

47. Hämäläinen, J.; Munnik, F.; Hatanpää, T.; Holopainen, J.; Ritala, M.; Leskelä, M.
Study of amorphous lithium silicate thin films grown by atomic layer deposition
Journal of Vacuum Science & Technology A **A30**, 01A106 (2012)

48. Heera, V.; Fiedler, J.; Voelskow, M.; Mücklich, A.; Skrotzki, R.; Herrmannsdörfer, T.; Skorupa, W.
Superconductor-insulator transition controlled by annealing in Ga implanted Si
Applied Physics Letters **100**, 262602 (2012)

49. Heintze, C.; Hernández-Mayoral, M.; Ulbricht, A.; Bergner, F.; Shariq, A.; Weissgärber, T.; Frielinghaus, H.
Nanoscale characterization of ODS Fe-9%Cr model alloys compacted by spark plasma sintering
Journal of Nuclear Materials **428**, 139 (2012)

50. Hinsche, N. F.; Mertig, I.; Zahn, P.
Thermoelectric transport in strained Si and Si/Ge heterostructures
Journal of Physics: Condensed Matter **24**, 275501 (2012)

51. Hinsche, N. F.; Yavorsky, B. Yu.; Gradhand, M.; Czerner, M.; Winkler, M.; König, J.; Böttner, H.; Mertig, I.; Zahn, P.
Thermoelectric transport in Bi_2Te_3/Sb_2Te_3 superlattices
Physical Review B **86**, 085323 (2012)

52. Houweling, Z.; Geus, J.; Harks, P.; Heller, R.; Schropp, R.
Self-assembled isolated monodisperse NiO_{1+Y} nanoparticles as catalytic templates for nanomaterials synthesis
Materials Chemistry and Physics **135**, 38 (2012)

53. Jacob, R.; Winnerl, S.; Fehrenbacher, M.; Bhattacharyya, J.; Schneider, H.; Wenzel, M. T.; von Ribbeck, H.-G.; Eng, L. M.; Atkinson, P.; Schmidt, O. G.; Helm, M.
Intersublevel spectroscopy on single InAs-quantum dots by terahertz near-field microscopy
Nano Letters **12**, 4336 (2012)

54. Jansen, R.; Deac, A. M.; Saito, H.; Yuasa, S.
Injection and detection of spin in a semiconductor by tunneling via interface states
Physical Review B **85**, 134420 (2012)

55. Jansen, R.; Deac, A. M.; Saito, H.; Yuasa, S.
Thermal spin current and magnetothermopower by Seebeck spin tunneling
Physical Review B **85**, 094401 (2012)

56. Jia, Y.; Chen, F.; de Aldana, J.; Akhmadaliev, Sh.; Zhou, S.
Femtosecond laser micromachining of Nd:GdCOB ridge waveguides for second harmonic generation
Optical Materials **34**, 1913 (2012)

57. Jia, Y.; Dong, N.; Chen, F.; de Aldana, J. R. V.; Akhmadaliev, Sh.; Zhou, S.
Continuous wave ridge waveguide lasers in femtosecond laser micromachined ion irradiated Nd:YAG single crystals
Optical Materials Express **2**, 657 (2012)

58. Jia, Y.; Dong, N.; Chen, F.; de Aldana, J. R. V.; Akhmadaliev, Sh.; Zhou, S.
Ridge waveguide lasers in Nd:GGG crystals produced by swift carbon ion irradiation and femtosecond laser ablation
Optics Express **20**, 9763 (2012)

59. Kaya, C.; Schneider, C.; Al Shemmary, A.; Seidel, W.; Kuntzsch, M.; Bhattacharyya, J.; Mittendorff, M.; Evtushenko, P.; Winnerl, S.; Staats, G.; Helm, M.; Stojanovic, N.; Michel, P.; Gensch, M.
Phase sensitive monitoring of electron bunch form and arrival time in superconducting linear accelerators
Applied Physics Letters **100**, 141103 (2012)

60. Keller, A.; Bald, I.; Rotaru, A.; Cauët, E.; Gothelf, K. V.; Besenbacher, F.
Probing electron-induced bond cleavage at the single-molecule level using DNA origami templates
ACS Nano **6**, 4392 (2012)

61. Kelling, J.; Ódor, G.; Nagy, M. F.; Schulz, H.; Heinig, K.-H.
Comparison of different parallel implementations of the 2+1-dimensional KPZ model and the 3-dimensional KMC model
European Physical Journal - Special Topics **210**, 175 (2012)

62. Kirchner, T.; Briechle, B.; Scheer, E.; Wolf, J.; Huhn, T.; Erbe, A.
Statistical investigation of current-voltage characterization in single molecule-metal junctions
Acta Physica Polonica A **121**, 410 (2012)

63. Kögler, R.; Anwand, W.; Richter, A.; Butterling, M.; Ou, X.; Wagner, A.; Chen, C.-L.
Nanocavity formation and hardness increase by dual ion beam irradiation of oxide dispersion strengthened FeCrAl alloy
Journal of Nuclear Materials **427**, 133 (2012)

64. Kosobrodova, E. A.; Kondyurin, A. V.; Fisher, K.; Möller, W.; Mckenzie, D. R.; Bilek, M.
Free radical kinetics in a plasma immersion ion implanted polystyrene: Theory and experiment
Nuclear Instruments and Methods in Physics Research B **280**, 26 (2012)

65. Krause, M.; Haluska, M.; Abrasonis, G.; Gemming, S.
SWCNT growth from C:Ni nanocomposites
Physica Status Solidi (B) **249**, 2357 (2012)

66. Krause, M.; Mücklich, A.; Oates, T. W. H.; Zschornak, M.; Wintz, S.; Endrino, J. L.; Baehtz, C.; Shalimov, A.; Gemming, S.; Abrasonis, G.
Tilting of carbon encapsulated metallic nanocolumns in carbon-nickel nanocomposite films by ion beam assisted deposition
Applied Physics Letters **101**, 053112 (2012)

67. Kreuter, C.; Leiderer, P.; Erbe, A.
Determination of potential landscapes using video microscopy
Colloid and Polymer Science **290**, 575 (2012)

68. Kunert, G.; Dobkowska, S.; Li, T.; Reuther, H.; Kruse, C.; Figge, S.; Jakiela, R.; Bonanni, A.; Grenzer, J.; von Borany, J.; Stefanowicz, W.; Sawicki, M.; Dietel, T.; Hommel, D.
$Ga_{1-x}Mn_xN$ epitaxial films with high magnetization
Applied Physics Letters **101**, 022413 (2012)

69. Li, L.; Hua, W.; Prucnal, S.; Yao, S.; Shao, L.; Potzger, K.; Zhou, S.
Defect induced ferromagnetism in 4H-SiC single crystals
Nuclear Instruments and Methods in Physics Research B **275**, 33 (2012)

70. Liedke, M. O.; Körner, M.; Lenz, K.; Grossmann, F.; Facsko, S.; Fassbender, J.
Magnetic anisotropy engineering: Single-crystalline Fe films on ion eroded ripple surfaces
Applied Physics Letters **100**, 242405 (2012)

71. Lišková, E.; Veis, M.; Višňovský, Š.; Ferré, J.; Mougin, A.; Mazalski, P.; Maziewski, A.; Liedke, M. O.; Fassbender, J.
Effect of Ga^+ irradiation on the magneto-optic spectra of Pt/Co/Pt sandwiches
Thin Solid Films **520**, 7169 (2012)

72. Macko, S.; Grenzer, J.; Frost, F.; Engler, M.; Hirsch, D.; Fritzsche, M.; Mücklich, A.; Michely, T.
Iron assisted ion beam patterning of Si(001) in the crystalline regime
New Journal of Physics **14**, 073003 (2012)

73. Markwitz, A.; Carder, D. A.; Hopf, T.; Kennedy, J.; Kuei, C. T.; Mücklich, A.; Osipowicz, T.
Formation of nanoclusters with varying Pb/Se concentration and distribution after sequential Pb^+ and Se^+ ion implantation into SiO_2
Nuclear Instruments and Methods in Physics Research B **273**, 199 (2012)

74. Martinavicius, A.; Abrasonis, G.; Scheinost, A. C.; Danoix, R.; Danoix, F.; Stinville, J. C.; Talut, G.; Templier, C.; Liedke, M. O.; Gemming, S.; Möller, W.
Nitrogen interstitial diffusion induced decomposition in AISI 304L austenitic stainless steel
Acta Materialia **60**, 4065 (2012)

75. Matlak, K.; Wall, J.; Kim, J.-Y.; Qu, J.; Jacobs, L. J.; Viehrig, H.-W.
Evaluation of radiation damage using nonlinear ultrasound
Journal of Applied Physics **111** (2012)

76. Maziewski, A.; Mazalski, P.; Kurant, Z.; Liedke, M.; McCord, J.; Fassbender, J.; Ferre, J.; Mougin, A.; Wawro, A.; Baczewski, L.; Rogalev, A.; Wilhelm, F.; Gemming, T.
Tailoring of magnetism in Pt/Co/Pt ultrathin films by ion irradiation
Physical Review B **85**, 1103 (2012)

77. Melone, J. J.; McCanny, T.; Schramm, U.; Akhmadaliev, Sh.; Spohr, M.; Cowan, T.; Mitchell, M. R.; Ledingham, K. W. D.; Burris-Mog, T.; Grötzschel, R.; Hanf, D.; Bussmann, M.; Wiggins, S. M.
Characterisation of permanent magnetic quadrupoles for focussing proton beams
Nuclear Instruments and Methods in Physics Research A **676**, 126 (2012)

78. Merchel, S.; Bremser, W.; Akhmadaliev, Sh.; Arnold, M.; Aumaître, G.; Bourlès, D. L.; Braucher, R.; Caffee, M.; Christl, M.; Fifield, L. K.; Finkel, R. C.; Freeman, S. P. H. T.; Ruiz-Gómez, A.; Kubik, P. W.; Martschini, M.; Rood, D. H.; Tims, S. G.; Wallner, A.; Wilcken, K. M.; Xu, S.
Quality assurance in accelerator mass spectrometry: Results from an international round-robin exercise for ^{10}Be
Nuclear Instruments and Methods in Physics Research B **289**, 68 (2012)

79. Morozov, S.; Joludev, M.; Antonov, A.; Rumyantsev, V.; Gavrilenko, V.; Aleshkin, V.; Dubinov, A.; Mikhailov, N.; Dvoretskiy, S.; Drachenko, O.; Winnerl, S.; Schneider, H.; Helm, M.
Study of lifetimes and photoconductivity relaxation in heterostructures with $Hg_x Cd_{1-x}$ Te/$Cd_y Hg_{1-y}$ Te quantum wells
Semiconductors **46**, 1362 (2012)

80. Morris, C. M.; Stehr, D.; Kim, H. C.; Truong, T. A.; Pryor, C.; Petroff, P. M.; Sherwin, M. S.
Terahertz ionization of highly charged quantum posts in a perforated electron gas
Nano Letters **12**, 1115 (2012)

81. Neelmeijer, C.; Roscher, R.
PIXE-RBS survey of a Meissen porcelain snuffbox: First version or not?
X-Ray Spectrometry **41**, 93 (2012)

82. Neudert, A.; Lai, Y. W.; Schäfer, R.; Kustov, M.; Schultz, L.; McCord, J.
Magnetic domains and twin boundary movement of NiMnGa magnetic shape memory

crystals
Advanced Engineering Materials **14**, 601 (2012)

83. Ódor, G.; Liedke, B.; Heinig, K.-H.; Kelling, J.
Ripples and dots generated by lattice gases
Applied Surface Science **258**, 4186 (2012)

84. Ou, X.; Kögler, R.; Zhou, H.; Anwand, W.; Grenzer, J.; Hübner, R.; Voelskow, M.; Butterling, M.; Zhou, S.; Skorupa, W.
Release of helium from vacancy defects in yttria-stabilized zirconia under irradiation
Physical Review B **86**, 224103 (2012)

85. Patschurek, C.; Lenz, K.; Strache, T.; Liedke, M. O.; Mönch, I.; Schäfer, R.; Schultz, L.; McCord, J.
Magnetization dynamics of buckling domain structures in patterned thin films
Physical Review B **86**, 054426 (2012)

86. Perez-Flores, J. C.; Baehtz, C.; Hoelzel, M.; Kuhn, A.; Garcia-Alvarado, F.
$H_2Ti_6O_{13}$, a new protonated titanate prepared by Li^+/H^+ ion exchange: synthesis, crystal structure and electrochemical Li insertion properties
RSC Advances **2**, 3530 (2012)

87. Pérez-Flores, J. C.; Baehtz, C.; Hoelzel, M.; Kuhn, A.; García-Alvarado, F.
Full structural and electrochemical characterization of $Li_2Ti_6O_{13}$ as anode for Li-ion batteries
Physical Chemistry, Chemical Physics **14**, 2892 (2012)

88. Persechini, L.; Ranjan, M.; Grossmann, F.; Facsko, S.; McGilp, J. F.
The linear and nonlinear optical response of native-oxide covered rippled Si templates with nanoscale periodicity
Physica Status Solidi (B) **249**, 1173 (2012)

89. Philipp, P.; Bischoff, L.
Investigation of conductive nanostructures on ta-C films made by FIB lithography
Nuclear Instruments and Methods in Physics Research B **282**, 121 (2012)

90. Philipp, P.; Bischoff, L.
Investigations of nano structures on ta-C films made by gallium FIB lithography
Diamond and Related Materials **23**, 140 (2012)

91. Philipp, P.; Bischoff, L.; Schmidt, B.
Taming of Ga droplets on DLC layers – Size tuning and local arrangement with nanometer accuracy
Nanotechnology **23**, 475304 (2012)

92. Pinto, S. R. C.; Buljan, M.; Marques, L.; Martin-Sanchez, J.; Conde, O.; Chahboun, A.; Ramos, A. R.; Barradas, N. P.; Alves, E.; Bernstorff, S.; Grenzer, J.; Mücklich, A.; Ramos, M. M. D.; Gomes, M. J. M.
Influence of annealing conditions on the formation of regular lattices of voids and Ge quantum dots in an amorphous alumina matrix
Nanotechnology **23**, 405605 (2012)

93. Potzger, K.
Ion-beam synthesis of magnetic semiconductors
Nuclear Instruments and Methods in Physics Research B **272**, 78 (2012)

94. Preu, S.; Mittendorff, M.; Lu, H.; Weber, H. B.; Winnerl, S.; Gossard, A. C.
1550 nm ErAs:In(Al)GaAs large area photoconductive emitters
Applied Physics Letters **101**, 101105 (2012)

95. Prucnal, S.; Abendroth, B.; Krockert, K.; König, K.; Henke, D.; Kolitsch, A.; Möller, H. J.; Skorupa, W.
Millisecond annealing for advanced doping of dirty-silicon solar cells
Journal of Applied Physics **111**, 123104 (2012)

96. Prucnal, S.; Gao, K.; Anwand, W.; Helm, M.; Skorupa, W.; Zhou, S.
Temperature stable 1.3 μm emission from GaAs
Optics Express **20**, 26075 (2012)

97. Prucnal, S.; Shalimov, A.; Ozerov, M.; Potzger, K.; Skorupa, W.
Magnetic and optical properties of virgin arc furnace grown MgO crystals
Journal of Crystal Growth **339**, 70 (2012)

98. Prucnal, S.; Zhou, S.; Ou, X.; Reuther, H.; Liedke, M. O.; Mücklich, A.; Helm, M.; Zuk, J.; Turek, M.; Pyszniak, K.; Skorupa, W.
InP nanocrystals on silicon for optoelectronic applications
Nanotechnology **23**, 485204 (2012)

99. Ranjan, M.; Facsko, S.
Anisotropic surface enhanced Raman scattering in nanoparticle and nanowire arrays
Nanotechnology **23**, 485307 (2012)

100. Rebohle, L.; Lehmann, J.; Prucnal, S.; Helm, M.; Skorupa, W.
The electrical and electroluminescence properties of rare earth implanted MOS light emitting devices in the near infrared
Journal of Luminescence **132**, 3151 (2012)

101. Redondo-Cubero, A.; Gago, R.; Palomares, F. J.; Mücklich, A.; Vinnichenko, M.; Vazquez, L.
Nanopatterning dynamics on Si(100) during oblique 40-keV Ar+ erosion with metal codeposition: Morphological and compositional correlation
Physical Review B **86**, 085436 (2012)

102. Reuther, H.; Talut, G.; Mücklich, A.; Stromberg, F.
Magnetism in Ge by ion implantation with Fe and Mn
Journal of Physics D: Applied Physics **45**, 395001 (2012)

103. Ritter, R.; Wilhelm, R. A.; Ginzel, R.; Kowarik, G.; Heller, R.; El-Said, A. S.; Papaléo, R. M.; Rupp, W.; Crespo López-Urrutia, J. R.; Ullrich, J.; Facsko, S.; Aumayr, F.
Pit formation on poly(methyl methacrylate) due to ablation induced by individual slow highly charged ion impact
EPL - Europhysics Letters **97**, 13001 (2012)

104. Roshchupkina, O. D.; Grenzer, J.; Strache, T.; McCord, J.; Fritzsche, M.; Mücklich, A.; Baehtz, C.; Fassbender, J.
Focused ion beam induced structural modifications in thin magnetic films.
Journal of Applied Physics **112**, 033901 (2012)

105. Saint-Cast, P.; Kania, D.; Heller, R.; Kuehnhold, S.; Hofmann, M.; Rentsch, J.; Preu, R.
High-temperature stability of c-Si surface passivation by thick PECVD Al_2O_3 with and without hydrogenated capping layers
Applied Surface Science **258**, 8371 (2012)

106. Sério, S.; Melo Jorge, M. E.; Nunes, Y.; Barradas, N. P.; Alves, E.; Munnik, F.
Incorporation of N in TiO_2 films grown by DC-reactive magnetron sputtering
Nuclear Instruments and Methods in Physics Research B **273**, 109 (2012)

107. Shuai, Y.; Ou, X.; Wu, C.; Zhang, W.; Zhou, S.; Bürger, D.; Reuther, H.; Slesazeck, S.; Mikolajick, T.; Helm, M.; Schmidt, H.
Substrate effect on the resistive switching in $BiFeO_3$ thin films
Journal of Applied Physics **111**, 07D906 (2012)

108. Simonin, L.; Colin, J.-F.; Ranieri, V.; Can-Évet, E.; Martin, J.-F.; Bourbon, C.; Baehtz, C.; Strobel, P.; Daniel, L.; Patoux, S.
In situ investigations of a Li-rich Mn–Ni layered oxide for Li-ion batteries
Journal of Materials Chemistry **22**, 11316 (2012)

109. Srivastava, P.; Ghosh, S.; Joshi, B.; Satyarthi, P.; Kumar, P.; Kanjilal, D.; Bürger, D.; Zhou, S.; Schmidt, H.; Rogalev, A.; Wilhelm, F.
Probing origin of room temperature ferromagnetism in Ni ion implanted ZnO films with X-ray absorption spectroscopy
Journal of Applied Physics **111**, 013715 (2012)

110. Staiger, M.; Rafailov, P.; Gartsman, K.; Telg, H.; Krause, M.; Radovsky, G.; Zak, A.; Thomsen, C.
Excitonic resonances in WS_2 nanotubes
Physical Review B **86**, 161523 (2012)

111. Sterba, J. H.; Munnik, F.; Pearce, N. J. G.
Raising the temper - µ-spot analysis of temper inclusions in experimental ceramics
Journal of Radioanalytical and Nuclear Chemistry **291**, 25 (2012)

112. Takahashi, T.; Iskandar, R.; Munnik, F.; Music, D.; Mayer, J.; Schneider, J. M.
Synthesis, microstructure, and mechanical properties of YPd_3B thin films
Journal of Alloys and Compounds **540**, 75 (2012)

113. Talati, M.; Posselt, M.; Bonny, G.; Al-Motasem, A.; Bergner, F.
Vibrational contribution to the thermodynamics of nanosized precipitates: vacancy–copper clusters in bcc-Fe
Journal of Physics: Condensed Matter **24**, 225402 (2012)

114. Thorn, A.; Ritter, E.; Ullmann, F.; Pilz, W.; Bischoff, L.; Zschornack, G.
Liquid metal alloy ion source based metal ion injection into a room temperature electron beam ion source
Review of Scientific Instruments **83**, 02A511 (2012)

115. Tiagulskyi, S. I.; Tyagulskiy, I. P.; Nazarov, A. N.; Nazarova, T. M.; Rymarenko, N. L.; Lysenko, V. S.; Rebohle, L.; Lehmann, J.; Skorupa, W.
Thermal effect on electroluminescence quenching in SiO_2 with Ge and ReOx nanoclusters
Electrochemical Society Transactions **45**, 161 (2012)

116. Tiagulskyi, S.; Nazarov, A.; Tyagulskii, I.; Lysenko, V.; Rebohle, L.; Lehmann, J.; Skorupa, W.
Shell model for REOx nanoclusters in amorphous SiO_2: charge trapping and electroluminescence quenching
Physica Status Solidi (C) **9**, 1468 (2012)

117. Toimil-Molares, M. E.; Röntzsch, L.; Sigle, W.; Heinig, K.-H.; Trautmann, C.; Neumann, R.
Pipetting nanowires: In situ visualization of solid-state nanowire-to-nanoparticle transformation driven by surface diffusion-mediated capillarity
Advanced Functional Materials **22**, 695 (2012)

118. Tripathi, J. K.; Liedke, M. O.; Strache, T.; Sarangi, S. N.; Grötzschel, R.; Gupta, A.; Som, T.
Effect of low energy He^+-ion irradiation on structural and magnetic properties of thin Pt/Cr/Co multilayers
Nuclear Instruments and Methods in Physics Research B **272**, 96 (2012)

119. Verleger, S.; Grimm, A.; Kreuter, C.; Tan, H. M.; van Kan, J. A.; Erbe, A.; Scheer, E.; van der Maarel, J. R. C.
A single-channel microparticle sieve based on Brownian ratchets
Lab on a Chip **12**, 1238 (2012)

120. Viehrig, H.-W.; Altstadt, E.; Houska, M.; Valo, M.
Fracture mechanics characterisation of the beltline welding seam of the decommissioned WWER-440 reactor pressure vessels of nuclear power plant Greifswald Unit 4
International Journal of Pressure Vessels and Piping **89**, 129 (2012)

121. Vieluf, M.; Munnik, F.; Neelmeijer, C.; Kosmata, M.; Teichert, S.
High resolution RBS investigations of ZrO_2 layer growth in the initial stage on native silicon oxide and titanium nitride
Thin Solid Films **520**, 5900 (2012)

122. Wagner, A.; Ulbricht, A.; Bergner, F.; Altstadt, E.
Influence of the copper impurity level on the irradiation response of reactor pressure vessel steels investigated by SANS
Nuclear Instruments and Methods in Physics Research B **280**, 98 (2012)

123. Wagner, M.; Teich, M.; Helm, M.; Stehr, D.
Temperature dependence of the intraexcitonic AC Stark effect in semiconductor quantum wells
Applied Physics Letters **100**, 051109 (2012)

124. Wang, X.; Liu, S.; Ma, D.; Zheng, X.; Chen, G.; Xu, F.; Tang, N.; Shen, B.; Zhang, P.; Cao, X.; Wang, B.; Huang, S.; Chen, K.; Zhou, S.; Yoshikawa, A.

Fe-doped InN layers grown by molecular beam epitaxy
Applied Physics Letters **101**, 171905 (2012)

125. Wang, X.; Liu, S.; Ma, N.; Feng, L.; Chen, G.; Xu, F.; Tang, N.; Huang, S.; Chen, K. J.; Zhou, S.; Shen, B.
High-electron-mobility InN layers grown by boundary-temperature-controlled epitaxy
Applied Physics Express **5**, 015502 (2012)

126. Weatherup, R. S.; Bayer, B. C.; Blume, R.; Baehtz, C.; Kidambi, P. R.; Fouquet, M.; Wirth, C. T.; Schlögl, R.; Hofmann, S.
On the mechanisms of Ni-catalysed graphene chemical vapour deposition
ChemPhysChem **13**, 2544 (2012)

127. Winnerl, S.
Scalable microstructured photoconductive terahertz emitters
Journal of Infrared, Millimeter and Terahertz Waves **33**, 431 (2012)

128. Winnerl, S.; Hubrich, R.; Mittendorff, M.; Schneider, H.; Helm, M.
Universal phase relation between longitudinal and transverse fields observed in focused terahertz beams
New Journal of Physics **14**, 103049 (2012)

129. Wintz, S.; Bunce, C.; Banholzer, A.; Körner, M.; Strache, T.; Mattheis, R.; McCord, J.; Raabe, J.; Quitmann, C.; Erbe, A.; Fassbender, J.
Interlayer coupled spin vortex pairs and their response to external magnetic fields
Physical Review B **85**, 224420 (2012)

130. Wintz, S.; Strache, T.; Körner, M.; Bunce, C.; Banholzer, A.; Mönch, I.; Mattheis, R.; Raabe, J.; Quitmann, C.; McCord, J.; Erbe, A.; Lenz, K.; Fassbender, J.
Control of vortex pair states by post-deposition interlayer exchange coupling modification
Physical Review B **85**, 134417 (2012)

131. Winzer, T.; Knorr, A.; Mittendorff, M.; Winnerl, S.; Sun, D.; Norris, T. B.; Helm, M.; Malic, E.
Absorption saturation in optically pumped graphene
Applied Physics Letters **101**, 221115 (2012)

132. Wirth, C. T.; Bayer, B. C.; Gamalski, A. D.; Esconjauregui, S.; Weatherup, R. S.; Ducati, C.; Baehtz, C.; Robertson, J.; Hofmann, S.
The phase of iron catalyst nanoparticles during carbon nanotube growth
Chemistry of Materials **24**, 4633 (2012)

133. Wojcik, H.; Junige, M.; Bartha, W.; Albert, M.; Neumann, V.; Merkel, U.; Peeva, A.; Gluch, J.; Menzel, S.; Munnik, F.; Liske, R.; Utess, D.; Richter, I.; Klein, C.; Engelmann, H. J.; Ho, P.; Hossbach, C.; Wenzel, C.
Physical characterization of PECVD and PEALD Ru(-C) films and comparison with PVD ruthenium film properties
Journal of the Electrochemical Society **159**, H166 (2012)

134. Wojcik, H.; Kaltofen, R.; Merkel, U.; Krien, C.; Strehle, S.; Gluch, J.; Knaut, M.; Wenzel, C.; Preusse, A.; Bartha, J.; Geidel, M.; Adolphi, B.; Neumann, V.; Liske, R.; Munnik, F.
Electrical evaluation of Ru-W(-N), Ru-Ta(-N) and Ru-Mn films as Cu diffusion barriers
Microelectronic Engineering **92**, 71 (2012)

135. Xie, Y.; Yang, Z.; Li, L.; Yin, L.; Hu, X.; Huang, Y.; Jian, H.; Song, W.; Sun, Y.; Zhou, S.; Zhang, Y.
Annealing induced colossal magnetocapacitance and colossal magnetoresistance in In-doped $CdCr_2S_4$
Journal of Applied Physics **112**, 123912 (2012)

136. Xu, Q.; Wen, Z.; Shuai, Y.; Wu, D.; Zhou, S.; Schmidt, H.
Forming-free unipolar resistive switching in $BiFe_{0.95}Co_{0.05}O_3$ films
Journal of Superconductivity and Novel Magnetism **25**, 1679 (2012)

137. Yankov, R. A.; Kolitsch, A.; von Borany, J.; Mücklich, A.; Munnik, F.; Donchev, A.; Schütze, M.
Surface protection of titanium and titanium-aluminum alloys against environmental degradation at elevated temperatures
Surface & Coatings Technology **206**, 3595 (2012)

138. Yilgin, R.; Yurtisigi, M.; Parabas, A.; Turksoy, M.; Ozdemir, M.; Aktas, B.; Kolitsch, A.
Ferromagnetic behavior of Fe^+ implanted Si(100) semiconductor
Journal of Superconductivity and Novel Magnetism **25**, 2731 (2012)

139. Zhou, S.; Chen, L.; Shalimov, A.; Zhao, J.; Helm, M.
Depth profile of the tetragonal distortion in thick GaMnAs layers grown on GaAs by Rutherford backscattering/channeling
AIP Advances **2**, 042102 (2012)

140. Zhou, S.; Wang, Y.; Jiang, Z.; Weschke, E.; Helm, M.
Ferromagnetic InMnAs on InAs prepared by ion implantation and pulsed laser annealing
Applied Physics Express **5**, 093007 (2012)

141. Zhou, S.; Zhang, W.; Shalimov, A.; Wang, Y.; Huang, Z.; Bürger, D.; Mücklich, A.; Zhang, W.; Schmidt, H.; Helm, M.
Magnetic Mn_5Ge_3 nanocrystals embedded in crystalline Ge: a magnet/semiconductor hybrid synthesized by ion implantation
Nanoscale Research Letters **7**, 528 (2012)

142. Zier, M.; Reinholz, U.; Riesemeier, H.; Radtke, M.; Munnik, F.
Accurate stopping power determination of ^{15}N ions for hydrogen depth profiling by a unique combination of ion beams and synchrotron radiation
Nuclear Instruments and Methods in Physics Research B **273**, 18 (2012)

143. Zimmermann, B.; Fietzke, F.; Klostermann, H.; Lehmann, J.; Munnik, F.; Möller, W.
High rate deposition of amorphous hydrogenated carbon films by hollow cathode arc PECVD
Surface & Coatings Technology **212**, 67 (2012)

Concluded scientific degrees

PhD theses

1. Al-Asqalani Al Motasem, A.T.
   Nanoclusters in diluted Fe-based alloys containing vacancies, copper and nickel: Structure, energetics and thermodynamics
   TU Dresden, 15.06.2012
2. Baumgart, C.
   Quantitative dopant profiling in semiconductors: A new approach to Kelvin probe force microscopy
   TU Dresden, 19.07.2012
3. Bürger, D.
   Charakterisierung von ferromagnetischen Ge:Mn-Nanonetzen nach Synthese mittels Mn-Ionenimplantation und gepulster Laserausheilung
   TU Dresden, 08.11.2012
4. Höwler, M.
   Präparation und Charakterisierung von TMR-Nanosäulen
   TU Dresden, 24.07.2012
5. Numazawa, S.
   Modeling of metal nanocluster growth on patterned substrates and surface pattern formation under ion bombardment
   TU Dresden, 22.05.2012
6. Thorn, A.
   Ladungsbrüten mit Raumtemperatur-Elektronenstrahlionenquellen
   TU Dresden, 02.03.2012
7. Zschintzsch, M.
   Self organized formation of Ge nanocrystals in multilayers
   TU Dresden, 27.04.2012

Diploma theses

1. Kelling, J.
   Kinetic Monte Carlo simulations on self-organization of nanostructures accelerated by massive parallelization
   TU Dresden, 18.04.2012
2. Langer, M.
   Herstellung und Charakterisierung magnetischer Metastrukturen
   TU Dresden, 14.02.2012
3. Sasse, H.
   Untersuchungen zu Beladungstechniken von Elektronenstrahl-Ionenquellen (EBIS) mit Metallionen
   TU Dresden, 18.06.2012
4. Trache, M.
   Analyse eines Messplatzes für frequenzaufgelöste magnetooptische Kerr-Effektmessungen (FR-MOKE) sowie dessen Ansteuerung auf der Basis von LabVIEW
   W.-Büchner-Hochschule Darmstadt, 17.12.2012

MSc theses

1. Wutzler, R.
   Influence of implantation and annealing conditions on the optoelectronic properties of Nd and Er doped MOS layers
   TU BA Freiberg, 20.12.2012

BSc theses

1. Böttger, C.
   Terahertz-Nahfeldmikroskopie an optisch angeregten Proben
   FH Darmstadt, 21.06.2012
2. Opherden, L.
   Metallisierung von DNA-Origami-Strukturen
   TU Dresden, 07.06.2012
3. Schreiber, B.
   Plasmonische Nanopartikel auf DNA-Origami-Strukturen
   TU Dresden, 08.06.2012

Appointments and honors

Awards and honors

1. **Facsko, Stefan**
   Leader of the research group „Ion Induced Nanostructures“ of the Ion Beam Center was appointed "HZDR Research Fellow“

2. **Fiedler, Jan**
   PhD candidate in the „Semiconductor Materials“ division received the DFCNA Sonderpreis 2011 des Dresdner Fraunhofer-Cluster Nanoanalytik Dresdner Barkhausen-Poster-Preis 2011, 10 February 2012, Dresden, Germany

3. **Fiedler, Jan**
   PhD candidate in the „Semiconductor Materials“ division received the 1st Award for the best oral presentation of "Young Scientist Contest" at the IX-th International Conference on Ion Implantation and Other Applications of Ions and Electrons, ION 2012, 25-28 June 2012, Kazimierz Dolny, Poland

4. **Fiedler, Jan**
   PhD candidate in the „Semiconductor Materials“ division received the Best Poster Award for the excellent poster presentation at the 18th International Conference on Ion Beam Modification of Materials, IBMM 2012, 02-07 September 2012, Qingdao, China

5. **Martin, Norbert**
   Alumni PhD candidate in the division “Magnetism” received the HZDR Award for Doctoral Candidates 2011 for his dissertation „Herstellung und Charakterisierung von magnetisch heterogenen Schichten und Elementen“ (TU Dresden, 07.06.2011), 13 March 2012

6. **Schönitz, Isabel**
   PhD candidate in the research group “Materials Characterization” of the division “Structural Materials” received a Poster Prize at the MUNECO (Materials UNder Extreme COnditions) Summerschool, 11-15 June 2012, Madrid, Spain

7. **Winnerl, Stephan**
   Senior scientist at the division "Spectroscopy" received the HZDR Research Award 2012 for his outstanding contributions to terahertz science

8. **Zhou, Shengqiang**
   Leader of the Helmholtz Young Investigators group “Functional Materials” of the division “Semiconductor Materials” received the IBMM Young Scientist Award 2012 at the 18th International Conference on Ion Beam Modifications of Materials, 02-07 September 2012, Qingdao, China, for his use of ion beams to induce magnetism in semiconductors and oxides.

Participation in conferences and lectures / talks

Invited conference talks

1. Bergner, F.
Small angle neutron scattering
Symposium on irradiation effects in structural materials for nuclear reactors, 17.-21.09.2012, Sevilla, Spain

2. Bernert, K.; Sluka, V.; Fowley, C.; Fassbender, J.; Deac, A. M.
Switching voltages and back-hopping in magnetic tunnel junctions with different geometries
NordicSpin'12 - Third Nordic Workshop on Spintronics and Nanomagnetism, 22.-25.04.2012, Varberg, Sweden

3. Bernert, K.; Sluka, V.; Fowley, C.; Fassbender, J.; Deac, A. M.
Switching voltages and back-hopping in magnetic tunnel junctions with different geometries
Spin Caloritronics 4, 02.-06.06.2012, Sendai, Japan

4. Bernert, K.; Sluka, V.; Fowley, C.; Fassbender, J.; Deac, A. M.
Switching voltages and back-hopping in magnetic tunnel junctions with different geometries
Magnetism and Magnetic Nanomaterials, MMN' 2012, 04.-06.09.2012, Boumedes, Algeria

5. Bernert, K.; Sluka, V.; Fowley, C.; Fassbender, J.; Deac, A. M.
Generalized switching voltages in magnetic tunnel junctions
Joint Dresden-Japan Workshop on Molecular Scale and Organic Electronic Materials, 11.-13.12.2012, Dresden, Germany

6. Bischoff, L.
Focused ion beams - Status and new trends
ITG WORKSHOP: Vacuum Electronics 2012, 20.-21.08.2012, Bad Honnef, Germany

7. Bischoff, L.
Modern trends in FIB development
7. FIB-Workshop Focused Ion Beams in Research, Science and Technology, 25.-27.06.2012, Dresden, Germany

8. Brenner, F.; Haas, S.; Schneider, F.; Klemm, V.; Schreiber, G.; von Borany, J.; Heitmann, J.
Semiconductor nanocrystals embedded in high-k matarials
221st Meeting of Electrochemical Society, Symposium Advanced Nanomaterials and Processing, 06.-10.05.2012, Seattle, USA

9. Donchev, A.; Schütze, M.; Kolitsch, A.; Yankov, R. A.
Enhancing the high temperature capability of Ti-alloys
Dresdner Werkstoffsymposium 2012, 06.-07.12.2012, Dresden, Germany

10. Erbe, A.; Wiesenhütter, U.; Pohl, D.; Rellinghaus, B.; Fassbender, J.
Coulomb blockade effects in FePt nanoparticles
DPG Spring Meeting of the Condensed Matter Section, 25.-30.03.2012, Berlin, Germany

11. Facsko, S.; Fritzsche, M.; Ou, X.; Böttger, R.; Bischoff, L.
Ion irradiation of Ge: from sponge-like structure to periodic pattern formation
18th International Conference on Ion Beam Modification of Materials (IBMM-18), 02.-07.09.2012, Qingdao, China

12. Gemming, S.; Weissbach, T.; Zschornak, M.; Stöcker, H.; Meyer, D. C.; Leisegang, T.; Ronneberger, I.; Potzger, K.
Multifunctional oxides – Modifying the ferroic properties by defects due to irradiation, doping and annealing
MRS Spring Meeting, 09.-13.04.2012, San Francisco, USA

13. Gensch, M.
Coherent THz pulses from linear SRF accelerators: Perspectives for naturally synchronized THz pump probe experiments and novel electron beam diagnostic
Workshop on Terahertz Sources for Time Resolved Studies of Matter, 30.-31.07.2012, Chicago, USA

14. Gensch, M.
Super-radiant coherent THz sources: Challenges and opportunities
Frontiers of THz Science, 05.-06.09.2012, Stanford, USA

15. Greene, P. K.; Gilbert, D. A.; Kirby, B. J.; Borchers, J.; Lau, J. W.; Shull, R.; Chih-Huang, L.; Osten, J.; Fassbender, J.; Davies, J.; Fitzsimmons, M.; Zimanyi, G.; Liu, K.
Probing graded perpendicular anisotropy with polarized neutron reflectometry
ACNS American Conference on Neutron Scattering, 24.-28.06.2012, Washington, DC, USA

16. Greene, P. K.; Gilbert, D. A.; Kirby, B. J.; Borchers, J.; Lau, J. W.; Lai, C.-H.; Osten, J.; Fassbender, J.; Davies, J. E.; Fitzsimmons, M.; Liu, K.
Magnetization reversal in nanostructures with graded perpendicular anisotropy
NordicSpin'12 - Third Nordic Workshop on Spintronics and Nanomagnetism, 22.-25.04.2012, Varberg, Sweden

17. Grenzer, J.
Materialforschung „zu Hause“ und am Synchrotron: Röntgenuntersuchungen an nano-kristallinen dünnen Filmen
Bruker XRD Anwendertreffen, 09.-10.10.2012, Lüneburg, Germany

18. Heinig, K.-H.
Kinetic Monte Carlo simulations at spatiotemporal scales of experiments
International Workshop on "Beyond Molecular Dynamics: Long Time Atomic-Scale Simulations", 26.03.2012, Dresden, Germany

19. Heinig, K.-H.; Schmidt, B.; Mücklich, A.; Liedke, B.; Kelling, J.; Friedrich, D.; Hauschild, D.; Stegemann, K.-H.; Keles, U.; Bulutay, C.; Aydinli, A.
Si nanowire networks embedded in SiO_2 formed by spinodal decomposition of SiO – a novel absorber material for 3rd generation solar cells
E-MRS Spring Meeting 2012, Symp. Y, 14.-18.05.2012, Strasbourg, France

20. Heinig, K.-H.; Schmidt, B.; Mücklich, A.; Liedke, B.; Kelling, J.; Friedrich, D.; Hauschild, D.; Stegemann, K.-H.; Bulutay, C.; Keles, U.; Aydinli, A.
Si nanowire networks for 3rd generation solar cells
4th International Conference on Nanostructure Selfassembly (NANOSEA2012), 25.-29.06.2012, Margherita di Pula, Sardinia/Italy

21. Heinig, K.-H.; Aydinli, A.; Turan, R.; Hauschild, D.
The German-Turkish project RainbowEnergy: A Si-based nanocomposite absorber for thin film PV cells
Solar Electricity Conference & Exhibition (SOLARTR-2), 07.-09.11.2012, Antalya, Turkey

22. Heintze, C.; Bergner, F.; Hernández-Mayoral, M.
Ion-irradiation induced damage in FeCr alloys characterized by nanoindentation
CAARI 2012 - 22nd International Conference on the Application of Accelerators in Research and Industry, 05.-10.08.2012, Fort Worth, USA

23. Helm, M.
Intra-excitonic coherent nonlinear optics in quantum wells: the Autler-Townes effect and beyond
31th International Conference on the Physics of Semiconductors (ICPS 2012), 29.07.-03.08.2012, Zürich, Switzerland

24. Helm, M.
Terahertz nonlinear optics of excitons in quantum wells using a free-electron laser
Viennese Symposium on Heterostructures, 07.09.2012, Wien, Austria

25. Helm, M.; Winnerl, S.; Mittendorff, M.; Schneider, H.; Winzer, T.; Malic, E.; Knorr, A.; Orlita, M.; Potemski, M.; Sprinkle, M.; Berger, C.; de Heer, W. A.
Carrier dynamics in graphene near the Dirac point

Joint Dresden-Japan Workshop on Molecular Scale and Organic Electronic Materials, 11.-13.12.2012, Dresden, Germany

26. Keller, A.
Nanostrukturierung von Oxidoberflächen mit Ionenstrahlen: Einfluss auf Zelladhäsion und -proliferation
12. Sitzung des Arbeitskreises Biokeramik, 16.11.2012, Aachen, Germany

27. Kolitsch, A.; Yankov, R.
Ionenstrahlbasierte Oberflächenmodifizierung von TiAl-Werkstoffen
3. Dresdner Werkstoffsymposium 2012, 06.-07.12.2012, Dresden, Germany

28. Lindner, J.
Magnetism at the nanoscale: Importance of Surfaces and Interfaces
14th Joint Vacuum Conference, 04.-04.06.2012, Dubrovnik, Croatia

29. Lipp Bregolin, F.; Sias, U. S.; Behar, M.; Prucnal, S.; Rebohle, L.; Skorupa, W.
Ion implantation techniques for silicon based photovoltaics and light emitters
IXth International Conference Ion Implantation and other applications of Ions and Electrons - ION 2012, 25.-28.06.2012, Kazimierz Dolny, Poland

30. Meyer, D. C.; Stöcker, H.; Hanzig, J.; Hanzig, F.; Zschornak, M.; Abendroth, B.; Gemming, S.
Electric Formation of Metal/SrTiO3 Junctions and its Correlation to Multi-Dimensional Defects
DPG Spring Meeting of the Condensed Matter Section, 25.-30.03.2012, Berlin, Germany

31. Mittendorff, M.; Winnerl, S.; Schneider, H.; Helm, M.; Orlita, M.; Potemski, M.; Winzer, T.; Malic, E.; Knorr, A.; Sprinkle, M.; Berger, C.; de Heer, W. A.
Relaxation dynamics in Landau quantized graphene
THz Dynamics in Carbon Based Nanostructures, 07.03.2012, Dresden, Germany

32. Möller, W.
Ion beams for application in science and industry: Activities in Germany and the European infrastructure project SPIRIT
Ion Beams '12: Multidisciplinary Applications of Nuclear Physics with Ion Beams, 06.-08.06.2012, Legnaro, Italy

33. Prucnal, S.; Facsko, S.; Mücklich, A.; Zhou, S. Q.; Ou, X.; Liedke, M. O.; Turek, M.; Zuk, J.; Skorupa, W.
III-V compound semiconductors integrated with silicon for functional photronic devices
E-MRS 2012 Spring Meeting, 14.-18.05.2012, Strasbourg, France

34. Prucnal, S.; Zuk, J.; Pyszniak, K.; Drozdziel, A.; Facsko, S.; Mücklich, A.; Zhou, S. Q.; Ou, X.; Liedke, M. O.; Liedke, B.; Turek, M.; Skorupa, W.
Flash lamp processing of III/V compound semiconductors on silicon and SOI wafers for functional photronic devices
IXth International Conference Ion Implantation and other applications of Ions and Electrons - ION 2012, 25.-28.06.2012, Kazimierz Dolny, Poland

35. Redondo-Cubero, A.; Lorenz, K.; Alves, E.; Gago, R.; Hierro, A.; Vinnichenko, M.; Chauveau, J.-M.; Nakamura, A.; Krause, M.; Temmyo, J.; Muñoz, E.; Brandt, M.; Henneberger, F.
Ion beams as a tool for advanced structural characterization in ZnO-based materials
SPIE Photonics West, Optoelectronic Materials and Devices, Oxide-based Materials and Devices III (Conference 8263), 22.-25.01.2012, San Francisco, USA

36. Rugel, G.
Acclerator Mass Spectrometry
496. Wilhelm und Else Heraeus-Seminar - Astrophysics with modern small-scale accelerators, 06.-10.02.2012, Bad Honnef, Germany

37. Schneider, H.
Exciton dynamics in GaAs quantum wells studied with a free-electron laser
The 6th International Symposium on Ultrafast Phenomena and THz Waves (ISUPTW2012), POEM OSA Topical Meeting, 01.-02.11.2012, Wuhan, China

38. Skorupa, W.
Subsecond thermal processing for advanced electronics and photovoltaics
E-MRS 2012 Spring Meeting, Symposium A: Advanced Silicon Materials Research for Electronic and Photovoltaic Applications III, 14.-18.05.2012, Strasbourg, France

39. Skorupa, W.
Advanced approaches to electronic materials using subsecond thermal processing
IXth International Conference Ion Implantation and other applications of Ions and Electrons - ION 2012, 25.-28.06.2012, Kazimierz Dolny, Poland

40. Skorupa, W.
More Moore or more-than-Moore or nothing more? A nanoview on silicon & germanium...
E-MRS 2012 Fall Meeting, 17.-21.09.2012, Warsaw, Poland

41. Skorupa, W.
s-Temperung von HL & Dielektrika more Moore & more than Moore & Nothing more...
EFDS-Workshop "Struktur und Eigenschaften dielektrischer Schichten für die Optik", 07.11.2012, Jena, Germany

42. Skrotzki, R.; Herrmannsdörfer, T.; Heera, V.; Fiedler, J.; Schönemann, R.; Philipp, P.; Bischoff, L.; Voelskow, M.; Mücklich, A.; Schmidt, B.; Skorupa, W.; Helm, M.; Wosnitza, J.
On-chip superconductivity above 7 K in microstructured 10 nm thin Ga films embedded in Si wafers
M2S 2012 - Materials and Mechanisms of Superconductivity, 29.07.-03.08.2012, Washington, USA

43. Vinnichenko, M.; Hauschild, D.; Cornelius, S.; Krause, M.; Gago, R.; Mücklich, A.; Lissotschenko, V.; Kolitsch, A.
Modification of ZnO:Al properties: post-deposition millisecond thermal processing vs direct growth at elevated substrate temperature
10th International Symposium on Ceramic Materials and Components for Energy and Environmental Applications (10th CMCEE), 21.-23.05.2012, Dresden, Germany

44. Werniewicz, K.
In the search for a dream job - discovering your own potential.
The BioTiNet Summer School "Titanium in Medicine", 04.-08.06.2012, Caldes d'Estrac, Barcelona, Spain

45. Werniewicz, K.
Scientific publishing – writing successful papers
The BioTiNet Summer School "Titanium in Medicine", 04.-08.06.2012, Caldes d'Estrac, Barcelona., Spain

46. Werniewicz, K.
Scientific publishing – writing successful papers
IXth International Conference Ion Implantation and other applications of Ions and Electrons - ION 2012, 25.-28.06.2012, Kazimierz Dolny, Poland

47. Winnerl, S.
Semiconductor quantum structures in high THz fields
503th Wilhelm and Else Heraeus Seminar Free-Electron Lasers: from Fundamentals to Applications, 10.-13.04.2012, Bad Honnef, Germany

48. Winnerl, S.
Graphene excited with short infrared pulses: fundamental aspects and application perspectives
7th International Conference on Surfaces, Coatings and Nanostructured Materials, 18.-21.09.2012, Prague, Czech Republic

49. Zhou, S.
Introducing ferromagnetism into semiconductors by ion beams
18th International Conference on Ion Beam Modifications of Materials, 02.-07.09.2012, Qingdao, China

Conference talks

1. Abrasonis, G.; Krause, M.; Gemming, S.; Bilek, M. M. M.; Möller, W.
Ion-assisted deposition of carbon-transition metal nanocomposite thin films
13th International Conference on Plasma Surface Engineering - PSE 2012, 10.-14.09.2012, Garmisch-Partenkirchen, Germany

2. Abrasonis, G.; Krause, M.; Oates, T. W. H.; Mücklich, A.; Facsko, S.; Baehtz, C.; Shalimov, A.; Gemming, S.
Ion-guided phase separation of carbon-nickel composite films during ion beam assisted deposition: 3D sculpting at the nanoscale
AVS 59th International Symposium & Exhibition, 28.10.-02.11.2012, Tampa, Florida, USA

3. Akhmadaliev, Sh.; Rugel, G.; Kolitsch, A.; von Borany, J.
The new 6 MV tandem accelerator at HZDR
Workshop Ionenstrahlphysik, 10.-11.07.2012, Augsburg, Germany

4. Anwand, W.; Butterling, M.; Brauer, G.; Wagner, A.; Richter, A.; Chen, C.-L.; Kögler, R.
Ion implantation-induced defects in Oxide Dispersion Strengthened (ODS) steel probed by positron annihilation spectroscopy
DPG Spring Meeting of the Condensed Matter Section, 25.-30.03.2012, Berlin, Germany

5. Ball, D. K.; Fritzsche, M.; Osten, J.; Lenz. K.; Facsko, S.; Mücklich, A.; Fassbender, J.
Tailoring the magnetic damping and anisotropy of Permalloy deposited on GaSb nanocones.
IEEE International Magnetics Conference 2012 (Intermag 2012), 07.-11.05.2012, Vancouver, Canada

6. Baumgart, C.; Habicht, S.; Feste, S.; Helm, M.; Mantl, S.; Schmidt, H.
Kelvin probe force microscopy imaging on horizontal locally doped silicon nanowires
DPG Spring Meeting of the Condensed Matter Section, 25.-30.03.2012, Berlin, Germany

7. Baumgart, C.; Habicht, S.; Feste, S.; Helm, M.; Müller, A.-D.; Schmidt, H.
Kelvin probe force microscopy for characterizing functionalized semiconductor surfaces for nano and biotechnologies
E-MRS Fall Meeting 2012, 17.-21.09.2012, Warsaw, Poland

8. Bergner, F.; Anwand, W.; Butterling, M.; Heintze, C.; Jungmann, M.; Kolitsch, A.; Krause-Rehberg, R.; Ulbricht, A.; Wagner, A.
Application of positron annihilation spectroscopy to the study of irradiated Fe-Cr alloys
21st Workshop on Iron-Chromium Alloys and 3rd Workshop on nuclear Fe alloys: modelling and experiments, 29.-31.10.2012, Alicante, Spain

9. Bergner, F.; Ulbricht, A.; Wagner, A.; Kuksenko, S.; Pareige, C.; Pareige, P.; Malerba, L.
Critical assessment of Cr-rich precipitates in neutron-irradiated Fe-12at%Cr
Joint IAEA - EC Topical meeting on Development of new structural materials for advanced fission and fusion reactor systems, 16.-20.04.2012, JRC Ispra, Italy

10. Bernert, K.; Sluka, V.; Fowley, C.; Gan, H.; Fassbender, J.; Deac, A. M.
Switching phase diagrams and backhopping in Magnetic Tunnel Junctions (MTJs)
IEEE International Magnetics Conference 2012 (Intermag 2012), 07.-11.05.2012, Vancouver, Canada

11. Bernert, K.; Sluka, V.; Fowley, C.; Gan, H.; Fassbender, J.; Deac, A. M.
Switching phase diagrams and backhopping in Magnetic Tunnel Junctions (MTJs)
The IEEE International Conference on Microwave Magnetics, 26.-29.08.2012, Kaiserslautern, Germany

12. Bernert, K.; Sluka, V.; Fowley, C.; Gan, H.; Fassbender, J.; Deac, A. M.
Switching voltages and back-hopping in magnetic tunnel junctions with different geometries
The IEEE International Conference on Microwave Magnetics, 26.-29.08.2012, Kaiserslautern, Germany

13. Bhattacharyya, J.; Zybell, S.; Helm, M.; Schneider, H.; Andrews, A. M.; Strasser, G.; Schneebeli, L.; Böttge, C. N.; Breddermann, B.; Chatterjee, S.; Kira, M.; Koch, S. W.

Time-resolved photoluminescence quenching by intra-excitonic transitions in presence of external magnetic field
11th International Workshop on Nonlinear Optics and Excitation Kinetics in Semiconductors, 23.-27.09.2012, Stuttgart, Germany

14. Bhattacharyya, J.; Zybell, S.; Winnerl, S.; Hopkinson, M.; Wilson, L. R.; Andrews, A. M.; Strasser, G.; Helm, M.; Schneider, H.
Intraband carrier dynamics in quantum dots and quantum wells
International Conference on Superlattices, Nanostructures and Nanodevices, 22.-27.07.2012, Dresden, Germany

15. Bischoff, L.
Status and new trends in FIB processing
Workshop Ionenstrahlphysik 2012, 10.-11.07.2012, Augsburg, Germany

16. Böttger, R.; Bischoff, L.; Heinig, K.-H.; Schmidt, B.; Anders, C.; Urbassek, H.
Taming nanostructures: From sponge to dot pattern on Ge controlled by heavy-ion-deposited energy
56th International Conference on Electron, Ion and Photon Beam Technology and Nanofabrication, 29.05.-01.06.2012, Waikoloa, USA

17. Buljan, M.; Baehtz, C.; Holý, V.; Radić, N.; Roshchupkina, O.; Prucnal, S.; Mücklich, A.; Valeš, V.; Bernstorff, S.; Grenzer, J.
Manipulation of Ge quantum dot ordering in alumina matrix by deposition conditions
DPG Spring Meeting of the Condensed Matter Section, 25.-30.03.2012, Berlin, Germany

18. Bürger, D.; Zhou, S.; Höwler, M.; Ou, X.; Kovacs, G.; Reuther, H.; Mücklich, A.; Skorupa, W.; Helm, M.; Schmidt, H.
Anomalous hysteretic Hall effect in a ferromagnetic, Mn-rich, amorphous Ge:Mn nano-network
DPG Spring Meeting of the Condensed Matter Section, 25.-30.03.2012, Berlin, Germany

19. Bürger, D.; Zhou, S.; Höwler, M.; Ou, X.; Kovacs, György J.; Reuther, H.; Mücklich, A.; Skorupa, W.; Helm, M.; Schmidt, H.
Synthesis and characterization of a percolating, ferromagnetic, Mn-rich Ge:Mn nanonet with hysteretic transport properties
E-MRS 2012 Fall Meeting, 17.-21.09.2012, Warschau, Poland

20. Butterling, M.; Anwand, W.; Bergner, F.; Cowan, T. E.; Heinze, C.; Ulbricht, A.; Wagner, A.; Krause-Rehberg, R.
Defect characterization of ion-implanted Fe-Cr alloys using positron Doppler broadening spectroscopy
Workshop Ionenstrahlphysik 2012, 09.-11.07.2012, Augsburg, Germany

21. Butterling, M.; Anwand, W.; Cowan, T. E.; Skorupa, W.; Wagner, A.; Häberle, J.; Jungmann, M.; Krille, A.; Krause-Rehberg, R.; Eule, A. C.
Structural characterization of lead sheets for organ pipes by positron annihilation spectroscopy
DPG Spring Meeting of the Condensed Matter Section, 25.-30.03.2012, Berlin, Germany

22. Cherkouk, C.; Rebohle, L.; Gerlach, T.; Kunze, G.; Lenk, J.; Ou, X.; Pietzsch, J.; Skorupa, W.
A controlled immobilization of His-tagged estrogen receptor hERa: Comparison study between the kinetics and morphology
E-MRS 2012 Spring Meeting, 14.-18.05.2012, Strasbourg, France

23. Cornelius, S.; Vinnichenko, M.; Munnik, F.; Heller, R.; Kolitsch, A.; Möller, W.
Process control, performance limits and dopant activation for Al-doped ZnO grown by reactive pulsed magnetron sputtering
13th International Conference on Plasma Surface Engineering (PSE 2012), 09.-14.09.2012, Garmisch-Partenkirchen, Germany

24. Cornelius, S.; Vinnichenko, M.; Munnik, F.; Möller, W.
Quantification of Al and Ga electrical activation in ZnO films grown by reactive magnetron sputtering
4th Symposium on Transparent Conductive Materials 2012, 21.-26.10.2012, Chersonissos, Crete, Greece

25. Donchev, A.; Schütze, M.; Yankov, R. A.; Kolitsch, A.
Efficient oxidation protection of Ti- and TiAl-alloys by fluorine treatments
TMS Annual Meeting 2012, 11.-15.03.2012, Orlando, Florida, USA

26. Endler, R.; Voelskow, M.; Mücklich, A.; Schumann, T.; Skorupa, W.
Thin silicon films - texture and grain size improvement
31. Deutsches Nutzertreffen RTP und Heißprozesse, 21.03.2012, Erlangen, Germany

27. Facsko, S.; Fritzsche, M.; Ou, X.; Keller, A.; Mücklich, A.
Ion induced patterns on Ge surfaces
Workshop Ionenstrahlphysik, 10.-11.07.2012, Augsburg, Germany

28. Facsko, S.
Periodic nanoscale patterns induced by ion irradiation: Ripples, dots, and holes
19th International Workshop on Inelastic Ion-Surface Collisions (IISC-19), 16.-21.09.2012, Frauenchiemsee, Germany

29. Fassbender, J.; Körner, M.; Lenz, K.; Strache, T.; Banholzer, A.; Grebing, J.; Lindner, J.; Barsukov, I.; Römer, F.; Meckenstock, R.; Hemken To Krax, S.; Farle, M.; McCord, J.; Mönch, I.; Mattheis, R.
Magnonic crystals by means of patterned ion implantation
18th International Conference on Ion Beam Modification of Materials (IBMM2012), 02.-07.09.2012, Qingdao, China

30. Fiedler, J.; Heera, V.; Skrotzki, R.; Herrmannsdörfer, T.; Voelskow, M.; Mücklich, A.; Facsko, S.; Reuther, H.; Perego, M.; Schmidt, B.; Skorupa, W.; Gobsch, G.; Helm, M.
Superconductivity in Ga-implanted group-IV semiconductors
18th International Conference on Ion Beam Modifications of Materials (IBMM 2012), 02.-07.09.2012, Qingdao, China

31. Fiedler, J.; Heera, V.; Skrotzki, R.; Herrmannsdörfer, T.; Voelskow, M.; Mücklich, A.; Schmidt, B.; Skorupa, W.; Gobsch, G.; Helm, M.
Superconducting layers by Ga implantation and short-term annealing in Si
IXth International Conference Ion Implantation and other applications of Ions and Electrons - ION 2012, 25.-28.06.2012, Kazimierz Dolny, Poland

32. Fiedler, J.; Heera, V.; Skrotzki, R.; Herrmannsdörfer, T.; Voelskow, M.; Mücklich, A.; Skorupa, W.; Gobsch, G.; Helm, M.
Properties of Ga implanted germanium and silicon
Struktur und Eigenschaften Dielektrischer Schichten für die Optik, 07.11.2012, Jena, Germany

33. Gao, K.; Prucnal, S.; Anwand, W.; Skorupa, W.; Helm, M.; Zhou, S.
Quasi-temperature stable luminescence at 1.3 µm from flash lamp annealed GaAs
European Materials Research Society Spring Meeting, 14.-18.05.2012, Strasbourg, France

34. Gao, K.; Prucnal, S.; Jiang, Z.; Skorupa, W.; Helm, M.; Yastrubchak, O.; Gluba, L.; Zhou, S.
Millisecond flash lamp annealed GaAs: a promising light emitter material at 1.3 um
DPG Spring Meeting of the Condensed Matter Section, 25.-30.03.2012, Berlin, Germany

35. Gao, K.; Prucnal, S.; Mücklich, A.; Skorupa, W.; Zhou, S.
Fabrication of Si(1-x)Ge(x) alloy on silicon by Ge-ion-implantation and short-time-annealing
IXth International Conference Ion Implantation and other applications of Ions and Electrons - ION 2012, 25.-28.06.2012, Kazimierz Dolny, Poland

36. Germer, S.; Rebohle, L.; Helm, M.; Skorupa, W.
Si-based light emitters in integrated photonic circuits for smart biosensor applications
DPG Spring Meeting of the Section AMOP, 12.-16.03.2012, Stuttgart, Germany

37. Geyer, N.; Tonkikh, A. A.; Ou, X.; Kögler, R.; Skorupa, W.; Werner, P.
Tailoring the properties of semiconductor nanowiresfor thermoelectric applicationsby means of metal-assisted chemical etching
31th International and 10th European Conference on Thermoelectrics, 09.-12.07.2012, Aalborg, Denmark

38. Greene, P. K.; Osten, J.; Fassbender, J.; Endo, T.; Iwata, N.; Liu, K.
Tuning perpendicular anisotropy gradients in Co/Pd multilayers by Ar ion irradiation

IEEE International Magnetics Conference 2012 (Intermag 2012), 07.-11.05.2012, Vancouver, Canada

39. Grenzer, J.; Buljan, M.; Roshchupkina, O.; Baehtz, C.; Holý, V.
In-situ observation of the Self-assembled growth of ordered Ge nanocrystals embedded within a dielectrical matrix
DPG Spring Meeting of the Condensed Matter Section, 25.-30.03.2012, Berlin, Germany

40. Grenzer, J.; Buljan, M.; Holý, V.; Baehtz, C.; Horák, L.; Bernstorff, S.; Radić, N.
In-situ real-time observation of the self-assembled growth of ordered germanium nanocrystals embedded within a dielectric matrix
The 11th Biennial Conference on High Resolution X-Ray Diffraction and Imaging, 15.-20.09.2012, Saint-Petersburg, Russia

41. Gündoğdu, S.; Özen, E. S.; İlday, S.; Heinig, K.-H.; Turan, R.; Aydinli, A.
Si nanocrystal networks by Si/SiO_2 phase separation in SiOx thin films for third generation solar cells
Solar Electricity Conference & Exhibition (SOLARTR-2), 07.-09.11.2012, Antalya, Turkey

42. Heinig, K.-H.; Schmidt, B.; Mücklich, A.; Liedke, B.; Kelling, J.; Friedrich, D.; Hauschild, D.; Stegemann, K.-H.; Keles, U.; Bulutay, C.; Aydinli, A.
Networks of Si nanowires in SiO_2 for solar cells
E-MRS Spring Meeting 2012, Symp. A, 14.-18.05.2012, Strasbourg, France

43. Heinig, K.-H.; Böttger, R.; Bischoff, L.; Liedke, B.; Urbassek, H.; Anders, C.
Morphology of Ge surfaces after Bi, Bi2 and Bi3 ion impacts: holes, dots and sponge
Workshop Ionenstrahlphysik, 10.-11.07.2012, Augsburg, Germany

44. Heinig, K.-H.; Böttger, R.; Liedke, B.; Bischoff, L.; Anders, C.; Urbassek, H.
Surface patterning of Ge and Si by heavy ion and cluster impacts: Experiments, atomistic simulations and theory
19th International Workshop on Inelastic Ion-Surface Collisions (IISC-19), 16.-21.09.2012, Frauenchiemsee, Germany

45. Hinsche, N. F.; Yavorsky, B. Yu.; Mertig, I.; Zahn, P.
Thermoelectric transport in Bi_2Te_3/Sb_2Te_3 heterostructures
DPG Spring Meeting of the Condensed Matter Section, 25.-30.03.2012, Berlin, Germany

46. Hölzer, M.; Hinsche, N. F.; Ernst, A.; Mertig, I.; Zahn, P.
Boltzmann transport theory applied to Bi_2Te_3
Thermoelectric properties related to nanostructure and dimensionality in Bi2Te3 nanomaterials, 05.-06.07.2012, Darmstadt, Germany

47. Jacob, R.; Fehrenbacher, M.; Winnerl, S.; Bhattacharyya, J.; Schneider, H.; Helm, M.; von Ribbeck, H.-G.; Eng, L. M.; Atkinson, P.; Rastelli, A.; Schmidt, O. G.
Scanning near-field infrared micro-spectroscopy on buried InAs quantum dots
DPG Spring Meeting of the Condensed Matter Section, 25.-30.03.2012, Berlin, Germany

48. Junghähnel, M.; Fietzke, F.; Vinnichenko, M.; Cornelius, S.
Recent developments of TiO_2:Nb sputtered with high deposition rates from a rotatable magnetron system
55th Annual Society of Vacuum Coaters Technical Conference, 28.04.-03.05.2012, Santa Clara, USA

49. Keller, A.; Andersen, O. Z.; Foss, M.; Facsko, S.; Kraft, D. C.; Besenbacher, F.
Response of human mesenchymal stem cells to ion-sputtered surfaces
Workshop Ionenstrahlphysik, 10.-11.07.2012, Augsburg, Germany

50. Körner, M.; Lenz, K.; Banholzer, A.; Grebing, J.; Barsukov, I.; Römer, F. M.; Lindner, J.; Farle, M.; Fassbender, J.
Extrinsically controlled spin relaxation in NiFe thin films induced by a periodic scattering potential
DPG Spring Meeting of the Condensed Matter Section, 25.-30.03.2012, Berlin, Germany

51. Körner, M.; Lenz, K.; Fritzsche, M.; Facsko, S.; Fassbender, J.
Morphology induced two-magnon scattering in thin NiFe films

IEEE International Magnetics Conference 2012 (Intermag 2012), 07.-11.05.2012, Vancouver, Canada

52. Lehmann, J.; Mücklich, A.; von Borany, J.; Skorupa, W.; Schäfer, A.; Schubert, J.; Mantl, S.
Post-deposition flash-lamp annealing of high-k materials
E-MRS 2012 Spring Meeting, 14.-18.05.2012, Strassbourg, France

53. Liedke, B.; Heinig, K.-H.; Gulseren, O.; Akguc, G. B.; Vinnichenko, M.
Thin film PV cell with Ag nanoparticle layers in TCO and Si nanosponge absorber
E-MRS 2012 Spring Meeting, 14.-18.05.2012, Strasbourg, France

54. Liedke, B.; Heinig, K.-H.; Schmidt, B.; Friedrich, D.; Mücklich, A.; Kelling, J.; Hauschild, D.
Si-nanosponge embedded in SiO_2 as a new absorber material for photovoltaics
DPG Spring Meeting of the Condensed Matter Section, 25.-30.03.2012, Berlin, Germany

55. Liedke, B.; Mücklich, A.; Heinig, K.-H.; Schmidt, B.; Friedrich, D.; Keles, U.; Bulutay, C.
EFTEM studies of Si nanowire networks in SiO_2 for thin film PV cells
E-MRS 2012 Spring Meeting, 14.-18.05.2012, Strasbourg, France

56. Martinavičius, A.; Danoix, R.; Danoix, F.; Abrasonis, G.; Drouet, M.; Templier, C.; Hannoyer, B.
Atom probe tomography characterization of the decomposition in austenitic stainless steels 304L and 316L induced by low temperature plasma nitriding
13th International Conference on Plasma Surface Engineering - PSE 2012, 10.-14.09.2012, Garmisch-Partenkirchen, Germany

57. Martins, R. M. S.; Barradas, N.; Alves, E.; Henke, D.; Reuther, H.; Schell, N.; Carmezim, M. J.; Silva, T. M.; Fernandes, J. C. S.
Modification of Ni-Ti surface composition and morphology by plasma immersion ion implantation for biomedical applications
MPA 2012 - 6th International Meeting on Developments in Materials, Processes and Applications of Emering Technologies, 02.-04.07.2012, Alvor, Portugal

58. Masset, P.; Bleicher, F.; Bortolotto, L.; Geiger, G.; Kolitsch, A.; Langlade, C.; Paul, J.; Pelic, B.; Pyczak, F.; Rafaja, D.; Schumacher, P.; Schütze, M.; Wolf, G.; Yankov, R.
Improvement of the resistance of titanium aluminides to environmental embrittlement
Pacific Rim Meeting on Electrochemical and Solid-State Science (PRIME 2012), 07.-12.10.2012, Honolulu, Hawaii, USA

59. Matlack, K.; Wall, J.; Kim, J. Y.; Qu, J.; Jacobs, L. J.; Viehrig, H.-W.
Capability of nonlinear ultrasonic methods to monitor radiation damage in reactor pressure vessel steels
NuMat 2012: The Nuclear Materials Conference, 22.-25.10.2012, Osaka, Japan

60. Mazalski, P.; Maziewski, A.; Liedke, M. O.; Fassbender, J.; Ferré, J.; Mougin, A.; Baczewski, L. T.; Wawro, A.; Rogalev, A.; Wilhelm, F.
XAS/XMCD studies of Ga^+ irradiation driven magnetization reorientation in Pt/Co/Pt nanostructures
ESRF Users' Meeting 2012, 06.-09.02.2012, Grenoble, France

61. Merchel, S.; Akhmadaliev, Sh.; Fimiani, L.; Haubold, R.; Herrmann, S.; Korschinek, G.; Ott, U.; Pavetich, S.; Rugel, G.
Reconstruction of Gebel Kamil's irradiation history
Joint meeting "Paneth Kolloquium", "The first 10 million years of the solar system" (DFG SPP 1385) & "MEMIN" (DFG FOR 887), 09.-12.10.2012, Nördlingen, Germany

62. Merchel, S.; Akhmadaliev, Sh.; Rugel, G.; Cartwright, J. A.; Ott, U.; Faestermann, T.; Fimiani, L.; Korschinek, G.; Ludwig, P.
Cosmogenic nuclides in meteorites
DPG Spring Meeting of the Section AMOP, 12.-16.03.2012, Stuttgart, Germany

63. Mittendorff, M.; Winnerl, S.; Schneider, H.; Helm, M.; Orlita, M.; Potemski, M.; Berger, C.; de Heer, W. A.
Relaxation dynamics in Landau-quantized graphene probed in the mid-infrared range
DPG Spring Meeting of the Condensed Matter Section, 25.-30.03.2012, Berlin, Germany

64. Mittendorff, M.; Winnerl, S.; Schneider, H.; Helm, M.; Orlita, M.; Potemski, M.; Wendler, F.; Malic, E.; Knorr, A.; Sprinkle, M.; Berger, C.; de Heer, W. A.

Selective pump-probe measurements in Landau quantized graphene
International Conference on Superlattices, Nanostructures, and Nanodevices, 22.-27.07.2012, Dresden, Germany

65. Mok, K. M.; Scarlat, C.; Kovacs, G. J.; Li, L.; Zviagin, V.; McCord, J.; Helm, M.; Schmidt, H.
Magneto-optical coupling in ferromagnetic thin films investigated by VMOGE
7th Workshop Ellipsometry, 05.-07.03.2012, Leipzig, Germany

66. Mok, K. M.; Scarlat, C.; Kovacs, G. J.; Li, L.; Zviagin, V.; McCord, J.; Helm, M.; Schmidt, H.
Magneto-optical coupling in ferromagnetic thin films investigated by VMOGE
DPG Spring Meeting of the Condensed Matter Section, 25.-30.03.2012, Berlin, Germany

67. Munnik, F.; Hanf, D.; Wilhelm, R. A.; von Borany, J.; Lange, H.
Comparison of a new simple system for high depth resolution RBS with the magnetic spectrometer
Workshop Ionenstrahlphysik, 10.-11.07.2012, Augsburg, Germany

68. Murali, D.; Kaur, G.; Jegadeesan, P.; Panigrahi, B. K.; Valsakumar, M. C.; Posselt, M.
Y-Ti-O nanocluster formation in Bcc Fe using DFT and kinetic Monte Carlo simulations
Multiscale Materials Modeling (MMM) 2012, 15.-19.10.2012, Singapore, Singapore

69. Neubert, M.; Vinnichenko, M.; Cornelius, S.; Kolitsch, A.
Tantalum incorporation in TiO_2 based transparent conductive thin films
DPG Spring Meeting of the Condensed Matter Section, 25.-30.03.2012, Berlin, Germany

70. Neubert, M.; Vinnichenko, M.; Cornelius, S.; Kolitsch, A.
TCOs auf Basis Tantal-dotierter TiO_2 Schichten
Workshop „Transparente leitfähige Oxide - Festkörperphysikalische Grundlagen und Technologie", 21.-22.05.2012, Dresden, Germany

71. Neubert, M.; Vinnichenko, M.; Fiedler, J.; Gebel, T.; Liepack, H.; Kolitsch, A.
Low electrical resistivity polycrystalline TiO_2-based transparent conductive thin films by DC magnetron sputter deposition
4th International Symposium on Transparent Conductive Materials, 21.-26.10.2012, Hersonnisos, Greece

72. Nogay, G.; İlday, S.; Turan, R.; Heinig, K.-H.; Friedrich, D.
Spectroscopic ellipsometry studies of nc-Si/a-Si and nc-Si/SiOx systems: Optical characterization of crystallization
Solar Electricity Conference & Exhibition (SOLARTR-2), 07.-09.11.2012, Antalya, Turkey

73. Ou, X.; Kögler, R.; Mücklich, A.; Skorupa, W.; Facsko, S.; Helm, M.
Fabrication of Si and Ge nanostructure arrays by ion beam irradiation
International Conference on Superlattices, Nanostructures and Nanodevices (ICSNN 2012), 22.-27.07.2012, Dresden, Germany

74. Ou, X.; Kögler, R.; Wei, X.; Mücklich, A.; Skorupa, W.; Facsko, S.; Wang, X
Fabrication of Si and Ge nanostructure arrays
The 18th International Conference on Ion Beam Modifications of Materials (IBMM2012), 02.-07.09.2012, Qingdao, China

75. Pavetich, S.; Akhmadaliev, Sh.; Merchel, S.; Rugel, G.
Development of an ion source for volatile elements at DREAMS
DPG Spring Meeting of Section AMOP, 12.-16.03.2012, Stuttgart, Germany

76. Philipp, P.; Bischoff, L.; Schmidt, B.
Taming of Ga droplets on DLC layers – Size tuning and local arrangement with nanometer accuracy
56th international conference on electron, ion, and photon beam technology and nanofabrication (EIPBN), 29.05.-01.06.2012, Waikoloa Village, Hawaii, USA

77. Posselt, M.
Free energy of embedded nanoclusters: Role of the configurational contributions
MMM 2012 - 6th International Conference on Multiscale Materials Modeling, 15.-19.10.2012, Singapore, Singapore

78. Prucnal, S.; Facsko, S.; Mücklich, A.; Zhou, S. Q.; Ou, X.; Liedke, M. O.; Turek, M.; Zuk, J.; Skorupa, W.

III-V compound semiconductors integrated with silicon for functional optoelectronic devices
Workshop Ionenstrahlphysik 2012, 10.-11.07.2012, Augsburg, Germany

79. Radek, M.; Bracht, H.; Posselt, M.; Schmidt, B.
Ion-beam mixing in crystalline and amorphous germanium isotope multilayers
DPG Spring Meeting of the Condensed Matter Section, 25.-30.03.2012, Berlin, Germany

80. Rebohle, L.; Prucnal, S.; Lehmann, J.; Germer, S.; Skorupa, W.
Lumineszenz von Seltenen Erden in SiO_2
EFDS Seminar "Struktur und Eigenschaften dielektrischer Schichten für die Optik", 07.11.2012, Jena, Germany

81. Rebohle, L.; Wutzler, R.; Germer, S.; Lehmann, J.; Helm, M.; Skorupa, W.
Er- and Nd-implanted MOS light emitting devices and their use for integrated photonic applications
SPIE Photonics Europe, 16.-19.04.2012, Brüssel, Belgium

82. Richter, R.; Neelmeijer, C.
The Waldenburg beakers and Johann Kunckel: Analytical and technological study of four corner-cut colored glasses
IIC Congress - The Decorative: Conservation and the Applied Arts, 10.-14.09.2012, Wien, Austria

83. Ritter, R.; Wilhelm, R. A.; Stöger-Pollach, M.; Mücklich, A.; Werner, U.; Beyer, A.; Facsko, S.; Gölzhäuser, A.; Aumayr, F.
Nanopores milled in carbon nanomembranes due to impact of individual slow highly charged ions
Workshop Ionenstrahlphysik, 10.-11.07.2012, Augsburg, Germany

84. Rugel, G.; Akhmadaliev, Sh.; Merchel, S.; Pavetich, S.
Status von AMS–Messungen an DREAMS
DPG Spring Meeting of the Section AMOP, 12.-16.03.2012, Stuttgart, Germany

85. Schmidt, K.; Akhmadaliev, Sh.; Anders, M.; Bemmerer, D.; Boretzky, K.; Caciolli, A.; Dietz, M.; Elekes, Z.; Fülöp, Z.; Gyürky, G.; Hannaske, R.; Junghans, A.; Marta, M.; Menzel, M.-L.; Schwengner, R.; Szücs, T.; Wagner, A.; Yakorev, D.; Zuber, K.
The $^{40}Ca(\alpha,\gamma)^{44}Ti$ reaction studied by activation
VIII Tours Symposium on Nuclear Physics and Astrophysics, 02.-07.09.2012, Lenzkirch-Saig, Germany

86. Schmidt, K.; Akhmadaliev, Sh.; Anders, M.; Bemmerer, D.; Boretzky, K.; Caciolli, A.; Dietz, M.; Elekes, Z.; Fülöp, Z.; Gyürky, G.; Hannaske, R.; Junghans, A.; Marta, M.; Menzel, M.-L.; Schwengner, R.; Szücs, T.; Wagner, A.; Yakorev, D.; Zuber, K.
Untersuchung der $^{40}Ca(\alpha,\gamma)^{44}Ti$ -Reaktion bei E_α ~ 3.5 MeV
DPG Spring Meeting 2012, 19.-23.03.2012, Mainz, Germany

87. Schmidt, K.; Akhmadaliev, Sh.; Anders, M.; Bemmerer, D.; Boretzky, K.; Caciolli, A.; Elekes, Z.; Fülöp, Z.; Gyürky, G.; Hannaske, R.; Junghans, A.; Marta, M.; Schwengner, R.; Szücs, T.; Wagner, A.; Zuber, K.
Resonanzstärken in der $^{40}Ca(\alpha,\gamma)^{44}Ti$ -Reaktion
496. Wilhelm und Else Heraeus-Seminar - Astrophysics with modern small-scale accelerators, 05.-10.02.2012, Bad Honnef, Germany

88. Schneider, H.; Bhattacharyya, J.; Zybell, S.; Winnerl, S.; Helm, M.; Andrews, A. M.; Strasser, G.; Köhler, K.
Free-electron laser spectroscopy of quantum well exciton dynamics
37th International Conference on Infrared, Millimeter and Terahertz Waves (IRMMW-THZ 2012), 23.-28.09.2012, Wollongong, Australia

89. Skorupa, W.; Cherkouk, C.; Henke, D.; Prucnal, S.; Reuther, H.; Werner, H.; Pfeifer, D.; Eule, A.-C.
Anticorrosion studies for pipe organ-related materials using plasma processing
13th International Conference on Plasma Surface Engineering, 10.-14.09.2012, Garmisch-Partenkirchen, Germany

90. Sluka, V.; Kákay, A.; Deac, A. M.; Bürgler, D. E.; Hertel, R.; Schneider, C. M.
Core-core interaction in spin-torque double-vortex oscillators
IEEE International Magnetics Conference 2012 (Intermag 2012), 07.-11.05.2012, Vancouver, Canada

91. Teich, M.; Wagner, M.; Stehr, D.; Schneider, H.; Helm, M.; Chatterjee, S.; Gibbs, H.; Khitrova, G.
Intra-excitonic extreme nonlinear optics
DPG Spring Meeting of the Condensed Matter Section, 25.-30.03.2012, Berlin, Germany

92. Vinnichenko, M.; Hauschild, D.; Cornelius, S.; Krause, M.; Gago, R.; Mücklich, A.; Neidhardt, J.; Lissotschenko, V.; Kolitsch, A.
Mechanisms of electrical and optical properties modification of ZnO:Al films induced by very rapid thermal processing
E-MRS Spring Meeting, 14.-18.05.2012, Strasbourg, France

93. Vinnichenko, M.; Hauschild, D.; Krause, M.; Cornelius, S.; Gago, R.; Mücklich, A.; Lissotschenko, V.; Kolitsch, A.
Effects of millisecond thermal processing on the properties of ZnO-based transparent conducting materials
4th Symposium on Transparent Conductive Materials 2012, 21.-26.10.2012, Chersonissos, Crete, Greece

94. Wagner, M.; Stehr, D.; Schneider, H.; Winnerl, S.; Teich, M.; Andrews, A. M.; Schartner, S.; Strasser, G.; Helm, M.
Intraexcitonic Autler-Townes effect in terahertz-driven semiconductor quantum wells
APS March Meeting 2012, 27.02.-02.03.2012, Boston, Massachusetts, USA

95. Wallner, A.; Feige, J.; Fifield, K.; Korschinek, G.; Melber, K.; Merchel, S.; Ott, U.; Paul, M.; Rugel, G.; Steier, P.; Tims, S.; Vockenhuber, C.
AMS within Eurogenesis: Nanodiamonds and SN-signatures
XII International Symposium on Nuclei in the Cosmos, 05.-10.08.2012, Cairns, Australia

96. Werniewicz, K.; Skorupa, W.
Low-cost and large-area electronics, roll-to-roll processing and beyond
IXth International Conference Ion Implantation and other applications of Ions and Electrons - ION 2012, 25.-28.06.2012, Kazimierz Dolny, Poland

97. Wilde, C.; Vinnichenko, M.
DC magnetron sputtering of ZnO:Al from metallic and reduced ceramic targets: comparison of ion energy distributions
DPG Spring Meeting of the Condensed Matter Section, 25.-30.03.2012, Berlin, Germany

98. Wilhelm, R. A.; Heller, R.; Facsko, S.
***In-situ* analysis of nanostructures induced by slow highly charged ions**
DPG Spring Meeting of the Condensed Matter Section, 25.-30.03.2012, Berlin, Germany

99. Winnerl, S.; Mittendorff, M.; Schneider, H.; Helm, M.; Orlita, M.; Potemski, M.; Winzer, T.; Malic, E.; Knorr, A.; Berger, C.; de Heer, W. A.
Relaxation dynamics in graphene excited with low photon energies
Graphene Week, 03.-08.06.2012, Delft, The Netherlands

100. Zahn, P.; Hinsche, N. F.; Mertig, I.
Thermoelectric transport in strained Si and Si/Ge heterostructures
DPG Spring Meeting of the Condensed Matter Section, 25.-30.03.2012, Berlin, Germany

Posters

1. Abrasonis, G.; Krause, M.; Mücklich, A.; Heller, R.; Heinig, K.-H.; Gemming, S.; Möller, W.
Ion beam assisted deposition of nano-structured C:Ni films
DPG Spring Meeting of the Condensed Matter Section, 25.-30.03.2012, Berlin, Germany

2. Abrasonis, G.; Morawetz, K.
Instability types at ion-assisted alloy deposition: from surface to bulk nanopatterning
DPG Spring Meeting of the Condensed Matter Section, 25.-30.03.2012, Berlin, Germany

3. Abrasonis, G.; Martinavicius, A.; Scheinost, A. C.; Danoix, R.; Danoix, F.; Stinville, J. C.; Templier, C.; Gemming, S.; Möller, W.
Low temperature plasma nitriding induced decomposition in AISI 304L austenitic stainless steel
13th International Conference on Plasma Surface Engineering, 10.-14.09.2012, Garmisch-Partenkirchen, Germany

4. Andermann, C.; Bonnet, S.; Gloaguen, R.; Crave, A.; Merchel, S.; Braucher, R.; Bourlès, Didier L.
Decadal to Millennial scale erosion rates in the Nepal Himalayas
American Geophysical Union, Fall Meeting 2012, 03.-07.12.2012, San Francisco, USA

5. Ball, D. K.; Günther, S.; Fritzsche, M.; Lenz, K.; Varvaro, G.; Makarov, D.; Mücklich, A.; Facsko, S.; Fassbender, J.; Albrecht, M.
Magnetic properties of Co/Pd multilayers films deposited on GaSb nanocones
Joint European Magnetic Symposia (JEMS 2012), 09.-14.09.2012, Parma, Italy

6. Banholzer, A.; Wintz, S.; Bunce, C.; Strahe, T.; Körner, M.; Erbe, A.; Puzic, A.; Raabe, J.; Quitmann, C.; Lenz, K.; Fassbender, J.
Investigation of the dynamics of magnetic vortices in trilayer systems
DPG Spring Meeting of the Condensed Matter Section, 25.-30.03.2012, Berlin, Germany

7. Banholzer, A.; Wintz, S.; Osten, J.; Raabe, J.; Quitmann, C.; Lenz, K.; Fassbender, J.
Investigation of vortex dynamics in coupled trilayer systems
Joint European Magnetic Symposia (JEMS 2012), 09.-14.09.2012, Parma, Italy

8. Bernert, K.; Sluka, V.; Fowley, C.; Gan, H.; Fassbender, J.; Deac, A.
Switching Phase Diagrams and Backhopping in Magnetic Tunnel Junctions (MTJs)
International Colloquium on Magnetic Films and Surfaces (ICMFS), 24.-28.09.2012, Shanghai, China

9. Bernert, K.; Sluka, V.; Fowley, C.; Gan, H.; Fassbender, J.; Deac, A. M.
Switching voltages and back-hopping in magnetic tunnel junctions with different geometries
International Colloquium on Magnetic Films and Surfaces (ICMFS), 24.-28.09.2012, Shanghai, China

10. Bhattacharyya, J.; Zybell, S.; Helm, M.; Andrews, A. M.; Strasser, G.; Schneider, H.
Transient magneto-photoluminescence quenching by intra-excitonic THz absorption
ICPS2012 - 31st International Conference on the Physics of Semiconductors, 29.07.-03.08.2012, Zürich, Switzerland

11. Bürger, D.; Zhou, S.; Höwler, M.; Ou, X.; Kovacs, G. J.; Reuther, H.; Mücklich, A.; Skorupa, W.; Helm, M.; Schmidt, H.
Anomalous hysteretic Hall effect in a ferromagnetic, Mn-rich, amorphous Ge:Mn nano-network
DPG Spring Meeting of the Condensed Matter Section, 25.-30.03.2012, Berlin, Germany

12. Bürger, D.; Zhou, S.; Höwler, M.; Ou, X.; Kovacs, G. J.; Reuther, H.; Mücklich, A.; Skorupa, W.; Helm, M.; Schmidt, H.
Hysteretic anomalous Hall effect in a Mn-rich, amorphous Ge:Mn nanonet
IFW Winterschool, 15.-18.01.2012, Oberwiesenthal, Germany

13. Butterling, M.; Anwand, W.; Cornelius, S.; Potzger, K.; Smekhova, A.; Vinnichenko, M.; Wagner, A.
Optimization of growth parameters of TiO_2 thin films using a slow positron beam
16th International Conference on Positron Annihilation (ICPA-16), 19.-24.08.2012, Bristol, Great Britain

14. Caglar, K.; Mamidala, V.; Lehnert, U.; Schneider, C.; Seidel, W.; Schlarb, H.; Kuntzsch, M.; Staats, G.; Al-Shemmary, A.; Stojanovic, N.; Geloni, G.; Helm, M.; Michel, M.; Gensch, M.
(THz based) electron bunch diagnostic at superconducting continuous wave accelerators
IPAC 2012 - International Particle Accelerator Conference 2012, 21.-25.05.2012, New Orleans, USA

15. Cartwright, J. A.; Merchel, S.; Rugel, G.; Fimiani, L.; Ludwig, P.; Llorca, J.; Ott, U.
The 100th Martian meteorite Ksar Ghilane 002 (KG 002): Noble gases and radionuclides

point to a strong relationship with Los Angeles
43rd Lunar and Planetary Science Conference, 19.-23.03.2012, The Woodlands, Texas, USA

16. Cornelius, S.; Vinnichenko, M.; Möller, W.
Understanding and using the current-voltage-pressure relationship in reactive magnetron sputtering for the growth of transparent conductive oxides
13th International Conference on Plasma Surface Engineering (PSE 2012), 09.-14.09.2012, Garmisch-Partenkirchen, Germany

17. Cornelius, S.; Vinnichenko, M.; Munnik, F.; Heller, R.; Möller, W.
Approaching physical limits of ZnO:Al film performance for application in photovoltaics
EMRS Spring Meeting 2012, 14.-18.05.2012, Strasbourg, France

18. Deßmann, N.; Pavlov, S. G.; Shastin, V. N.; Zhukavin, R. Kh.; Winnerl, S.; Mittendorff M.; Hübers, H.-W.
Time-resolved electronic capture in germanium doped with hydrogen-like impurity centers
37th International Conference on Infrared, Millimeter and Terahertz Waves, 23.-28.09.2012, Wollogon, Australia

19. Eder, F. M.; Neelmeijer, C.; Pearce, Nicholas J. G.; Sterba, Johannes H.; Bichler, M.; Merchel, S.
Chemical fingerprinting of Hungarian and Slovakian obsidian using three complementary analytical techniques
39th International Symposium on Archaeometry: "50 years of ISA", 28.05.-01.06.2012, Leuven, Belgium

20. Eder, F.; Neelmeijer, C.; Pearce, Nick J. G.; Sterba, Johannes H.; Bichler, M.; Merchel, S.
New direction in Melos obsidian characterization
Archäometrie und Denkmalpflege 2012, 28.-31.03.2012, Tübingen, Germany

21. El-Said, A. S.; Wilhelm, R. A.; Facsko, S.; Trautmann, C.
Surface nanostructuring of $LiNbO_3$ by high-density electronic excitations
25th International Conference on Atomic Collisions in Solids (ICACS), 21.-25.10.2012, Kyoto, Japan

22. El-Said, Ayman S.; Wilhelm, R. A.; Heller, R.; Facsko, S.; Lemell, C.; Wachter, G.; Burgdorfer, J.; Ritter, R.; Aumayr, F.
Phase diagram for nanostructuring CaF_2 surfaces by slow highly charged ions
25th International Conference on Atomic Collisions in Solids (ICACS), 21.-25.10.2012, Kyoto, Japan

23. Endler, R.; Voelskow, M.; Schumann, T.; Gebel, T.; Liepack, H.; Kolitsch, A.; Skorupa, W.
Formation of dendritic structures in thin silicon films on amorphous substrates by high intensity flash lamp annealing
E-MRS 2012 Spring Meeting, 14.-18.05.2012, Strasbourg, France

24. Facsko, S.; Ou, X.; Mücklich, A.
Ion induced patterns on crystalline Ge surfaces
25th International Conference on Atomic Collisions in Solids (ICACS 25), 21.-25.10.2012, Kyoto, Japan

25. Feige, J.; Wallner, A.; Fifield, L. K.; Korschinek, G.; Merchel, S.; Rugel, G.; Winkler, S. R.
Supernova dust in terrestrial deep-sea archives
Joint meeting "Paneth Kolloquium", "The first 10 million years of the solar system" (DFG SPP 1385) & "MEMIN" (DFG FOR 887), 09.-12.10.2012, Nördlingen, Germany

26. Feige, J.; Wallner, A.; Winkler, S. R.; Merchel, S.; Fifield, L. K.; Korschinek, G.
The search for supernova-produced radionuclides in deep-sea sediments with AMS
496. Wilhelm und Else Heraeus-Seminar - Astrophysics with modern small-scale accelerators, 06.-10.02.2012, Bad Honnef, Germany

27. Feige, J.; Wallner, A.; Winkler, S. R.; Merchel, S.; Fifield, L. K.; Korschinek, G.; Rugel, G.
AMS measurements of supernova-produced radionuclides in deep-sea sediment cores
62. Jahrestagung der Österreichischen Physikalischen Gesellschaft, 18.-21.09.2012, Graz, Austria

28. Feige, J.; Wallner, A.; Winkler, S. R.; Merchel, S.; Fifield, L. K.; Korschinek, G.; Rugel, G.
Supernova-dust in deep-sea sediment cores
International conference of the European Science Foundation EuroGENESIS CoDustMas network action, 05.-08.11.2012, Ascona, Switzerland

29. Fiedler, J.; Heera, V.; Skrotzki, R.; Herrmannsdörfer, T.; Skorupa, W.; Gobsch, G.; Helm, M.
Superconducting layers in semiconductors – Ready for the quantum interference?
18th International Conference on Ion Beam Modifications of Materials (IBMM 2012); 02.-07.09.2012, Qingdao, China

30. Fiedler, J.; Skrotzki, R.
Superconducting layers in silicon - Get ready for the quantum interference -
Dresdner Barkhausen-Poster-Preis 2011, 10.02.2012, Dresden, Germany

31. Fischer, T.; Pronin, A. V.; Stehr, D.; Wosnitza, J.; Niemeier, T.; Holzapfel, B.
Direct observation of the superconducting energy-gap opening in the optical conductivity spectra of $LuNi_2B_2C$
DPG Spring Meeting of the Condensed Matter Section, 25.-30.03.2012, Berlin, Germany

32. Fowley, C.; Bernert, K.; Sluka, V.; Fassbender, J.; Deac, A. M.; Rippard, W. H.; Pufall, M. R.; Russek, S. E.
Initial magnetisation angle dependence for microwave oscillation in a metallic spin valve
IEEE International Magnetics Conference 2012 (Intermag 2012), 07.-11.05.2012, Vancouver, Canada

33. Fowley, C.; Sluka, V.; Bernert, K.; Gan, H. D.; Deac, A. M.; Rippard, W. H.; Pufall, M. R.; Russek, S. E.
Microwave dynamics in point contact spin valve structures combining in-plane and out-of-plane magnetic layers with in-plane magnetic fields
21th International Colloquium on Magnetic Films and Surfaces (ICMFS), 24.-28.09.2012, Shanghai, China

34. Franke, C.; Schneider, H.; Faist, J.; Liu, H. C.
Intersubband dynamics in two-photon quantum well infrared photodetectors
International Conference on Superlattices, Nanostructures and Nanodevices, 22.-27.07.2012, Dresden, Germany

35. Franke, C.; Schneider, H.; Faist, J.; Liu, H. C.
Intersubband dynamics in two-photon quantum well infrared photodetectors
DPG Spring Meeting of the Condensed Matter Section, 25.-30.03.2012, Berlin, Germany

36. Gemming, S.; Weissbach, T.; Zschornak, M.; Stöcker, H.; Meyer, D. C.; Leisegang, T.; Ronneberger, I.; Potzger, K.
Multifunctional oxides - influence of defects on the ferroic properties
DPG Spring Meeting of the Condensed Matter Section, 25.-30.03.2012, Berlin, Germany

37. Germer, S.; Rebohle, L.; Skorupa, W.; Helm, M.
Basic structures of integrated photonic circuits for smart biosensor applications
DOKDOK 2012, 07.-11.10.2012, Oppurg, Germany

38. Hampe, D.; Gleisberg, B.; Köhler, M.; Akhmadaliev, Sh.; Rugel, G.; Merchel, S.
Determination of ^{41}Ca with LSC and AMS: method development, modifications and applications
Ninth International Conference Methods and Applications of Radioanalytical Chemistry (MARC IX), 25.-30.03.2012, Kailua-Kona, Hawaii, USA

39. Jacob, R.; Fehrenbacher, M.; Winnerl, S.; Bhattacharyya, J.; Schneider, H.; Helm, M.; von Ribbeck, H.-G.; Eng, L. M.; Atkinson, P.; Schmidt, A. Rastelli O. G.
Scanning near-field infrared nano-spectroscopy on buried InAs quantum dots
503. WE-Heraeus-Seminar on Free-Electron Lasers: from Fundamentals to Applications, 10.-13.04.2012, Bad Honnef, Germany

40. Keller, A.; Bald, I.; Rotaru, A.; Cauët, E.; Gothelf, K. V.; Besenbacher, F.
Probing electron-induced bond cleavage at the single-molecule level using DNA origami templates
Electron Controlled Chemical Lithography 2012 Meeting, 18.-22.05.2012, Stykkishólmur, Iceland

41. Kelling, J.; Heinig, K.-H.
Large scale atomistic simulations on nanostructure evolution
Response Treatment for the Dynamical Properties of Materials with the ABINIT Package, 22.-26.10.2012, ETH Zürich, Switzerland

42. Körner, M.; Barsukov, I.; Römer, F. M.; Lenz, K.; Meckenstock, R.; Hemken To Krax, S.; Banholzer, A.; Grebing, J.; Lindner, J.; Farle, M.; Fassbender, J.
Frequency dependence of spin relaxation in periodic systems
International Colloquium on Magnetic Films and Surfaces (ICMFS) 2012, 24.-28.09.2012, Shanghai, China

43. Körner, M.; Lenz, K.; Fritzsche, M.; Facsko, S.; Fassbender, J.
Morphology induced two-magnon scattering in thin NiFe films
International Colloquium on Magnetic Films and Surfaces (ICMFS) 2012, 24.-28.09.2012, Shanghai, China

44. Krause, M.; Haluska, M.; Wenisch, R.; Kunze, T.; Abrasonis, G.; Gemming, S.
CNT growth from C:Ni nanocomposites
International winterschool on electronic properties of novel materials, 03.-10.03.2012, Kirchberg, Austria

45. Krause, M.; Kunze, T.; Mücklich, A.; Fritzsche, M.; Wenisch, R.; Posselt, M.; Gemming, S.; Abrasonis, G.
Structure, mechanical, and tribological properties of C:Ni nanocomposite films grown by IBAD
13th International Conference on Plasma Surface Engineering, 10.-14.09.2012, Garmisch-Partenkirchen, Germany

46. Krause, M.; Mücklich, A.; Fritzsche, M.; Facsko, S.; Oates, T. W. H.; Buljan, M.; Gemming, S.; Abrasonis, G.
Nanostructuring of C:Ni nanocomposite films using ion-beam assisted ion-beam co-sputtering
13th International Conference on Plasma Surface Engineering, 10.-14.09.2012, Garmisch-Partenkirchen, Germany

47. Kunze, T.; Posselt, M.; Gemming, S.; Lautz, J.v., Pastewka, L.; Moseler, M.; Seifert, G.
Tribosimulation of ta-C nanocoatings - Friction and wear on the atomic scale
Gordon Research Conference 2012, 08.-13.07.2012, Waterville, ME, USA

48. Kunze, T.; Posselt, M.; Gemming, S.; Lautz, J.v., Pastewka, L.; Moseler, M.; Seifert, G.
Tribosimulation of ta-C nanocoatings
Materials Science and Engineering 2012, 25.-27.09.2012, Darmstadt, Germany

49. Kunze, T.; Seifert, G.; Posselt, M.; Gemming, G.; Lautz, J.v.; Pastewka, L.; Moseler, M.
Wear in tetrahedral amorphous carbon induced by sp3/sp2 phase transition
ADGLASS Workshop 2012, 14.-16.11.2012, Bremen, Germany

50. Kutschan, B.; Morawetz, K.; Gemming, S.
Modeling the morphogenesis of brine channels in sea ice
DPG Spring Meeting of the Condensed Matter Section, 25.-30.03.2012, Berlin, Germany

51. Langer, M.; Neudert, A.; Osten, J.; Körner, M.; Mönch, I.; Mattheis, R.; Fassbender, J.; McCord, J.
Magnetization reversal of ferromagnetic elements surrounded by a synthetic antiferromagnet
IEEE International Magnetics Conference 2012 (Intermag 2012), 07.-11.05.2012, Vancouver, Canada

52. Lehmann, J.; von Borany, J.; Skorupa, W.; Schäfer, A.; Schubert, J.; Mantl, S.
Flash-lamp annealing of ternary rare earth oxides for use as alternative high-k materials
19th International Conferenz on Ion Implantation Technology, 25.-29.06.2012, Valladolid, Spain

53. Lenz, K.; Körner, M.; Banholzer, A.; Liedke, M. O.; Grebing, J.; Fassbender, J.; Barsukov, I.; Römer, F. M.; Lindner, J.; Landeros, P.
Frequency-tunable magnetic relaxation in periodic nanostructures tailored by ion beam irradiation

IEEE International Magnetics Conference 2012 (Intermag 2012), 07.-11.05.2012, Vancouver, Canada

54. Martins, R. M. S.; Schell, N.; Mahesh, K. K.; Silva, R. J. C.; Braz Fernandes, F. M.
Growth mode and texture development in Ni-Ti shape memory alloy (SMA) films during co-sputtering deposition – An in situ synchrotron radiation study
MPA 2012 – 6th International Meeting on Developments in Materials, Processes and Applications of Emerging Technologies, 02.-04.07.2012, Alvor, Portugal

55. Mazalski, P.; Dobrogowski, W.; Sveklo, I.; Maziewski, A.; Fritzsche, M.; Liedke, M. O.; Fassbender, J.; Baczewski, L. T.; Wawro, A.
Alteration of magnetic anisotropy of Pt/Co/Pt trilayers by FIB irradiation
Joint European Magnetic Symposia (JEMS 2012), 09.-14.09.2012, Parma, Italy

56. Meriaux, A.-S.; Delunel, R.; Merchel, S.; Finkel, R. C.
Evidences for a more restricted Icelandic Ice cap re-advance after the Bølling warming period
American Geophysical Union, Fall Meeting 2012, 03.-07.12.2012, San Francisco, USA

57. Meyer, T.; Obry, B.; Pirro, P.; Brächer, T.; Neb, R.; Osten, J.; Strache, T.; Fassbender, J.; Hillebrands, B.
Microscopic magnetic structuring of spin-wave waveguides by ion implantation in a NiFe layer
DPG Spring Meeting of the Condensed Matter Section, 25.-30.03.2012, Berlin, Germany

58. Meyer, T.; Obry, B.; Pirro, P.; Brächer, T.; Neb, R.; Osten, J.; Strache, T.; Fassbender, J.; Hillebrands, B.
Microscopic magnetic structuring of spin-wave waveguides by ion implantation in a NiFe layer
IEEE International Magnetics Conference 2012 (Intermag 2012), 07.-11.05.2012, Vancouver, Canada

59. Michalak, P. P.; Munnik, F.; Radtke, M.; Buzanich, G.; Reinholz, U.; Riesemeier, H.; Merchel, S.; Renno, A. D.
Spatially-resolved analysis of natural minerals as carriers of high-tech metals and Rare Earth Elements: comparison of EPMA, PIXE and Sy-µXRF
13th International Conference on Nuclear Microprobe Technology & Applications (ICNMTA), 22.-27.07.2012, Lisbon, Portugal

60. Michalak, P. P.; Renno, A. D.; Munnik, F.; Radtke, M.; Buzanich, G.; Reinholz, U.; Merchel, S.
Three natural minerals - sanidine, pyrite and columbite - as potential geologic reference materials. Characterization of chemical homogeneity at a micrometer scale
European Mineralogical Conference 2012, 02.-06.09.2012, Frankfurt am Main, Germany

61. Mittendorff, M.; Winnerl, S.; Schneider, H.; Helm, M.; Orlita, M.; Potemski, M.; Berger, C.; de Heer, W. A.
Carrier relaxation in Landau-quantized graphene
Graphene Week 2012, 04.-08.06.2012, Delft, The Netherlands

62. Mook, A.; Pientka, F.; Mertig, I.; Zahn, P.
Anomalous Hall effect as a Fermi surface property
DPG Spring Meeting of the Condensed Matter Section, 25.-30.03.2012, Berlin, Germany

63. Müller, A.-D.; Müller, F.; Wengel, S.; Baumgart, C.; Skorupa, S.; Reuther, H.; Mücklich, A.; Schmidt, H.
Gold diffusion into silicon during thermal annealing
DPG Spring Meeting of the Condensed Matter Section, 25.-30.03.2012, Berlin, Germany

64. Neubert, M.; Vinnichenko, M.; Gebel, T.; Liepack, H.; Kolitsch, A.
Sputter deposition of TiO_2-based transparent conductive thin films
E-MRS 2012 Spring Meeting, 13.-18.05.2012, Strasbourg, France

65. Neudert, A.; Bali, R.; Kostylev, M.; Adeyeye, A.; Römer, F. M.; Wagner, K.; Farle, M.; Lenz, K.; Lindner, J.; Fassbender, J.
Magnetization dynamics of Co antidot lattices
2012 IEEE International Conference on Microwave Magnetics (ICMM 2012), 26.-29.08.2012, Kaiserslautern, Germany

66. Osten, J.; Greene, P.; Ende, T.; Iwata, N.; Lenz, K.; Liu, K.; Fassbender, J.
Tailoring perpendicular anisotropy in Co/Pd multilayers by ion irradiation
18th International Conference on Ion Beam Modification of Materials (IBMM 2012), 02.-07.09.2012, Qingdao, China

67. Osten, J.; Greene, P.; Endo, T.; Iwata, N.; Lenz, K.; Liu, K.; Fassbender, J.
Tailoring perpendicular anisotropy in Co/Pd multilayers by ion irradiation
DPG Spring Meeting of the Condensed Matter Section, 25.-30.03.2012, Berlin, Germany

68. Osten, J.; Greene, P.; Endo, T.; Iwata, N.; Lenz, K.; Liu, K.; Fassbender, J.
Tailoring perpendicular anisotropy in Co/Pd multilayers by ion irradiation
MRS Spring Meeting and Exhibit, 09.-13.04.2012, San Francisco, USA

69. Ou, X.; Kögler, R.; Zhao, K.; Anwand, W.; Grenzer, J.; Voelskow, M.; Butterling, M.; Mücklich, A.; Zhou, S.; Skorupa, W.
Radiation damage in YSZ simulated by single and double beam ion irradiation
The 18th International Conference on Ion Beam Modifications of Materials (IBMM2012), 02.-07.09.2012, Qingdao, China

70. Ou, X.; Shuai, Y; Luo, W. B; Reuther, H.; Zhou, S.; Schmidt, H.
Tuning resistive switching behavior of $BiFeO_3$ by Ar^+ irradiation
The 18th International Conference on Ion Beam Modifications of Materials (IBMM2012), 02.-07.09.2012, Qingdao, China

71. Peplinski, B.; Adam, C.; Adamczyk, B.; Müller, R.; Schadrack, R.; Michaelis, M.; Emmerling, F.; Reuther, H.; Menzel, M.
Evidence of formation of $AlPO_4$ tridymite in some municipal sewage sludge ashes
European Powder Diffraction Conference 13 (EPDIC13), 28.-31.10.2012, Grenoble, France

72. Posselt, M.; Al-Motasem, A. T.
Configurational contributions to the free energy of embedded nanoclusters
11th International Conference on Computer Simulation of Radiation Effects in Solids, 24.-29.06.2012, Santa Fe, USA

73. Prucnal, S.; Abendroth, B.; Krockert, K.; König, K.; Henke, D.; Kolitsch, A.; Möller, H. J.; Skorupa, W.
Gettereing of metal impurities by flash lamp annealing in dirty-silicon solar cells
E-MRS 2012 Spring Meeting, 14.-18.05.2012, Strasbourg, France

74. Prucnal, S.; Abendroth, B.; Krockert, K.; König, K.; Kolitsch, A.; Steinert, M.; Möller, H. J.; Skorupa, W.
Plasma immersion ion implantation for the doping and texturization of silicon based solar cells
IXth International Conference Ion Implantation and other applications of Ions and Electrons - ION 2012, 25.-28.06.2012, Kazimierz Dolny, Poland

75. Prucnal, S.; Jiao, F.; Zhao, K.; Skorupa, W.; Helm, M.; Zhou, S.
Improvement of CIGS layer quality by flash lamp annealing
E-MRS 2012 Spring Meeting, 14.-18.05.2012, Strasbourg, France

76. Prucnal, S.; Rebohle, L.; Sun, J. M.; Skorupa, W.; Drozdziel, A.; Pyszniak, K.; Turek, M.; Zuk, J.
Sensitization of the blue-green electroluminescence by gadolinium coupled to Si nanocluster embedded in a SiO_2 matrix
Radiation Interaction with Material and Its Use in Technologies 2012, 14.-17.05.2012, Kaunas, Lithuania

77. Prucnal, S.; Voelskow, M.; Mücklich, A.; Liedke, M. O.; Pyszniak, K.; Drozdziel, A.; Turek, M.; Zuk, J.; Skorupa, W.
Conductivity type and crystal orientation of GaAs nanocrystals in silicon
Radiation Interaction with Material and Its Use in Technologies 2012, 14.-17.05.2012, Kaunas, Lithuania

78. Prucnal, S.; Zhou, S.; Ou, X.; Fritzsche, M.; Reuther, H.; Grebing, J.; Liedke, M. O.; Liedke, B.; Mücklich, A.; Helm, M.; Zuk, J.; Turek, M.; Drozdziel, A.; Skorupa, W.
Nanoarchitecture of a III-V semiconductor-on-silicon platform made by ion implantation and millisecond flash lamp annealing

18th International Conference on Ion Beam Modifications of Materials (IBMM2012), 02.09.-07.12.2012, Qingdao, China

79. Radek, M.; Bracht, H.; Posselt, M.; Schmidt, B.; Bougeard, D.; Haller, E. E.; Itoh, K.
Ion-beam mixing in crystalline and amorphous Si und Ge
11th International Conference on Computer Simulation of Radiation Effects in Solids, 24.-29.06.2012, Santa Fe, USA

80. Rebohle, L.; Wutzler, R.; Germer, S.; Lehmann, J.; Helm, M.; Skorupa, W.
Nd-implanted MOS light emitting devices for smart biosensor applications
E-MRS 2012 Spring Meeting, 14.-18.05.2012, Strasbourg, France

81. Reichel, D.; Skorupa, W.
Precise millisecond annealing for advanced material processing
EMRS Spring Meeting 2012, 14.-18.05.2012, Strasbourg, France

82. Ritter, R.; Shen, Q.; Teichert, C.; Wilhelm, R. A.; Facsko, S.; Ginzel, R.; Crespo López-Urrutia, J. R.; Aumayr, F.
Characterisation of nanostructures induced by slow highly charged ion bombardment of HOPG
25th Internation Conference on Atomic Collisions in Solids (ICACS), 21.-25.10.2012, Kyoto, Japan

83. Ritter, R.; Wilhelm, R. A.; Ginzel, R.; Schadauer, P.; Heller, R.; Rupp, W.; López-Urrutia, J. R. Crespo; Facsko, S.; Aumayr, F.
The effect of chemical etching on poly (methyl methacrylate) irradiated with slow highly charged ions
16th International Conference Physics of Highly Charged Ions, 02.-07.09.2012, Heidelberg, Germany

84. Ritter, R.; Wilhelm, R. A.; Stöger-Pollach, M.; Mücklich, A.; Werner, U.; Beyer, A.; Facsko, S.; Gölzhäuser, A.; Aumayr, F.
Nanopores milled in carbon nanomembranes due to impact of individual slow highly charged ions
16th International Conference Physics of Highly Charged Ions, 02.07.-07.09.2012, Heidelberg, Germany

85. Rugel, G.; Akhmadaliev, Sh.; Merchel, S.; Pavetich, S.
Ultrasensitive detection of actinides by accelerator mass spectrometry
International Workshop on Advanced Techniques in Actinide Spectroscopy (ATAS), 05.-07.11.2012, Dresden, Germany

86. Schönitz, I.; Bergner, F.; Weißgärber, T.; Shariq, A.
Fabrication and characterization of ODS Fe14Cr alloys for nuclear applications
Summer School on Materials under Extreme Conditions (Muneco), 11.-15.06.2012, Miraflores de la Sierra, Madrid, Spain

87. Schönitz, I.; Heintze, C.; Bergner, F.; García-Junceda, A.; Weißgärber, T.
Microstructural properties of spark plasma sintered ODS Fe-14Cr steels
Workshop on ODS steels, 24.-26.09.2012, Materials Department of the Oxford University, UK

88. Seidel, W.; Winnerl, S.; Bhattacharyya, J.; Teich, M.; Fehrenbacher, M.; Drachenko, O.; Schneider, H.; Helm, M.; Bauer, C.; Gensch, M.; Schurig, R.; Lehnert, U.; Michel, P.
The FELBE user facility
503th Wilhelm and Else Heraeus Seminar Free-Electron Lasers: from Fundamentals to Applications, 10.-13.04.2012, Bad Honnef, Germany

89. Skrotzki, R.; Herrmannsdörfer, T.; Fiedler, J.; Heera, V.; Voelskow, M.; Mücklich, A.; Schmidt, B.; Skorupa, W.; Helm, M.; Wosnitza, J.
Two concepts of introducing thin-film superconductivity in Ge and Si by use of Ga-ion implantation
DPG Spring Meeting of the Condensed Matter Section, 25.-30.03.2012, Berlin, Germany

90. Sluka, V.; Kákay, A.; Deac, A. M.; Bürgler, D. E.; Hertel, R.; Schneider, C. M.
Quenched Slonczewski-windmill in spin-torque vortex-oscillators
IEEE International Magnetics Conference 2012 (Intermag 2012), 07.-11.05.2012, Vancouver, Canada

91. Sluka, V.; Fowley, C. J.; Bernert, K.; Deac, A. M.; Rippard, W. H.; Pufall, M. R.; Russek, S. E.
Spin-transfer torque-induced dynamics of CoFe/Pd superlattice-based nano-oscillators in perpendicular magnetic field
21th International Colloquium on Magnetic Films and Surfaces (ICMFS2012), 24.-28.09.2012, Shanghai, China

92. Sluka, V.; Kákay, A.; Deac, A. M.; Bürgler, D. E.; Hertel, R.; Schneider, C. M.
Core-core interaction in spin-torque double-vortex oscillators
21th International Colloquium on Magnetic Films and Surfaces (ICMFS2012), 24.-28.09.2012, Shanghai, China

93. Steinbach, G.; Gemming, S.; Döscher, H.; Hannappel, T.; Schreiber, M.
Gallium phosphide - silicon interface: Structure and anisotropy investigations
DPG Spring Meeting of the Condensed Matter Section, 25.-30.03.2012, Berlin, Germany

94. Teich, M.; Wagner, M.; Stehr, D.; Helm, H. Schneider M.; Chatterjee, S.; Klettke, A. C.; Koch, S. W.; Kira, M.; Gibbs, H. M.; Khitrova, G.
Intraexcitonic Autler-Townes effect in semiconductor quantum wells
NOEKS11 - Nonlinear Optics and Excitation Kinetics in Semiconductors, 23.-27.09.2012, Stuttgart, Germany

95. Teich, M.; Wagner, M.; Stehr, D.; Schneider, H.; Helm, M.; Chatterjee, S.; Gibbs, H.; Khitrova, G.
Intraexcitonic coherent optics
Free-Electron Lasers: From Fundamentals to Applications, 10.-13.04.2012, Bad Honnef, Germany

96. Teich, M.; Wagner, M.; Stehr, D.; Schneider, H.; Helm, M.; Chatterjee, S.; Klettke, A.; Koch, S. W.; Gibbs, H.; Khitrova, G.
Intraexcitonic coherent nonlinear optics in quantum wells
International Conference on Superlattices, Nanostructures and Nanodevices - ICSNN 2012, 22.-27.07.2012, Dresden, Germany

97. Turek, M.; Prucnal, S.; Voelskow, M.; Mücklich, A.; Liedke, M. O.; Pyszniak, K.; Drozdziel, A.; Zuk, J.; Skorupa, W.
Flash lamp processing of III/V nanostructures in silicon
Radiation Interaction with Material and its Use in Technologies 2012, 14.-17.05.2012, Kaunas, Lithuania

98. Vinnichenko, M.; Junghähnel, M.; Neubert, M.; Gago, R.; Mücklich, A.; Kolitsch, A.
Crystallization of TiO2:Nb/Ta: effect of the as-deposited film morphology and local order structure
4th Symposium on Transparent Conductive Materials 2012, 21.-26.10.2012, Chersonnisos, Crete, Greece

99. Vinnichenko, M.; Liedke, B.; Heinig, K.-H.; Gulseren, O.; Friedrich, D.; Mücklich, A.; Schmidt, B.; Akguc, G. B.; Aydinli, A.
Plasmonic nano-Ag layers in TCO and Si nanosponge for photovoltaic applications
E-MRS Spring Meeting, 14.-18.05.2012, Strasbourg, France

100. Vogel, A.; Wintz, S.; Gerhardt, T.; Bocklage, L.; Strache, T.; Im, M.-Y.; Fischer, P.; Fassbender, J.; McCord, J.; Meier, G.
Domain-wall motion in permalloy nanowires with magnetic soft spots
19th International Conference on Magnetism (ICM 2012), 08.-13.07.2012, Busan, Korea

101. Wagner, A.; Ulbricht, A.; Bergner, F.
Robust Monte-Carlo fitting of small-angle neutron scattering curves for determining cluster-size distributions
German Neutron Scattering Conference, 24.-26.09.2012, FZ Jülich/GSI-Bonn, Germany

102. Wagner, A.; Ulbricht, A.; Bergner, F.
Small-angle neutron scattering and mechanical properties of low-Cu reactor pressure vessel steels neutron-irradiated at 255 °C and post-irradiation annealed at 290 °C
NuMat 2012: The Nuclear Materials Conference, 22.-25.10.2012, Osaka, Japan

103. Wallner, A.; Vockenhuber, C.; Güttler, D.; Feige, J.; Fifield, L. K.; Korschinek, G.; Melber, K.; Merchel, S.; Ott, U.; Paul, M.; Rugel, G.; Steier, P.; Tims, S.

AMS within CoDustMas: Nanodiamonds and SN-signatures
International Conference of the European Science Foundation EuroGENESIS CoDustMas network action, 05.-08.11.2012, Ascona, Switzerland

104. Wieser, M.; Sendler, T.; Liu, S.-P.; Weisbrod, S.; Tang, Z.; Marx, A.; Wolf, J.; Scheer, E.; Moresco, F.; Grebing, J.; Erbe, A.
Electrical characterization of single molecules in liquid environments
DPG Spring Meeting of the Condensed Matter Section, 25.-30.03.2012, Berlin, Germany

105. Wilde, C.; Cornelius, S.; Vinnichenko, M.
Ion mass and energy distributions in the DC magnetron sputtering of AZO from metallic and ceramic targets
13th International Conference on Plasma Surface Engineering (PSE 2012), 09.-14.09.2012, Garmisch-Partenkirchen, Germany

106. Wilhelm, R. A.; Facsko, S.; Wagner, J.; Heller, R.
A new facility for *in-situ* characterization of slow highly charged ion modifications of various materials
16th International Conference Physics of Highly Charged Ions, 02.-07.09.2012, Heidelberg, Germany

107. Wilhelm, R. A.; Facsko, S.; Wagner, J.; Heller, R.
A new facility for *in-situ* characterization of slow highly charged ion modifications of various materials
25th International Conference on Atomic Collisions in Solids (ICACS), 21.-25.10.2012, Kyoto, Japan

108. Winnerl, S.; Göttfert, F.; Mittendorff, M.; Schneider, H.; Helm, M.; Orlita, M.; Potemski, M.; Winzer, T.; Knorr, A.; Malic, E.; Sprinkle, M.; Berger, C.; de Heer, W. A.
Relaxation dynamics in epitaxial graphene investigated in the whole infrared spectral range
International Conference on Superlattices, Nanostructures and Nanodevices, 22.-27.07.2012, Dresden, Germany

109. Winnerl, S.; Malic, E.
Ultrafast relaxation dynamics close to the Dirac point in graphene
International Workshop on THz dynamics in carbon based nanostructures, 05.-07.03.2012, Dresden, Germany

110. Wintz, S.; Banholzer, A.; Raabe, J.; Quitmann, C.; Erbe, A.; Fassbender, J.
Interlayer coupled magnetic vortex pairs in trilayer disks
IEEE International Magnetics Conference 2012 (Intermag 2012), 07.-11.05.2012, Vancouver, Canada

111. Wintz, S.; Banholzer, A.; Raabe, J.; Quitmann, C.; Erbe, A.; Fassbender, J.
Interlayer coupled magnetic vortex pairs in trilayer disks
PNI in-house research workshop on "Magnetism and highly correlated electron systems", 11.-12.06.2012, Freising, Germany

112. Wintz, S.; Bunce, C.; Banholzer, A.; Körner, M.; Gemming, S.; Erbe, A.; Raabe, J.; Quitmann, C.; Fassbender, J.
Diverging-converging spin vortex pairs in biquadratically interlayer exchange coupled elements
19th International Conference on Magnetism (ICM 2012), 08.-13.07.2012, Busan, Korea

113. Wintz, S.; Bunce, C.; Banholzer, A.; Strache, T.; Körner, M.; Gemming, S.; Erbe, A.; McCord, J.; Raabe, J.; Quitmann, C.; Fassbender, J.
Pairs of diverging-converging spin vortices in biquadratically interlayer exchange coupled elements
DPG Spring Meeting of the Condensed Matter Section, 25.-30.03.2012, Berlin, Germany

114. Wintz, S.; Körner, M.; Gemming, S.; Erbe, A.; Raabe, J.; Quitmann, C.; Fassbender, J.
Direct imaging of effective spin meron pairs in magnetic multilayers
The 21th International Colloqium on Magnetic Films and Surfaces (ICMFS), 24.-28.09.2012, Shanghai, China

115. Wintz, S.; Raabe, J.; Banholzer, A.; Erbe, A.; Quitmann, C.; Fassbender, J.
Coupled vortex pairs in magnetic multilayer elements
Annual Meeting of the Swiss Physical Society 2012, 21.-22.06.2012, Zürich, Switzerland

116. Yankov, R. A.; Kolitsch, A.; von Borany, J.; Bortolotto, L.; Schütze, M.
Combination of a chemical vapor deposition coating and plasma immersion ion implantation of fluorine for oxidation protection and suppression of oxygen embrittlement in titanium aluminide alloys
13th International Conference on Plasma Surface Engineering, 10.-14.09.2012, Garmisch-Partenkirchen, Germany

117. Yankov, R.; von Borany, J.; Kolitsch, A.; Munnik, F.; Friedle, S.; Donchev, A.; Schütze, M.; Nießen, N.; Braun, R.
Fluorine-implanted titanium aluminide alloys for use in high-temperature oxidizing environments
19th International Conference on Ion Implantation Technology, 25.-29.06.2012, Valladolid, Spain

118. Zajac, D. A.; Ellmer, K.; Bikowski, A.; Vinnichenko, M.
Near order structure of transparent conducting oxides: X-ray absorption study of Al-doped ZnO and ZnMgO in low doping regime
11th International School and Symposium on Synchrotron Radiation in Natural Science, 20.-25.05.2012, Krakow, Poland

Lectures / talks

1. Abrasonis, G.
Control over surface and bulk atomistic processes in carbon-transition metal films
Seminar at TU Chemnitz: Topical Problems in Theoretical Physics, 25.01.2012, Chemnitz, Germany

2. Baehtz, C.; Shalimov, A.; Grenzer, J.; von Borany, J.
ROssendorf BeamLine II - New experimental possibilities for in-situ diffraction experiments
7. Wissenschaftliches Seminar des Dresdner Fraunhofer-Clusters Nanoanalytik, 27.01.2012, Dresden, Germany

3. Bischoff, L.
Liquid metal ion sources and their application in nanotechnology
Seminar, 19.11.2012, Mainz, Germany

4. Blaschke, D.; Skorupa, I.; Scheumann, B.; Scholz, A.; Zahn, P.; Gemming, S.; Potzger, K.
Resistive switching in TiO_2
Seminar at TU Chemnitz: Topical Problems in Theoretical Physics, 28.11.2012, Chemnitz, Germany

5. Bogusz, A.
Investigation of resistive switching in $YMnO_3$ thin films grown by PLD technique
Seminar at TU Chemnitz: Topical Problems in Theoretical Physics, 28.11.2012, Chemnitz, Germany

6. Deac, A. M.
Spin-torque devices for information-communication technology applications
Seminar at TU Dresden, 26.06.2012, Dresden, Germany

7. Deac, A. M.
Spin-torque devices for information-communication technology applications
Seminar at TU Chemnitz, 09.10.2012, Chemnitz, Germany

8. Facsko, S.
Periodic pattern induced by low energy ion irradiation
SPIRIT Workshop, 18.-20.07.2012, Lisbon, Portugal

9. Fassbender, J.
Ion beam modification of magnetic materials
IMW-Seminar des IFW Dresden, 19.01.2012, Dresden, Germany

10. Fassbender, J.
Ions hit magnetism - new challenges for the design of artificial nanostructures
Kolloquium at the University of Electronic Science and Technology, Chengdu, 10.09.2012, Chengdu, China

11. Fassbender, J.
Ions hit magnetism - new challenges for the design of artificial nanostructures
Physikalisches Kolloquium an der Universtität Osnabrück, 18.10.2012, Osnabrück, Germany

12. Gemming, S.; Dittmann, R.; Meyer, D. C.; Mikolajick, T.; Ronning, C.; Schmidt, H.; Waser, R.; Spaldin, N. A.; Basov, D.
Virtual Institute MEMRIOX - Memory Effects in Resistive Ion-beam Modified Oxides
HGF In-House Workshop PNI, 11.-12.06.2012, Freising, Germany

13. Gensch, M.
Coherent THz radiation from linear accelerators and 4t^{h} generation X-ray light sources: status, challenges and opportunities
Kolloquium des Fachbereichs Physik der Freien Universität Berlin, 27.04.2012, FU Berlin, Germany

14. Gensch, M.
Accelerator-based super-radiant coherent THz sources: Challenges and opportunities
Seminar des Fritz Haber Instituts, 22.10.2012, Berlin, Germany

15. Grenzer, J.
In-situ X-ray scattering & diffraction: Studying the formation of nanostructure
Gemeinsames Festkörperphysik-Seminar, Institut für Theoretische Physik, Universität Bremen, 18.12.2012, Bremen, Germany

16. Helm, M.
Terahertz spectroscopy of semiconductor nanostructures with the free-electron laser
Physikkolloquium TU Chemnitz, 23.05.2012, Chemnitz, Germany

17. Helm, M.
Terahertz spectroscopy of semiconductor nanostructures with the free-electron laser
Physikkolloquium Universität Konstanz, 26.06.2012, Konstanz, Germany

18. Helm, M.
Terahertz spectroscopy of semiconductor nanostructures with the free-electron laser
Physikkolloquium Universität Paderborn, 12.07.2012, Paderborn, Germany

19. Helm, M.
Terahertz spectroscopy of semiconductor nanostructures with the free-electron laser
Seminar talk at Southeastern University, 18.09.2012, Nanjing, China

20. Helm, M.
From terahertz science and technology to semiconductor quantum structures and back
Lecture at Southeastern University, 18.09.2012, Nanjing, China

21. Keller, A.
DNA origami
Seminar at TU Chemnitz: Topical Problems in Theoretical Physics, 12.12.2012, Chemnitz,Germany

22. Kelling, J.
Accelerated atomistic simulations of nanostructure evolution using graphics cards
Seminar at TU Chemnitz: Topical Problems in Theoretical Physics, 16.05.2012, Chemnitz, Germany

23. Kelling, J.
GPGPU for kinetic lattice Monte Carlo simulations
CCoE Seminar, 11.10.2012, TU-Dresden WIL/A317, Germany

24. Körner, M.
Morphology induced magnetic anisotropy and damping in thin films
Seminar at Lawrence Berkeley National Lab, 14.05.2012, Berkeley, CA, USA

25. Körner, M.
Morphology induced magnetic anisotropy and damping in thin films
Seminar at HGST, a Western Digital company, 17.05.2012, San Jose, CA, USA

26. Körner, M.
Morphology induced magnetic anisotropy and damping in thin films
Seminar at IBM Almaden Research Center, 15.05.2012, San Jose, CA, USA

27. Kranz, A.; Heinig, K.-H.; Liedke, B.
The influence of the surface slope on ion induced mass drift
Spring meeting of the DFG FOR 845 "Selbstorganisierte Nanostrukturen durch niederenergetische Ionenstrahlerosion", 07.-08.02.2012, Kaiserslautern, Germany

28. Merchel, S.
Wann ist denn das passiert? – Ko(s)mische Strahlung und einstürzende Berge
TU Dresden, Ringvorlesung im Studium generale / öffentliche Vorträge, 19.04.2012, Dresden, Germany

29. Merchel, S.; Rugel, G.; Akhmadaliev, Sh.
Bestimmung langlebiger Radionuklide zur Datierung in den Geowissenschaften und der Kosmochemie
Dresdener Geowissenschaftliches Kolloquium, 15.05.2012, Dresden, Germany

30. Ou, X.
Doping of nanostructure and defect engineering by ion beam implantation and irradiation
Lecture at Beihang University and Peking University, 28.09.2012, Beijing, China

31. Ou, X.; Grenzer, J.; Facsko, S.
Nano structure induced by ion beam sputtering
Forschergruppe 845 project workshop, 07.-08.02.2012, Kaiserslautern, Germany

32. Ou, X.; Grenzer, J.; Facsko, S.
Nanopattering on crystal Ge surfaces
Forschergruppe 845 project workshop, 07.-08.11.2012, Dresden, Germany

33. Ou, X.; Kögler, R.; Facsko, S.
Fabrication of nanostructure arrays by ion beam irradiation
Lecture at University of Konstanz, 12.-15.11.2012, Konstanz, Germany

34. Pavetich, S.; Akhmadaliev, Sh.; Merchel, S.; Rugel, G.
Development of an ion source for volatile elements
Lecture at Vienna Enviromental Research Accelerator, 20.11.2012, Wien, Austria

35. Posselt, M.; Kunze, T.; Al-Motasem, A.
Atomic-level simulations of materials properties and processes
Lecture at Department of Physics, Beihang University, 22.10.2012, Beijing, China

36. Schmidt, B.
Ion beam shaping of nanomaterials
SPIRIT Workshop, 18.-20.07.2012, Lisbon, Portugal

37. Schneider, H.
Experiments with strong far-infrared radiation at the free-electron laser
Kolloquium FB Physik, Universität Marburg, 14.05.2012, Marburg, Germany

38. Skorupa, W.
Subsecond thermal processing for advanced electronics and photovoltaics
Seminar at CEMES (Centre d'Elaboration de Matériaux et d'Etudes Structurales), 12.07.2012, Toulouse, France

39. Skorupa, W.
Millisecond annealing and beyond
Seminar at the Deptartment of Physics, University of Oslo, 12.10.2012, Oslo, Norway

40. Schneider, H.
Quantum well infrared photodetectors for dual-band thermal imaging and two-photon detection

Seminar, University of Electronic Science and Technology of China (UESTC), 18.10.2012, Chengdu, China

41. Wieser, M.; Berger, S.; Kunze, S.; Gemming, S.; Grebing, J.; Erbe, A.; Morawetz, K.; Huhn, K.; Wolf, J.
Conducting molecules
Seminar at TU Chemnitz: Topical Problems in Theoretical Physics, 09.05.2012, Chemnitz, Germany

42. Winnerl, S.
Relaxation dynamics in graphene
Seminar der Arbeitsgruppe Prof. Wieck, 06.07.2012, Bochum, Germany

43. Zahn, P.; Gemming, S.
Virtual Institute MEMRIOX
Seminar at TU Chemnitz: Topical Problems in Theoretical Physics, 11.01.2012, Chemnitz, Germany

44. Ziegenrücker, R.
Super-SIMS
Short course - Introduction to Secondary Ion Mass Spectrometry in the Earth Sciences, 22.-26.10.2012, Potsdam, Germany

Conferences, workshops, colloquia and seminars

Organization of conferences and workshops

1. Helm, M.; Winnerl, S.; Hertel, T.; Huber, R.; Tonouchi, M.
International workshop: THz dynamics in carbon based nanostructures
05.-07.03.2012, Dresden, Germany

2. Becquart, C.; Posselt, M.; Smith, R.
International workshop "Beyond molecular dynamics: Long time atomic scale simulations
16.-29.03.2012, Dresden, Germany

3. Helm, M.; Gensch, M.; Feldhaus, J.
503th Wilhelm and Else Heraeus Seminar: "Free-electron lasers: from fundamentals to applications"
10.-13.04.2012, Bad Honnef, Germany

4. Erbe, A.; Karl, M.
Helmholtz-Zeiss industry workshop
04.05.2012, Dresden, Germany

5. Helm, M.; Schmidt, O.G.
International Conference on Superlattices, Nanostructures and Nanodevices – ICSNN 2012
22.-27.07.2012, Dresden, Germany

Colloquia

1. Adeyeye, Adekunle
Information Storage Materials Laboratory, Department of Electrical and Computer Engineering, National University of Singapore
Artificial ferromagnetic nanostructures: An experimental platform for magnonics
09.10.2012

2. Banhart, John
Helmholtz-Zentrum Berlin
The complexity of ageing in Al 6000 alloys
01.03.2012

3. Bauer, Michael
Institut für Experimentelle und Angewandte Physik, Christian-Albrechts-Universität zu Kiel
Ultrafast plasmon dynamics probed by photoemission electron microscopy
18.10.2012

4. Felser, Claudia
Max Planck Institute for Chemical Physics of Solids and Johannes Gutenberg Universität Mainz
Tetragonal Heusler compounds for spintronics
19.07.2012

5. Heinrich, Bret
Physics Department, Simon Fraser University, Burnaby, BC, Canada
Spin pumping effects: magnetic metal and insulator interfaces
09.07.2012

6. Hertel, Riccardo
Institut de Physique et Chimie des Matériaux de Strasbourg, Université de Strasbourg, France
Simulation of ultrafast vortex dynamics in magnetic nanotubes: Cherenkov-type spin wave radiation and chiral symmetry breaking
19.04.2012

7. Schultheiß, Helmut
Materials Science Division, Argonne National Laboratory, France
Spin wave transport in microscopic magnetic structures
12.07.2012

8. Schmitz-Antoniak, Carolin
Universität Duisburg-Essen
X-ray absorption spectroscopy on nanoscale systems for modern applications
11.10.2012

9. Thomson, Tom
Nano Engineering and Storage Technology Group, University of Manchester, UK
Nano-magnetism: Understanding and exploiting perpendicular anisotropy materials
29.05.2012

10. Weig, Eva
Center for NanoScience & Fakultät für Physik, LMU München
Nanomechanical systems
25.10.2012

Seminars

1. Aleksandrov, Yuriy
Universität Duisburg-Essen
Electrical detection studies of inverse spin Hall effect induced by spin pumping
23.05.2012

2. Alexandru, Mihaela
Polytechnical University of Catalonia, National Center of Microelectronics, Spain
Radiation hardness Investigations of SiC devices by electron and proton irradiation
13.07.2012

3. Babonneau, David
Département Physique et Mécanique des Matériaux, Université de Poitiers, France
GISAXS analysis of ion-beam nanostructured thin films: experiences and simulations
23.05.2012

4. Bogusz, Agnieszka
TU Bergakademie Freiberg
Research activities in the field of high temperature processes involving oxides
09.02.2012

5. Bradley, Mark
Colorado State University, USA
Nanoscale patterns produced by ion bombardment of surfaces: The crucial effect of impurities
25.06.2012

6. Camarota, Benedetta
PTB Braunschweig
The electron counting capacitance standard experiment at PTB Braunschweig: recent progress
16.03.2012

7. Deniz, Okan
Graduate School of Science Department of Advanced Technologies, Department of Materials Science and Engineering, Anadolu University, Eskişehir, Turkey
Determination of correlation between magnetic and structural properties in nano-scale IrMn/CoFe thin film systems for magnetic storage systems
23.10.2012

8. Dimakis, Emmanouil
Paul Drude Institut, Berlin
Molecular beam epitaxy of III-V nanostructures: from growth mechanisms to light emitting

diodes
12.11.2012

9. Fedoryshyn, Yuriy
ETH Zürich, Switzerland
MBE growth of InP-based structures in FIRST-lab at ETH Zurich
12.11.2012

10. Gago, Raul
Instituto de Ciencia de Materiales de Madrid, Consejo Superior de Investigaciones Científicas, Madrid, Spain
X-ray absorption studies of pure and N-doped TiO_2 films grown by reactive pulsed magnetron sputtering
05.09.2012

11. Garrido, Blas
Departamento de Electrónica, Facultad de Física, Universidad de Barcelona, Spain
Silicon quantum dot multilayered structures for tandem solar cells and light emitting devices
14.12.2012

12. Geyer, Nadine
MPI für Mikrostrukturphysik Halle
Nanostructuration of silicon by means of metal-assisted chemical etching
22.06.2012

13. Grydlik, Martyna und Brehm, Moritz
IFW Dresden
SiGe nanostructures towards applications in Si-based photonics
29.08.2012

14. Hilgendorff, Michael
FU Berlin
Colloid chemistry: Preparation and surface manipulation of inorganic nanoparticles for multiple applications
25.07.2012

15. Khalid, Muhammad
Universität Leipzig
Defect-induced magnetism in non-magnetic oxides
06.08.2012

16. Kostylev, Mikhail
University of Western Australia
Microwave dynamics in magnetic multi-layers and nanostructures for magnonic and spintronic applications
07.03.2012

17. Lomakina, Faina
Universität Regensburg
Origin of the magnetogyrotropic photogalvanic effect in GaAs quantum wells
22.02.2012

18. Mascher, Peter
Department of Engineering Physics and Center for Emerging Device Technologies, McMaster University, Hamilton, Ontario/Canada
Visible light emission from rare-earth doped silicon-based nanostructures
12.12.2012

19. Matias, Vladimir
iBeam Materials, Inc. and Los Alamos National Laboratory, NM, USA
Ion-beam assisted nano-texturing of templates for epitaxial film growth
18.06.2012

20. Pérez, Nicolas
1 Dep. Física Fonamental and Institut de Nanociència i Nanotecnologia (IN2UB), Universitat de Barcelona, Spain

Magnetite nanoparticles with bulk like behaviour
01.08.2012

21. Preu, Sascha
Universität Erlangen
N-i-pn-i-p THz sources and field effect transistor detectors
12.06.2012

22. Röder, Falk
Speziallabor für höchstauflösende Elektronenmikroskopie und Elekronenholographie Triebenberg, TU Dresden
Electron holography of electric and magnetic fields
04.04.2012

23. Romstedt, Friedrich
Universität Göttingen
Measurements of 3D magneto-optical properties of a thin ferromagnetic film
02.04.2012

24. Schmult, Stefan
NamLab, TU Dresden
Quantum Hall effect in GaAs/AlGaAs bilayers or excitons in two half-filled Landau levels
25.04.2012

25. Schultes, Günter
HTW Saarbrücken
Metal-carbon thin films for mechanical sensors
28.02.2012

26. Shi, Jing
Department of Physics and Astronomy, University of California, Riverside, USA
Searching for transport evidence of surface states in Bi_2Se_3 topological insulator
22.05.2012

27. Stenner, Charlotte
Universität Hamburg
Manipulation of magnetic properties of permalloy microstructures via chromium implantation
30.10.2012

28. Stevenson, Stephanie
Swiss Light Source, Paul Scherrer Institut, Switzerland
Magnetisation dynamics of mesoscopic structures studied with X-ray microscopy
05.09.2012

29. Vogt, Katrin
TU Kaiserslautern
Optical detection of spin wave transport in microstructures
13.07.2012

30. Windl, Wolfgang
Department of Materials Science and Engineering, The Ohio State University, Columbus, USA
Ab initio modeling of functional materials – From double perovskites to graphene
24.07.2012

31. Wurstbauer, Ursula
Columbia University, New York, USA
State-of-the-art structures by MBE: quantum phases of electrons and properties of magnetic hole systems
05.11.2012

32. Yildirim, Oguz
Ankara University, Engineering Physics Department, Magnetic Materials Research Group, Ankara, Turkey
The investigation of the effect of the substitution of Ti for Mn on the structural, magnetic and magnetocaloric properties of CoMnGe alloy
04.04.2012

Exchange of researchers

SPIRIT visitors

1. Beck, L.
   CEA Saclay, Gif sur Yvette, France; 01.-03.05.2012
2. Chenwei, H.
   CNRS/CEMHTI, Orléans, France; 02.-05.09.2012
3. Dekov, V.
   IFREMER Département Géosciences Marines Laboratoire Géochimie Métallogénie, Plouzané, France ; 22.01.-04.02.2012
4. Dimova, M.
   Institute of Mineralogy and Crystallography - Bulgarian Academy of Sciences, Sofia, Bulgaria; 22.01.-04.02.2012
5. Hardi, Ch.
   Loughborough University, Loughborough, United Kingdom; 23.-26.09.2012
6. Kostova-Dimeva, I.
   University of Sofia, Sofia, Bulgaria; 13.-31.05.2012
7. Koutsokeras, L.
   University of Ioannina, Ioannina, Greece; 05.-07.06.2012
8. Mackova, A.
   Nuclear Physics Institute of ASCR, Rez, Czech Republic; 12.-13.06.2012; 17.-18.10.2012
9. Malinsky, P.
   Nuclear Physics Institute of ASCR, Rez, Czech Republic; 11.-15.06.2012; 15.-18.10.2012
10. Meissl, W.
    Technische Universität Wien, Austria; 19.02.-10.03.2012
11. Moll, S.
    CEA Saclay, Gif sur Yvette, France; 01.-04.05.2012
12. Nowak, M.
    University Poznan, Poznán, Poland; 11.-16.11.2012
13. Pochrybniak, C.
    Soltan Institute for Nuclear Studies, Otwock, Poland; 28.05.-02.06.2012
14. Ritter, R.
    Technische Universität Wien, Austria; 19.-24.02.2012; 22.-27.04.2012; 14.-18.10.2012
15. Schrempf, D.
    Technische Universität Wien, Austria; 26.02.-10.03.2012
16. Toms, P.
    Nuclear Physics Institute of ASCR, Rez, Czech Republic; 11.-15.06.2012; 15.-18.10.2012
17. Werner, Z.
    Soltan Institute for Nuclear Studies, Otwock, Poland; 28.05.-02.06.2012
18. Williams, C.
    Loughborough University, Loughborough, United Kingdom; 03.-07.06.2012

FEL visitors

1. Chatterjee, S.
   Philipps-Universität Marburg, Germany; 11.-18.03.2012; 20.-26.05.2012; 11.-22.11.2012
2. Chernikov, A.
   Philipps-Universität Marburg, Germany; 11.-18.03.2012; 20.-26.05.2012
3. Deßmann, N.
   Aerospace Center DLR, Berlin, Germany; 19.-24.03.2012; 06.-10.08.2012; 24.-27.10.2012
4. Diakonova, N.
   Laboratoire Charles Coulomb, CNRS-UM2, Département semiconducteurs, Matériaux et Capteurs, Université Montpellier 2, Montpellier, France; 05.-09.08.2012
5. Kamann, J.
   Universität Regensburg,Germany; 20.-21.06.2012
6. *Lörincz, I.*
   Eotvos University, Budapest, Hungary; 14.-15.02.2012; 11.-12.09.2012; 10.-15.10.2012
7. Malnasi-Csizmadia, A.
   Eotvos University, Budapest, Hungary; 14.-15.02.2012; 11.-12.09.2012; 10.-15.10.2012
8. Ortolani, M.
   CNR-IFN, Institute for Photonics and Nanotechnology, Rome, Italy; 18.-23.06.2012
9. Orlita, M.
   Grenoble High Magnetic Field Laboratory (GHMFL), Grenoble, France; 30.05.-01.06.2012
10. Pavlov, S.
    Aerospace Center DLR, Berlin, Germany; 19.-24.03.2012; 06.-10.08.2012; 25.-27.10.2012
11. Pohl, A.
    Aerospace Center DLR, Berlin, Germany; 19.-24.03.2012; 06.-10.08.2012
12. Preu, S.
    Universität Erlangen-Nürnberg, Erlangen, Germany; 17.-21.10.2012
13. *Rauscher, A.*
    Eotvos University, Budapest, Hungary; 14.-15.02.2012
14. *Rosemann, N.*
    Philipps-Universität Marburg, Germany; 11.-22.11.2012
15. *Schay, G.*
    Eotvos University, Budapest, Hungary; 14.-15.02.2012; 11.-12.09.2012; 10.-15.10.2012
16. Shastin, V.
    Institute for Physics of Microstructures of the Russian Academy of Sciences, Nizhny Novgorod, Russia; 06.-10.08.2012
17. Tsyplenkov, V.
    Aerospace Center DLR, Berlin, Germany; 25.-27.10.2012
18. Virgilio, M.
    University of Pisa, Pisa, Italy; 18.-23.06.2012
19. *Wall, S.*
    ICFO - Institut de Ciències Fotòniques, Castelldefels, Spain; 11.-13.09.2012
20. Zhukavin, R.
    Institute for Physics of Microstructures of the Russian Academy of Sciences, Nizhny Novgorod, Russia; 06.-10.08.2012

ROBL-MRH visitors

1. Barchasz, C.
   CEA Grenoble, LITEN.DEHT.LBA, Grenoble, France; 05.-08.12.2012
2. Bayer B. C.
   University of Cambridge, Department of Engineering , Cambridge, UK; 20.-26.06.2012
3. Burlaka, V.
   Georg-August-Universität Göttingen, Institut für Materialphysik, Göttingen, Germany; 08.-12.12.2012
4. Caha, O.
   Masaryk University, Institute of Condensed Matter Physics, Brno, Czech Republic; 27.07.-01.08.2012
5. Cavaleiro, A.
   University of Coimbra, CEMUC, Department of Mechanical Engineering, Coimbra, Portugal; 03.-07.10.2012
6. Chmelik, D.
   TU BA Freiberg, Institute of Materials Science, Freiberg, Germany; 16.-20.11.2012
7. Colin, J.-F.
   CEA Grenoble, LITEN.DEHT.LBA, Grenoble, France; 05.-08.12.2012
8. Gruber, W.
   TU Clausthal, Institute of Metallurgy, Clausthal-Zellerfeld, Germany; 07.-10.10.2012
9. Holy, V.
   Charles University, Dept. of Condensed Matter Physics, Praha, Czech Republic; 07.-10.11.2012, 27.07.-01.08.2012
10. Hrauda, N.
    Johannes Kepler University, Institute of Semiconductor Physics, Linz, Austria; 26.09.-02.10.2012
11. Keplinger, M.
    Johannes Kepler University, Institute of Semiconductor Physics, Linz, Austria; 26.09.-02.10.2012
12. Kidambi, P. R.
    University of Cambridge, Department of Engineering , Cambridge, UK; 20.-26.06.2012
13. Kriegner, D.
    Johannes Kepler University, Institute of Semiconductor Physics, Linz, Austria; 26.09.-02.10.2012
14. Kurz, S.
    MPI for Intelligent Systems, Stuttgart, Germany; 30.06.-03.07.2012
15. Leineweber A.
    MPI Metallforschung, Stuttgart, Germany; 30.06.-03.07.2012
16. Michaelis, B.
    University of Cambridge, Department of Engineering, Cambridge, UK; 20.-26.06.2012
17. Perez-Flores, J. C.
    Universidad San Pablo CEU, Facultad de Farmacia, Madrid, Spain; 29.11.-04.12.2012
18. PiskorskaI-Hommel, E.
    University Bremen, Institute of Solid State Physics, Bremen, Germany; 07.-10.11.2012
19. Rahn, J.
    TU Clausthal, Institute of Metallurgy, Clausthal-Zellerfeld, Germany; 07.-10.10.2012
20. Ramos, A. S.
    University of Coimbra, CEMUC, Department of Mechanical Engineering, Coimbra, Portugal; 03.-07.10.2012

21. Ratayski, U.
TU BA Freiberg, Institute of Materials Science, Freiberg, Germany; 16.-20.11.2012

22. Santos-Martins, R. M.
IST.ITN - Campus Tecnologico e Nuclear, UFA - Unidade de Física e Aceleradores, Sacavém, Portugal; 03.-07.10.2012

23. Schimpf, C.
TU BA Freiberg, Institute of Materials Science, Freiberg, Germany; 16.-20.11.2012

24. Schmidt, H.
TU Clausthal, Institute of Metallurgy, Clausthal-Zellerfeld, Germany; 07.-10.10.2012

25. Steiner, H.
Johannes Kepler University, Institute of Semiconductor Physics, Linz, Austria; 27.07.-01.08.2012

26. Uchida, H. T.
Georg-August-Universität Göttingen, Institut für Materialphysik, Göttingen, Germany; 08.-12.12.2012

27. Walus, S.
CEA Grenoble, LITEN.DEHT.LBA, Grenoble, France; 05.-08.12.2012

28. Waninger, M.
Georg-August-Universität Göttingen, Institut für Materialphysik, Göttingen, Germany; 08.-12.12.2012

Other guests

1. Baulin, R.
Lomonossov Moscow State University, Moscow, Russia; 10.-16.09.2012

2. Bilek, M.
University of Sydney, Sydney, Australia; 25.-29.06.2012

3. Bradley, M.
Colorado State University, Fort Collins, USA; 17.-29.06.2012

4. Buljan, M.
Ruder Boskovic Institute, Zagreb, Croatia; 01.-22.07.2012

5. Chatterjee, S.
Indian Institute of Technology, Bhubaneswar, India; 03.-29.05.2012

6. Eder, F.
TU Wien, Wien, Austria; 01.07.-31.12.2012

7. El-Said, A. S.
Mansoura University, Mansoura, Egypt; 04.06.-31.08.2012

8. Gago, R.
Instituto de Ciencia de Materiales de Madrid, Madrid, Spain; 08.08.-07.09.2012

9. Gallardo, R.
Universidad Tecnica Federico Santa Maria, Valparaiso, Chile; 31.08.-24.11.2012

10. Gan, H.
Sendai, Japan; 01.04.-30.09.2012

11. Gokhman, A.
South Ukrainian Pedagogical University, Odessa, Ukraine; 01.08.-30.09.2012

12. Gollwitzer, J.
New York University, USA; 06.06.-28.08.2012

13. Granovskiy, A.
Lomonossov Moscow State University, Moscow, Russia; 10.-16.09.2012

14. Holybee, B.
Purdue University, West Lafayette, USA; 01.11.-31.12.2012

15. Hou, F.
Lanzhou, P.R. China; 01.04.-30.06.2012

16. Incecam, S.
Ankara, Turkey; 01.07.-31.08.2012

17. Keles, U.
Bilkent University, Ankara, Turkey; 29.05.-29.06.2012

18. Kilibarda, F.
University of Belgrad, Belgrad, Serbia; 01.10.-20.12.2012

19. Konopik, P.
COMTES FHT a.s., Dobrany, Czech Republic; 16.01.-13.04.; 09.-17.08.2012

20. Mikhaylovskiy, Y.
Lomonossov Moscow State University, Moscow, Russia; 10.-16.09.2012

21. Moiseev, K.
IOFFE Institute, St. Petersburg, Russia; 13.-28.04.2012

22. Nikolaev, S.
RRC Kurchatov Institute, Moscow, Russia; 10.-16.09.2012

23. Ostapenko, A.
Lomonossov Moscow State University, Moscow, Russia; 16.-19.01.2012

24. Pankratyev, F.
Lomonossov Moscow State University, Moscow, Russia; 10.-16.09.2012

25. Ranjan, M.
Institute for Plasma Research, Gandhinagar, India; 15.09.-31.10.2012

26. Semisalova, A.
Lomonossov Moscow State University, Moscow, Russia; 10.-16.09.2012

27. Smekhova, A.
Lomonossov Moscow State University, Moscow, Russia; 01.-15.07.; 10.-16.09.; 08.10.-19.11.2012

28. Som, T.
Institute of Physics, Bhubaneswar, India; 12.06.-13.08.2012

29. Song, W.
Institute of Solid State Physics, Hefei, P. R. China; 15.05.-15.08.2012

30. Windl, W.
Ohio State University, Columbus, USA; 12.-26.07.2012

31. Yildirim, H.
Karabuk University, Karabuk, Turkey; 01.07.-30.09.2012

32. Yildirim, O.
Ankara University, Ankara, Turkey; 02.-06.04.2012

33. You, T.
TU Chemnitz, Chemnitz, Germany; 22.10.-04.11.; 02.-18.11.; 17.-21.12.2012

34. Zhou, H.-B.
Beihang University, Beijing, P. R. China; 10.07.-11.08.2012

Laboratory visits

1. Bali, R.
DESY Hamburg, Germany; 04.-07.07.; 20.-23.07.; 05.-07.08.; 21.-24.09.; 18.-22.10.2012

2. Banholzer, A.
Swiss Light Source, PSI Villigen, Switzerland; 24.06.-03.07.; 17.-23.10.; 25.11.-04.12.2012

3. Buhl, M.
Swiss Light Source, PSI Villigen, Switzerland; 31.01.-06.02.; 24.06.-03.07.; 17.-23.10.; 29.11.-04.12.2012

4. Bürger, D.
DESY Hamburg, Germany; 04.-11.07.; 01.-07.08.2012

5. Cornelius, S.
BESSY Berlin, Germany; 16.-23.07.2012

6. Deac, A.
Swiss Light Source, PSI Villigen, Switzerland; 25.-29.11.2012

7. Drachenko, O.
LNCMP Toulouse, France; 13.-22.03.; 29.08.-17.09.2012

8. Erbe, A.
BESSY Berlin, Germany; 30.04.-03.05.2012
Swiss Light Source, PSI Villigen, Switzerland; 29.06.-03.07.2012

9. Facsko, S.
University of Twente, Enschede, The Netherlands; 15.-19.04.2012

10. Fowley, C.
Trinity College, Dublin, Ireland; 23.04.-01.05.; 04.-10.11.2012
Swiss Light Source, PSI Villigen, Switzerland; 17.-23.10.; 26.-30.11.2012

11. Fries, F.
Swiss Light Source, PSI Villigen, Switzerland; 31.01.-06.02.2012

12. Gollwitzer, J.
Swiss Light Source, PSI Villigen, Switzerland; 23.06.-03.07.2012

13. Grebing, J.
BESSY Berlin, Germany; 27.04.-07.05.2012
Swiss Light Source, PSI Villigen, Switzerland; 24.06.-03.07.2012

14. Grenzer, J.
ESRF Grenoble, France; 28.05.-01.06.; 05.-16.11.2012

15. Heintze, C.
Oxford, UK; 04.-09.03.2012

16. Keller, A.
University of Twente, Enschede, The Netherlands; 15.-19.04.2012
Reykjavik University, Reykjavik, Island; 15.-23.05.2012

17. Khalid, M.
BESSY Berlin, Germany; 27.11.-02.12.2012

18. Langer, M.
Swiss Light Source, PSI Villigen, Switzerland; 29.11.-04.12.2012

19. Luo, W.
UESTC Chengdu, P. R. China; 24.06.-30.06.2012

20. Meutzner, F.
DESY Hamburg, Germany; 04.-07.07.; 20.-23.07.2012

21. Ou, X.
Beihang University, Beijing, P. R. China; 08.09.-02.10.2012
Universität Konstanz, Germany; 11.-15.11.2012

22. Potzger, K.
Moscow State University, Moscow, Russia; 11.-15.04.2012

23. Roshchupkina, O.
ESRF Grenoble, France; 28.05.-05.06.; 27.06.-09.07.; 18.-21.09.; 05.-20.11.2012

24. Schneider, H.
Shanghai Jiatong University, Shanghai, P. R. China; 14.-29.04.; 20.10.-04.11.2012
Universität Freiburg, Germany; 26.05.-03.06.2012

25. Schönitz, I.
CIEMAT Madrid, Spain; 03.-16.06.2012

26. Sendler, T.
Swiss Light Source, PSI Villigen, Switzerland; 31.01.-07.02.2012

27. Sluka, V.
Swiss Light Source, PSI Villigen, Switzerland; 25.11.-30.11.2012

28. Steinbach, G.
Swiss Light Source, PSI Villigen, Switzerland; 31.01.-07.02.; 17.-23.10.2012

29. Ulbricht, A.
Budapest, Hungary; 21.05.-01.06.2012
ILL Grenoble, France; 04.-07.12.2012

30. Vinnichenko, M.
BESSY Berlin, Germany; 09.-16.07.2012

31. Wagner, A.
Budapest, Hungary; 21.05.-01.06.2012
Rouen University, Rouen, France; 08.-14.07.2012
CRIEP, Tokyo, Japan; 12.-21.10.2012

32. Wang, Y.
BESSY Berlin, Germany; 22.-29.04.; 27.11.-02.12.2012
Advanced Light Source, Berkeley, USA; 20.06.-02.07.2012
DESY Hamburg, Germany; 01.-07.08.2012

33. Wilde, C.
BESSY Berlin, Germany; 05.-10.06.2012

34. Wintz, S.
Advanced Light Source, Berkeley, USA; 08.-26.03.2012
BESSY Berlin, Germany; 30.04.-04.05.2012
Swiss Light Source, PSI Villigen, Switzerland; 25.-29.11.2012

35. Yildirim, O.
BESSY Berlin, Germany; 14.-21.11.2012

36. Zhou, S.
BESSY Berlin, Germany; 22.-29.04.; 27.11.-02.12.2012
Advanced Light Source, Berkeley, USA; 20.06.-02.07.2012
DESY Hamburg, Germany; 06.-11.07.2012

Projects

The projects are listed by funding institution and project starting date. In addition, the institute has several bilateral service collaborations with industrial partners and research institutions. These activities are not included in the following overview.

European Projects

1. 10/2006 – 03/2012 European Union EU
NULIFE – Nuclear plant life prediction
Dr. E. Altstadt Phone: 0351 260 2276 e.altstadt@hzdr.de

2. 02/2008 – 10/2013 European Union EU
GETMAT– Generation IV and transmutation materials
Dr. F. Bergner Phone: 0351 260 3186 f.bergner@hzdr.de

3. 03/2009 – 08/2013 European Union EU
SPIRIT – Support of public and industrial research using ion beam technology
Prof. W. Möller Phone: 0351 260 2245 w.moeller@hzdr.de

4. 03/2009 – 12/2013 European Union EU
PERFORM60 – Radiation effects in reactor materials (modelling)
Dr. E. Altstadt Phone: 0351 260 2276 e.altstadt@hzdr.de

5. 02/2010 – 01/2014 European Union EU
LONGLIFE – Long term irradiation embrittlement effects
Dr. E. Altstadt Phone: 0351 260 2276 e.altstadt@hzdr.de

6. 01/2011 – 12/2014 European Union EU
MATTER – Materials testing and rules
Dr. F. Bergner Phone: 0351 260 3186 f.bergner@hzdr.de

7. 06/2012 – 05/2015 European Union EU
CALIPSO – Coordinated access to lightsources
Prof. M. Helm Phone: 0351 260 2260 m.helm@hzdr.de

Helmholtz Association Projects

1. 03/2011 – 02/2016 Helmholtz–Gemeinschaft HGF
Functional Materials – Helmholtz Young Investigators' Group
Dr. S. Zhou Phone: 0351 260 2484 s.zhou@hzdr.de

2. 07/2011 – 09/2018 Helmholtz–Gemeinschaft HGF
NANONET – International Helmholtz research school on nanoelectronic networks
Dr. A. Erbe Phone: 0351 260 2366 a.erbe@hzdr.de

3. 08/2011 – 07/2012 Helmholtz–Gemeinschaft HGF
HEF–ALION – Spinoff funding
Prof. A. Kolitsch Phone: 0351 260 3348 a.kolitsch@hzdr.de

4. 10/2011 – 09/2016 Helmholtz–Gemeinschaft HGF
MEMRIOX – Virtual Institute – Memory effects in oxides
Prof. S. Gemming Phone: 0351 260 2470 s.gemming@hzdr.de

5. 02/2012 – 01/2015 Helmholtz–Gemeinschaft HGF
HRJRG–DETI.2 – Helmholtz Russia joint research group – Magnetic TiO_2
Dr. K. Potzger Phone: 0351 260 3244 k.potzger@hzdr.de

German Science Foundation Projects

1. 07/2008 – 06/2012 Deutsche Forschungsgemeinschaft DFG
MIMAD – Magnetische Anisotropie und Dämpfungsphänomene
Prof. J. Fassbender Phone: 0351 260 3096 j.fassbender@hzdr.de

2. 02/2009 – 09/2012 Deutsche Forschungsgemeinschaft DFG
Magtemplat – Magnetismus von nanoskaligen Filmen
Prof. J. Fassbender Phone: 0351 260 3096 j.fassbender@hzdr.de

3. 09/2009 – 12/2012 Deutsche Forschungsgemeinschaft DFG
DAFS – Bestimmung der elektronischen Struktur von Punktdefekten
Prof. S. Gemming Phone: 0351 260 2470 s.gemming@hzdr.de

4. 11/2009 – 03/2013 Deutsche Forschungsgemeinschaft DFG
TCOMR – Electric field control of magnetoresistance
Dr. H. Schmidt Phone: 0351 260 2724 heidemarie.schmidt@hzdr.de

5. 02/2010 – 06/2014 Deutsche Forschungsgemeinschaft DFG
HybMagMat – Hybride magnetische Materialien
Prof. J. Fassbender Phone: 0351 260 3096 j.fassbender@hzdr.de

6. 04/2010 – 03/2013 Deutsche Forschungsgemeinschaft DFG
Strukturbildende Prozesse in amorphen Kohlenstoffschichten
Dr. L. Bischoff Phone: 0351 260 2963 l.bischoff@hzdr.de

7. 08/2010 – 09/2013 Deutsche Forschungsgemeinschaft DFG
SuSi – Supraleitung in hochdotierten Gruppe IV Halbleitern
Dr. V. Heera Phone: 0351 260 3343 v.heera@hzdr.de

8. 09/2010 – 08/2013 Deutsche Forschungsgemeinschaft DFG
TERATOP – Terahertz non–linear detection and quantum optical studies by resonant two–photon transitions in semiconductor quantum wells
Dr. H. Schneider Phone: 0351 260 2880 h.schneider@hzdr.de

9. 11/2010 – 10/2013 Deutsche Forschungsgemeinschaft DFG
Atomistische Simulation der Selbstorganisation bei der Ionenstrahlerosion
Dr. K.–H. Heinig Phone: 0351 260 3288 k.h.heinig@hzdr.de

10. 11/2010 – 10/2013 Deutsche Forschungsgemeinschaft DFG
Relaxation dynamics in graphene investigated in the mid– and far–infrared spectral range
Dr. S. Winnerl Phone: 0351 260 3522 s.winnerl@hzdr.de

11. 01/2011 – 01/2014 Deutsche Forschungsgemeinschaft DFG
Wechselwirkung langsamer hochgeladener Ionen mit der Oberfläche von Ionenkristallen und Isolatoren
Dr. S. Facsko Phone: 0351 260 2987 s.facsko@hzdr.de

12. 01/2011 – 12/2013 Deutsche Forschungsgemeinschaft DFG
Selbstorganisierte Oberflächenmuster auf Germanium durch schwere Clusterionen
Dr. L. Bischoff Phone: 0351 260 2963 l.bischoff@hzdr.de

13. 03/2011 – 02/2014 Deutsche Forschungsgemeinschaft DFG
HISENSE – High–field studies of the band dispersion in novel semiconductor materials
Dr. O. Drachenko Phone: 0351 260 3593 o.drachenko@hzdr.de

14. 04/2011 – 03/2014 Deutsche Forschungsgemeinschaft DFG
FRUSTPART – Nukleation von Spinordnung in niederdimensionalen kolloidalen Partikelsystemen
Dr. A. Erbe Phone: 0351 260 2366 a.erbe@hzdr.de

15. 04/2011 – 03/2013 Deutsche Forschungsgemeinschaft DFG
CONDDNA – Quantum transport at the molecular scale of DNA
Dr. A. Erbe Phone: 0351 260 2366 a.erbe@hzdr.de

16. 08/2011 – 07/2014 Deutsche Forschungsgemeinschaft DFG
Nanostrukturierung von Oberflächen mit direkter Extraktion der Ionen aus Plasmaquellen
Dr. S. Facsko Phone: 0351 260 2987 s.facsko@hzdr.de

17. 09/2011 – 04/2013 Deutsche Forschungsgemeinschaft DFG
Terahertz dynamics in carbon based nanostructures
Prof. M. Helm Phone: 0351 260 2260 m.helm@hzdr.de

18. 03/2012 – 04/2014 Deutsche Forschungsgemeinschaft DFG
Ortsaufgelöste ferromagnetische Resonanz
Dr. J. Lindner Phone: 0351 260 3221 j.lindner@hzdr.de

19. 09/2012 – 09/2015 Deutsche Forschungsgemeinschaft DFG
ATOMIX – Atomares Mischen in Halbleitermultischichtstrukturen
Dr. M. Posselt Phone: 0351 260 3279 m.posselt@hzdr.de

Federally Funded Projects

1. 06/2009 – 05/2012 Bundesministerium für Bildung und Forschung BMBF
BioLED – Sensorik zur Detektion von (anti–) östrogen– und (anti–) androgenwirkenden Substanzen
Dr. L. Rebohle Phone: 0351 260 3368 l.rebohle@hzdr.de

2. 01/2010 – 03/2012 AG Industrieller Forschungseinrichtungen (AiF) BMWi
Advanced coatings to suppress environmental embrittlement of TiAl alloys
Prof. A. Kolitsch Phone: 0351 260 3348 a.kolitsch@hzdr.de

3. 04/2010 – 03/2013 Bundesministerium für Bildung und Forschung BMBF
WTZ–Türkei: Rainbow Energy – Development of new solar cells
Dr. K–.H. Heinig Phone: 0351 260 3288 k.h.heinig@hzdr.de

4. 05/2010 – 07/2013 AG Industrieller Forschungseinrichtungen (AiF) BMWi
TCO Grenzflächenoptimierung
Prof. A. Kolitsch Phone: 0351 260 3348 a.kolitsch@hzdr.de

5. 06/2010 – 11/2013 Gesellschaft für Anlagen– und Reaktorsicherheit (GRS) BMBF
Alterungseffekte in RDB–Stahl
Dr. F. Bergner Phone: 0351 260 3186 f.bergner@hzdr.de

6. 07/2010 – 06/2013 Gesellschaft für Chemische Technik und Biotechnologie DECHEMA
Ionenimplantation für Hochtemperatur–Oxidationsschutz
Prof. A. Kolitsch Phone: 0351 260 3348 a.kolitsch@hzdr.de

7. 10/2010 – 09/2013 Bundesministerium für Bildung und Forschung BMBF
Photoinitiated dynamics studied in the fs to ns time and the THz to PHz frequency domain: Picosecond beamline at FELBE (PIDID)
Dr. H. Schneider Phone: 0351 260 2880 h.schneider@hzdr.de

8. 05/2011 – 09/2013 Gesellschaft für Chemische Technik und Biotechnologie DECHEMA
Ionenimplantation für TiAl–Proben
Prof. A. Kolitsch Phone: 0351 260 3348 a.kolitsch@hzdr.de

9. 10/2011 – 10/2013 Bundesministerium für Bildung und Forschung BMBF
WTZ Indien: Plasmonische Strukturen
Dr. S. Facsko Phone: 0351 260 2987 s.facsko@hzdr.de

10. 10/2011 – 09/2012 Swiss National Science Foundation SNF
Spin–dependent transport in superlattice nanostructures
Dr. A. Deac Phone: 0351 260 3709 a.deac@hzdr.de

11. 01/2012 – 11/2014 AG Industrieller Forschungseinrichtungen (AiF) BMWi
Hochtemperaturoxidationsschutz für Titanlegierungen
Prof. A. Kolitsch *Phone: 0351 260 3348* *a.kolitsch@hzdr.de*

Saxony State Funded Projects

1. 07/2009 – 12/2012 Sächsische Aufbaubank SAB
High–k Gate Dielektrika 2. Generation (KZWEI)
Dr. W. Skorupa *Phone: 0351 260 3612* *w.skorupa@hzdr.de*

2. 12/2010 – 05/2013 Sächsische Aufbaubank SAB
Kelvin–Kraft–Mikroskopie
Dr. H. Schmidt *Phone: 0351 260 2724* *heidemarie.schmidt@hzdr.de*

3. 04/2012 – 03/2014 Sächsische Aufbaubank SAB
ADDE II: Untersuchung der H–Passivierung
Dr. W. Skorupa *Phone: 0351 260 3612* *w.skorupa@hzdr.de*

4. 06/2012 – 05/2014 Sächsische Aufbaubank SAB
NanoKlang – Korrosionsunterdrückung an Metall–Orgelpfeifen
Dr. W. Skorupa *Phone: 0351 260 3612* *w.skorupa@hzdr.de*

Personnel Exchange Projects

1. 09/2009 – 08/2012 Alexander–von–Humboldt–Stiftung AvH
Gastaufenthalt Dr. El–Said (Mansoura University, Egypt)
Dr. S. Facsko *Phone: 0351 260 2987* *s.facsko@hzdr.de*

2. 01/2011 – 12/2012 Deutscher Akademischer Austauschdienst DAAD
Projektbezogener Personenaustausch mit Spanien (Universidad Politécnica de Madrid)
Dr. F. Munnik *Phone: 0351 260 2174* *f.munnik@hzdr.de*

3. 11/2011 – 10/2012 Alexander–von–Humboldt–Stiftung AvH
Rückkehrstipendium Dr. A. Keller
Prof. J. Fassbender *Phone: 0351 260 3096* *j.fassbender@hzdr.de*

Bilateral Projects

1. 05/2008 – 04/2012 FHR Anlagenbau Ottendorf–Okrilla/IHP Frankfurt/O. Industry
Blitztemperung 200
Dr. W. Skorupa *Phone: 0351 260 3612* *w.skorupa@hzdr.de*

2. 07/2008 – 06/2012 TU Bergakademie Freiberg TU–BA
Eigenschaften nano– und mikrokristalliner Si–Dünnfilme
Dr. W. Skorupa *Phone: 0351 260 3612* *w.skorupa@hzdr.de*

3. 04/2010 – 03/2012 FHR Anlagenbau / Centrotherm Industry
Entwicklung industrietauglicher Temperaturmessung
Dr. W. Skorupa *Phone: 0351 260 3612* *w.skorupa@hzdr.de*

4. 04/2010 – 05/2013 Swiss Federal Nuclear Safety Inspectorate ENSI
Bruchmechanik bei Neutronenversprödung
Dr. H.–W. Viehrig *Phone: 0351 260 3246* *h.w.viehrig@hzdr.de*

5. 10/2010 – 09/2013 DTF Technology Dresden Industry
DTF– Industriedoktoranden
Prof. A. Kolitsch *Phone: 0351 260 3348* *a.kolitsch@hzdr.de*

6. 05/2012 – 03/2013 IXYS Semiconductor Industry
Machbarkeitsstudie
Dr. J. v. Borany *Phone: 0351 260 3378* *j.v.borany@hzdr.de*

7.	07/2012 – 06/2016	Abengoa Research, Seville, Spain		Industry
	AR framework collaboration			
	Dr. G. Abrasonis	*Phone: 0351 260 3578*	*g.abrasonis@hzdr.de*	
8.	10/2012 – 12/2015	Carl–Zeiss Microscopy		Industry
	Kooperation Ionenmikroskopie			
	Dr. J. v. Borany	*Phone: 0351 260 3378*	*j.v.borany@hzdr.de*	

Doctoral training programme

International Helmholtz Research School NANONET

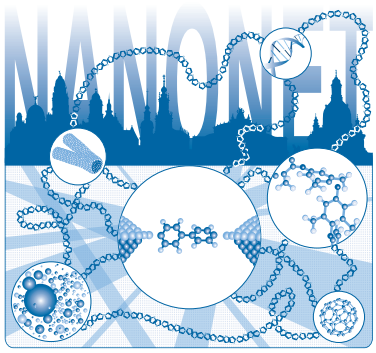

The Institute of Ion Beam Physics and Materials Research is coordinating the International Helmholtz Research School for Nanoelectronic Networks (IHRS NANONET) supported by the Initiative and Networking Fund of the Helmholtz Association. The project started in October 2012. The total funding is 1.200.000 € for a period of 6 years.

The IHRS NANONET is an international, interdisciplinary and thematically focused doctoral programme in the field of molecular electronics. The research school aims at attracting and promoting excellence by educating promising doctoral candidates with backgrounds in physics, chemistry, materials science and electrical engineering. During a period of 3 years PhD candidates benefit from well-structured, comprehensive training curricula and multiple mentorship, while performing cutting edge research projects within one of the 15 NANONET research groups. Under the supervision of outstanding scientists leading the field of nanoelectronics, the doctoral candidates have the unique opportunity to contribute to the advancement of molecular electronics by developing strategies for the real integration of single nanosized building blocks into large interconnected networks

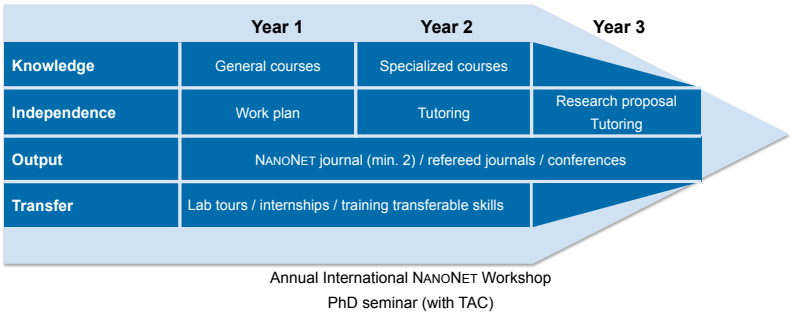

The period of doctoral studies is crucial in the academic career of young scientists. Therefore, the IHRS NANONET fosters not only professional qualification but also personal development by equipping young graduates with competencies for successful careers in a wide variety of positions in academia and industry. The training programme invests on professional competencies, such as the capability to work across disciplines and cultures by promoting networking and the exchange of ideas and knowledge with fellows, mentors and collaboration partners. The cooperation with international scientific and industrial partners complements and broadens the expertise of the IHRS NANONET by establishing a unique research and training network for its doctoral candidates.

The consortium

Helmholtz-Zentrum Dresden-Rossendorf
Technische Universität Dresden
Leibniz Institute of Polymer Research Dresden
Fraunhofer Institute for Nondestructive Testing
NaMLab gGmbH

For further information please contact the NANONET coordinator, Dr. Ana Cordeiro (nanonet@hzdr.de) or visit the IHRS NANONET website: www.ihrs-nanonet.de

Experimental equipment

Accelerators, ion implanters and ion-assisted-deposition

Van de Graaff Accelerator (VdG)	1.8 MV	*TuR Dresden, DE*
Tandetron Accelerator (T1)	3 MV	*HVEE, NL*
Tandetron Accelerator (T2)	6 MV	*HVEE, NL*
Low-Energy Ion Implanter	0.5 - 50 kV	*Danfysik, DK*
High-Current Ion Implanter	20 - 200 kV	*Danfysik, DK*
High-Energy Ion Implanter	40 - 500 kV	*HVEE, NL*
Plasma Immersion Ion Implantation	5 - 60 keV	*GBR, DE / Home-built*
Focused Ion Beam (15 nm, variable ions)	30 keV, 10 A/cm^2	*Orsay Physics, FR*
Highly-Charged Ion Facility	25 eV – 25 keV × Q Q = 1…40 (Xe)	*Home-built*
Dual-Beam Magnetron Sputter Deposition		*Roth & Rau, DE*
Ion-Beam-Assisted Deposition		*Danfysik, DK*
Ion-Beam Sputtering	200 - 2000 V	*Home-built*
UHV Ion Irradiation (Ar, He, etc.)	0 - 5 keV Scan 10×10 mm^2	*VG, USA*

Ion Beam Analysis (IBA)

A wide variety of advanced IBA techniques are available at the MeV accelerators (see figure).

RBS	Rutherford Backscattering Spectrometry	(1), (9), (11), (12), (21)	*vdG, T1, T2*
RBS/C	RBS + Channelling	(1), (9), (11), (12)	*vdG, T1, T2*
HR-RBS	High-Resolution RBS/C	(9), (13)	*T1*
ERDA	Elastic Recoil Detection Analysis	(1), (4)	*vdG, T2*
HR-ERDA	High-resolution ERDA	(7)	*T2*
PIXE	Particle-Induced X-ray Emission	(1), (5), (6), (12)	*vdG, T1, T2*
PIGE	Particle-Induced γ Emission	(6), (12)	*T1, T2*
NRA	Nuclear Reaction Analysis	(3)	*T2*
NRRA	Nuclear Resonance Reaction Analysis	(11)	*T1*
NMP	Nuclear Microprobe	(12)	*T1*
AMS	Accelerator Mass Spectrometry (focused to cosmogenic radionuclides: ^{10}Be, ^{26}Al, ^{36}Cl, ^{41}Ca, ^{129}I)	(10)	*T2*

Some stations are equipped with additional process facilities enabling *in-situ* IBA investigations during ion irradiation, sputtering, deposition, annealing etc..

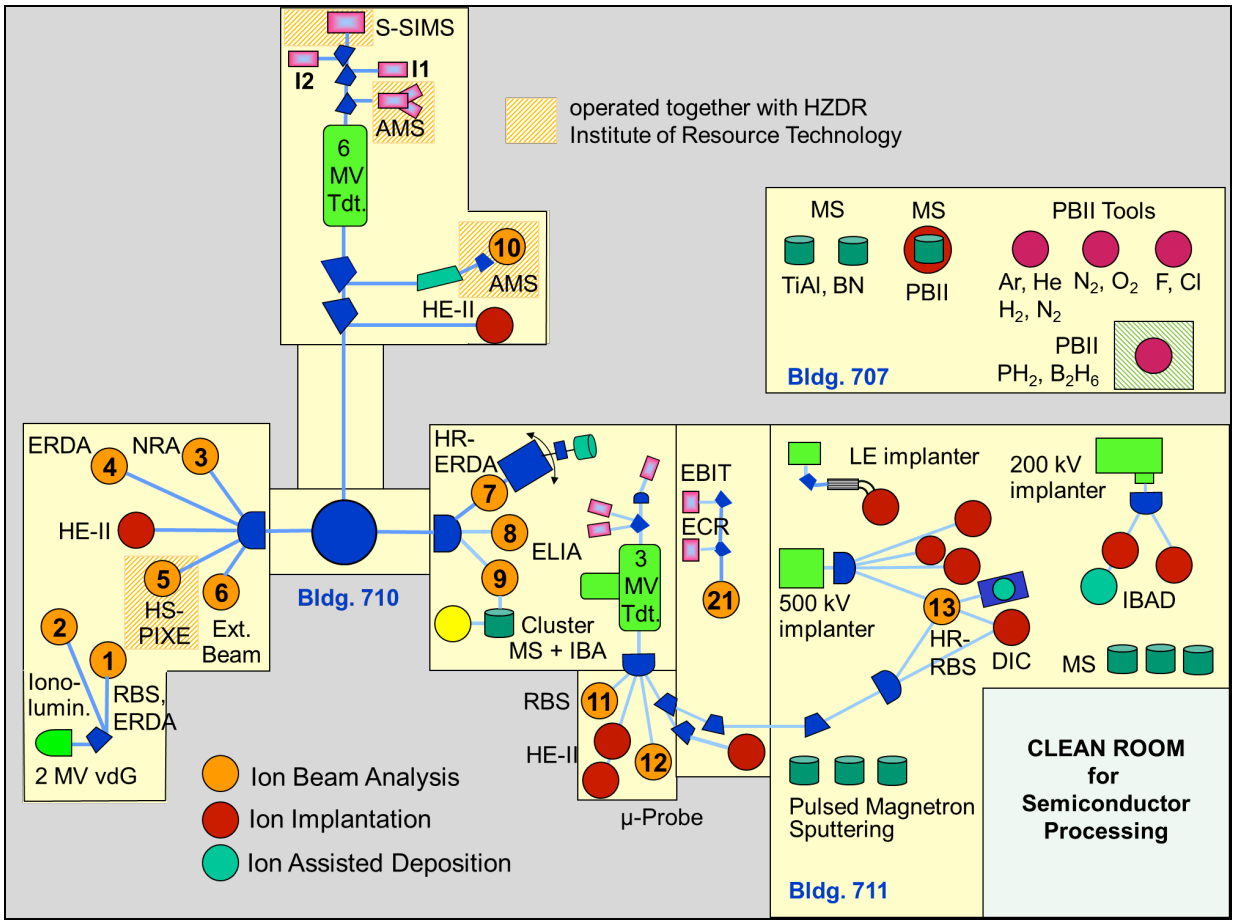

Schematic overview of the Ion Beam Center

Other particle-based analytical techniques

SEM	Scanning Electron Microscope	1 - 30 keV + EDX	*Hitachi, JP*
TEM	Transmission Electron Microscope (Titan 80-300 with Image Corrector)	80 - 300 keV + EDX, +GIF	*FEI, NL*
FIB/SEM	Focused Ion / Electron Cross Beam (NVision 40 with Elphy Plus Litho)	0.5 – 30 keV + IL, + EDX	*Zeiss-NTS, DE* *Raith, Bruker, DE*
AES	Auger Electron Spectroscopy	+ XPS	*Fisions, UK*
CEMS	Mössbauer Spectroscopy	^{57}Fe source	*Home-built*
PAS	Positron Annihilation Spectroscopy	^{22}Na source 30 V - 36 kV	*Home-built*

Photon-based analytical techniques

XRD/XRR	X-Ray Diffraction and Reflection	Cu-Kα	*Bruker AXS, DE*
HR-XRD	High-Resolution XRD	Cu-Kα	*GE Inspection, DE*
TFA	Thin Film Analysis, including Grazing Incidence Small Angle Scattering (GiSAXS)	Cu-Kα	*PANalytical, NL*
XRD/XRR	with Synchrotron Radiation	5 – 35 keV	*ROBL at ESRF, FR*
SE	Spectroscopic Ellipsometry	250 - 1700 nm	*Woollam, US*
FTIR	Fourier-Transform Infrared Spectrometer	600 - 7000 cm^{-1}	*Nicolet, US*
FTIR	Fourier-Transform Infrared Spectrometer	50 - 15000 cm^{-1}	*Bruker, DE*
	Ti:Sapphire Femtosecond Laser	78 MHz	*Spectra Physics, US*
	Femtosecond Optical Parametric Osci.		*APE, DE*
	Ti:Sapphire Femtosecond Amplifier	1 kHz	*Femtolasers, AT*
	Ti:Sapphire Femtosecond Amplifier	250 kHz	*Coherent, US*
	Femtosecond Optical Parametric Amplifier		*Light Conversion, LI*
THz-TDS	Terahertz Time-Domain Spectroscopy	0.1 - 4 THz	*Home-built*
Raman	Raman Spectroscopy	> 45 cm^{-1} shift	*Jobin-Yvon-Horiba, FR*
PL	Photoluminescence	300 - 1500 nm	*Jobin-Yvon-Horiba, FR*
TRPL	Time-Resolved PL	τ = 3 ps - 2 ns τ > 5 ns	*Hamamatsu Phot., JP* *Stanford Research, US*
EL	Electroluminescence (10-300 K)	300 - 1500 nm	*Jobin-Yvon-Horiba, FR*
	Optical Split-Coil Supercond. Magnet	7 T	*Oxford Instrum., UK*
PR	Photomodulated Reflectivity	300 - 1500 nm	*Jobin-Yvon-Horiba, FR*
PLE	Photoluminescence Excitation	300 - 1500 nm	*Jobin-Yvon-Horiba, FR*
OES	Optical Emission Spectroscopy	250 – 800 nm	*Jobin-Yvon-Horiba, FR*

Magnetic thin film deposition and analysis

MBE	Molecular Beam Epitaxy with in-situ FIB		*CreaTec, DE*
MBE	Molecular Beam Epitaxy		*Home-built*
PLD	Pulsed Laser Deposition		*SURFACE, DE*
MFM	Magnetic Force Microscope	~ 50 nm resol	*VEECO / DI, US*
SQUID	Supercond. Quantum Interference Device	± 7 T	*Quantum Design, US*
MOKE	Magneto-Optic Kerr Effect (in-plane)	± 0.35 T	*Home-built*
MOKE	Magneto-Optic Kerr Effect (perpend.)	± 2 T	*Home-built*
SKM	Scanning Kerr Microscope		*Home-built*
	Kerr Microscope		*Evico Magnetics, DE*
TR-MOKE	Time-Resolved MOKE (Pump-Probe)		*Home-built*
VNA-FMR	Vector Network Analyzer Ferromagnetic Resonance		*Agilent / Home-built*
ME	Magnetoellipsometer		*LOT, DE; AMAC, US*

Other analytical and measuring techniques

STM	Scanning Tunneling Microscope (with AFM-Option)		*DME, DK*
STM	*In-situ* Scanning Tunneling Microscope (T variable)		*Omicron, DE*
AFM	Atomic Force Microscope (Tapping Mode)		*SIS, DE*
AFM	Atomic Force Microscope (with c-AFM, SCM-Module)		*Veeco Instruments, UK*
KFM	Kelvin Probe Force Microscopy		*Anfatec, DE*
	Dektak Surface Profilometer		*Veeco, US*
	Micro Indenter / Scratch Tester		*Shimatsu, JP*
MS	Mass Spectrometers (EQP-300, HPR-30)		*HIDEN, DE & US*
	Wear Tester (pin-on disc)		*Home-built*
LP	Automated Langmuir Probe		*Impedans, IE*
HE	Hall Effect Equipment	2 - 400 K, ≤ 9 T	*LakeShore, US*
RS	Sheet-Rho-Scanner		*AIT, South Korea*
DLTS	Deep Level Transient Spectroscopy	(+ I-U / C-V) (10 - 300 K, 1 MHz)	*PhysTech, DE*
IV / CV	Photocapacitance (+I-V/G-V)	(250 - 2500 nm)	*Home-built*
IV / CV	I-V and C-V Analyzer		*Keithley, US*
IV / CV	I-V and C-V Semi-Automatic Prober	(-60 – 300°C)	*Süss, DE; Keithley, US*
IV	I-V Prober	(4.2 – 600 K)	*LakeShore, Agilent, US*

Processing and preparation techniques

Physical Deposition	Sputtering DC / RF, Evaporation	*Nordiko, UK*
	Electron Beam Evaporation System	*Leybold Optics, DE*
	Thermal Evaporation	*Bal-Tec, LI*
Chemical Deposition	Plasma Enhanced CVD (for a-Si, SiO_2, SiON, Si_3N_4)	*Oxford Instruments, UK*
Dry Etching	Plasma and RIE Mode	*Sentech, DE*
Reactive Ion Beam Etching	∅ 6”, Ar, CF_4	*Roth & Rau, DE*
Etching / Cleaning	incl. Anisotropic Selective KOH Etching	
Photolithography	Mask-Aligner, 2 µm-level	*Süss, DE*
Electron Beam Lithography	Raith 150-TWO: ∅ 6”, 10 nm res.	*Raith, DE*
Thermal Treatment	Room Temperature - 2000°C	
• Furnace		*InnoTherm, DE*
• Rapid Thermal Annealing		*ADDAX, FR*
• Flash-Lamp Units (0.5 – 20 ms)		*Home-built; FHR, DE*
• RF Heating (Vacuum)		*JIP.ELEC, FR*
• Laser annealing (CW, 808 nm, 450 W)		*LIMO, DE*
• Laser annealing (30 ns pulse,10 Hz, 308 nm, 500 mJ)		*COHERENT, USA*
Bonding Techniques	Ultrasonic Wire Bonding	*Kulicke & Soffa, US*
Cutting, Grinding, Polishing		*Bühler, DE*
TEM Sample Preparation	Plan View and Cross Section incl. Ion Milling Equipment	*Gatan, US*

Hot cells laboratory

Mechanical testing of neutron irradiated structural materials	max. total activity 5 TBq (Co-60), T = -150 ... +315 °C	
Fracture mechanics testing	max load ±50 kN	MTS, US
Charpy impact testing	300 J	WPM Leipzig, DE
Small punch test	10 kN	Hegewald & Peschke, DE
Specimen preparation	Electrical discharge machining	AGIE, DE
Depth sensing nanoindentation/ AFM	UNAT, load range 1 … 500 mN	ASMEC, DE

User facilities and services

Ion Beam Center (IBC)

The IBC is a leading European user facility primarily dedicated to research and application of ion beam techniques in materials science. The IBC comprises various ion beam facilities providing a wide energy range between eV and about 60 MeV. Besides these facilities, structural analysis (electron microscopy and spectroscopy, X-ray scattering techniques) and sample or device processing under clean-room conditions belong to the IBC to deliver a “complete” user service. The use of the IBC facilities includes the scientific and technical support during planning, execution and subsequent evaluation of the experiments.

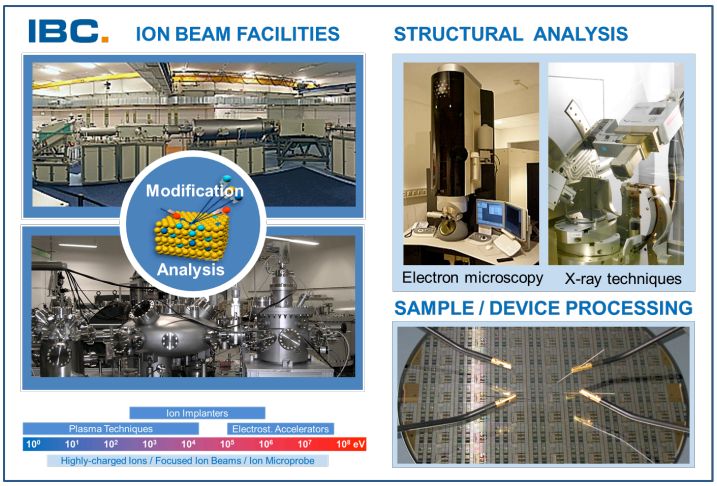

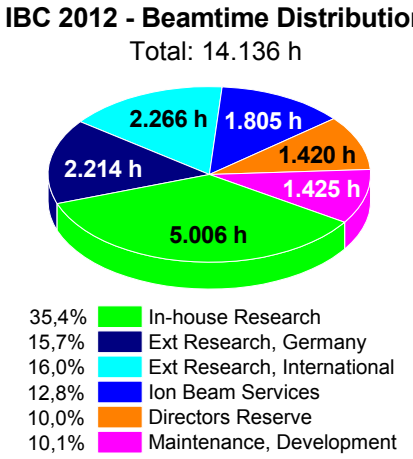

The IBC is recognized as a qualified large-scale facility within the “BMBF Verbundforschung” promoting long-term collaborations with universities. In addition, the IBC coordinates the European Infrastructure Project “SPIRIT” (see page 122) dedicated to transnational user access to different European Ion Beam Centres. With respect to other ion beam centres worldwide, the IBC may be characterized by three specific features: (i) the research is focused to materials science, (ii) the activities cover both, material modification and analysis, and (iii) the operation as a competence centre for ion beam applications in a close collaboration with industry. At IBC most common ion beam techniques are available, including dedicated end-stations for ion beam modification and analysis such as:

- High-energy ion implantation for semiconductor processing,
- Plasma-based ion implantation for fast semiconductor doping or surface patterning processes,
- Surface patterning or micromechanics on the nano-scale by various focus ion beam facilities,
- Experiments using highly charged ions,
- End-stations allowing the simultaneous use of different IBA-techniques (e.g. RBS, He-ERDA, PIXE), partly as *in-situ* analysis during deposition or annealing experiments,
- Hydrogen (or other light elements) depth profiling using nuclear reaction analysis,
- Depth profiling (ERDA, RBS) with near-surface sub-nm resolution using magnetic spectrometers,
- IBA with µm spatial resolution using an ion microprobe or state-of-the art x-ray cameras,
- Accelerator mass spectrometry @ DREAMS beamline (excluding ^{14}C detection)

Presently, access to IBC installations is provided on the basis of scientific collaborations with research groups, by proposals of external users or taking advantage of the commercial service activities by the HZDR Innovation GmbH (www.hzdr-innovation.de). For further information please contact Dr. Johannes von Borany (j.v.borany@hzdr.de) or visit the IBC webpage (www.hzdr.de/IBC).

SPIRIT

The Institute of Ion Beam Physics and Materials Research is coordinating the Integrated Infrastructure SPIRIT under the FP7 Capacities Programme of the European Union. The duration of the project is from March 2009 to August 2013, the total funding is 6.991.000 €.

SPIRIT integrates 11 leading ion beam facilities from 6 European Member States and 2 Associated States. Nine of the partners provide Transnational Access to European researchers and industry at their infrastructures. Ion beams in an energy range from ~10 keV to ~100 MeV are supplied for modification and analysis of solid surfaces, interfaces, thin films and nanostructured systems, being mainly applied in research related to materials, biomedicine, environment, and cultural heritage. SPIRIT aims at increasing user access and the quality of research by sharing best practice, balancing supply and demand, harmonizing procedures and extending the services into new emerging fields and to new users especially from the New European Member States and industry. The project comprises a management section (4% of the total funding) and three interlinked activities of Transnational Access (45%), Networking (19%) and Joint Research (32%).

Potential users from public of industrial research are invited for free use of the ion beam facilities at the SPIRIT partners laboratories, either by conducting experiments personally or by sending samples in case of standard ion implantation or ion beam materials analysis. Regularly, access is given on a transnational basis, i.e. the user has to be employed in a European Member or Associate State in which the specific infrastructure is not situated.

Also in 2012, all SPIRIT activities continued to demonstrate excellent performance. The second periodic report (covering months 19-36) was readily accepted by the European Commission. Although close to 100% of all deliverables and milestones will be accomplished, residual resources enable additional Joint Research activities and an increase of the Transnational Access volume by ~5%. For this purpose, a prolongation of SPIRIT by six months was agreed with the Commission.

Under the coordination of the University of Surrey, U.K., the SPIRIT consortium successfully applied for an EU Marie Curie Initial Training Network project SPRITE (“Supporting Postgraduate Research with Internships in industry and Training Excellence”) with a total funding of 3.537.036 €, starting in January 2013.

The SPIRIT Consortium
The top nine partners provide Transnational Access.

Helmholtz-Zentrum Dresden-Rossendorf	Germany
CNRS – CENBG Bordeaux	France
Katholieke Universiteit Leuven	Belgium
Jozef Stefan Institut Ljubljana	Slovenia
Universität der Bundeswehr München	Germany
CEA – JANNUS Saclay and CIMAP Caen	France
University of Surrey	U.K.
University de Pierre et Marie Curie Paris	France
Ruder Boskovic Institute Zagreb	Croatia
Institute Tecnologico e Nuclear Lisboa	Portugal
Swiss Federal Institute of Technology Zurich	Switzerland

Free Electron Laser FELBE

ELBE is an acronym for the free-electron laser (FEL) at the Electron Linear accelerator with high Brilliance and Low Emittance (ELBE) located at the Helmholtz-Zentrum Dresden-Rossendorf, Germany. The heart of ELBE is a superconducting linear accelerator operating in cw mode with a pulse repetition rate of 13 MHz. The electron beam (40 MeV, 1 mA max.) is guided to several laboratories where secondary beams (particle and electromagnetic) are generated. Two free-electron lasers (U27-FEL and U100-FEL) produce intense, coherent electromagnetic radiation in the mid and far infrared, which is tunable over a wide wavelength range (4 – 250 µm) by changing the electron energy or the undulator magnetic field. Main parameters of the infrared radiation produced by FELBE are as follows:

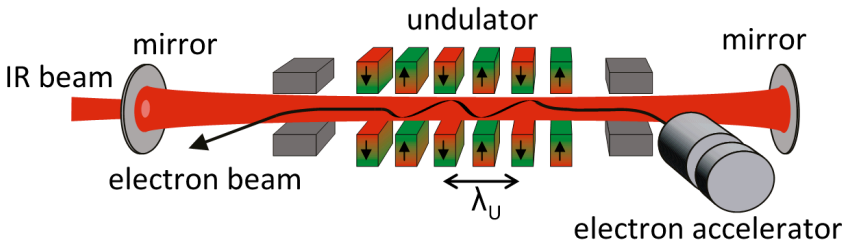

Wavelength λ	4 – 22 µm 18 – 250 µm	FEL with undulator U27 FEL with undulator U100
Pulse energy	0.01 – 2 µJ	depends on wavelength
Pulse length	1 – 25 ps	depends on wavelength
Repetition rate	13 MHz	3 modes: • cw • macropulsed (> 100 µs, < 25 Hz) • single pulsed (Hz…kHz)

The free electron laser is a user facility. Applications for beam time can be submitted twice a year, typically by April 15 and October 15. Users from EU countries can receive support through the FP7 Integrated Infrastructure Initiative (I3) CALIPSO (**C**oordinated **A**ccess to **LI**ghtsources to **P**romote **S**tandards and **O**ptimization).

Typical applications are picosecond pump-probe spectroscopy (also in combination with several other femtosecond lasers, which are synchronized to the FEL), near-field microscopy and nonlinear optics. The FELBE facility also serves as a far-infrared source for experiments at the High-Field Laboratory Dresden (HLD) involving pulsed magnetic fields up to 70 Tesla.

The statistics shows that the FEL used 1050 hours beamtime of the ELBE accelerator. This corresponds to 27 % of total beamtime, which is again distributed among internal and external users.

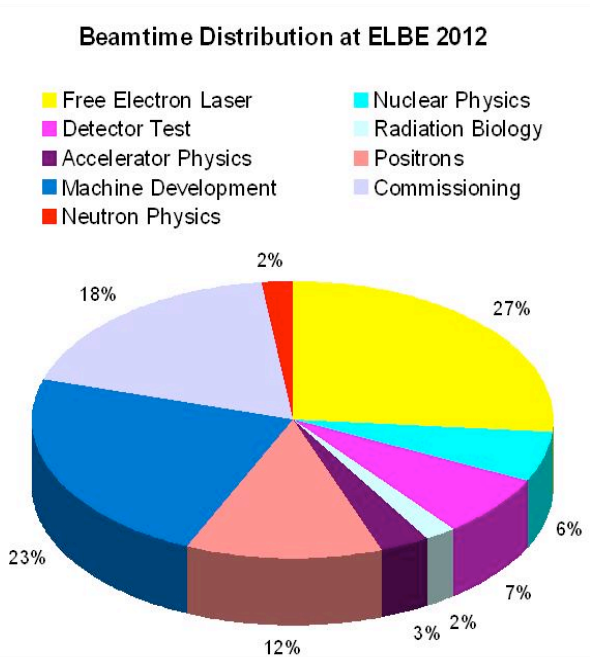

For further information please contact:
Prof. Manfred Helm (m.helm@hzdr.de)
or visit the FELBE webpage www.hzdr.de/FELBE.

ROssendorf BeamLine (ROBL)

The **RO**ssendorf **B**eam**L**ine (ROBL), operated by the HZDR since 1998, is a bending magnet synchrotron beam line located at the European Synchrotron Radiation Facility (ESRF) in Grenoble, France. It consists of two high specialized experimental stations, one unique for spectroscopic investigation of actinide and other radionuclides (Radiochemistry RCH) and one for diffraction experiments (Materials Science MRH). The latter is run by the Institute of Ion Beam Physics and Materials Research. In summer 2011 the complete beamline optics was renewed, since spring 2012 the beamline is back in user operation. Beside conventional silicon single crystals for monochromatisation in (111) and (311) orientation also a modern multilayer optics is available increasing the flux by two orders of magnitude by reduced energy resolution. By the use of mirrors with three different coatings (Si, Rh, Pt) the complete energy range from 6 to 35 keV is now accessible. Additionally, the beam can be focused by toroidal shape mirrors at the sample position in MRH down to approx 0.3*0.3 mm^2. The set-up and main parameters are sketched as follows:

Energy resolution	< 5×10^{-4} ΔE/E (Si(111)) < 1×10^{-4} ΔE/E (Si(311)) ~2×10^{-2} ΔE/E (multilayer ML)
Beam size	(10×0.5) mm^2 unfocussed (0.3×0.3) mm^2 focussed
Photon flux	8×10^{9} phot./(s.mm^2) unfocussed > 3×10^{11} phot./(s.mm^2) focussed > 2×10^{13} phot./(s.mm^2) focussed ML

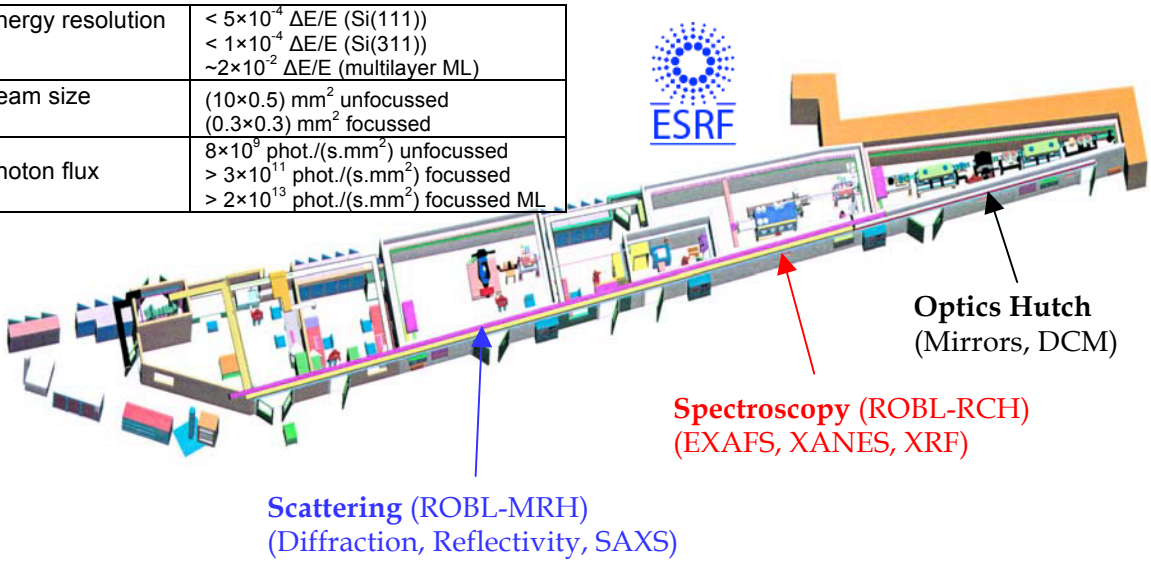

The core competence of ROBL-MRH is the analysis of thin films, multilayers and (ion-beam-synthesized) nanostructures using X-ray scattering techniques. Hereby phase formation or transformations; nanostructure, surface and interface evolution or strain/stress states are investigated. Of special attraction are experiments under *in-situ* conditions at ROBL-MRH. These studies are using process chambers for magnetron sputter deposition or annealing under vacuum or using various also reactive gases. All scattering experiments can be complemented by spectroscopic investigations.

ROBL is a user facility. Applications for beam time can be submitted as an official ESRF proposal at March 1st and September 1st. The ESRF covers travel and accommodation costs of successfully reviewed proposals. In addition, there is also the possibility to use in-house research beam time for collaborative experiments between external users and HZDR scientists for studies of common interest.

For further information please contact

Dr. Andreas Scheinost (ROBL-RCH): scheinost@esrf.fr
Dr. Carsten Bähtz (ROBL-MRH): baehtz@esrf.fr

or visit the ROBL webpage: www.hzdr.de/ROBL

Services

Main areas of competence

- Ion implantation in a broad range of ion energy (~ 200 eV to ~ 50 MeV) and substrate temperature
- Advanced ion beam technologies (high energy ion implantation, plasma immersion ion implantation, focused ion beam) for (micro)electronic applications
- Deposition of functional coatings using ion-assisted physical vapor deposition
- Advanced annealing technologies with flash lamps and lasers in the subsecond range
- Development and fabrication of sensors and detectors for charged particle spectroscopy
- High energy ion implantation service for power devices and laser structures
- Surface analysis of solid materials with high energy ion beams
- Computer simulation of ion beam interaction with materials
- Optical characterization of materials (luminescence, FTIR, Raman)
- Mechanical testing of neutron irradiated structural materials

Offers

- Consultation and problem evaluation for ion beam applications
- Process development for ion beam processing of metals, ceramics, semiconductors, thin films
- Preparation and treatment of material samples, tools or complex parts of devices
- Ion implantation and ion beam analysis services
- Fabrication of silicon radiation sensors under clean room conditions
- Structural diagnostics of materials surfaces including e-beam (SEM, TEM, AES) and X-ray techniques (XRD, XRR with both Cu-K and Synchrotron (5-35 keV) radiation).

Contact

Please direct your inquiries to one of the following experts:

Field of application	Responsible	Phone / Fax*	E-mail
Ion implantation and high-energy ion beam analysis	Dr. Johannes von Borany	3378 / 3438	j.v.borany@hzdr.de
Ion technologies for surface modification and doping	Prof. Andreas Kolitsch	3348 / 2703	a.kolitsch@hzdr.de
Advanced surface annealing	Dr. Wolfgang Skorupa	3612 / 3411	w.skorupa@hzdr.de
Semiconductor preparation Detector / Sensor fabrication	Dr. Bernd Schmidt	2726 / 3285	bernd.schmidt@hzdr.de
Focused ion beams	Dr. Lothar Bischoff	2963 / 3285	l.bischoff@hzdr.de
Structural diagnostics	Dr. Johannes von Borany	3378 / 3438	j.v.borany@hzdr.de
Materials research with Synchrotron radiation at ROBL (ESRF)	Dr. Carsten Bähtz	2367	baehtz@esrf.fr
Optical materials characterization	Dr. Harald Schneider	2880 / 3285	h.schneider@hzdr.de
Mechanical testing of irradiated structural materials	Dr. Hans-Werner Viehrig	3246	h.w.viehrig@hzdr.de

*For all phone/ fax-numbers choose the country / local code: +49 351 260 - xxxx (for HZDR)
+33 47 688 - xxxx (for ROBL)

The institute also recommends the homepages of its spin-off companies

• HZDR Innovation GmbH		www.hzdr-innovation.de
• GeSiM mbH	Si-Microsystems	www.gesim.de
• APT Dresden	Applied Pulse Technology	www.apt-dresden.de
• DTF GmbH	Thin Film Technology	www.dtf-technology.de

Organization chart

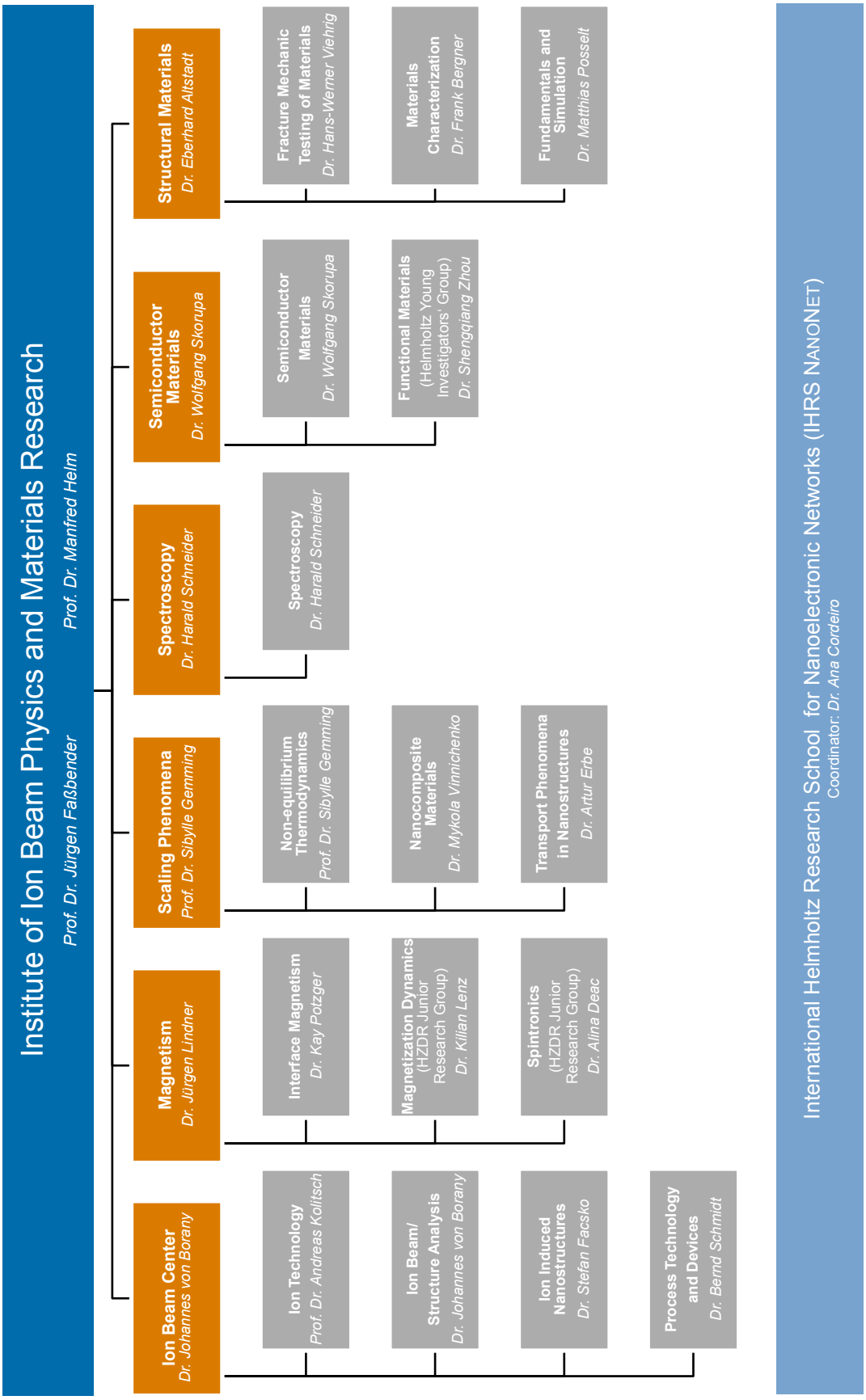

List of personnel 2012

DIRECTORS
Prof. Dr. M. Helm, Prof. Dr. J. Fassbender

OFFICE
S. Gebel, S. Kirch

SCIENTIFIC STAFF

Permanent staff

Dr. G. Abrasonis
Dr. C. Akhmadaliev
Dr. E. Altstadt
Dr. C. Bähtz
Dr. F. Bergner
Dr. L. Bischoff
Dr. J. von Borany
Dr. S. Facsko
Dr. S. Gemming
Dr. J. Grenzer
Dr. V. Heera
Dr. K.-H. Heinig
Dr. R. Hübner
Dr. R. Kögler
Prof. A. Kolitsch
Dr. J. Lindner
Dr. A. Mücklich
Dr. G. Müller
Dr. F. Munnik
Dr. C. Neelmeijer
Dr. M. Posselt
Dr. K. Potzger
Dr. L. Rebohle
Dr. H. Reuther
Dr. B. Schmidt
Dr. H. Schneider
Dr. W. Skorupa
Dr. A. Ulbricht
Dr. H.-W. Viehrig
Dr. M. Voelskow
Dr. M. Werner
Dr. S. Winnerl

Non-permanent

Dr. R. Bali
Dr. J. Bhattacharyya
Dr. F. Bregolin (P)
Dr. C. Cherkouk (P)
Dr. A. Cordeiro (P)
Dr. A. Deac
Dr. M. Devaraj (P)
Dr. O. Drachenko (P)
Dr. A. S. El-Said (P)
Dr. A. Erbe
Dr. C. Fowley
Dr. M. Friedrich (P)
Dr. J. Grebing
Dr. R. Heller
M. Houska (P)
Dr. A. Keller (P)
Dr. E. Kerimov (P)
Dr. M. Khalid (P)
Dr. M. Krause (P)
Dr. K. Lenz
Dr. B. Liedke (P)
Prof. W. Möller (P)
Dr. A. Neudert
Dr. X. Ou (P)
Dr. W. Pilz (P)
Dr. S. Prucnal (P)
K. Saravanan (P)
Dr. A. Shalimov
Dr. H. Schmidt (P)
Dr. V. Sluka
Dr. M. Vinnichenko (P)
Dr. K. Werniewicz (P)
Dr. R. Yankov (P)
Dr. P. Zahn (P)
Dr. S. Zhou (P)

TECHNICAL STAFF

Permanent staff

Rb. Aniol
Ry. Aniol
E. Christalle
S. Eisenwinder
B. Gebauer
D. Hanf
J. Haufe
A. Henschke
H. Hilliges
S. Klare
J. Kreher
A. Kunz
H. Lange
U. Lucchesi
F. Ludewig
R. Mester
M. Mißbach
C. Neisser
J. Pietzsch
A. Reichel
H. Richter
M. Roßner
S. Rott
B. Scheumann
G. Schnabel
A. Schneider
A. Scholz
T. Schumann
U. Skorupa
M. Steinert
U. Strauch
A. Thiel
K. Thiemig
A. Vetter
J. Wagner
W. Webersinke
R. Weidauer
A. Weise
R. Weiss
J. Winkelmann
I. Winkler
L. Zimmermann
J. Zscharschuch

Non-permanent

A. Barth
C. Frenzel (P)
F. Nierobisch
T. Putzke (P)
T. Schönherr (P)
I. Skorupa (P)
A. Weißig (P)

(P) Projects

PhD STUDENTS

Y. Aleksandrov
D. Ball
A. Banholzer
C. Baumgart
K. Bernert
D. Blaschke
A. Bogusz
R. Böttger
M. Buhl
D. Bürger
S. Cornelius
R. Endler
M. Fehrenbacher
J. Fiedler
C. Franke
D. Friedrich
M. Fritzsche
K. Gao
S. Germer
A. Heidarian
C. Heintze
T. Kaspar
N. Klingner
M. Körner
E. Kowalska
A. Kranz
M. Langer
J. Lehmann
F. Lomakina
M. Mittendorff
K. M. Mok
M. Neubert
J. Osten
B. Pelic
P. Philipp
D. Reichel
O. Roshchupkina
C. Scarlat
I. Schönitz
E. Schumann
Y. Shuai
T. Sendler
G. Steinbach
D. Stephan
M. Teich
A. Wagner
Y. Wang
R. Wenisch
U. Wiesenhütter
M. Wieser
C. Wilde
R. Wilhelm
S. Wintz
O. Yildirim
M. Zschintzsch
S. Zybell

STUDENTS (diploma / MSc / BSc)

C. Böttger
J. Kelling
M. Kretschmer
A. Mrotzek
L. Opherden
H. Sasse
J. Schmidt
B. Schreiber
M. Trache
R. Wutzler
R. K. Yadav

HZDR

HELMHOLTZ
ZENTRUM DRESDEN
ROSSENDORF

Institute of Ion Beam Physics and Materials Research
P.O. Box 51 01 19 · 01314 Dresden/Germany
Phone +49 351 260-2345
Fax +49 351 260-3285
http://www.hzdr.de

Member of the Helmholtz Association